



UNIVERSIDAD NACIONAL AUTÓNOMA
DE MÉXICO



FACULTAD DE QUÍMICA
POSGRADO EN CIENCIAS BIOQUÍMICAS

“Papel de las proteínas de choque térmico 90 en la fisiología renal”

*Tesis que para obtener el grado en:
Doctor en ciencias Bioquímicas*

Presenta:

M en C. Victoria Ramírez González.

*Tutor
Dra. Norma A. Babadilla Sandoval
Investigador titular C.
Instituto de Investigaciones Biomédicas, UNAM*

México D. F., Abril de 2009.



UNAM – Dirección General de Bibliotecas

Tesis Digitales
Restricciones de uso

DERECHOS RESERVADOS ©
PROHIBIDA SU REPRODUCCIÓN TOTAL O PARCIAL

Todo el material contenido en esta tesis está protegido por la Ley Federal del Derecho de Autor (LFDA) de los Estados Unidos Mexicanos (México).

El uso de imágenes, fragmentos de videos, y demás material que sea objeto de protección de los derechos de autor, será exclusivamente para fines educativos e informativos y deberá citar la fuente donde la obtuvo mencionando el autor o autores. Cualquier uso distinto como el lucro, reproducción, edición o modificación, será perseguido y sancionado por el respectivo titular de los Derechos de Autor.

Reconocimientos

Este trabajo se realizó en la Unidad de Fisiología Molecular del departamento de Medicina Genómica y Toxicología Ambiental del Instituto de Investigaciones Biomédicas UNAM, y el departamento de Nefrología del Instituto Nacional de Ciencias Médicas y Nutrición “Salvador Zubirán” bajo la tutoría de la Dra. Norma Araceli Bobadilla Sandoval. México, Distrito Federal. Febrero 2005 - Diciembre 2008.

Al comité tutorial que asesoró el desarrollo de esta tesis estuvo formado por investigadores de la Universidad Nacional Autónoma de México. UNAM.

Dra. Norma A. Bobadilla Sandoval

Instituto de Investigaciones Biomédicas.

Dr. Fernando López Casillas

Instituto de Fisiología Celular.

Dr. Armando Tovar Palacio

Facultad de Química.

Al programa de maestría y doctorado en ciencias bioquímicas de la Facultad de Química UNAM, por todas las facilidades otorgadas.

Este trabajo fue realizado con el apoyo otorgado por el CONACyT a Dra. Norma Bobadilla con el número de registro (48483) y por la UNAM-DGAPA (IN228206-3)

El jurado de examen estuvo formado por:

Dra. Victoria Chagoya de Sánchez	Presidente
Dr. Rogelio Hernández Pando	Vocal
Dr. Gerardo Gamba Ayala	Secretario
Dra. Clorinda Arias Álvarez	Suplente
Dr. Fernando López Casillas	Suplente

Agradezco al Dr. Gerardo Gamba por sus comentarios durante el desarrollo de este trabajo.

Agradezco la asesoría del MVZ. Octavio Villanueva en el manejo de los animales en el bioterio del INCMNSZ.

Durante la realización de mis estudios de doctorado recibí una beca otorgada por el **CONACyT** con el número de registro 17030

Agradecimientos

A mis padres: Martha y Ángel: Por estar en todo momento conmigo, enseñándome a valorar las cosas buenas y malas de la vida, por enseñarme a perseverar y alcanzar mis sueños, por mostrarme que cada uno hace su propio destino. Siempre se han alegrado de mis aciertos pero sobre todo han comprendido mis fracasos, mostrándome que las adversidades se superan con valor, entereza y un profundo compromiso. Les agradezco haber hecho de mí la persona que ahora soy, por alentar mis sueños y por su mantener su fe en mi. Este sueño también es suyo, pues siempre hemos caminado juntos, los amo, gracias.

A mis hermanos Angy, Adry, Miguel, Ale y la nueva adquisición Héctor: Gracias por su apoyo, paciencia y consejos, por darme palabras de aliento cuando las necesité, por corregir mis errores y sobre todo, por mostrarme que no importa lo que pase siempre cuento con ustedes y sé que su cariño es incondicional, los quiero mucho.

A Norma Bobadilla: Porque al ser parte de su equipo alcance uno más de mis sueños, le agradezco su ayuda, paciencia, su trato personal, su esfuerzo y compromiso, sin su ayuda no hubiera sido posible. Durante este tiempo no solo crecí profesionalmente, aprendí a ser tolerante, paciente y que para lograr los objetivos, es necesario conducirse con ética y honradez, aprendí que en la ciencia no todo está dicho, no todo es cierto y no todo es fácil, ahora sé que en este camino hay que ser paciente y perseverante. De usted obtuve, una guía, un ejemplo y una amiga, gracias.

A Joyce, Erika y Paola: Por todas sus palabras de aliento y por aguantar mis innumerables quejas. Gracias por mostrarme su cariño y sorprenderme con su desinteresado apoyo, chicas sin ustedes no hubiera sido lo mismo pues gane tres grandes amigas.

A mis amigos, Ale, Isaías, Vero, Rolando,, Miguel, Mario, Rosibel, Maru, Ita, Damián, Juan, Jorge, Juan Manuel y Tino: Gracias por los buenos y malos momentos, por ser parte de esta aventura y sacarme de la rutina.

A mis compañeros del Departamento de Nefrología y Metabolismo Mineral. Por sus valiosos consejos y por hacer un agradable ambiente de trabajo.

A Leticia García y Nayeli Ortega: Por su amistad además de hacer mi vida más fácil y ayudarme en todos los trámites administrativos durante mis estudios doctorales.

A la UNAM por lograr formar parte de su comunidad y llevar en alto sus valores y colores.

Victoria.

Índice	Páginas
Abreviaturas	iii
Índice de figuras	v
Resumen	vii
1) Introducción	2
1.1) Proteínas de choque térmico	2
1.2) Principales funciones de las subfamilias de proteínas de choque térmico.	3
1.2.1) Small Hsps (sHsps)	4
1.2.2) Hsp40	6
1.2.3) Hsp60	7
1.2.4) Hsp70	7
1.2.5) Hsp110	8
1.3) Proteínas de choque térmico de 90 KDa (Hsp90)	9
1.4) Las proteínas citosólicas: Hsp90 α y Hsp90 β .	9
1.5) Estructura cuaternaria de Hsp90 α y de Hsp90 β	12
1.6) Forma activa de Hsp90	15
1.7) Inhibidores farmacológicos de Hsp90	17
1.8) Hsp90 y sus proteínas cliente	20
1.9) Hsp90 y su interacción con la sintasa de óxido nítrico endotelial (eNOS)	21
1.10) Localización de Hsp90 en el tejido renal	29
1.11) Hsp90 en la reabsorción renal de sodio y en la regulación osmótica	31
1.12) Hsp90 en condiciones fisiopatológicas renales	34

2) Hipótesis	38
3) Objetivos	39
4) Métodos	41
4.1) Inclusión de animales	41
4.2) Cirugía	41
4.3) Estudios bioquímicos	44
4.3.1) Determinación de la filtración glomerular	44
4.3.2) Excreción urinaria de nitritos y nitratos	45
4.3.3) Lipoperoxidación.	45
4.3.4) Peróxido de hidrógeno urinario	46
4.3.5) Niveles de isoprostanos $F_{2\alpha}$ urinarios.	47
4.4.) Estudios moleculares	49
4.4.1) Extracción de RNA total	49
4.4.2) Transcripción reversa	49
4.4.3) RT-PCR en tiempo real	50
4.4.4) Análisis de Western blot	51
5) Resultados	55
6) Discusión	70
7) Referencias	71
8) Artículos	89
9) Otros Artículos	100

Abreviaturas

Hsp	Proteínas de choque térmico.
sHsp	small Hsp
HSF1	Factor de transcripción de choque térmico de 90KDa
HSE	Elemento de respuesta de choque térmico
eNOS	Sintasa de óxido nítrico endotelial
NO	Óxido nítrico
GA	Geldanamicina
Rad	Radicicol
TAM	Tensión arterial media
FSR	Flujo sanguíneo renal
FG	Filtración glomerular
NO ₂ ⁻	Nitritos
NO ₃ ⁻	Nitratos
O ₂ ⁻	Anión superóxido
NADPH	Nicotina adenina dinucleótido fosfato
BH ₄	Tetrahidrobioptерина
FAD	Flavina adenina dinuclótido
FMN	Flavina mononucleótido
GCs	Guanilato ciclasa soluble
GMPc	Guanosina monofosfato cíclico
Akt	Proteína cinasa B
BAEC's	Células endoteliales de aorta de bobino
L-NAME	L-metil-nitro-arginina

VEGFR2	Receptor 2 del factor de crecimiento del endotelio vascular
TonEBP	Proteína de unión que potencia la respuesta a tonicidad
INUTEST	Polímero de fructosa altamente soluble.

Índice de Figuras.

Figura	Páginas
1. Funciones fisiológicas de las proteínas de choque térmico.	2
2. Localización celular de las proteínas que conforman a las proteínas de choque térmico de 90KDa.	9
3. Representación esquemática de los transcritos primarios de las Hsp90 citosólicas.	10
4. Representación esquemática de los sitios regulatorios de los genes hsp90 α y Hsp90 β .	11
5. Dominios de Hsp90.	13
6. Representación esquemática del ciclo ATPasa de Hsp90.	15
7. Estructura química de los inhibidores de Hsp90	18
8. Mecanismo de reacción y estequioterapia de la biosíntesis de NO	22
9. Fosforilación in vitro de eNOS	24
10. Sitios de interacción de Hsp90 en eNOS	26
11. Expresión de Hsp90 α y Hsp90 β en el tejido renal	29
12. Localización de Hsp90 α y Hsp90 β en el tejido renal	30
13. Parámetros fisiológicos durante la inhibición de Hsp90	54
14. Efecto de la inhibición de Hsp90 durante la inhibición de Hsp90 empleando INUTEST	56
15. RNA total extraído de cortezas de ambos grupos de estudio	56
16. Cinéticas de amplificación hechas por RT PCR en tiempo real	57
17. Efecto de la inhibición de Hsp90 sobre las niveles de RNAm de Hsp90	59
18. Efecto de la inhibición de Hsp90 sobre las niveles de proteína de Hsp90	60
19. Producción de NO durante la inhibición de Hsp90	61
20. Niveles de estrés oxidativo durante la inhibición de Hsp90	62
21. Expresión de eNOS durante la inhibición de Hsp90	64
22. Efecto de la fosforilación de eNOS durante la inhibición de Hsp90	65
23. Efecto de la inhibición de Hsp90 sobre el estado de dimerización de eNOS	67

Tablas

Tabla 1 Clasificación y propiedades de las proteínas de choque térmico	5
Tabla 2 Abundancia relativa de Hsp90 α y Hsp90 β	16

Resumen

Introducción. La subfamilia de proteínas de choque térmico de 90 Kda, comprenden del 1-2 % de la proteína citosólica total, en las células eucariontes, está formada por 5 miembros, siendo Hsp90 α y Hsp90 β las más abundantes ocupando el 85%. Estas proteínas se han asociado a un gran número de procesos fisiológicos a través de interactuar con más de 100 proteínas, a las cuales se les denomina clientes moleculares de Hsp90. Diferentes estudios han mostrado que Hsp90 regula la actividad de la sintasa de óxido nítrico endotelial (eNOS), incrementando su actividad y por ende aumentando la producción de óxido nítrico (NO) en las células del endotelio vascular donde ejerce acciones vasodilatadoras.

Objetivo. Conocer si la inhibición de Hsp90 con Radicicol modifica el flujo sanguíneo renal (FSR) y la filtración glomerular (FG) al inhibir la formación del complejo Hsp90-eNOS.

Métodos. Se incluyeron 20 ratas Wistar macho de 300g de peso, fueron divididas en dos grupos. Al primer grupo se les infundió vehículo (DMSO 10% y etanol 10% en solución salina) y al segundo grupo se le infundió radicicol (25mg/ml/min) durante 60 min. Se realizaron mediciones basales antes de la infusión de vehículo o radicicol. Durante todo el experimento se monitoreo la presión arterial media (TAM), FSR, se determinó la FG, la excreción urinaria de nitritos y nitratos, se cuantificó la producción de isoprostanos F_{2 α} y de peróxido de hidrógeno en orina. En el tejido renal se evaluaron los niveles de lipoperoxidación, los niveles de RNAm y cantidad de proteína de Hsp90 α , Hsp90 β y eNOS. Además se determinaron los niveles de fosforilación de eNOS en la serina 1177 y en la

treonina 497 de eNOS, finalmente se evaluó la relación dímero/monómero de eNOS.

Resultados y Conclusiones. Observamos que la inhibición de Hsp90 con radicicol, redujo de manera significativa el FSR y la FG, efecto que se acompañó con la reducción urinaria de nitritos y nitratos. No observamos cambios en la cantidad de RNAm, ni de proteína de eNOS. La infusión de radicicol incrementó de manera significativa la fosforilación de la treonina 497 de eNOS asociada con reducción en la producción de NO, este efecto se asocio con menor cantidad de dímeros activos e incremento en la formación de monómeros inactivos. Por lo que nuestros resultados sugieren que la hipoperfusión e hipofiltración observada durante la infusión de radicicol puede ser mediada en parte por la pérdida de la interacción entre Hsp90-eNOS.

Introducción

1) Introducción

Las células y tejidos están expuestos constantemente a condiciones extremas que alteran la homeostasis celular y que pueden llegar a producir estrés celular en forma aguda o crónica. En consecuencia, las células han desarrollado mecanismos protectores que son capaces de percibir y responder a estos cambios ya sea en el medio ambiente interno o en externo para evitar que sea dañada la fisiología celular.

1.1) Proteínas de choque térmico

Uno de los mecanismos de protección celular fue descrito por primera vez en 1962 por Ritossa y col (1), quienes observaron un aumento repentino en la síntesis de RNAm en glándulas salivales de *Drosophila melanogaster* cuando la temperatura se incrementaba 5°C. Posteriormente mostraron que estos transcritos generaban proteínas de pesos moleculares entre 27 y 70 (kDa), las proteínas recién sintetizadas se les denominó proteínas de choque térmico Hsp, por sus siglas en inglés Heat Shock Proteins. A partir de ese momento se iniciaron diversos estudios para investigar el papel de estas proteínas y su conservación a lo largo de la evolución (1, 2).

Las proteínas de choque térmico conforman una numerosa familia de proteínas con un peso molecular que varía entre 10 y los 160 kDa y que han sido divididas en seis subfamilias por la similitud de su masa molecular conocidas

como: la Hsp de 100-110 KDa, la de 90 KDa, la de 70 KDa, la de 60 KDa, la de 40 KDa y la subfamilia de Hsp's con peso molecular de 18-40KDa (3).

1.2) Principales funciones de las subfamilias de proteínas de choque térmico.

En la Figura 1 se resumen las principales funciones de las proteínas de

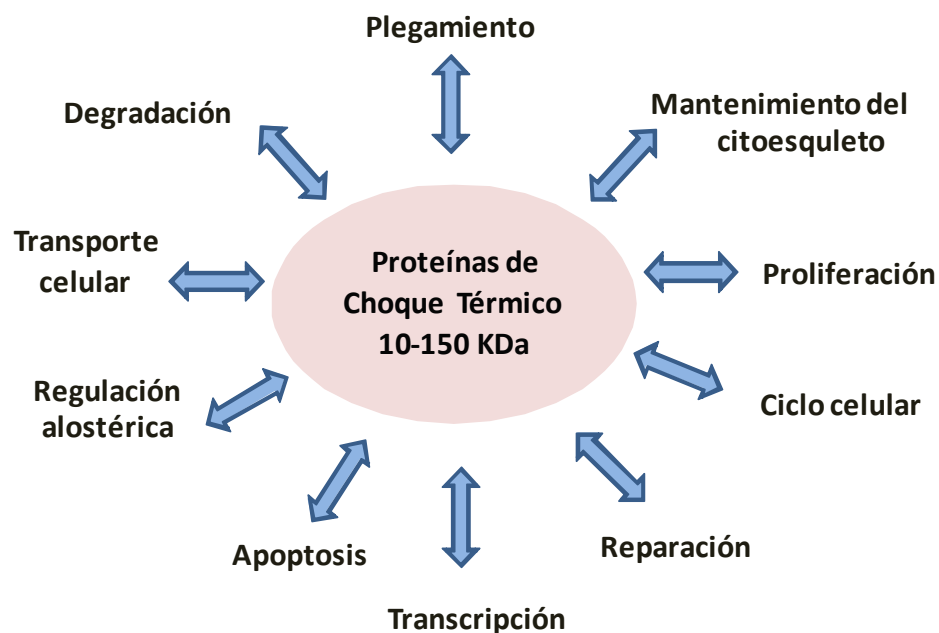


Fig. 1. Funciones fisiológicas de las proteínas de choque térmico

choque térmico en condiciones fisiológicas, dentro las que destacan: ayudar a ensamblar los complejos de la RNA polimerasa II, participar en la maduración y plegamiento de proteínas recién sintetizadas, reparar proteínas dañadas, regular allostéricamente a otras proteínas y transportarlas a sus compartimientos celulares, además de que participan en mantener la conformación del citoesqueleto. También se conoce que participan en el ciclo celular y en procesos

de proliferación, también son capaces de evitar agregados celulares no funcionales que comprometan la viabilidad celular. Cabe señalar que esta función chaperónica es, en la mayoría de las casos, dependiente de ATP (4).

Las proteínas de choque térmico se expresan en forma constitutiva y la mayoría de ellas se inducen bajo condiciones de estrés celular como la hipertermia o la hipotermia, la hipoxia, la inflamación, la exposición a radiación ionizante, fármacos tóxicos y por la presencia de metales pesados como zinc, hierro, cadmio, mercurio y arsénico (5, 6, 7, 8, 9).

Las Hsps también funcionan en otra gran cantidad de procesos celulares, los cuales dependen de la localización y de la estructura cuaternaria pues se ha reportado que las proteínas de choque térmico son activas en su forma monómera y hasta en conformaciones tan complejas de anillos hexaédricos o gránulos de 27 subunidades. A continuación se mencionan generalidades de cada una de las subfamilias de Hsp Tabla 1 (10, 11, 12).

1.2.1) Small Hsp (*sHsp*)

La sub-familia de proteínas de menor peso molecular o small Hsp está compuesta por proteínas de peso molecular monomérico que varía entre los 15 a los 45 KDa. Pueden formar dímeros, hexámeros y oligómeros localizándose principalmente en el citoplasma de las células. Se han descrito la presencia de gránulos de estas proteínas de hasta 450 KDa en roedores.

Las *sHsp* se caracterizan por la presencia de un dominio conocido como α cristalino que está conformado de 90 aminoácidos en el extremo carboxilo

encargado de las interacciones entre las diferentes subunidades. Se conoce que la actividad de estas proteínas es regulada principalmente por cambios en su estado de fosforilación y no por interacción con diferentes nucleótidos o con otras proteínas, por lo que hasta ahora no se les atribuye funciones de co-chaperonas.

Sub-familia	Localización celular	Estado cuaternario	Funciones
<i>Small Hsp</i> <i>(sHsp)</i> 15-40 KDa	Citoplasma Núcleo	Dímeros Hexámeros Hexadecámeros Esferas de 24 unidades	Evitar agregados proteicos Plegamiento Polimerización de actina
<i>Hsp40</i>	Citoplasma Retículo endoplásmico	Dímeros Complejos proteicos	Actividad chaperona Síntesis de colágeno
<i>Hsp60</i> <i>Sistema de chaperoninas</i>	Citoplasma Mitocondria	Tetrámeros Doble anillo hexaédrico y heptaédrico Anillos de multímeros	Complejo chaperónico Plegamiento y transporte de proteínas Degradación
<i>Hsp70</i>	Citoplasma Núcleo Mitocondria Retículo Endoplasmico	Heterodímeros con otras Hsp	Plegamiento Transporte Importación
<i>Hsp90</i>	Citoplasma Mitocondria Retículo endoplasmico	Dímeros	Plegamiento y Transporte de proteínas Prevención de agregados proteicos Modulador alostérico
<i>Hsp110</i>	Citoplasma Núcleo Retículo endoplasmico	Dímeros Anillos hexaédricos y heptaédricos Multímeros	Solubilización de agregados proteicos Plegamiento proteico Regulación osmótica

Tabla 1. Clasificación y propiedades de las proteínas de choque térmico.

Las sHsps desempeñan sus funciones dependiendo de su dimerización u oligomerización, por ejemplo, se ha descrito que el dímero de Hsp26 modula el plegamiento de cadenas peptídicas nacientes. Sin embargo la fosforilación de estas proteínas puede promover su disociación como ocurre con Hsp27 ya que reduce su actividad. En contraste Hsp25 incrementa su actividad cuando se encuentra formando hexadecámeros interactuando con proteínas entre las que se encuentran los filamentos de actina, la unión de Hsp25 evita la precipitación de la actina (10,.11, 12, 13, 14).

1.2.2) *Hsp 40*

Esta sub-familia es considerada como co-chaperonas que integran el complejo de chaperonas citosólica. La subfamilia de Hsp40 posee un dominio altamente conservado de 70 aminoácidos conocido como dominio J que se localiza en el extremo amino y es necesario para su interacción con otras proteínas de choque térmico como la Hsp70. La mayoría de estas Hsps se localizan en el citoplasma, pero miembros de esta familia se han localizado en el retículo endoplasmico. La variedad de esta subfamilia es tan extensa que ha sido necesaria ser subclasicificada en tres grupos de acuerdo a su conservación del dominio J en tipo I, II y III.

Dependiendo de su estado de polimerización el peso molecular puede variar de 40 a 500 KDa. Sus principales funciones son la de co-chaperonas y facilitar el plegamiento y movimiento de las cadenas del colágeno (11, 12, 15, 16).

1.2.3) Hsp60.

La subfamilia de Hsp60 es conocida como la familia de las chaperoninas. Se clasifican en dos sub grupos conocidos como el de las proteínas homologas a GroEL y el de las chaperoninas. El peso molecular varía dependiendo de su conformación y generalmente las pertenecientes al primer grupo se encuentran formando anillos cilíndricos de 7 subunidades, mientras que las segundas se encuentran formando dos anillos de diferentes subunidades. Se ha descrito la presencia de estas proteínas en la mitocondria y en el cloroplasto, aunque en las células de mamíferos estos complejos pueden localizarse en el citoplasma. La principal función de estas chaperonas es proporcionar un adecuado plegamiento a diversas proteínas, este proceso ocurre cuando las proteínas cliente se unen a la cavidad central formada en los anillos y se ha demostrado que este proceso es regulado por la hidrólisis de ATP así como por el desensamblaje de los diferentes anillos (10, 12, 14, 17, 18).

1.2.4) Hsp70

Constituye la familia más abundante de Hsps pues comprenden del 3.6% al 4% de la proteína soluble total, además es una de las mejores caracterizadas, se conocen tres miembros que se expresan de manera constitutiva e inducible. Se encuentran en diferentes compartimientos celulares como el citoplasma, el núcleo y el retículo endoplasmico. Se caracterizan por poseer dos dominios claramente identificados, el primero es el dominio amino donde se localiza un sitio de unión al ATP y un segundo dominio o carboxilo donde se unen sus proteínas cliente. Las principales funciones de esta subfamilia es el plegamiento de péptidos nacientes,

translocación de proteínas y recientemente se describió su papel en la regulación de la apoptosis (12, 13, 14).

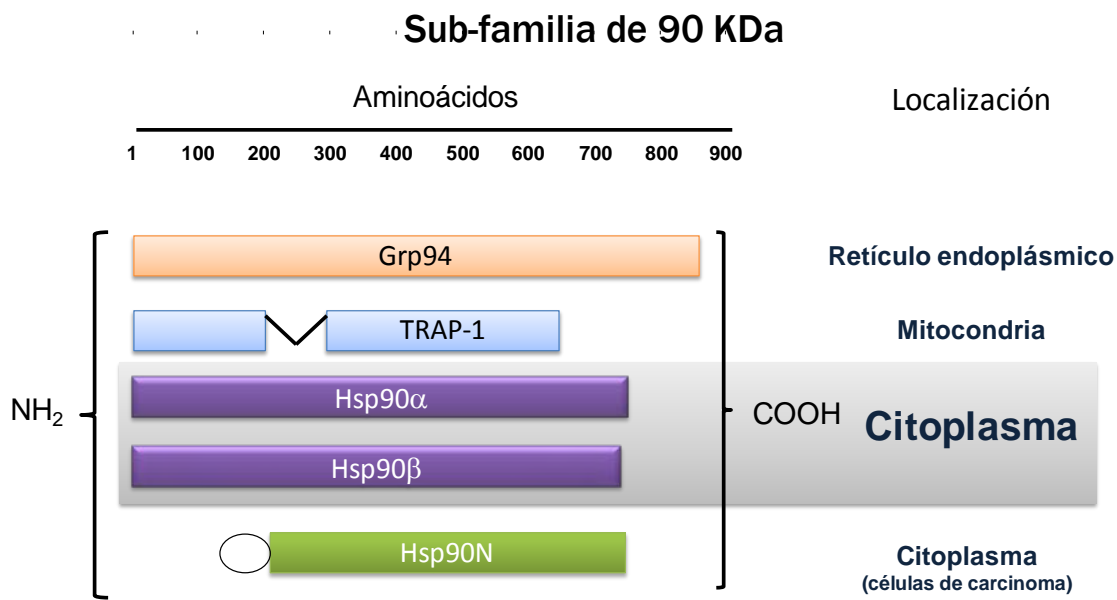
Se conoce que la actividad de estas proteínas es regulada por la presencia de otras co-chaperonas como Hsp40, pues facilita su actividad ATPasa permitiendo así asociarse a sus clientes moleculares. Se ha descrito que pueden formar de heterodímeros con otras proteínas como Hsp40, p23, Hip y Hsp110 pero no hay evidencia que las Hsp70 formen homodímeros (10, 15, 19).

1.2.5) *Hsp110*

Esta sub-familia es la tercera más abundante después de la de 70 y 90 KDa, su proporción es aproximadamente del 0.7% de la proteína celular total; Se expresan en la mayoría de los tejidos y se localizan tanto en el citoplasma como en el retículo endoplasmico. Al igual que la de 70 y 90 KDa tiene una región ATPasa en el dominio amino terminal. Esta subfamilia es activa solo cuando forma anillos multiproteicos de 400 a 700KDa. Las Hsp110 forman complejos principalmente con Hsp70 y Hsp25/27. Las principales funciones de esta subfamilia es evitar la formación de agregados proteicos, facilitando su degradación, ya que Las Hsp110 son subunidades formadoras de diferentes complejos de proteasas, sin embargo por sí mismas no poseen actividad proteolítica (10, 20)

1.3) Proteínas de Choque Térmico de 90 KDa.

La subfamilia de Hsp de 90 KDa está compuesta por cinco isoformas conocidas como Hsp90 α , Hsp90 β , Trap-1 (Hsp75), Gpr94 y Hsp90N (Figura 2). Se ha descrito que las Hsp90 constituyen del 1 al 2% de la proteína citosólica soluble total en las células eucariontes. Estas proteínas se diferencian en la célula por su abundancia y localización celular; Hsp90 α y Hsp90 β conforman el 85% de esta subfamilia y se localizan en el citoplasma mientras que el 15% restante lo conforman Trap-1, Gpr94 y Hsp90N, las dos primeras se localizan en la mitocondria y en el retículo endoplásmico respectivamente y finalmente Hsp90N se expresa únicamente en diferentes carcinomas (21, 22, 23, 24, 25, 26, 27).



1.3) Las proteínas citosólicas: Hsp90 α y Hsp90 β .

Ambas proteínas son codificadas por genes diferentes, se han mapeado copias de cada uno de ellos en diferentes cromosomas; Hsp90 α está ubicado en los cromosomas 1, 3, 4, 11 y 14 con un tamaño de 7393 pb, pero únicamente el

gen localizado en el cromosoma 14 se transcribe, este gen genera un RNAm de 2912 pb que traduce una proteína de 733 aminoácidos. Mientras que el gen de Hsp90 β se ha identificado en los cromosomas 4, 6, 10, 13, 14 y 15 con un tamaño de 8210 pb, pero el único que se transcribe está localizado en el cromosoma 6. El transcripto de este gen es de 2567 pb que se traduce en una proteína de 726 aminoácidos (28, 29).

Como se observa en la Figura 3 los transcritos primarios de Hsp90 α y de Hsp90 β presentan intrones y exones, pero particularmente el primer exón no se traduce y se ha propuesto que esta característica les puede conferir una regulación diferente como se detalla a continuación (30).

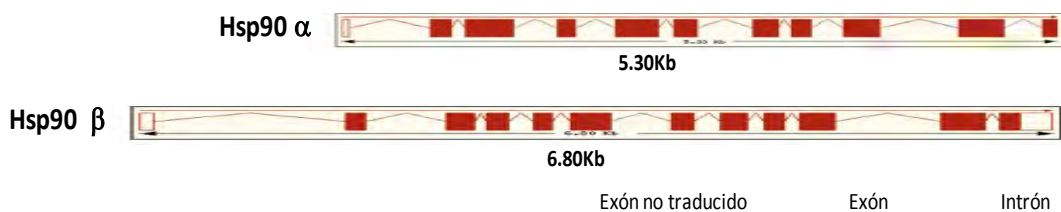


Figura. 3. Representación esquemática de la estructura de los transcritos primarios de las Hsp90s citosólicas, donde los cuadros blancos indican exones no traducidos, los cuadros rojos exones traducidos y las líneas continuas representan los intrones. Tomada de A. Subbarao et-al. *FEBS Letters*, 2004.

La transcripción de los genes de las proteínas de choque térmico está principalmente regulada por los elementos de respuesta a choque térmico (HSE) que se encuentran ubicados en su región promotora. (22). En el gen de Hsp90 α , la región promotora está conformada por el núcleo del promotor y dos regiones ricas en "GC" localizados río arriba entre -50 y -200pb. El promotor contiene una caja

TATA en el sitio -30pb donde se ensambla la RNA polimerasa II. En células Jurkat (células T en leucemia) se demostró que la transcripción inducible del gen de Hsp90 α es regulada por tres HSE, que contienen el motivo 'nGAA' localizados río arriba en la región -1031/-1022pb, -307/-288 pb y -96/-60 pb. También se ha identificado un HSE en el primer intrón +238/+247, al que se le ha atribuido la transcripción constitutiva del gen (31, 32).

Mientras que, el gen de Hsp90 β contiene un sitio CRE (elemento de respuesta a AMPc) en la posición -126 pb, así como una caja CAAT localizada en -87/-84pb río arriba de la caja TATA que se ubica a -27 pb. Se han caracterizado dos elementos de respuesta a estrés térmico en el primer intrón localizados en +680/+695 y +734/+747 pb respectivamente, que incrementan la transcripción del gen de manera inducible. Se han señalado otros dos HSE en la región +628/+642 pb y +1337/+1346 pb que se han denominado HSE atípicos, pero no son capaces de inducir la transcripción del gen en respuesta a estrés térmico. Finalmente, también se ha identificado un HSE que se localiza corriente arriba en la región -648/-634 que regula la transcripción constitutiva del gen, pues su delección no inhibe la transcripción durante el incremento de temperatura. La localización de estos elementos se muestran en la Figura 4 (31, 32). Se ha propuesto que la distribución de los HSE en Hsp90 α y Hsp90 β , parece conferirles una regulación transcripcional diferente, por lo que se considera que estos dos genes pueden responder de forma diferente ante el mismo estímulo.

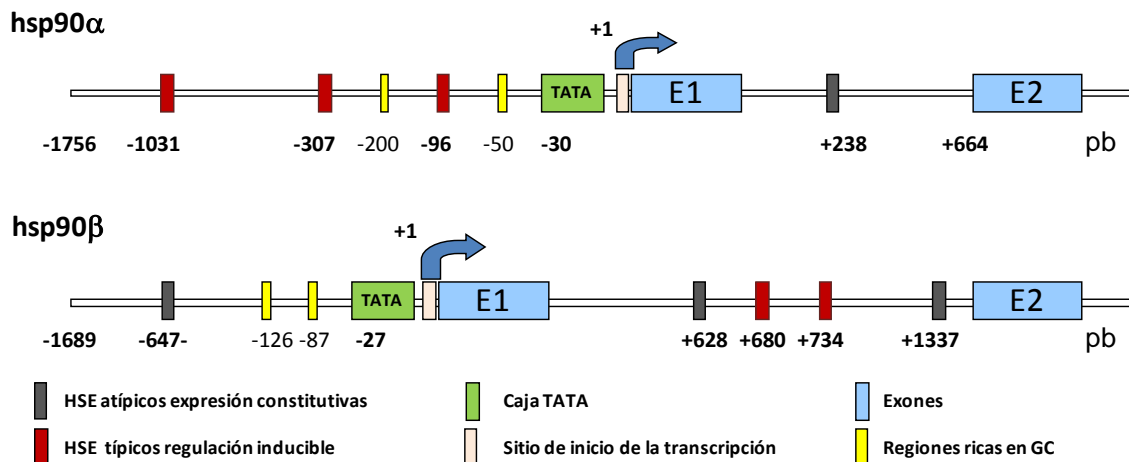


Figura. 4. Representación esquemática de los sitios regulatorios de los genes de hsp90 α y hsp90 β . En cuadros rojo se representan la localización de los elementos de respuesta de choque térmico (HSE) que regulan la expresión inducible de estos genes, en cuadros grises se ilustran los HSE con secuencia atípica, que regulan su transcripción constitutiva, también en cuadros verdes se ilustra el sitio de unión de la RNA polimerasa II y en amarillo los elementos del promotor localizados río arriba del núcleo del promotor. Se observa que la transcripción inducible de hsp90 α se regula en forma diferente a la de hsp90 β pues los HSE se localizan corriente arriba del núcleo del promotor y en el primer intrón respectivamente.

El factor de transcripción de choque térmico 1 (HSF-1) regula la transcripción de Hsp90 α y de Hsp90 β . En condiciones normales, HSF-1 se encuentra en el citoplasma unido a diferentes chaperonas incluyendo a las proteínas de choque térmico de 90KDa que lo mantienen reprimido. Cuando se produce estrés celular ya sea físico o químico, HSF-1 es liberado de complejo, propiciando su fosforilación y translocación al núcleo donde se forma un trímero activo que se une a los elementos de respuesta de estrés térmico HSE, activando así, la transcripción de la mayoría de los genes de choque térmico (33, 34, 35).

1.4) Estructura cuaternaria de Hsp90 α y de Hsp90 β

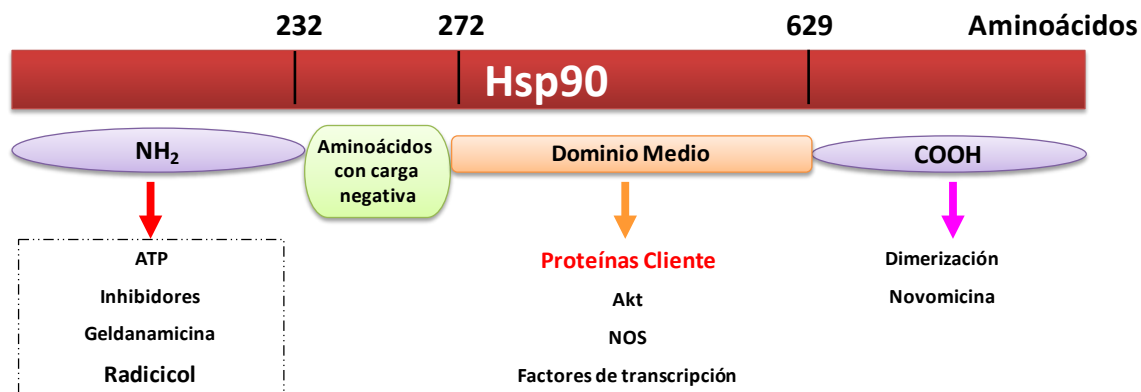


Figura. 5. Dominios de Hsp90. La estructura cuaternaria de Hsp90 presenta un dominio amino donde se localiza el sitio catalítico para la unión de ATP e inhibidores, seguido por una región rica en aminoácidos con carga negativa. En el dominio medio es donde se realizan la mayoría de sus interacciones y finalmente el dominio carboxilo, sitio de dimerización.

Hsp90 α y Hsp90 β están conformadas por cuatro dominios bien caracterizados como se detallan en la Figura 5. El primero es el dominio amino terminal donde se localiza el sitio de unión al ATP, también conocido como dominio ATPasa, donde el ATP es hidrolizado mediante diferentes ciclos de asociación y disociación entre Hsp90 y sus proteínas cliente como se muestra en la Figura 6 (21, 22, 23, 36, 37, 38, 39, 40, 41). Las proteínas cliente son todas aquellas proteínas con las que Hsp90 interactúa y puede modificar, estabilizar o incluso aumentar su actividad. La estructura cristalina de este extremo en levadura y en humano ha mostrado la presencia de 8 hojas beta plegadas antiparalelas y nueve alfa hélices que forman una estructura de sándwich α/β dando una estructura tridimensional similar a la DNA girasa y a la proteína MutL reparadora del DNA que requiere ATP para formar una unión o anclaje al DNA (38). El segundo dominio es llamado “cargado”, ya que es una región de 30 aminoácidos con carga negativa de la cual se desconoce su función específica. El tercer

dominio llamado “dominio medio” es donde se unen sus proteínas cliente dentro de las que destacan: cinasas, factores de transcripción, proteínas G, proteínas del citoesqueleto, receptor a mineralocorticoides, sintasas de óxido nítrico, entre otras. Finalmente, el dominio carboxilo terminal es donde se realiza la dimerización de Hsp90 (3). Así mismo, estudios recientes muestran que en este extremo hay un segundo sitio de unión a ATP, que es sensible a novomicina y cis-platino; aparentemente para que este sitio sea activo es necesario que Hsp90 adopte una conformación adecuada para permitirle unir al ATP. Pero, hay muy poca evidencia sobre las condiciones necesarias para que este sitio adquiera actividad. Los autores de estos estudios sugieren que este segundo sitio de unión a ATP parece estar disponible, solo cuando el extremo amino se encuentra ocupado, ya sea por ATP o por sus inhibidores. Sin embargo, la participación de este sitio sobre la actividad de Hsp90 no es clara , pero se ha propuesto que ambos sitios podrían funcionar de forma cooperativa (42, 43).

1.5) Forma activa de Hsp90

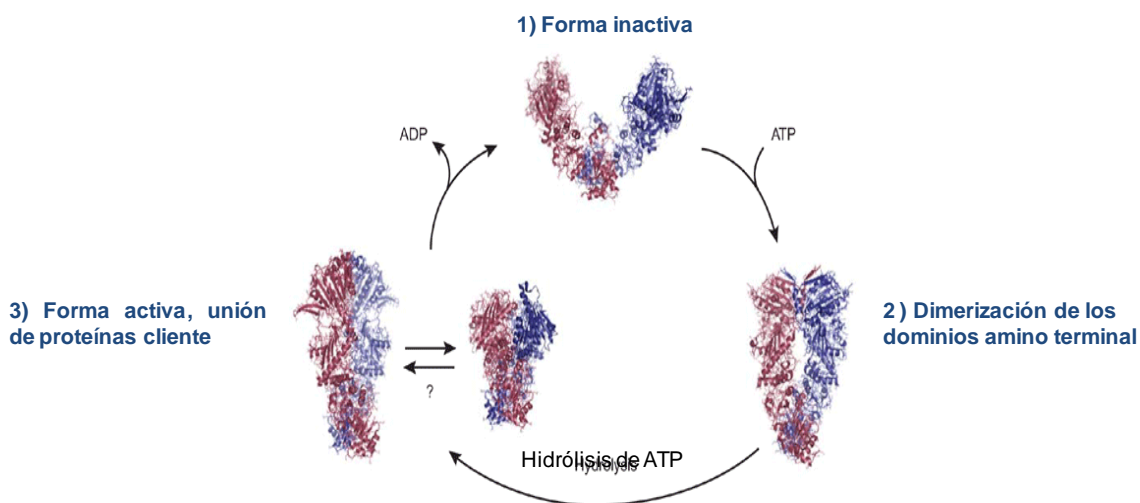


Figura 6. Representación del ciclo ATPasa de Hsp90 . 1)Se observa que la unión de una molécula de ADP favorece la conformación abierta inhibiendo la actividad de Hsp90. 2)La unión del ATP propicia el rearreglo del dímero facilitando el acercamiento de los extremos amino generando el sitio catalítico para el ATP. 3) Tras la unión del ATP, Hsp90 sufre una serie de torsiones que cambian la orientación de los monómeros, permitiendo la hidrólisis del ATP y la unión de sus clientes moleculares. Tomada de Klaus Richter et-al. *Nature*, 2007.

Diversos estudios han mostrado que las Hsp90 se encuentran activas cuando forman dímeros. En un trabajo reciente realizado por Buchner y col.; (39) reportaron que el dímero de Hsp90 funciona al adoptar dos conformaciones diferentes, la primera llamada “cerrada” o activa y la segunda conocida como “abierta” o inactiva (44, 45, 46, 47).

La conformación cerrada se establece cuando una molécula de ATP se une al dímero de Hsp90, esto genera un cambio conformacional que permite la formación de una especie de asa de interacción entre los extremos amino de cada monómero favoreciendo la hidrólisis del ATP y la unión a sus proteínas cliente. Por el contrario, si el dímero se encuentra en la conformación abierta ahora contendrá

una molécula de ADP unida que evitará que Hsp90 reclute a sus proteínas cliente. Esta asociación y disociación se conoce como ciclo ATPasa y es indispensable para la función correcta de Hsp90 (46,47).

Se ha observado que el cambio del estado abierto al cerrado produce cambios conformacionales en toda la proteína, principalmente en las regiones denominadas bisagras, estas se localizan en la transición del dominio carboxilo y el dominio medio, así como en la transición del dominio medio al dominio amino. El primer cambio observado mediante cristalografía de rayos X, muestra que el dominio carboxilo y medio sufren una fuerte torsión que modifica su orientación y aproxima a los extremos amino. El segundo movimiento es otra torsión de 90° de los extremos amino permitiendo el ensamble catalítico para la unión e hidrólisis del ATP y la interacción con sus clientes moleculares (46). Generalmente Hsp90 α se encuentra en forma de homodímeros, sin embargo se ha descrito la formación de heterodímeros, pero es poco frecuente encontrarla en forma de monómeros. Mientras que la isoformas constitutiva Hsp90 β se encuentra en mayor proporción en forma de monómeros también se han encontrado en forma de heterodímeros como se resume en la Tabla 2 (23).

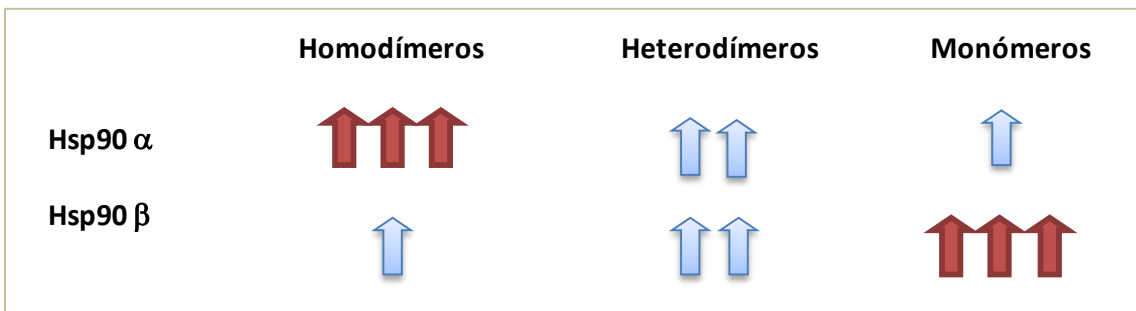


Tabla 2. Abundancia relativa del estado de agregación molecular de Hsp90 α y Hsp90 β en las células eucariontes. Se observa que Hsp90 α se encuentra principalmente en forma de homodímeros y en menor proporción su forma monomérica, mientras que Hsp90 β generalmente se localiza en su forma monomérica y pocas veces se encuentra formando homodímeros.

1.6) Inhibidores Farmacológicos de Hsp90.

Para conocer sobre el papel de estas proteínas se han empleado diversas estrategias, entre ellas se han descrito algunos inhibidores de Hsp90, como la geldanamicina y el radicicol entre otros (23, 25, 48).

El primer inhibidor descrito fue la Geldanamicina que es un antibiótico de la familia de las benzoquinonas que se extrajo del hongo *Streptomyces hygroscopicus* en la década de los setentas. En un principio fue empleado como antibacteriano por sus acciones contra bacterias gram positivas (49). Posteriormente se observó que la administración de este fármaco promovía la reducción de tumores, muchos autores especularon que la geldanamicina inhibía a las proteínas involucradas en procesos neoplásicos como ErbB2, EGF, c-Src, Raf-1 y CdK4. Ensayos de cristalografía de rayos X mostraron de manera clara que la geldanamicina se une con alta afinidad al sitio ATPasa de Hsp90 e inhibe el

complejo multichaperonico propiciando la ubiquitinación y degradación de sus clientes moleculares (50, 51, 52, 53).

En la década de los 90's comenzó el uso de este fármaco como tratamiento en diferentes canceres, sin embargo su uso fue restringido por su baja solubilidad aunada a altos índices de toxicidad observados en el hígado. Por su potencial uso en terapias antineoplásicas se desarrollaron diversos análogos conocidos como 17- alil-amino- geldanamicina y 17-de-metoxi-geldanamicina que presentan menos efectos tóxicos además de ser más solubles (54,55).

Poco se conoce acerca de la farmacología de estos inhibidores, pero se ha descrito que son metabolizados en el hígado por el citocromo P450 CYP3A4 a su metabolito estable 17 amino-geldanamicina que conserva la propiedad de inhibir a Hsp90, pero a este compuesto se le atribuye la hepatotoxicidad (54, 55).

La farmacocinética de estos inhibidores es variable y solo ha sido evaluada en pacientes oncológicos, el tiempo de vida media puede variar desde 90 minutos hasta 3.8 horas con depuración de 19.9 a 25 L/hr/m² y distribución variable de 92 a 106L/m². Por otro lado su metabolito estable el 17- amino geldanamicina ha presentado tiempos de vida media hasta de 9 horas (55).

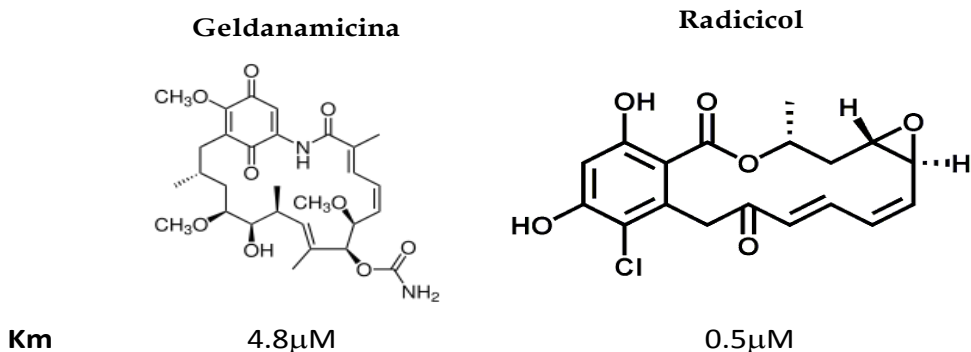


Figura 7. Estructura química de los inhibidores de Hsp90 Geldanamicina y Radicicol. También se muestran las constantes de afinidad con las que se unen a Hsp90. Para determinar las constantes de afinidad, Hsp90 de levadura fue transformada y purificada mediante cromatografía de afinidad en E coli.

Las dosis empleadas en este tipo de pacientes varían desde 10 a 450mg/m²/semana y los tratamientos pueden ser dosis bajas durante 5 días a la semana o una dosis en tres ciclos por semana. Como mencione previamente, la mayoría de estos inhibidores presentan severos efectos secundarios como: náusea, vómito, fatiga, anemia, trombocitopenia y toxicidad hepática (55, 56, 57, 58).

El radicicol es un antibiótico derivado de las ansamicinas que se extrajo del hongo *Monosporium Bonordem* que se une a Hsp90 con mayor afinidad que la geldanamicina e incluso que el propio ATP. Inicialmente se empleó como tranquilizante, sin embargo al igual que la geldanamicina mostró actividad antiproliferativa inhibiendo a diferentes cinasas que regulan la transcripción de oncogenes. La figura 7 muestra la estructura química de ambos inhibidores así como sus constantes de afinidad por Hsp90 las cuales se determinaron con Hsp90 de *Sacharomices cerevisiae* (48).

Este fármaco se ha empleado en diferentes modelos “in vitro” para inhibir las interacciones de Hsp90 en concentraciones del orden de micro y nano molar,

también se ha descrito que la administración de radicicol propicia la expresión de genes de choque térmico por la liberación del factor de transcripción de choque térmico HSF-1. Aunado a ello se le han asociado propiedades anti-angiogénicas en modelos “in vivo” inhibiendo la expresión de VEGF (48).

Al igual que los demás inhibidores la farmacología del radicicol es muy pobre pero en diversos trabajos se ha reportado que posee menor hepatotoxicidad que el resto de los inhibidores de Hsp90, Sin embargo su uso se ha limitado por su baja solubilidad (59, 60).

Hsp90 y sus proteínas cliente.

Se conoce que las Hsp90 participan en un gran número de funciones y esto lo realizan a través de interactuar con más de 100 proteínas cliente. Las interacciones son dependientes de otras proteínas conocidas como co-chaperonas entre ellas se encuentran algunas inmunofilinas y ciclofilinas así como chaperonas de menor peso molecular como Hip, Hop, Hsp40 entre otras. Esta unión estabiliza a Hsp90 facilitando la interacción con sus clientes moleculares (3, 22,44,61,62).

Esta unión a sus proteínas cliente le permite intervenir o mediar diferentes procesos celulares como el ciclo celular, respuesta inmune, estrés celular, apoptosis, cáncer, reestructuración del citoesqueleto, regulación del tono vascular; lo que sin duda hace complejo su estudio (22,44,61,62).

1.7) Hsp90 y su interacción con la sintasa de óxido nítrico endotelial (eNOS)

Una de las interacciones mejor estudiadas de Hsp90 es la que se establece con la sintasa de óxido nítrico endotelial (eNOS). La eNOS cataliza la oxidación del aminoácido L-arginina a óxido nítrico (NO) y L-citrulina.

La conversión de L-arginina a NO se realiza en dos etapas que son catalizadas por 1.5 mol de NADPH (nicotina adenina dinucleótido fosfato) y por dos moléculas de O₂ por mol de NO formado. También se requiere la presencia de otros cofactores y grupos prostéticos como, tetrahidrobioptерина (BH₄), flavina adenina dinucleótido (FAD), flavina mononucleótido (FMN), calcio y la unión de la calmodulina. La primera etapa en la reacción consiste de la mono-oxigenación del grupo guanidino de la L- arginina, en este paso se genera un intermediario estable llamado N^ω-hidroxi-L arginina. En la segunda reacción, un electrón del NADPH y otro del O₂ atacan al grupo guanidino de la N^ω- hidroxi- L arginina incorporando el O₂, lo que facilita la liberación de un átomo de nitrógeno y la formación de L-citrulina, a su vez el átomo de nitrógeno se une a un átomo de la molécula de O₂ para formar el NO, el otro átomo de oxígeno se reduce a agua, ver el detalle de la reacción en la Figura 8 (129).

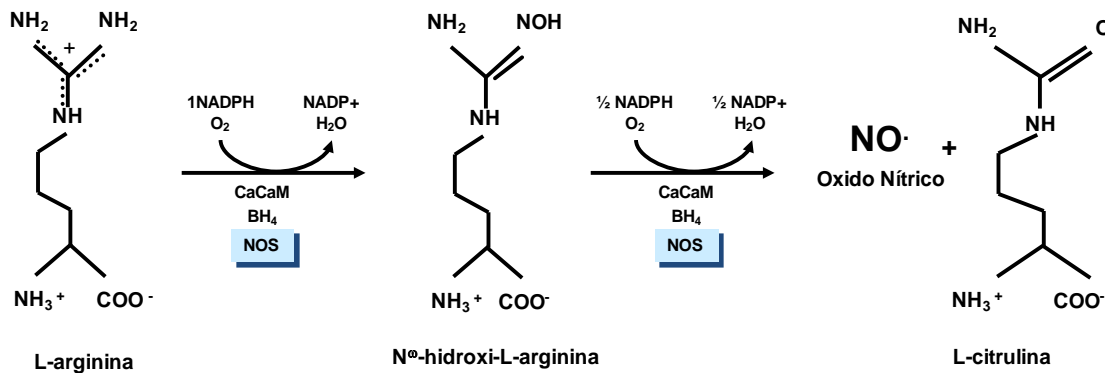
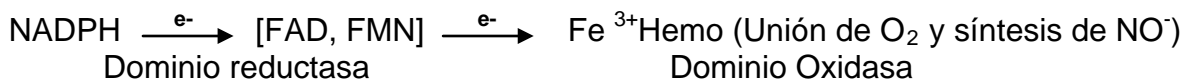


Figura 8. Mecanismo de reacción y estequiometría de la biosíntesis de óxido nítrico (NO) por la sintasa de óxido nítrico endotelial. La reacción se realiza en dos etapas sucesivas de monooxigenación con la presencia de diferentes cofactores como NADPH, FAD, FMN, BH₄, O₂ y Calmodulina (CaCaM). Tomada de Marletta M et-al. Cell, 1994

La estructura cuaternaria de sintasa de óxido nítrico endotelial eNOS, presenta diferentes motivos de unión a otras proteínas. En el centro de la proteína se localiza una región de unión para la calmodulina (CaCaM) flanqueada por el dominio oxidasa y el dominio reductasa. El dominio oxidasa contiene un motivo de unión para el NADPH y un sitio activo tipo citocromo P450 con un grupo hemo activo además de un motivo para la unión de BH₄, mientras que el dominio oxidasa contiene sitios de transferencia de electrones como FAD y FMN. La actividad de eNOS es dependiente de la formación de un homodímeros, la unión de la calmodulina y sus cofactores. La transferencia de electrones se da en forma lineal del dominio reductasa de un monómero al dominio oxidasa de otro monómero, como se detalla a continuación.



El NADPH dona un electrón que se transfiere sucesivamente a los nucleótidos de flavina para ser oxidado finalmente por el grupo hemo del citocromo P450. La oxidación del Fe ²⁺ permite la unión del oxígeno y formación de NO (130).

El óxido nítrico es un gas altamente volátil de vida media de 2 ms, que participa en regulación del tono vascular, evita la agregación plaquetaria y actúa como neurotransmisor entre otras funciones. Al respecto se conoce que la presencia de ligandos como angiotensina II, el incremento en los niveles de calcio intracelular o cambios en la fuerza de rozamiento en los vasos sanguíneos entre otros estímulos puede promover vasoconstricción, en respuesta a esto la célula endotelial es capaz de incrementar la síntesis de NO. Una vez que el NO es producido difunde libremente a la célula de músculo liso uniéndose a la guanilato ciclase soluble GCs. La GCs promueve la conversión de GTP a GMPc que produce tres efectos 1) Inhibe la entrada de calcio a la célula, reduciendo la concentración intracelular de este ión. 2) Activa canales de potasio, los cuales favorecen la hiperpolarización y por ende producen vasorelajación y 3) Activa a la fosfatasa de las cadenas ligeras de miosina, lo que favorece la defosforilación de las cadenas ligeras de miosina produciendo relajación del músculo liso (63, 64, 65, 66, 67).

Mediante ensayos de inmunoprecipitación en células endoteliales de aorta de bovino, se mostró que Hsp90 interactúa directamente con eNOS y esta unión se acompañó de mayor generación de óxido nítrico. Para conocer el papel de Hsp90 en la relajación dependiente del endotelio García Cardeña y Col.; (68) incubaron anillos de aorta preconstriñidos con un inhibidor de Hsp90,

geldanamicina y observaron que reduce la producción de NO dependiente del endotelio, de lo que concluyeron que Hsp90 tiene un papel fundamental en la regulación del tono vascular a través de mediar la producción NO (68).

Alteraciones en la formación del complejo Hsp90- eNOS puede ser de relevancia en procesos patológicos. Estudios previos han postulado que eNOS es regulada pos-transcripcionalmente, tanto por su interacción con otras proteínas (estimuladoras ó inhibitorias) (68, 69, 70,71), como por su estado de fosforilación (72, 73, 74,75). A este respecto, estudios recientes mostraron que eNOS tiene 6 sitios potenciales de fosforilación ubicados en las serinas 116, 617, 635, y 1177, la treonina 497 y recientemente se describió la presencia de un sitio de fosforilación de la tirosina (76, 77, 78). Si la fosforilación ocurre en las serinas 617, 635 y 1177 esto resulta en un aumento en la actividad de eNOS, pues la fosforilación en estos residuos confiere a la enzima que se establezca un adecuado flujo de electrones que se traduce en mayor producción de NO, mientras que la fosforilación de la serina 116 y treonina 497 parece tener un efecto contrario al reducir la función de eNOS y disminuir la síntesis de NO. Sobre la fosforilación en la tirosina 83 hasta ahora solo se especula que al ser fosforilado este residuo favorece la formación de sitios de unión con otras proteínas que podrían incrementar la actividad eNOS (76, 77, 78, 79, 80, 81, 82).

A este respecto Takahashi S y Col.; (83) mostraron “in vitro” que Hsp90 facilita la fosforilación de eNOS. Para lo cual incubaron a eNOS purificada a partir de lisados de células endoteliales y a la proteína cinasa B o Akt, en presencia o ausencia de Hsp90 y observaron que después de 2 minutos de la adición de Hsp90 al medio se incrementaba de manera significativa la fosforilación de la

serina 1177 de eNOS, mientras que la ausencia de Hsp90 en el medio no modificó los niveles basales de fosforilación como se observa en la Figura 9. Estos resultados indicaron que la fosforilación de eNOS está regulada por la presencia de Hsp90.

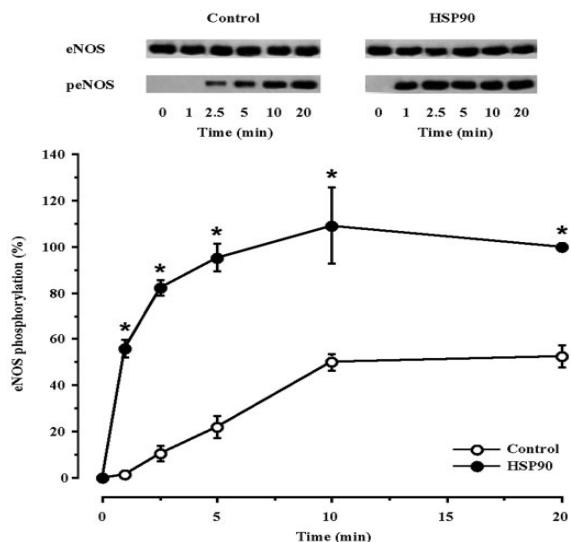


Figura 9. Fosforilación in vitro de eNOS en presencia y ausencia de Hsp90. La grafica muestra que la adición de Hsp90 incrementó significativamente la fosforilación de eNOS desde los 2 min con fosforilación máxima a los 10 min. En el panel superior se muestra un Western blot donde se observa el incremento de la fosforilación de la S1177 de eNOS, sin cambios en la cantidad total de eNOS o Hsp90. *p< vs. control. Tomada de Takahashi S et-al, *J. Biol. Chem.* 2003.

Un estudio posterior realizado en células endoteliales de bovino mostró de manera clara que Hsp90 promueve la actividad de eNOS incrementando la fosforilación del residuo de serina 1177 mediado por la proteína cinasa B o Akt concluyendo así, que el papel de Hsp90 es el de una proteína de andamiaje o adaptadora pues al reclutar a ambas proteínas favorece su proximidad y entonces Akt es capaz de fosforilar a eNOS incrementando así la producción de NO (69,72).

También, se ha propuesto que la fosforilación de la S1177 mejora el flujo de electrones en la enzima e incrementa la afinidad por calmodulina generando mayor producción de NO (71, 83). Por otro lado Pritchard y col.; (84) mostraron en células endoteliales de aorta de bovino (BAECs) que al inhibir a Hsp90 con geldanamicina, hay una reducción importante en la síntesis de óxido nítrico y este

efecto se acompaña con el incremento de la producción de anión superóxido, de esta forma eNOS parece tener un papel dual en la formación de dos radicales con función opuesta: el NO y al anión superóxido. Al respecto se propuso que la formación de radicales libres por eNOS esta directamente regulado por la fosforilación del sitio T495, pues cuando incrementa la fosforilación en este sitio, de la misma forma se eleva la concentración de anión superóxido (76, 84).

Recientemente este mismo grupo diseñó y sintetizó una serie de 12 péptidos señuelos de eNOS de 20 aminoácidos a los que nombraron B1 a B12 como se muestra en la Figura 10A, estos péptidos se diseñaron a partir del aminoácido 291 hasta el 420 de eNOS, porque esta región es en donde Hsp90 se asocia con esta enzima. Estos péptidos fueron incubados con lisados de células endoteliales de bovino y se observó, que de los doce péptidos, solo los péptidos B1 al B3 eran capaces de inhibir la interacción de eNOS y Hsp90 por competencia directa al sitio de interacción de estas proteínas, como se muestra en la Figura 10B. Debido a que el péptido B2 contenía secuencias comunes de B1 y B3, se evaluó la producción de NO empleando el péptido B2, al que además, se le agregó una secuencia que contenía un dominio de transducción de proteínas (PEP1), con el fin de facilitar la captura del péptido por las células. En otro ensayo, se observó que el péptido B2:PEP1 inhibe en forma significativa la producción de NO basal y durante su estimulación con el ionóforo de calcio, como se detalla en la Figura 10C. Para evaluar la significancia molecular de este hallazgo, el péptido B2 fue rediseñado y este vez se le agregó un dominio de transducción de proteínas en el extremo amino al que ahora llamarón TSB2. En la Figura 10D se muestra como la infusión de este péptido en aortas de ratón C57BL/6 aisladas y

perfundidas, aumentó la producción del anión superóxido, y este efecto no se observó cuando eNOS fue inhibida L- -nitro- metil-arginina (L-NAME). Este trabajo muestra que Hsp90 interactúa con eNOS en los aminoácidos 310-323 y que cuando se evita su interacción con esta proteína de choque térmico, hay una reducción en la actividad de esta enzima. Lo que sugiere, que Hsp90 juega un papel preponderante en la síntesis de NO (85,86).

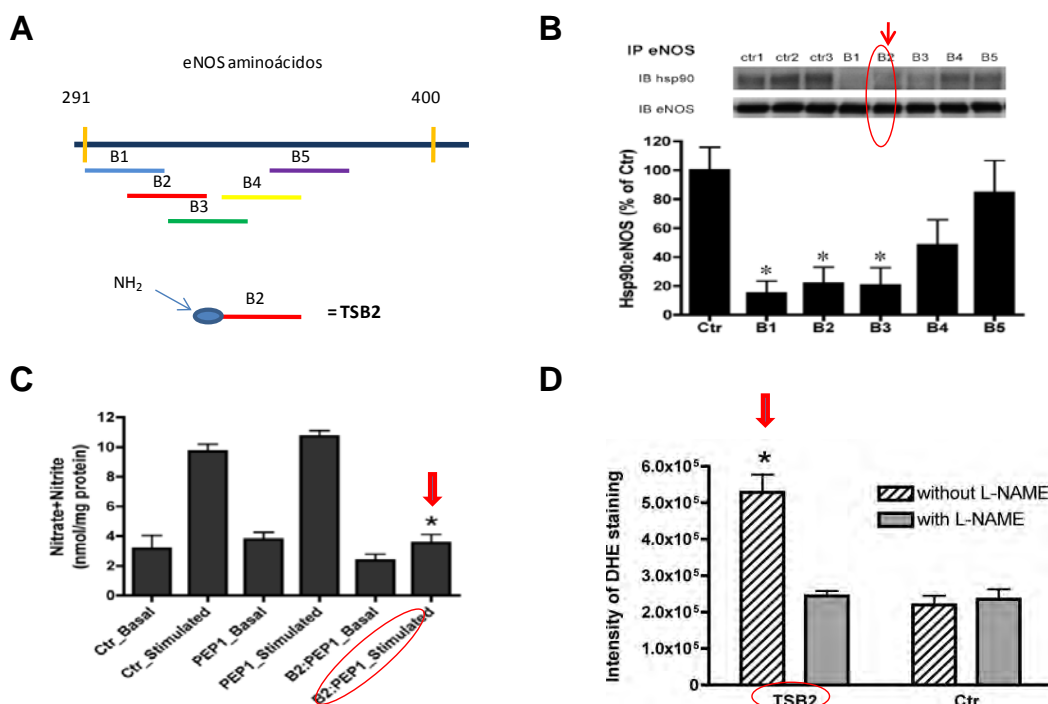


Figura 10. Sítios de interacción de Hsp90 en eNOS. A) Esquema del diseño de los péptidos señuelo. B) Inmunoprecipitación de eNOS-Hsp90 en (BAEC's) que muestra que el péptido B2 inhibe la interacción de Hsp90-eNOS. C) Producción de NO en BAEC's incubadas con el péptido B2 el cual inhibe la producción de Nitratos y nitritos en condiciones basales y en células estimuladas por incremento de la concentración de Ca^{2+} . D) La infusión del péptido TSB2 en aortas aisladas y perfundidas mostró incremento en producción de anión superóxido. *p<0.05 vs. Control. Tomada de Xu H. et-al. *J. Biol. Chem.* 2007.

Otra proteína importante en la vía de señalización del NO es la guanilato ciclase soluble (GCs) que es activada por el NO. La GCs una proteína heterodimérica que pertenece a la familia de las hemo- proteínas, está compuesta

por dos subunidades conocidas como α y β , que se activa por la unión directa del NO catalizando la conversión de GTP a GMPc, generando vasorelajación (88). Venema y Cols.; (87) mostraron en células endoteliales de bovino (BAECs) y aorticas de músculo liso de rata (RASMCs) que al menos una parte de la GCs existe en forma de complejo con Hsp90 y eNOS. Con la ayuda de proteínas de fusión observaron que la subunidad β de la GCs se une al dominio medio de Hsp90, efecto que fue abolido por la adición de geldanamicina concluyendo que Hsp90 podría estabilizar a GCs evitando su degradación, así mismo observaron que ambas proteínas coimmunoprecipitan a eNOS mostrando que Hsp90 es una proteína que permite la interacción de la GCs y eNOS, sugiriendo que la formación del complejo podría facilitar la producción de GMPc por incrementar la actividad de la GCs o por aumentar su capacidad de ser activada por NO (87).

Martine Duval y Cols.; (89) evidenciaron que Hsp90 participa en procesos angiogénicos mediados por la activación del receptor 2 del factor de crecimiento del endotelio vascular (VEGFR2). Ellos mostraron que la cotransfección de eNOS con VEGFR2 en células COS incrementa significativamente la síntesis de NO, y que la cotransfección con dinamina (proteína que inhibe la señalización del receptor facilitando su internalización), fue asociada con reducción de la síntesis de NO. Posteriormente observaron que la dinamina no modificó los niveles de autofosforilación del receptor, pero se observó aumento en la asociación con una proteína altamente fosforilada de aproximadamente 85 KDa, identificada más tarde como Hsp90, por lo que decidieron estudiar el papel de Hsp90 en la señalización del receptor. En cultivos de células endoteliales se observó que la

adicción de VEGF al medio incremento de manera significativa los niveles de fosforilación de Hsp90 β y debido a que la tirosina cinasa c-Src está involucrada en la señalización del VEGF, estos autores observaron que c-Src causa la fosforilación de la tirosina 300 de Hsp90 β y esto se asocio a con el incremento de la síntesis de NO, pues la cotransfección de c-Src con la mutante de Hsp90 β en la Y 300 por F no modificó la producción de NO. Estos resultados muestran de manera clara la participación de Hsp90 β en la regulación de la producción de NO mediados por VEGF (99).

1.8) Localización de Hsp90 en el tejido renal

En 1990 Matsubara y col.; (90) desarrollaron un anticuerpo dirigido hacia Hsp90 de cerebro de bovino y observaron que fue específico para células nerviosas, pero además mostraron que este anticuerpo era capaz de reconocer a Hsp90 en tejidos de otras especies.

Este grupo realizó estudios de inmunohistoquímica e inmunofluorescencia en el tejido renal de rata en condiciones normales y describieron la presencia de Hsp90 en el citoplasma de las células de los túbulos proximales y distales de la corteza renal y este fue uno de los primeros trabajos que mostró la presencia de Hsp90 en el tejido renal.

A pesar de que Hsp90 es muy abundante en la mayoría de las células y regula la función de diversa proteínas, se conoce muy poco de su papel fisiológico en el tejido renal y menos aún del papel específico de cada isoforma. En un estudio de nuestro laboratorio caracterizamos la expresión y localización de

Hsp90 α y Hsp90 β en la corteza y medula renal (91). Encontramos que estas proteínas se expresan en forma muy abundante siendo mayor su expresión en la medula renal con respecto a la corteza Figura. 11.

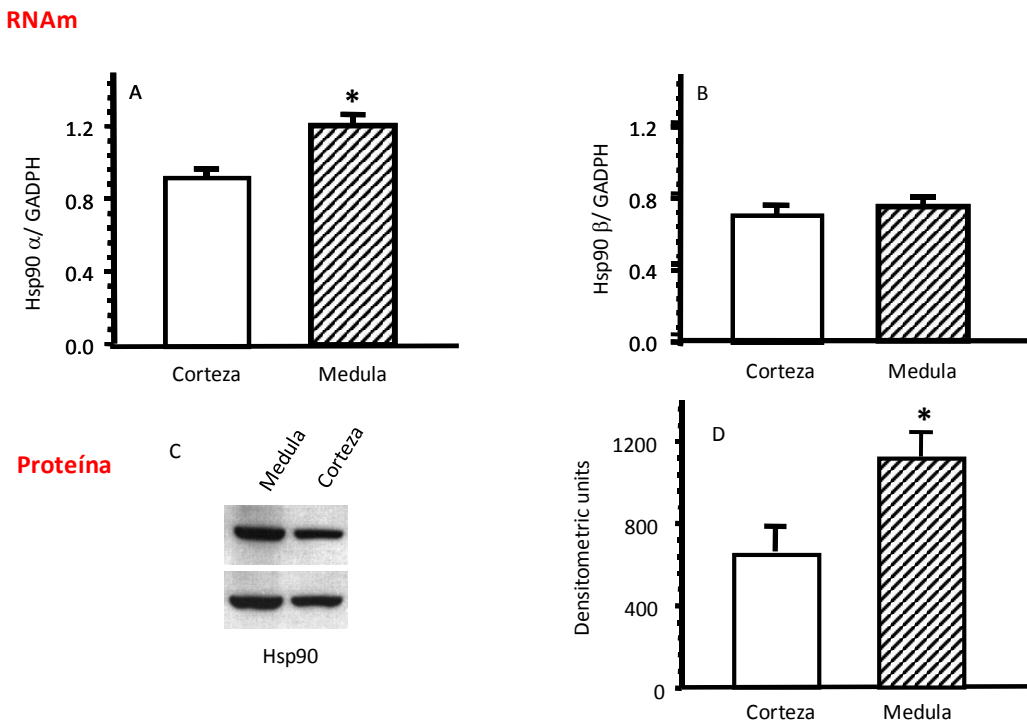


Figura. 11. Expresión de Hsp90 α y Hsp90 β en el tejido renal. A y B) Niveles de RNAm de Hsp90 α y Hsp90 β en la corteza (barras blancas) y medula (barras a rayas) determinados mediante RT-PCR semicuantitativa. C) Análisis de Western blot de Hsp90 realizado en dos mezclas de corteza y medula renal. D) Análisis densitométrico de los niveles proteicos de Hsp90. *p<0.05 Vs. Corteza. Tomado de Ramírez V et-al. *Cell and Stress Chaperones*, 2004.

Mediante inmunohistoquímica también observamos que Hsp90 α y Hsp90 β se localizan en la mayoría de las estructuras renales: capilares glomerulares, células mesangiales y a lo largo del epitelio tubular, pero no observamos diferencias entre la expresión y localización de cada una de sus isoformas como se observa en la Figura 12 (91).

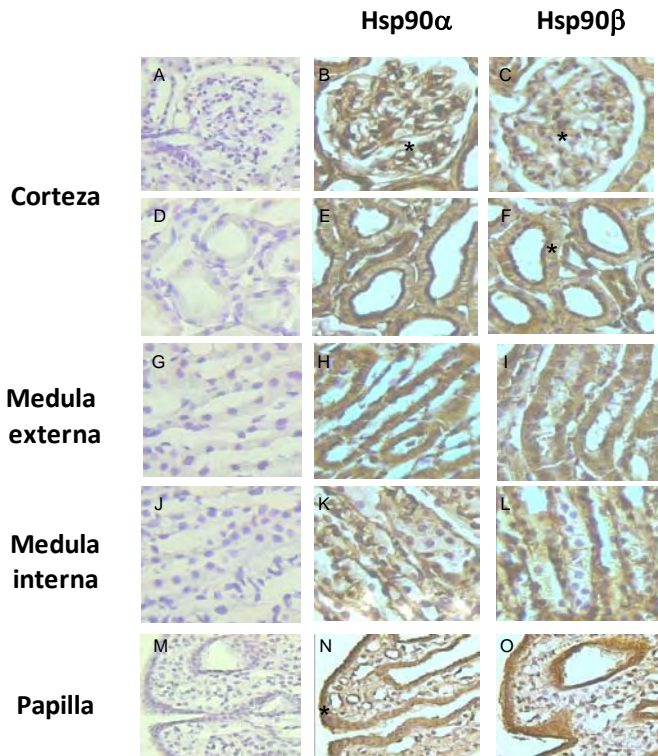


Figura 12. Localización de Hsp90 α y Hsp90 β en el tejido renal. A, D, G, J, y M son tinciones negativas para cada isoforma. B y C muestran inmunotinción en los capilares glomerulares, en las asas capilares (*), células mesangiales (flecha corta). Las flechas grandes muestran la tinción en la cápsula de Bowman. E-F muestran la tinción en el citoplasma de las células tubulares (*) y en el borde en cepillo de las células de los túbulos proximales (flechas). La inmunohistoquímica de la medula externa H-I muestra que Hsp90 α y Hsp90 β se localizan en el citoplasma de las células tubulares, en contraste en la medula interna la localización fue en la membrana basolateral K-L (flechas). Finalmente la pelvis renal mostró una intensa tinción en la punta de la papila (*) en los túbulos colectores medulares (flechas), en la células de la matriz extracelular y células intersticiales Ampliación 200X. Tomado de Ramírez V et-al. *Cell and Stress Chaperones*, 2004.

1.9) Hsp90 en la reabsorción renal de sodio y en la regulación osmótica

La función renal de Hsp90 más conocida hasta el momento es su unión y estabilización por aumento de la afinidad por aldosterona hacia los receptores mineralocorticoides, en donde además actúan Hsp70, Hip (p48), Hop (p56) y Hsp40 formando un complejo con Hsp90. La aldosterona es una hormona mineralocorticoide, que es secretada por las células de la zona glomerulosa en las glándulas suprarrenales. Es uno de los mayores reguladores de la concentración de Na⁺ en el organismo, pues está encargada de la reabsorción de sodio y secreción de potasio en el riñón. La aldosterona difunde libremente a través de la membrana y se une a sus receptores intracelulares localizados en los túbulos

dístales y colectores favoreciendo la transcripción de genes que codifican proteínas transportadoras de sodio como: el cotransportador de sodio/ cloro NCC, el canal epitelial de sodio ENAC y la bomba de sodio potasio ATP/asa, y el canal de potasio ROMK. Una vez que la hormona se une a su receptor, la Hsp90 y las co-chaperonas ayudan a translocar el complejo hormona-receptor al núcleo donde es liberado para activar la transcripción de genes lo cual potencia la reabsorción de Na^+ y agua en las células epiteliales renales del túbulo distal y colector (92-94). Hay evidencia que muestra que el complejo Hsp90 y co-chaperonas puede activar la transcripción de otros genes, como el de la calcineurina. (95, 96).

Ortiz y col., (97, 98) mostraron en asas de Henle perfundidas y aisladas que el NO producido por eNOS resulta en una reducción de la reabsorción de Na^+ y Cl^- por la inhibición del cotransportador de $\text{Na}^+ \text{K}^+ 2\text{Cl}^-$ (CSB). Es importante recordar que en este segmento de la nefrona se reabsorbe del 20 al 25% de sodio filtrado y además es impermeable al agua, lo que mantiene una adecuada tonicidad en la medula renal, por lo que cambios mínimos en el fluido tubular se verán reflejados en la excreción y reabsorción de sodio. En otro estudio realizado por el mismo grupo en las mismas condiciones, observaron que un aumento en el fluido luminal en el asa de Henle produce un aumento significativo de la actividad de eNOS conduciendo a una mayor liberación de NO y favoreciendo la migración de eNOS desde el citoplasma y la membrana basolateral, hacia la membrana apical, además mostraron que esta migración siempre está acompañada por Hsp90. También observaron que cuando no hay flujo luminal el patrón de localización de ambas proteínas es difuso en toda la célula. Por otro lado, debido a la interacción entre Hsp90 y eNOS incubaron las asas de Henle con geldanamicina, un inhibidor

específico de Hsp90, y no observaron translocación de Hsp90-eNOS. Esto sugiere que Hsp90 es necesaria para la translocación de eNOS y que la interacción de estas proteínas podría regular la reabsorción de sodio en el asa de Henle (99).

Se ha implicado la participación de diferentes chaperonas incluyendo a la Hsp90 en la regulación de la tonicidad renal. En células embrionarias de riñón humano HEK293, se describió la asociación de Hsp90 α y Hsp90 β con el factor de transcripción (TonEBP) proteína de unión que potencia la respuesta a tonicidad (100). Normalmente TonEBP/NFAT5 se encuentra en el citoplasma, una vez activado es translocado al núcleo donde se encarga de regular la transcripción de diversos genes como la aldosa reductasa, el cotransportador de sodio mio-inositol y el transportador de sodio-betaína entre otros (101,102). Estas proteínas son osmolitos orgánicos que conservan la viabilidad celular durante el aumento de la tonicidad.

En este trabajo observaron que Hsp90 forma parte del complejo que forman TonEBP y sus elementos de respuesta (TonEBP/OREBP) en condiciones isoosmóticas e hiperosmóticas. También determinaron la actividad de TonEBP en presencia o durante la inhibición de Hsp90 con geldanamicina. Como era de esperarse la hipertonicidad (500mosm/Kg) incrementa de manera significativa la actividad transcripcional de TonEPB, sin embargo la adición de geldanamicina abate la actividad transcripcional de TonEBP en un 30% a 300mosm/Kg y un 66% a 5000mosm/Kg. Estos resultados sugieren que Hsp90 tiene un papel fundamental en la regulación de moléculas que regulan la tonicidad en el tejido renal, facilitando la migración de TonEBP del citoplasma al núcleo (103).

1.10) Hsp90 en condiciones fisiopatológicas renales

En cuanto a condiciones fisiopatológicas se ha encontrado que la intoxicación con metales pesados como mercurio, zinc, cobalto, fierro y arsénico, producen aumento de la expresión de Hsp90 en el tejido renal.

Fukuda y col.; (9) administraron intraperitonealmente nitrilotriacetato férrico (Fe-NTA) en ratones produciendo daño oxidante e incremento la incidencia de adenocarcinoma renal. Estos autores observaron que una sola dosis de Fe-NTA es capaz de incrementar de manera significativa la expresión de Hsp90 en células tubulares renales y que si se prolonga su administración por varios días, de igual forma permanece la sobreexpresión de Hsp90 en el tejido renal, por lo que concluyeron que la presencia de Hsp90 podría conferir resistencia hacia el daño oxidante.

Somji y col., (104) analizaron el efecto del cloruro de cadmio CdCl_2 y arsenito de sodio NaAsO_2 en cultivos primarios de células de túbulo proximal humanas, las cuales fueron aisladas de biopsias de pacientes que padecían carcinoma renal. Estas células fueron incubadas con diferentes dosis de CdCl_2 y no observaron cambios en la expresión de ambas isoformas, sin embargo cuando las células fueron expuestas a arsenito de sodio o a mayor temperatura hasta 42.5°C, observaron un aumento significativo en la expresión de Hsp90 α y Hsp90 β , tanto en los niveles de RNAm como en la proteína.

Otro modelo en el cual se ha estudiado la expresión de Hsp90 es durante la administración de fármacos nefrotóxicos. Se ha demostrado que la

administración gentamicina en la rata durante 14 días, produce aumento en la concentración de creatinina y urea plasmática, además de propiciar aumento en la expresión de Hsp90 en el segmento S3 del túbulo proximal. Esto fue comprobado mediante análisis de inmunohistoquímica, de microscopia de luz y electrónica, donde se observó que hay acumulación de Hsp90 en los lisosomas de las células epiteliales del túbulo proximal después de 36 horas de la administración de la gentamicina. Así mismo se evaluó la presencia de Hsp90 durante 21 días y se comprobó que hay una expresión máxima a los 12 días post administración y esta tiende a disminuir durante el periodo de recuperación (105).

El cis-platino actualmente es utilizado en la práctica clínica como un medio de contraste (106). A pesar de ser útil se sabe que este fármaco es altamente tóxico ya que se ha reportado en ratas que una dosis única de 5 mg/Kg produce insuficiencia renal aguda. También se ha caracterizado que este fármaco produce cambios morfológicos de la arquitectura renal, como dilatación del segmento S3 del túbulo proximal. En este trabajo se demostró la inducción de Hsp90 en el asa de Henle y en la membrana apical del túbulo proximal después de 24 horas de la administración de cis-platino. Así mismo se comprobó la presencia de Hsp90 en el día 5 y 7 posterior a la administración en las células que se regeneran.

Morita y col., mostraron en ratas sometidas a isquemia renal unilateral por 60 min, produjo un abrupto incremento en la expresión de Hsp73 y Hsp90 después de 3 y 12 horas de reperfusión, estas proteínas fueron localizadas en el túbulo proximal y en células de asa de Henle. Aunado a esto, observaron la presencia Hsp90 después de 3, 7 y 28 días de reperfusión y comprobaron que esta persiste

en las regiones de regeneración celular. Estos autores proponen que además de que Hsp90 se expresa de manera constitutiva esta puede inducirse cuando hay daño tubular en etapas degenerativas y regenerativas lo que le confiere un papel protector en ambos casos.

Poco se conoce del papel de Hsp90 en condiciones fisiopatológicas, en humanos se ha reportado un caso único, en el cual un paciente padecía insuficiencia renal aguda con oliguria aunado a una severa hipertensión. A este sujeto se le tomó una biopsia renal, a partir de la cual se realizaron estudios de histológicos e inmunohistoquímica que revelaron la sobreexpresión de Hsp90 en el citoplasma de las células del segmento S3 del túbulo proximal en una etapa de recuperación y regeneración tubular (107).

Hipótesis Objetivos

1) Hipótesis

- Si Hsp90 desempeña un papel importante en la regulación de la función renal; entonces la inhibición de su actividad ATPasa con radicicol nos permitirá evaluar su participación en el mantenimiento del flujo sanguíneo renal y de la filtración glomerular.
- Si la formación del complejo Hsp90-eNOS regula el tono de la vasculatura renal; entonces la administración de radicicol producirá cambios en la producción de óxido nítrico.

2) Objetivos.

- I. Estudiar el efecto de la administración de radicicol sobre la filtración glomerular y el flujo plasmático renal.
- II. Estudiar el efecto de la disociación del complejo eNOS-Hsp90 sobre la fosforilación de eNOS en el tejido renal.

Métodos

4) Métodos

4.1) Inclusión de animales.

Se incluyeron 20 ratas Wistar macho de 300-320g de peso que fueron divididas aleatoriamente en dos grupos: el grupo control y el grupo en el que se inhibió a Hsp90. Los experimentos se realizaron en condiciones basales y durante la infusión (administración endovenosa) de vehículo o de radicicol el inhibidor de Hsp90.

4.2) Cirugía.

Previo al experimento los animales se anestesiaron con pentobarbital sódico intraperitonealmente a una dosis de 30mg/kg de peso posteriormente se colocaron en una mesa termoregulada colocándoles una sonda rectal para mantener la temperatura corporal a 37°C. Se cateterizó la tráquea con un tubo de polietileno PE-240 y con tubo de polietileno PE-50 las venas yugulares y las arterias femorales. Por una de las venas yugulares se infundió el plasma y según el caso el vehículo o el radicicol y la otra vena se utilizó para reponer la sangre que se tomó por una de las arterias femorales. La otra arteria cateterizada se utilizó para registrar la tensión arterial media (TAM) en un polígrafo Grass durante todo el experimento. También se cateterizó la vejiga con tubo de polietileno PE-90 para colectar muestras de orina durante el periodo basal y el experimental. Una vez cateterizado, al animal se le realizó una incisión media en el abdomen y se disecó la arteria renal izquierda para colocar una sonda de ultrasonido

previamente lubricada con gel (Flujoméetro Transonic System 1RB) y registrar el flujo sanguíneo renal (FSR) en forma continua.

Las ratas se mantuvieron en condiciones de euvolemia mediante la infusión de plasma (10 ml/kg) obtenido de una rata donadora. Todos los experimentos se realizaron en dos etapas, la primera de ellas consistió en la infusión de un marcador de la filtración glomerular azúcar baja en calorías (azúcar BC) al 5% (108) después de 30 min de iniciada la infusión se tomó una muestra de sangre y se inició la primera recolección de orina durante 30 a 45 min y al finalizar se tomó de nuevo una muestra de sangre de la arteria femoral reponiendo en cada toma, el mismo volumen con sangre de una rata donadora por la vena yugular. En la segunda etapa, además de infundir el azúcar BC, se infundió el vehículo (dimetil sulfoxido DMSO 20%) o el radicicol (25 μ g/0.1ml/h en DMSO) (109) nuevamente después de 30 min. de equilibrio empezó la recolección de orina de la vejiga por otros 30 a 45 min y al inicio y al final de la recolección se tomó una muestra de sangre de la arteria femoral reponiendo el mismo volumen con sangre de una rata donadora por la vena yugular. La concentración de azúcar BC en plasma y orina se determinó por el método de Davidson (110).:

Al finalizar el experimento, los animales fueron sacrificados se extrajeron ambos riñones y fueron separados macroscópicamente en corteza y medula renal. Los tejidos se congelaron a -80°C y se almacenaron para su posterior uso en estudios bioquímicos y moleculares como se detallara adelante.

Con el fin de corroborar nuestros resultados usando al azúcar BC como marcador de la filtración glomerular se incluyó un grupo de seis animales a los que en lugar de infundir azúcar BC como marcador de la filtración glomerular se les infundió el estándar de oro INUTEST® en una solución al 5%, el experimento se realizó de la misma forma descrita previamente en presencia y ausencia del inhibidor de Hsp90.

4.3) Estudios Bioquímicos

4.3.1) Determinación de la filtración glomerular.

Estos valores se determinan empleando el método de Davidson (110). Este método se basa en la hidrólisis acida de monosacáridos (hexosas y aldopentosas). La presencia del ácido favorece la ruptura de los enlaces glucosídicos y al reaccionar con la antrona los monosacáridos de oxidan tomando una coloración azul-verdosa. Para determinar su concentración se empleo una curva estándar de azúcar BC con concentraciones de 20 μ g/ml hasta 100 μ g/ml.

En un matraz se preparo la antrona (0.08mg/100ml), se colocaron 100ml de ácido sulfúrico concentrado y 26 ml de agua destilada hasta que estuvieran fríos, posteriormente se le agrego 100mg de antrona y se agito suavemente hasta que se disolvió. (Todo debe permanecer en hielo y protegido de la luz ya que es una reacción fotosensible)

Para determinar la concentración en plasma es necesario eliminar primero las proteínas del plasma, para ello se realiza un ensayo de precipitación empleando ácido tricloroacético 1N en la siguiente proporción.

125 μ l de TCA 1N

250 μ l de agua destilada

25 μ l de plasma problema

Se centrifugan por 10 min a 14000g y se emplea el sobrenadante.

El ensayo consiste en colocar 100 μ l de la curva estándar o del problema en un tubo limpio, enseguida congelar las muestras. Una vez que la antrona se ha disuelto en el ácido sulfúrico tenga una coloración amarillo canario, se adicionan

500 μ l a cada una de las muestras previamente congeladas, agitar vigorosamente e incubar a 42°C durante 50 minutos. Al finalizar este tiempo agitar vigorosamente y leer las muestras a una longitud de onda de 620nm. La concentración se determina con la curva estándar.

La filtración glomerular se cálculo de la siguiente forma.

$$FG = \frac{[Concentración\ de\ azúcar\ BC\ en\ orina]}{[Flujo]}$$
$$[Concentración\ de\ azúcar\ BC\ en\ orina]$$

Flujo= Volumen de orina/ Tiempo de recolección.

Nota: Para determinar la concentración de azúcar BC en plasma y orina se realizaron las diluciones apropiadas.

4.3.2) Excreción urinaria de nitritos y nitratos

Para determinar la concentración de nitritos y nitratos urinarios se empleó el estuche comercial nitric oxide de R & D, de acuerdo a las instrucciones del fabricante. Este ensayo determina los metabolitos estables del óxido nítrico presentes en las muestras, por conversión de nitratos a nitritos mediante la acción de la enzima nitrato reductasa. Este es un método colorimétrico basado en la reacción de Griess que produce la diazotización de los nitritos que reaccionan con el ácido sulfanilico produciendo un ion diazonio que se lee a una absorción máxima de 540nm.

4.3.3) Lipoperoxidación.

Se determinaron los niveles de lipoperoxidación como medida de los niveles de malondialdehido (MDA) en el tejido renal, mediante la técnica de especies reactivas al ácido tiobarbitúrico (TBARS).

Se homogenizaron 100 mg de corteza y medula renal en 1 ml de agua destilada, después de la homogenización el ensayo consistió en incubar 150 µl de homogenizado y agregar 350µl de una solución al 0.8% de ácido tiobarbitúrico en ácido tricloroacético al 15%, posteriormente las muestras fueron calentadas a 95°C por 45 minutos y al finalizar las muestra se centrifugaron a 3000g por 15 min. El sobrenadante fue leído en un espectrofotómetro a una longitud de onda de 532nm. Se determinó la concentración de TBARS utilizando su coeficiente de extinción molar de $1.56 \times 105 \text{ M}^{-1}\text{Cm}^{-1}$ y se expresaron como nmol de TBARS por mg de proteína. Los niveles de proteína de cada homogenizado se determinaron por el método de Bradford.

4.3.4) Peróxido de hidrógeno urinario.

Los niveles de peróxido de hidrógeno se determinan como una medida indirecta de la producción de anión superóxido como consecuencia del aumento en el estrés oxidativo.

Para corroborar que la administración de radicicol no produjo cambios en los niveles de anión superóxido, se determinó la concentración de peróxido de hidrógeno en orina en los animales infundidos con vehículo y radicicol durante

ambos periodos de estudio empleando el estuche comercial Amplex® Red Hydrogen Peroxide/Peroxidase Assay Kit (invitrogen) de acuerdo a las instrucciones del fabricante. Este es un método colorimétrico de un paso, empleando el 10-acetil-3,7-dihidroxifenoxyizano que reacciona con el peróxido de hidrógeno presente en las muestras produciendo resurfina de color rojo que tiene absorción máxima a 560nm.

El ensayo se realizo empleando una curva estándar de peróxido de hidrógeno de 1 a 10 μ M. Las muestras fueron diluidas en buffer de trabajo 1X. Se colocaron 50 μ L de cada estándar o muestra en una placa de ELISA posteriormente se les agrego 50 μ l de la solución de rojo de Amplex/HRP conjugado y las muestras se incubaron durante 30 minutos protegidas de la luz. Posteriormente la placa fue leída a 560nm y la concentración de H_2O_2 fue determinada por interpolación de la curva patrón. Los resultados se expresaron como nmol/ml de H_2O_2 .

4.3.5) Niveles de isoprostanos $F_{2\alpha}$ urinarios.

Los Isoprostanos son similares a las prostaglandinas, pero estos se producen por la lipoperoxidación de las proteínas de membrana y esta acción es inducida por la presencia de los radicales libres específicamente anión superóxido.

Por lo que para verificar si la infusión de radicicol modificaba la concentración de Isoprostanos $F_{2\alpha}$ (8-iso-PGF $_{2\alpha}$) estos fueron determinados en las orinas de ambos grupos de estudio mediante un ensayo de ELISA empleando el estuche comercial 8-iso-PGF $_{2\alpha}$ Elisa assay (Northwest. Vancouver. WA 98662)

siguiendo las instrucciones del fabricante. Se empleo una curva estándar de 8-iso PGF_{2α} de 0.01 a 100ng/ml

En una micro placa de Elisa en la cual se encontraba adherido un anticuerpo monoclonal hacia 8-iso-PGF_{2α} se colocaron 100μl de los estándares y muestras a las que se les adiciono 100ml de 8-iso PGF_{2α}/HRP conjugado y se incubaron durante 2 horas a temperatura ambiente. Después de 2 horas se realizaron tres lavados con buffer de trabajo 1X y se les adiciono 200μl del sustrato TMB (3,3', 5,5"-tetra-metil-benzidina) y se nuevamente se incubaron durante otros 40 min hasta el desarrollo de una coloración azul. La reacción fue detenida por adición de 50μl de H₂SO₄ 3M desarrollando una coloración amarilla. La placa se leyó a 450 nm. La concentración de isoprosanos se reporto como ng/ml de isoprostanos F_{2α}.

4.4) Estudios Moleculares

Se extrajeron ambos riñones y se separaron macroscópicamente en corteza y médula renal y se congelaron en nitrógeno líquido y se almacenaron a -80°C hasta su procesamiento.

4.4.1) Extracción de RNA total.

Se extrajo el RNA total de la corteza y medula renal por homogeneización en TRIZOL siguiendo las instrucciones del fabricante. Una vez aislado el RNA, se determinó la pureza, y concentración, mediante espectrofotometría y mediante un gel de agarosa al 1% se confirmó la integridad del mismo.

4.4.2) Trascipción reversa

La transcripción reversa se llevó a cabo a partir de 1 μ g de RNA total de corteza o médula tratadas previamente con DNAAasa. El RNA se ajustó a un volumen de 11 μ l con agua grado biología molecular y se sometió a 65° C durante 10 minutos para desnaturarizar la molécula de RNA. Se agregaron 9 μ l de una mezcla que contenía 200U unidades de transcriptasa reversa (MMLV Invitrogen), 100 pmol de hexámeros, 0.5 mM de cada nucleótido (dNTP) y 1x de buffer RT. La reacción se incubó a 37°C durante 1 hora y al finalizar se expuso a 95°C por 5 minutos para desnaturarizar la enzima y la reacción se llevó a un volumen final de 40 μ l (91,111).

4.4.3) RT-PCR en tiempo real:

Los niveles de RNAm de Hsp90 α , Hsp90 β y la sintasa de óxido nítrico endotelial eNOS, de la subunidad 18s del RNAr como gen control, se determinaron mediante RT-PCR en tiempo real, empleando los iniciadores específicos marcados con los fluoróforos FAM y VIC de Applied Biosystems. Para Hsp90 α de rata se utilizó el estuche comercial Rn00822023-g1, para Hsp90 β el ensayo número HSP90BRAT-X, para eNOS el ensayo número Rn02132634-s1.

Para corregir las variaciones de concentración de DNA o de la eficiencia de amplificación en cada reacción empleamos la subunidad 18S del RNAr como control endógeno. La cuantificación de la expresión de cada gen fue hecha empleando el método del umbral del ciclo (CT). (111,112). Para cuantificar la expresión de cada gen amplificado por PCR en tiempo real es necesario estimar la concentración de DNA presente en las muestras mediante la detección y cuantificación de la fluorescencia emitida en la fase exponencial de la curva de amplificación, esta fluorescencia es corregida por la concentración basal del trazador fluorescente y el fondo de las muestras.

El CT es una medida arbitraria, este debe ser fijado en la fase exponencial y deberá estar significativamente por arriba de la línea basal. Esta medida representa el número de ciclos en que el producto de PCR alcanza el umbral establecido. Sin embargo si este número es menor a 7 o mayor de 40 ciclos no deberá incluirse pues podría generar resultados erróneos. Una vez obtenido el CT se emplea un modelo matemático para cuantificar la expresión de ambos genes, este método se conoce como $2^{-(\Delta)(\Delta)ct}$.

Este valor se normaliza con respecto a un gen control restando el CT del gen problema menos el gen control, este valor se potencia en base dos, el valor matemático representa la expresión del gen en comparación con el gen control.(113)

4.4.4) Análisis de Western Blot:

Las proteínas fueron extraídas por homogenización de 100mg de corteza renal en 1 ml de buffer de lisis (50mM HEPES pH 7.4, 250mM NaCl, 5 mM EDTA, 0.1% NP-40 e inhibidor de proteasas Complete (Roche)) los homogenizados se centrifugaron a 4000 g por 8 min, se retiraron los restos celulares y se determinó la concentración de proteínas por el método de Lowry. Se corrieron de 20 – 50 µg proteínas en buffer de carga (6% SDS, 15% glicerol, 150 mM Tris, 3% azul de bromofenol, 2% - β-mercaptoetanol, pH 7.6).en un gel SDS- PAGE al 7.5% y se transfirieron a una membrana PVDF. Como control positivo de Hsp90α se cargaron 20µg de proteínas de células embrionarias de riñón humano HEK293 transfectadas con Hsp90α de rata, mientras que para eNOS se cargaron 0.6µg de eNOS recombinante de bovino (Abcam. Cambridge, MA).

Las membranas se incubaron durante 60 min a temperatura ambiente en agente bloqueante (BIO-RAD) al 0.4%,se lavaron durante 20 minutos en buffer tris salino (TBS-t 199mM TRIS, 1.36 M NaCl, 0.1% de Tween 20 pH 7.6), después las membranas se cortaron en dos partes, la parte inferior se incubó con el anticuerpo primario cabra anti- β- actina como proteína control (Santa Cruz Biotechnology) a una dilución de 1:5000 en solución de anticuerpo al 0.1% a 4°C durante toda la

noche, la parte superior se incubó con diferentes anticuerpos según el caso. Para Hsp90 α y Hsp90 β se incubó con los anticuerpos policlonales, de conejo anti-Hsp90 α y conejo anti- Hsp90 β (Abcam) a una dilución 1:5000 durante toda la noche a 4°C. En el caso de eNOS, eNOS S1177, eNOS T495, las membranas fueron bloquedas durante 60 min en agente bloqueante al 5% y dos lavados posteriores E incubadas según el caso con los anticuerpos policlonales anti-eNOS de conejo, ó anti- fosfo eNOS S1177 de conejo, o bien anti- eNOS T495 (Cell Signaling) de conejo, 1: 500 en albúmina sérica de bovino al 5%, durante toda la noche a 4°C. Al siguiente día, las membranas se lavaron en TBS-t por 30 min y se incubaron con el anticuerpo secundario por 60 min a temperatura ambiente. Para β -actina se empleo el anticuerpo conjugado HRP burro anti cabra (Santa Cruz Biotechnology) 1:10000, para Hsp90 α y Hsp90 β utilizamos el anticuerpo conjugado HRP- anti conejo a una dilución 1:10000 (Alpha Diagnostics) y finalmente para eNOS, fosfo eNOS S1177 y T495 se incubarón con el anticuerpo secundario HRP-anti-rabbit (Alpha Diagnostics) a una dilución 1:2500. Al finalizar las membranas fueron lavadas nuevamente por otros 60 min en TBS-t. Las proteínas□ fueron detectadas mediante un ensayo de quimioluminiscencia por autorradiografía de las bandas y se cuantificaron por análisis densitométrico (ECL PLUS, Amersham).

Para el ensayo de dimerización de eNOS se extrajeron proteínas totales de seis diferentes cortezas de cada grupo por homogenización en buffer de lisis (50mM TRIS-HCl pH 8.0, 0.1% Nonidet p-40, 180mM NaCl, 0.5mM EDTA e inhibidor de proteasas Complete). Los homogenizados se centrifugaron a 4000g

por 8 minutos a 4°C, se retiraron los restos celulares se le determinó la concentración de proteínas en el sobrenadante por el método de Lowry. Se colocaron 50μg de proteínas no desnaturalizadas en buffer de carga (6% SDS, 15% glicerol, 150 mM Tris, 3% azul de bromofenol, 2% β -mercaptoetanol, pH 7.6) y se separaron en un gel SDS-PAGE al 6% a 4°C (114, 115). Las proteínas se transfirieron a una membrana PVDF y el ensayo de western blot para eNOS se realizó como se describió previamente.

Resultados

5) Resultados.

Para conocer el papel de Hsp90 sobre la función renal y el flujo sanguíneo renal (FSR), incluimos 20 ratas que se dividieron en 2 grupos, 10 ratas recibieron de DMSO y alcohol etílico como vehículo y el resto se les infundió radicicol. Los animales se prepararon de acuerdo a lo descrito en los métodos. Durante todo el experimento se registró la tensión arterial media (TAM) y mediante una sonda de ultrasonido se monitoreó el FSR. Con el fin de determinar la función renal de estos animales durante todo el experimento se mantuvo una infusión de azúcar BC al 5% como marcador de la filtración glomerular (118).

Cada experimento consistió de dos etapas la primera se le denominó periodo basal o control y en la segunda etapa los animales recibieron una infusión de vehículo o radicicol durante 60 min más.

En la Figura 13 se muestran los valores de tensión arterial media (TAM),

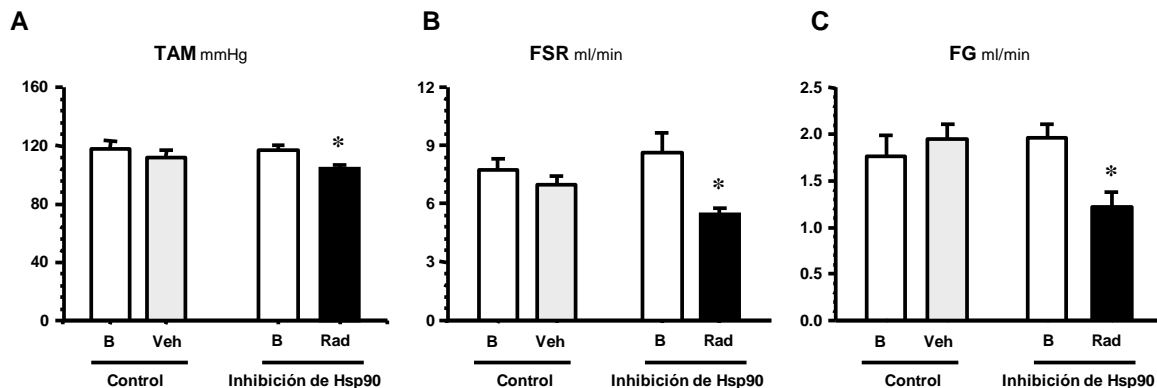


Figura. 13. Parámetros fisiológicos durante la inhibición de Hsp90. A) Tensión arterial media (TAM). B) Flujo sanguíneo renal (FSR). C) Filtración glomerular (FG) determinada por la infusión de azúcar BC. Basal barras blancas (B), Infusión de Vehículo barras grises (Veh) e infusión de radicicol barras negras(Rad). * $p \leq 0.05$ vs. B.

el FSR y la filtración glomerular (FG). En el grupo control, la infusión de vehículo produjo una ligera reducción no significativa de la TAM (123.4 ± 3.1 vs 115.9 ± 3.3 mmHg) y en el grupo que recibió radicicol se observó un efecto similar, que en

este caso alcanzó significancia estadística (117.5 ± 3.2 vs 103.2 ± 2.1 mmHg). el flujo sanguíneo renal no se modificó durante la infusión del vehículo (7.5 ± 0.6 vs. 6.9 ± 0.4 ml/min) mientras que, la infusión de radicicol produjo un descenso significativo del FSR con respecto a su periodo control (5.2 ± 0.3 vs. 8.36 ± 0.8 ml/min).

Como se puede apreciar en la figura 13C la infusión de vehículo no modifico la filtración glomerular en el grupo. En cambio la inhibición de Hsp90 con radicicol indujo una reducción significativa de la FG de un 32 % con respecto al su periodo basal (B 2.0 ± 0.02 vs Rad 1.2 ± 0.02 ml/min). Estos resultados sugieren que la infusión de radicicol produjo una caída de la función renal a través de inducir vasoconstricción renal, efecto que puede ser mediado por una reducción de factores vasodilatadores (como óxido nítrico o prostaglandinas) o bien por un aumento de los factores vasoconstrictores (como endotelina ó angiotensina).

Previamente mostramos el azúcar baja en calorías (BCS) es un marcador adecuado de la función renal, sin embargo para corroborar que los efectos mostrados anteriormente sean ocasionados por la inhibición de Hsp90, Incluimos un grupo de 6 ratas a las que les infundimos un marcado preciso empleado para medir la filtración glomerular INUTEST® en presencia o ausencia de radicicol. Como esperábamos, la inhibición de Hsp90 produjo una ligera caída de la TAM con respecto a su periodo basal Figura 14A. También comprobamos que la infusión de radicicol reduce el FSR (B 8.7 ± 0.5 vs. Rad 5.6 ± 0.3 ml/min) y la FG (B 1.9 ± 0.5 vs. Rad 1.3 ± 0.4 ml/min), niveles similares a los observados con el azúcar BC como se observa en la Figura. 14B. y 14C.

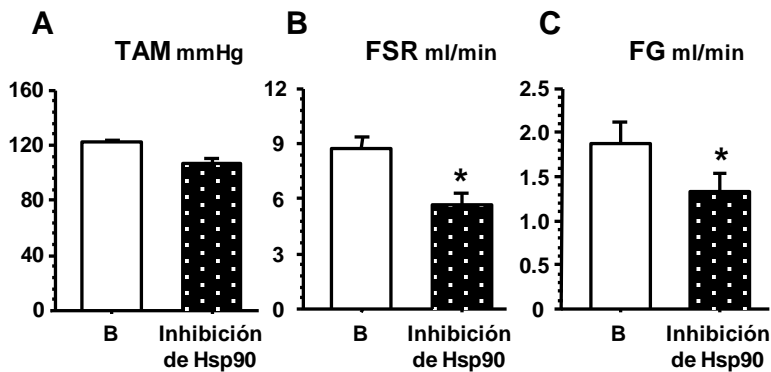


Figura 14. Efecto de la inhibición de Hsp90 sobre la función renal empleando INUTEST® como marcador de la filtración glomerular. A) TAM. B) FSR y C) FG . $p \leq 0.05$ vs. B.

De acuerdo con datos publicados por otros grupos se conoce que Hsp90 regula a su propio factor de transcripción HSF 1, y se ha mostrado que el radicicol o la geldanamicina propicia el desplazamiento de ese factor el cual es translocado al núcleo donde inicia la transcripción de genes de choque térmico incluyendo a Hsp90. Por lo que decidimos evaluar la expresión de Hsp90 en la corteza renal. Para ello se extrajo RNA total de las cortezas renales de los animales de ambos grupos.

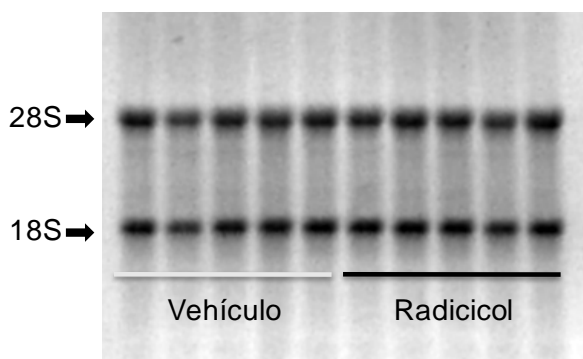


Figura 15. Foto representativa del RNA total extraído de las cortezas de ambos grupos de estudio. Cada carril contiene 1 μ g de RNA total de una rata diferente, infundida con vehículo o radicicol.

Una vez que se purificó el RNA total este fue tratado con DNAasa y se determinó su concentración mediante espectrofotometría. Para comprobar su integridad, 1 μ g de RNA de cada muestra se colocó y corrió en un gel de agarosa en condiciones desnaturizantes. La figura 15

muestra que el RNA se encontraba intacto pues se observan claramente dos RNA ribosomales 28 y 18S.

Para determinar los niveles de RNA mensajero de Hsp90, eNOS y del RNAr 18S en los animales de estudio. Se realizaron las curvas de amplificación para PCR en tiempo real, empleando diluciones seriadas del DNAc del grupo de animales control, iniciando con DNAc concentrado, 1:10, 1:100, 1:1000 y 1:10000. De igual forma se determinó si había o no competencia entre cada par de iniciadores con el gen control. Como se observa en la Figura 16A la amplificación del RNAr 18S es muy abundante pues al emplear el DNAc concentrado observamos que hay gran cantidad de producto de PCR amplificando antes de los 7 ciclos. En base a estas observaciones decidimos emplear la dilución 1:1000 del DNAc que amplifica productos de PCR aproximadamente a los 17 ciclos que nos permitirá su adecuado análisis. Para realizar los ensayos de competencia se realizó el mismo ensayo incubando ambas sondas en el mismo tubo (18S+gen problema) y comprobamos que la sonda de 18S es mucho más eficiente que las demás pues al analizar los resultados observamos que las graficas de amplificación de los genes problema se desplazan recorren hacia la derecha indicando indicando que una de las sondas es menos eficiente por lo que se dice que las sondas compiten entre sí. Para Hsp90 α , Hsp90 β y eNOS se realizaron las mismas pruebas y en base a las observaciones hechas decidimos emplear la dilución 1:100 como se observa en la figura 16B, C y D.

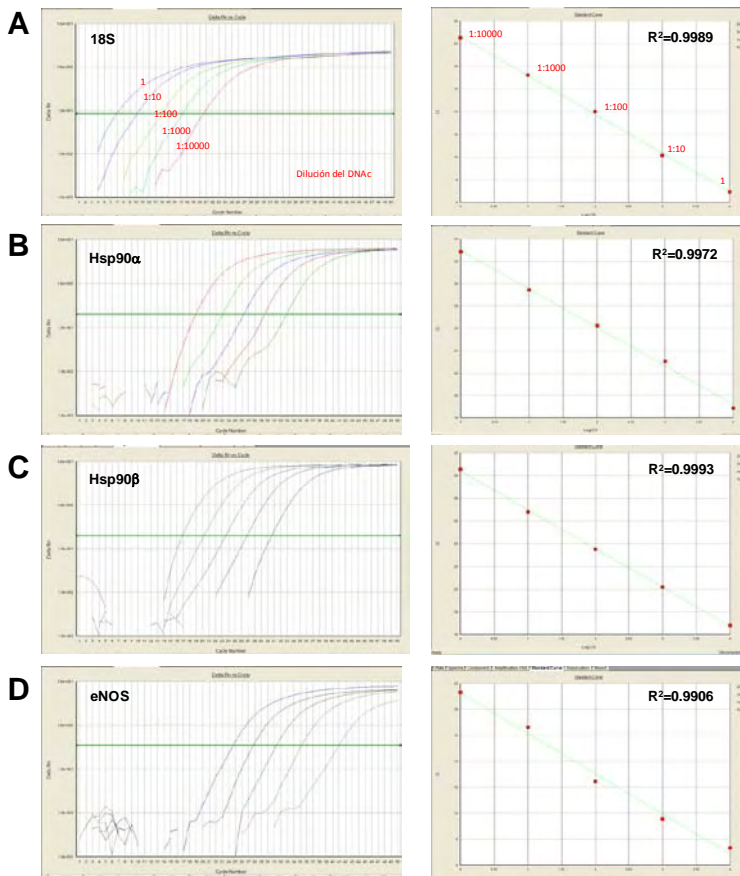


Figura 16. Cinéticas de amplificación hechas por PCR en tiempo real para los diferentes genes estudiados, se emplearon concentraciones diferentes del DNAc. En ellas se observa claramente que las curvas de amplificación se desplazan hacia la derecha conforme hay menos concentración de DNAc, manteniendo la proporción adecuada por cada orden de magnitud. Esto se comprobó al realizar una regresión lineal y observar un coeficiente de correlación cercano (R^2) a 1. A) Se muestran las curvas de amplificación de RNAr 18S empleado como gen control. B) Hsp90 α . C) Hsp90 β . D) eNOS.

Como era de esperarse al determinar los niveles de RNAm de Hsp90 observamos que la inhibición aguda con radicicol no produjo cambios en los niveles de RNAm de Hsp90 α /18S como se observa en la Fig.17A (Vehículo 1.0 ± 0.03 Vs radicicol 0.87 ± 0.1) así ni Hsp90 β / 18S como puede apreciarse en la Figura 17B (Vehículo 1.0 ± 0.04 Vs radicicol 1.2 ± 1.0).

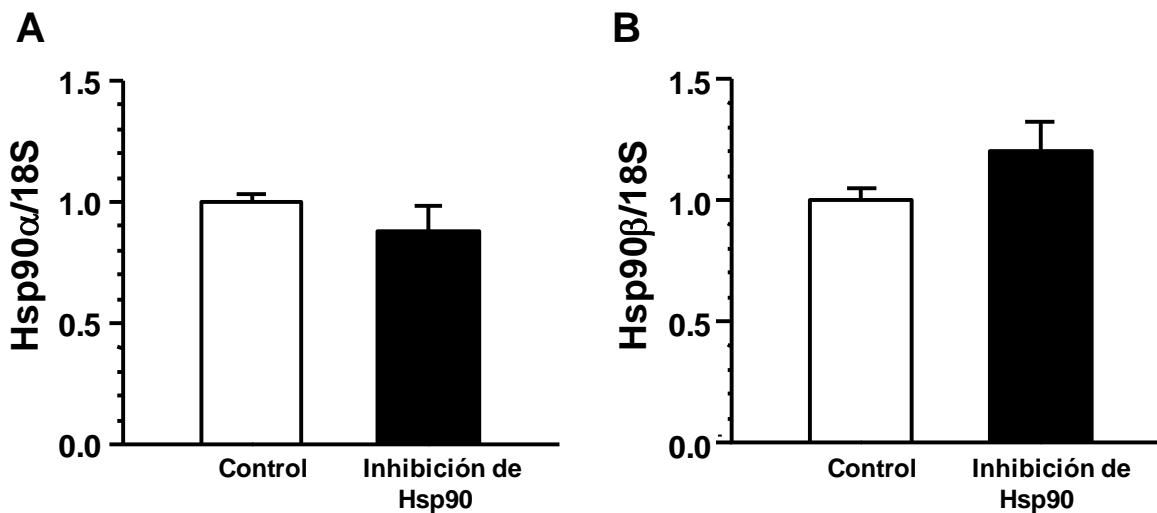


Figura 17. Efecto de la infusión de radicicol sobre los niveles de RNAm de Hsp90. A) Niveles de RNAm de Hsp90 α normalizado con RNAr 18S. B) Niveles de RNAm de Hsp90 β normalizado con 18S en la corteza renal. Barras blancas representan a los animales infundidos con vehículo y las barras negras representan a los animales infundidos con radicicol.

Se extrajeron proteínas totales para determinar los niveles de proteína de ambas isoformas y al igual que en el mensajero no observamos cambios como se observa en la Figura 18.

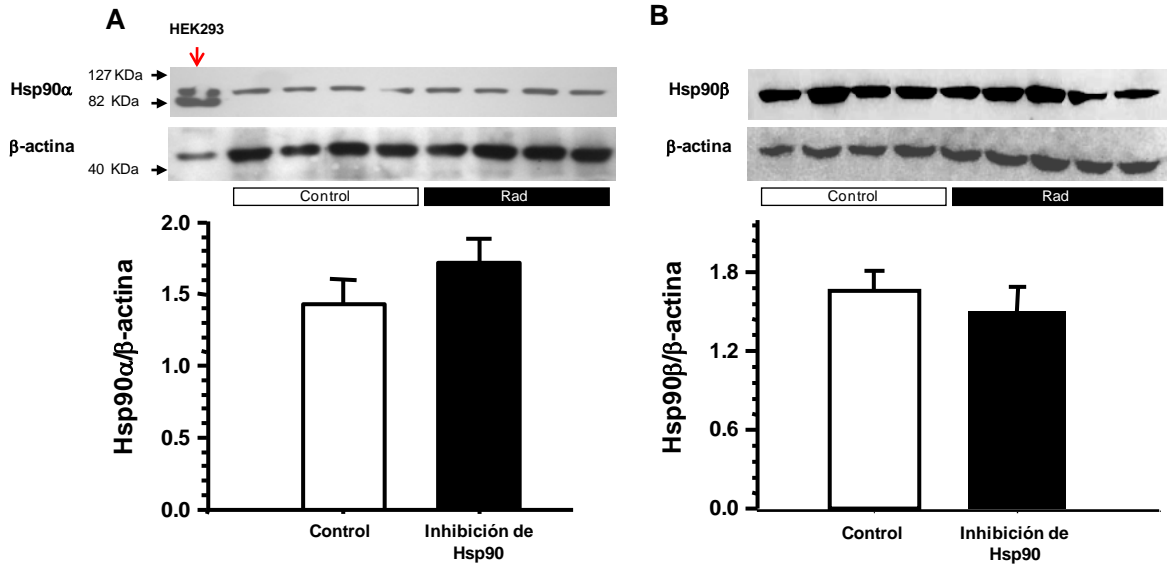


Figura 18. Niveles de proteína de Hsp90 en la corteza renal durante la infusión de vehículo o radicícol. A y B) Muestran el análisis de western blot de Hsp90 α y Hsp90 β normalizadas con β -actina. Como control positivo se emplearon células HEK 293 transfectadas con Hsp90 α . Las barras blancas representan el análisis densitométrico del western blot de Hsp90 α o β en las cortezas de 5 animales infundidos con vehículo, las barras negras representan el análisis densitométrico del Western blot de Hsp90 α o β en las cortezas de 5 animales infundidos con radicícol.

Debido a que la infusión de radicícol indujo reducción en la filtración glomerular propiciada por vasoconstricción renal, decidimos evaluar si este efecto fue mediado por reducción de agentes vasodilatadores o por incremento de factores vasoconstrictores.

El NO es un agente vasodilatador que se sintetiza por tres sintetasas de NO conocidas como la isoforma neuronal nNOS, la inducible iNOS y la endotelial eNOS, esta última es la que regula la generación de NO en el endotelio vascular e interviene en el mantenimiento de la hemodinámica renal. Aunado a esto se conoce que Hsp90 se une directamente a eNOS favoreciendo un aumento en su actividad y mayor producción de NO. Puesto que la inhibición de Hsp90 produjo reducción de la función renal es probable que la perdida de la interacción entre estas dos proteínas sea la consecuencia de la reducción en la producción de NO.

Para comprobar si la inhibición de Hsp90 produce reducción en los niveles de NO, determinamos la excreción urinaria de nitritos y nitratos ($\text{UNO}_2/\text{NO}_3\text{V}$) metabolitos estables de la síntesis de NO y como se muestra en la Figura 19A la infusión de radicicol redujo un 52% en la excreción urinaria de nitritos en el grupo de animales infundidos con radicicol y este cambio fue significativamente diferente con el grupo de vehículo. El mismo efecto fue observado en el grupo de animales infundidos con INUTEST® Figura 19B.

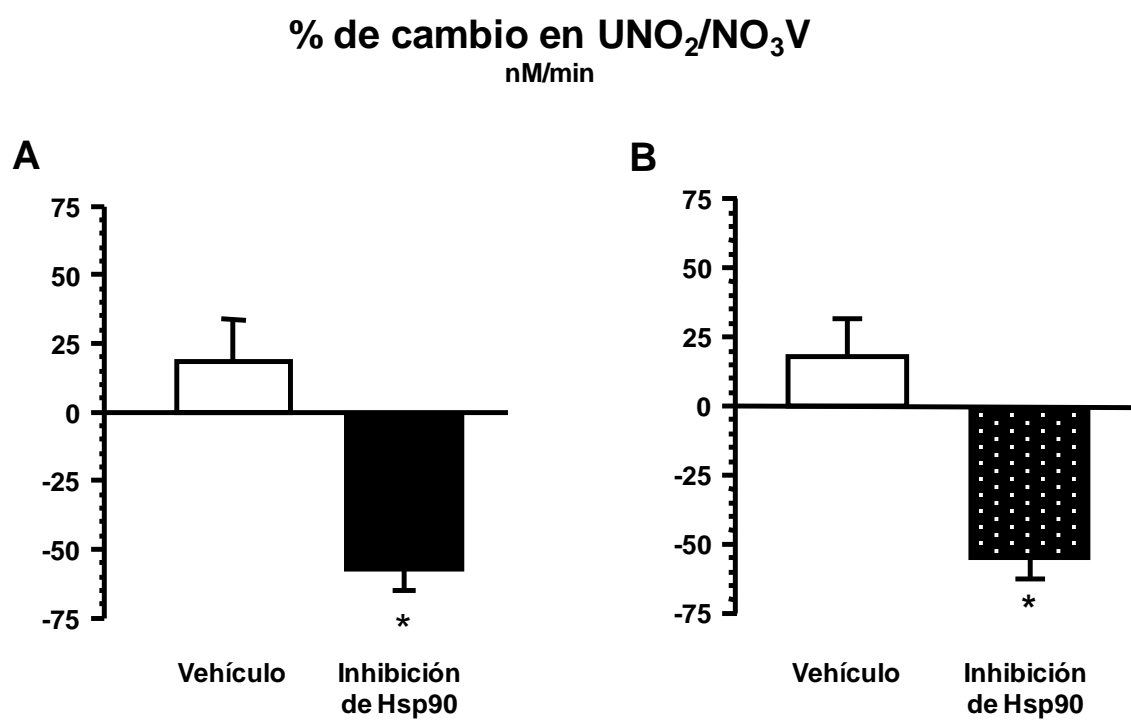


Figura 19. Producción de NO durante la inhibición de Hsp90. % de cambio en los niveles urinarios de nitritos y nitratos después de la infusión de vehículo (barras blancas) o de la inhibición de Hsp90 (Barras negras). A) Grupo infundido con azúcar BC. B) Grupo infundido con INUTEST®. p< 0.05 vs. Vehículo.

Para determinar si la reducción en la síntesis de NO se debe al desacople de Hsp90-eNOS y en consecuencia eNOS incremente los niveles intrarrenales de anión superóxido, determinamos los niveles de lipoperoxidación expresados como niveles de malondialdehído (MDA). Como se observa en la Figura 20A la infusión

de radicicol no modificó los niveles de MDA en la corteza renal con respecto a los animales infundidos con vehículo, en contraste se observó un incremento significativo en los niveles de MDA en la medula renal con respecto a la corteza renal; esto podría deberse a que la normalmente la medula está sometida a condiciones de hipoxia. La hipoxia se genera por una menor proporción de vasos sanguíneos y por la hiperosmolaridad que reduce la difusión de O_2

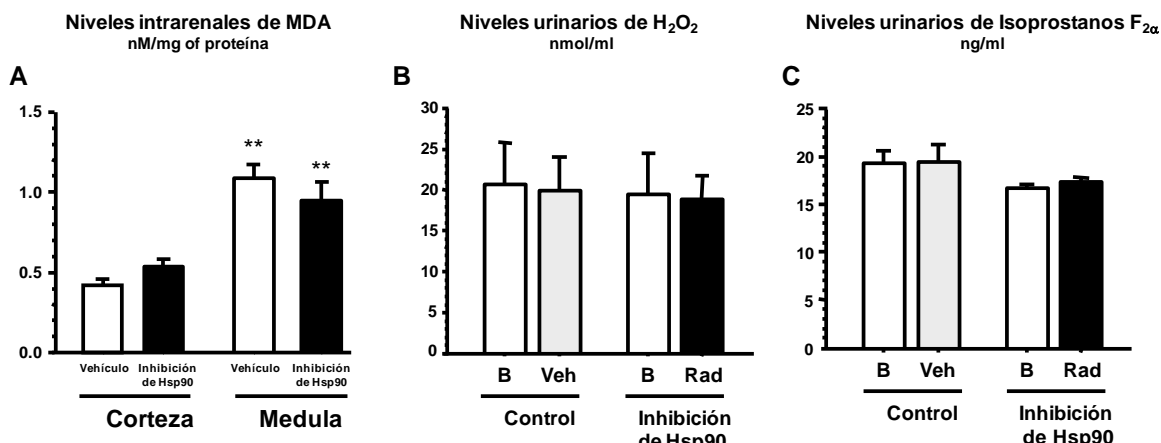


Figura 20. Niveles de estrés oxidativo observados al inhibir a Hsp90. A) Niveles de malondialdehído determinados en homogenados de corteza y medula renal. Barras blancas animales infundidos con vehículo y barras negras animales infundidos con radicicol. B) Niveles de peróxido de hidrógeno y C) Isoprostanos $F_{2\alpha}$ determinados en la orina durante el periodo basal (B) barras blancas, después de la infusión de vehículo (Veh) o radicicol (Rad) barras grises y negras respectivamente. ** p <0.05 vs. Corteza .

Para corroborar que la inhibición de Hsp90 no produce cambios en la concentración de anión superóxido, determinamos la concentración urinaria de peróxido de hidrogeno y de Isoprostanos $F_{2\alpha}$ como marcadores de estrés oxidativo. La Figura 20B y 20C muestra que la infusión de vehículo o radicicol no modificó la producción de O_2^- como previamente observamos en el tejido renal. Estos resultados muestran que la inhibición de Hsp90 reduce la síntesis de NO sin modificar la producción de anión superóxido.

Para conocer si la reducción de los niveles de NO observados durante la inhibición de Hsp90 se debe a cambios en la expresión de la sintasa de óxido nítrico endotelial eNOS. Para ello determinamos los niveles de RNAm en la corteza renal de eNOS mediante RT- PCR en tiempo real empleando el rRNA 18S como gen control en ambos grupos de estudio. Nuevamente determinamos las cinéticas de amplificación para la eNOS observando que amplifica de manera adecuada a la dilución 1:100 en el ciclo 30 como se observa en la Figura 16D.

No observamos cambios los niveles de RNAm de eNOS en los animales infundidos con radicicol y vehículo (1.1 ± 0.07 Vs 1.0 ± 0.006) como se muestra en la Figura 21 A, de igual forma el análisis densitométrico de los niveles proteicos de eNOS total/ β actina no mostró cambios en ambos grupos de estudio (Veh 0.57 ± 0.07 vs Rad 0.53 ± 0.06 unidades arbitrarias) Figura 21 B. Estos datos indican que la reducción de los niveles de NO no es una consecuencia de menor cantidad de proteína.

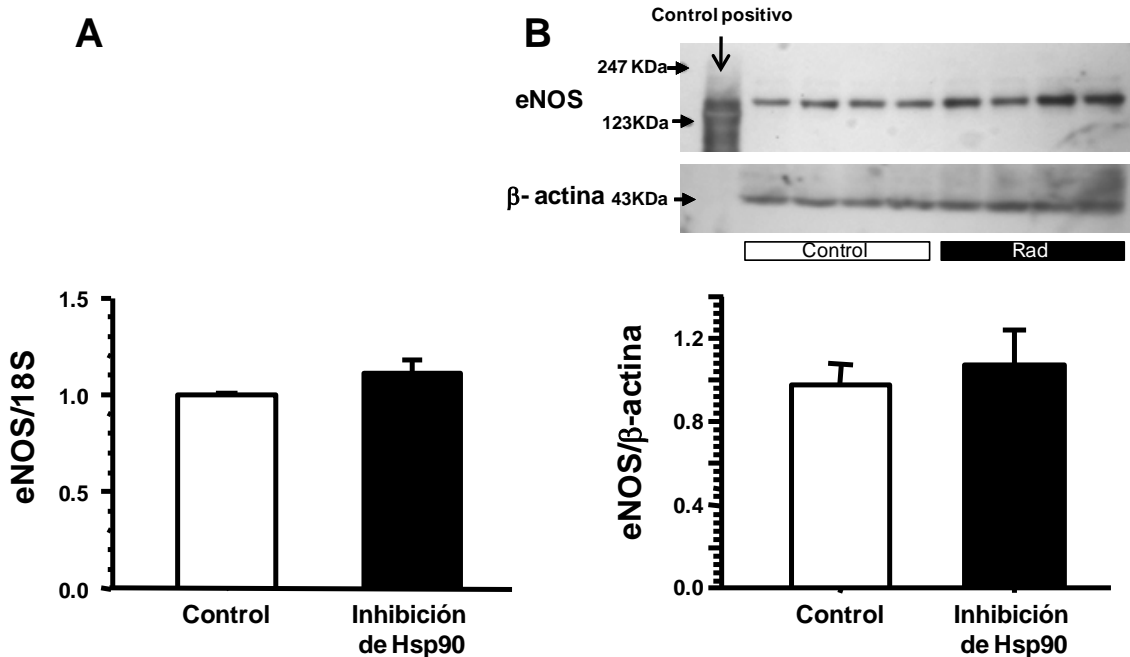


Fig.21 Expresión de eNOS durante la inhibición de Hsp90. A) Niveles de RNAm de eNOS determinados mediante RT-PCR en tiempo real normalizados con el rRNA 18S. B) Análisis de Western blot realizado en 5 cortezas diferentes de cada grupo y cuantificación densitométrica de eNOS normalizada con β -actina, primer carril control positivo (eNOS purificada). Animales control, barras blancas e inhibición de Hsp90, barras negras.

Es bien conocido que la actividad de eNOS está regulada por sus sitios de fosforilación por tal motivo evaluamos en el tejido renal el grado de fosforilación del residuo Thr 495 involucrado con reducción de la actividad de eNOS y biodisponibilidad del NO (76, 77, 78, 79, 80, 81, 82, 116).

La densitometría del análisis de Western blot para de este residuo muestra que los animales infundidos con radicicol muestran un aumento significativo en los niveles de fosforilación de la T497 eNOS/ β -actina (Veh 0.47 ± 0.18 vs. Rad 0.78 ± 0.12 Unidades arbitrarias) con respecto al grupo de animales infundidos con vehículo como se muestra en la Figura.22A.

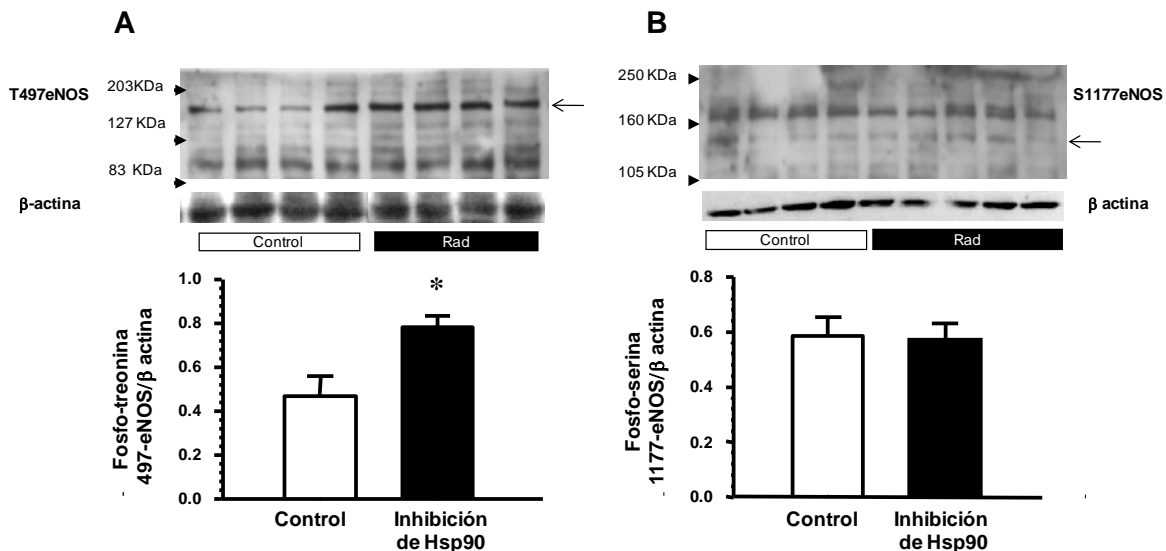


Figura 22. Efecto de la inhibición de Hsp90 en la fosforilación de eNOS. A) Western blot de la Thr 497 de eNOS empleando el fosfo anticuerpo específico donde se observa un incremento significativo de la fosforilación este residuo inactivante durante la infusión de radicicol. B) Western blot de la serina 1177 de eNOS la cual no se modificó durante la inhibición de Hsp90. Las barras blancas (control) y negras (inhibición de Hsp90) representan el análisis densitométrico de los análisis de Western blot, realizados en 5 diferentes cortezas de cada grupo de estudio, normalizados con la proteína β- actina. *p< 0.05 Vs.Control.

Por otro lado la densitometría del análisis de Western blot del sitio activador de eNOS en la S1177 expresado como la relación de eNOS S1177/ β-actina no muestra cambios significativos en la fosforilación de este residuo entre el grupo vehículo y el infundido con radicicol como se observa en la Figura 22B (0.11 ± 0.06 Vs 0.14 ± 0.04 Unidades arbitrarias).

Estos resultados sugieren que el aumento de la fosforilación de la T497 es suficiente para modificar de manera importante la función renal favoreciendo la reducción en la producción de NO.

Así mismo, se ha descrito que eNOS es una enzima activa cuando se encuentra formando dímeros (114,115) mientras que cuando se encuentra en forma monomérica no es activa, debido a que el flujo de electrones para la síntesis de NO se lleva a cabo del dominio reductor de un monómero al domino oxidante

del otro monómero. Por lo tanto, en este estudio evaluamos la proporción de dímero/monómero de eNOS en estos animales.

La Figura 23A muestra un Western blot representativo de eNOS en condiciones no desnaturalizantes que muestra la forma dimérica y monomérica de esta proteína y observamos en los animales infundidos con radicicol un descenso significativo en la cantidad de dímero con respecto a los animales control, en consecuencia se observa una mayor proporción de eNOS monomérica después de la inhibición de Hsp90. El análisis densitométrico confirmo los cambios de la dimerización de eNOS como se observa en las Figuras 23B y 23C.

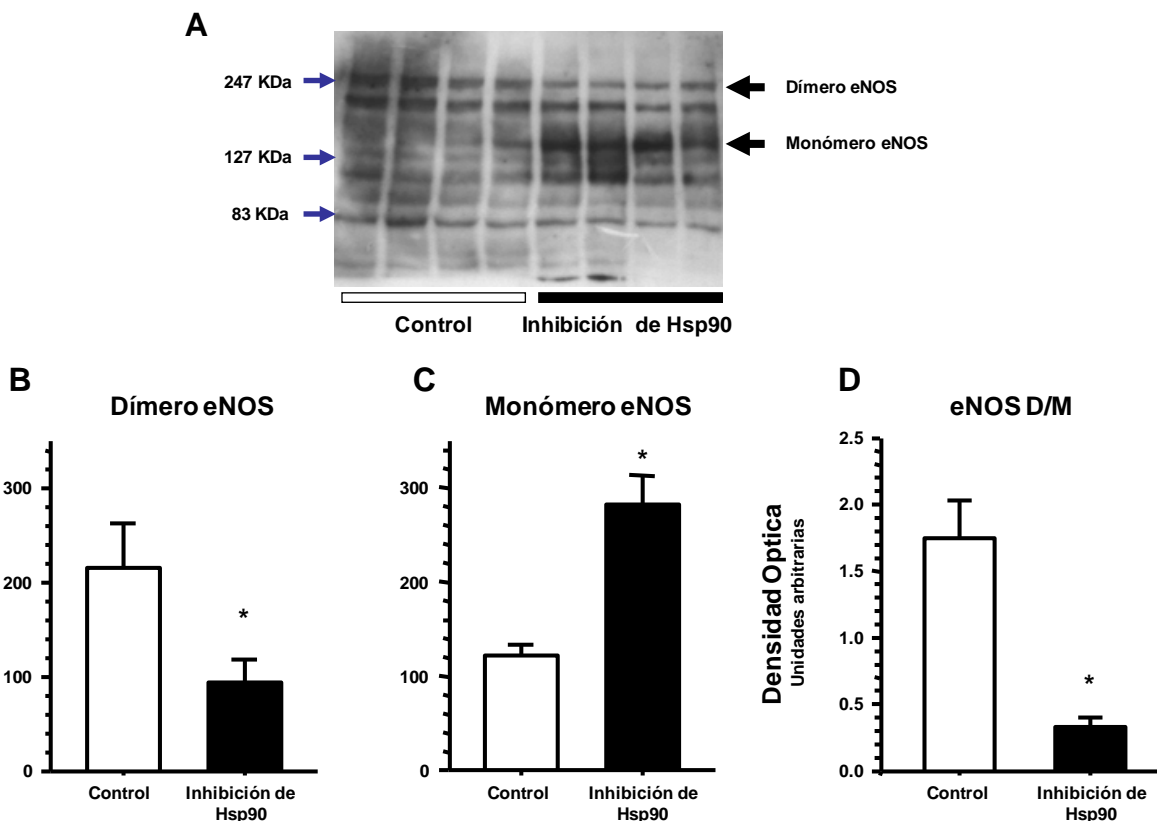


Figura 23. Efecto de la inhibición de Hsp90 sobre el estado de dimerización de eNOS. A) Western blot de eNOS en condiciones no desnaturalizantes, donde se observa la proporción del monómero y dímero de 5 cortezas de animales infundidos con vehículo (control) y 5 con radicicol (Inhibición de Hsp90). B y C) Análisis densitométrico de la forma dimérica y monomérica de eNOS. D) Relación dímero/monómero. Barras blancas (animales control), barras negras (Inhibición de Hsp90). * $p<0.05$ vs. Control.

De igual forma al evaluar la relación dímero/monómero observamos reducción significativa de la forma activa de eNOS en el grupo de radicicol con respecto al grupo control (Rad 1.74 ± 0.32 Vs Veh 0.33 ± 0.07 Unidades arbitrarias) Figura 20D, estos resultados aunados al incremento de los niveles de fosforilación de la T495 de eNOS sugieren que los cambios observados se deben al desacople de Hsp90-eNOS producido por el radicicol.

Discusión

6) Discusión.

Las proteínas citosólicas de choque térmico de 90 KDa, Hsp90 α y Hsp90 β desempeñan múltiples funciones que son realizadas al unirse y estabilizar a otras proteínas, denominadas proteínas cliente, de las que se han descrito más de 100 clientes moleculares de Hsp90, entre las que destacan enzimas, cinasas, receptores y factores de transcripción (44).

En un estudio reciente de nuestro laboratorio mostramos que Hsp90 α y Hsp90 β se expresan y localizan en el riñón (91), sin embargo poco se conoce del papel que desempeñan en el tejido renal. Por lo que el presente estudio se diseñó para evaluar si las Hsp90 están involucradas en regular la función renal en condiciones fisiológicas. Para lograr este objetivo, se utilizó un inhibidor farmacológico de Hsp90 conocido como radicicol. El radicicol es un compuesto que inhibe a Hsp90 a través de unirse al dominio ATPasa de esta proteína, lo que evita que sus proteínas cliente interactúen con Hsp90 (44).

En este trabajo observamos que la inhibición aguda de Hsp90 con radicicol indujo hipoperfusión renal, que fue detectada por la reducción significativa del flujo sanguíneo renal en un 40% con respecto al grupo control. Este efecto se acompañó por una disminución significativa de la filtración glomerular, evidenciando así, que Hsp90 está implicada en la regulación del tono vascular renal, ya que su inhibición produjo vasoconstricción.

Una de las interacciones más estudiadas de Hsp90 es la que puede mantener con la sintasa de óxido nítrico endotelial (eNOS), esta enzima se encarga de producir el NO en el endotelio y participar en la regulación del tono vascular a través de producir un efecto vasodilatador (66). La vasoconstricción renal que observamos al administrar radicicol nos sugería que podría resultar de una reducción de los factores vasodilatadores o bien de un incremento de factores vasoconstrictores. En estudios realizados por Garcia Cardeña y Col.; (68) y por Yetik-Anakack y Col.; (88) se demostró que la incubación de anillos de aorta de rata en presencia de geldanamicina o radicicol, incrementaba la fuerza de tensión en los anillos de aorta, estos resultados se interpretaron como un efecto vasoconstrictor, una vez observado este efecto estimularon la producción de NO dependiente del endotelio por la adición de acetilcolina al medio y observaron que estos anillos tenían una pobre producción de NO. Simultáneamente en células COS y células endoteliales vasculares de bovino (BAECs) observaron que la adición de geldanamicina redujo la actividad de eNOS y en consecuencia, la síntesis de NO se vió abatida por completo.

Por lo tanto, la hipoperfusión e hipofiltración renal inducida por la infusión de radicicol nos hizo suponer que estos efectos podrían estar mediados por una reducción en la síntesis de NO, aunado al hecho de que no se conocía si las observaciones hechas por Garcia- Cardeña también se podrían aplicar al lecho vascular renal, por lo que en este trabajo evaluamos la síntesis de NO, observando que la inhibición de Hsp90 con radicicol redujo en un 52% la excreción urinaria de nitritos y nitratos, los metabolitos estables de la síntesis de NO. En apoyo a nuestros resultados Cheng J y Cols.; (127) demostraron en arterias

interlobares de riñón un efecto similar. El 20-HETE es un eicosanoide que contribuye a la regulación del tono vascular, funcionando como vasoconstrictor. Estos autores demostraron en BAECs que el 20-HETE reduce significativamente la síntesis de NO, efecto que fue mediado por una reducción de la interacción entre Hsp90 y eNOS. Posteriormente, este grupo estudió el papel del 20-HETE en la relajación inducida por acetilcolina y encontraron que este ácido reduce de manera significativa la síntesis de NO y por ende la relajación del músculo liso.

También existe evidencia de que Hsp90 no solo regula la producción de NO durante la homeostasis celular sino que también puede desregular la actividad de eNOS en condiciones fisiopatológicas. En un estudio reciente se mostró que la falta de interacción de eNOS y Hsp90 juega un papel preponderante en un modelo de nefropatía diabética. Esta enfermedad se caracteriza por daño endotelial, lo que se ha asociado con una reducción de la síntesis de NO e incremento en la generación de radicales libres. En ratas con diabetes tipo I, inducida por la administración de estreptozotocina se mostró, que los niveles elevados de glucosa propiciaron la fosforilación de Hsp90 α en la treonina 89 de manera AMPc dependiente, lo que promovió la migración de Hsp90 α del citoplasma hacia la membrana, efecto que se asoció con una caída significativa de la síntesis de NO. Por lo que estos autores propusieron que la migración de Hsp90 α impidió la interacción con eNOS lo que no solo resultó con menor producción de NO, sino también aumento la generación de radicales libres (125).

Estos hallazgos sugieren que Hsp90 α participa en promover daño en este tipo de nefropatía y plantea que este podría ser el mecanismo por el cual, en la

diabetes se observa una reducción de NO (125). En apoyo a lo anterior, Frossard y Col.; (126) describieron la importancia de la formación del complejo Hsp90 y eNOS en el síndrome hepatopulmonar. Este síndrome puede desarrollarse en pacientes que presentan cirrosis o hipertensión portal y se caracteriza por hipoxemia y vasodilatación pulmonar. De forma paradójica, esta enfermedad se asocia con una sobreproducción de NO en el pulmón, mientras que en el hígado se observa una reducción en los niveles de NO, lo que contribuye a la hipertensión portal observada. En ese estudio se evaluó, la actividad diferencial de la actividad de eNOS por Hsp90 en un modelo de cirrosis biliar en la rata. Mediante ensayos de inmunoprecipitación se observó que la mayor actividad de eNOS en el pulmón se debe al incremento significativo en la asociación con Hsp90 efecto que fue prevenido por la adición de geldanamicina que redujo la interacción entre estas dos proteínas. Para tratar de explicar el efecto contrarió, en el hígado mostraron que la reducción de NO fue debida a un incremento en la interacción de eNOS con caveolina-1, proteína que mantiene a eNOS en la membrana en su forma inactiva y en consecuencia una pérdida significativa de la interacción con Hsp90 (71, 126).

En un estudio publicado recientemente, se mostró la secuencia de aminoácidos de eNOS responsable de mantener la interacción con Hsp90, mediante una estrategia novedosa como lo son, los péptidos señuelos. Los autores diseñaron 12 péptidos señuelos de eNOS, que nombraron B1 a B12 y que se incubaron con lisados de células endoteliales de bovino y observaron que solo los péptidos B1 al B3 reducían la interacción entre eNOS y Hsp90, teniendo además la particularidad de reducir la síntesis de NO. Por lo que rediseñaron un péptido que contenía los aminoácidos de B1, B2 y B3, al que llamaron TSB2 y que

incluía los residuos 301 a 330 de eNOS y observaron que la incubación del este péptido, en arterias facialis o su administración durante dos semanas en ratas produce vasoconstricción, lo que se asoció con una reducción de la producción de $\text{NO}_2/\text{NO}_3\text{V}$. Este descenso en la producción de NO se asoció con el incremento la síntesis de anión superóxido, mostrando nuevamente el papel de Hsp90 en la regulación del tono vascular (85, 86). También Pritchard y Cols.; (84) observaron que la inhibición de Hsp90 con geldanamicina en BAECs ocasionaba una reducción significativa de los nitritos y nitratos, pero también simultáneamente detectaron un incremento en la producción de anión superóxido. La producción de radicales libres por eNOS ha sido explicada por cambios en la fosforilación de la Tre 495 por PKC. Esta modificación produce un cambio conformacional en la enzima capaz de interrumpir el flujo de electrones produciendo un desacople; por lo que ahora eNOS es capaz de producir el anión superóxido (76, 118). Por lo que, estos dos últimos estudios muestran el papel dual de eNOS en la producción de dos radicales libres con papeles fisiológicos diferentes el NO y el anión O_2^- . De acuerdo con la reducción de la síntesis de NO observada en nuestro estudio durante la inhibición de Hsp90 nos hizo suponer que quizá esto podría generar que eNOS ahora produjera anión superóxido. En base a esto evaluamos si la infusión de radicicol modificaba los niveles de estrés oxidativo en el tejido renal a través de medir los niveles de lipoperoxidación en el tejido renal (malondialdehído) y por cuantificar los niveles de peróxido de hidrógeno e isoprostanos $\text{F}_{2\alpha}$ presentes en la orina. La inhibición de Hsp90 no alteró la síntesis de radicales libres a pesar de producir una importante reducción en la producción de NO. Estos

resultados sugieren que el desacople de eNOS/Hsp90 puede tener dos fases: una rápida con menor producción de NO y otra tardía, en donde eNOS ahora pudiera producir anión superóxido, pero debido a que solo infundimos el radicícol por menos de una hora es probable que solo detectemos el primer efecto, esto también fue observado por Whistett y Col.; (119) en BAECs, donde la adición de radicícol al medio de cultivo no modificó la producción de radicales libres.

Es probable que la inhibición del complejo Hsp90-eNOS y la reducción de NO hallan propiciado la hipoperfusión observada, pero no podemos dejar de mencionar que Hsp90 pueda regular el tono vascular por otras vías independientes a la de eNOS, pues se conoce que Hsp90 es capaz de regular la función de las otras dos sintetasas de óxido nítrico conocidas como la isoforma neuronal (nNOS) y la inducible (iNOS) que también se expresa en el tejido renal (120). Aunque prácticamente podemos excluir la participación de la iNOS, pues se ha descrito que solo incrementa la producción de NO en condiciones adversas como la inflamación o el shock aunado a su baja expresión en el tejido renal (121). En cambio la nNOS se expresa de manera abundante en el tejido renal específicamente en las células de la macula densa, desempeñando papeles importantes en el riñón como los son la regulación del sistema de retroalimentación túbulo glomerular y la liberación de la renina (97, 98, 121) Yang Sonn y Cols.; (122) determinaron que la actividad de nNOS es regulada por Hsp90, efecto que fue demostrado al transfectar y purificar a nNOS a partir de células HEK293. Estos autores observaron que la actividad de nNOS se incrementó de manera significativa después de la adición de Hsp90 purificada, concluyendo así que la interacción de esta chaperona facilita la unión de la

calmodulina, este efecto se vio abatido por la adición de geldanamicina o radicicol o por la adición de Hsp90 desnaturalizada (123). En base a estos trabajos no es difícil suponer que la administración del radicicol también inhibía la interacción con nNOS y esto pueda también contribuir a la reducción de la síntesis de NO por otra vía. Es importante resaltar que para poder determinar el papel de esta isoforma en el tejido renal durante la inhibición aguda de Hsp90, será necesario emplear inhibidores específicos de nNOS como el 7 nitroindazol (7NI).

Para conocer cuáles fueron los mecanismos que propiciaron la caída de los metabolitos estables de la síntesis de NO, decidimos evaluar si la inhibición de Hsp90 modificaba la expresión de eNOS. Como era de esperarse la inhibición aguda de Hsp90 con radicicol no modificó los niveles de RNAm, ni los de proteína de eNOS confirmado resultados observados por otros grupos, que han mostrado que ni la sobreexpresión o la inhibición de Hsp90 modifica a eNOS transcripcionalmente (117). No obstante, Hsp90 es capaz de modificar el estado de fosforilación de eNOS. Se conocen 6 sitios potenciales de fosforilación de eNOS, pero solo dos de ellos han sido involucrados en la regulación de la síntesis de oxido nítrico: la serina 1177 y la treonina 495, mientras que la fosforilación de la serina 1177 activa a eNOS y la fosforilación de la treonina la inactiva. Satoru T y cols.; (83) observaron en BAECs que Hsp90 incrementa la actividad de eNOS por dos mecanismos: 1) por aumentar la afinidad de eNOS por la calmodulina y 2) por reclutar a la cinasa Akt que fosforila la serina 1177 mejorando el transporte de electrones e incrementando la síntesis de NO. Así mismo, se ha descrito que la sobreexpresión de Hsp90 en células endoteliales de cordón umbilical de humano incrementa la unión con la proteína fosfatasa 2B (calcineurina) encargada de

defosforilar el residuo de la treonina 495 de eNOS (117) favoreciendo la fosforilación de eNOS en residuos activadores. Por el contrario, la inhibición del complejo Hsp90-eNOS promueve la proximidad de la proteína cinasa C que favorece la fosforilación del residuo inactivante de eNOS en la Tre 495, produciendo un cambio conformacional en la proteína que impide la unión de la calmodulina y con ello se inhibe la actividad de eNOS (63, 64, 65). En este trabajo nosotros observamos que la administración del inhibidor de Hsp90 indujo un incremento significativo de la fosforilación inactivante de eNOS en la treonina 495 lo que correlacionó con la reducción en la UNO₂/NO₃V que podría explicar en parte la vasoconstricción observada en los animales que recibieron radicicol. Para conocer el papel citoprotector de Hsp90 o su participación en la regulación de eNOS Kuppat y Col.;,(117) sobreexpresaron a Hsp90 mediante su transfección “in vivo”, posteriormente realizaron isquemia/reperfusión cardiaca, y observaron que la sobreexpresión de Hsp90 mejoraba la función cardiaca después de el proceso de isquemia/reperfusión y propusieron que este efecto era mediado por el incremento en la síntesis de NO que se evaluó mediante los niveles de GMPc. En base a sus resultados plantearon el siguiente mecanismo, la sobreexpresión de Hsp90 incrementó la interacción con eNOS y esto propicia que Akt incrementara la fosforilación de eNOS en la serina 1177 y evita la fosforilación de la treonina 495, efecto que no se observó en los animales que no fueron transfectados, concluyendo así que el incremento de la interacción de Hsp90-eNOS aumenta la síntesis de NO restablece la función cardiaca y reduce el tamaño del infarto. Así mismo Miao y Cols,; (128) generaron una dominante negativa de Hsp90β, por la

mutación del ácido aspartico 88 (Hsp90 D88N), residuo que es crucial para la unión de ATP a Hsp90. Por lo tanto, la transfección de esta proteína en BAECs, redujó de manera significativa la producción de NO después de la estimulación con VEGF, el mecanismo propuesto es que la presencia de esta dominante negativa impidió la interacción de Hsp90 con sus clientes moleculares, ya que la transfección de Hsp90D88N se asoció con una reducción en la fosforilación de la Ser 473 de Akt y en consecuencia con una reducción de la fosforilación de eNOS en la Ser 1177 de eNOS.

Otra vía que exploramos fue el papel de Hsp90 en la formación del homodímero de eNOS al desempeñar su principal función como chaperona permitiendo el plegamiento adecuado a otras proteínas entre ellas eNOS, al respecto se conoce que la conformación activa de eNOS es la forma dimérica ya que la oxidación de la L-arginina a NO ocurre del dominio reductasa de un monómero al dominio oxidasa del otro (114, 1159). Por lo tanto era importante conocer si el radicícol modificaba la conformación de la enzima y hallamos que la inhibición de Hsp90 incrementó de manera significativa la formación de monómeros inactivos y en consecuencia propició la reducción de la forma dimérica activa. Sugiriendo de manera clara que la unión de Hsp90 es indispensable para proporcionar estabilidad a la formación dimérica activa de eNOS.

Nuestros resultados muestran que la inhibición de Hsp90 es capaz de inducir vasoconstricción renal y reducir de la tasa de filtración glomerular, efecto que fue mediado por el incremento en la fosforilación de la treonina 495 de eNOS y reducción de la forma dimérica de eNOS generando monómeros inactivos y en consecuencia una reducción de la síntesis de NO que puede explicar la

vasoconstricción renal observada. Este estudio abre un campo nuevo de estudio para evaluar si la interacción de Hsp90 con eNOS es alterada en la insuficiencia renal.

Referencias

7) Referencias

1. Ritossa FA (1962) *Experientia* **18**, 571-573
2. Ritossa, F. (1996) *Cell Stress. Chaperones.* **1**, 97-98
3. Borkan, S. C. and Gullans, S. R. (2002) *Annu. Rev. Physiol* **64**, 503-527
4. Beck, F. X., Neuhofen, W., and Muller, E. (2000) *Am. J. Physiol Renal Physiol* **279**, F203-F215
5. Bidmon, B., Endemann, M., Muller, T., Arbeiter, K., Herkner, K., and Aufricht, C. (2002) *Kidney Int.* **62**, 1620-1627
6. Bidmon, B., Endemann, M., Muller, T., Arbeiter, K., Herkner, K., and Aufricht, C. (2000) *Kidney Int.* **58**, 2400-2407
7. Jiang, B., Xiao, W., Shi, Y., Liu, M., and Xiao, X. (2005) *Cell Stress. Chaperones.* **10**, 252-262
8. Morita, K., Wakui, H., Komatsuda, A., Ohtani, H., Miura, A. B., Itoh, H., and Tashima, Y. (1995) *Ren Fail.* **17**, 405-419
9. Fukuda, A., Osawa, T., Oda, H., Tanaka, T., Toyokuni, S., and Uchida, K. (1996) *Biochem. Biophys. Res. Commun.* **219**, 76-81
10. Benjamin, I. J. and McMillan, D. R. (1998) *Circ. Res.* **83**, 117-132
11. Narberhaus, F. (2002) *Microbiol. Mol. Biol. Rev.* **66**, 64-93
12. Kosmaoglou, M., Schwarz, N., Bett, J. S., and Cheetham, M. E. (2008) *Prog. Retin. Eye Res.* **27**, 434-449
13. Arrigo, A. P., Paul, C., Ducasse, C., Manero, F., Kretz-Remy, C., Virot, S., Javouhey, E., Mounier, N., and Diaz-Latoud, C. (2002) *Prog. Mol. Subcell. Biol.* **28**, 185-204
14. Mounier, N. and Arrigo, A. P. (2002) *Cell Stress. Chaperones.* **7**, 167-176
15. Fliss, A. E., Rao, J., Melville, M. W., Cheetham, M. E., and Caplan, A. J. (1999) *J. Biol. Chem.* **274**, 34045-34052
16. Cheetham, M. E. and Caplan, A. J. (1998) *Cell Stress. Chaperones.* **3**, 28-36
17. Maguire, M., Poole, S., Coates, A. R., Tormay, P., Wheeler-Jones, C., and Henderson, B. (2005) *Immunology* **115**, 231-238

18. Maguire, M., Coates, A. R., and Henderson, B. (2002) *Cell Stress. Chaperones*. **7**, 317-329
19. Fan, C. Y., Lee, S., and Cyr, D. M. (2003) *Cell Stress. Chaperones*. **8**, 309-316
20. Park, J., Easton, D. P., Chen, X., MacDonald, I. J., Wang, X. Y., and Subjeck, J. R. (2003) *Biochemistry* **42**, 14893-14902
21. Chiosis, G., Vilenchik, M., Kim, J., and Solit, D. (2004) *Drug Discov. Today* **9**, 881-888
22. Sreedhar, A. S., Kalmar, E., Csermely, P., and Shen, Y. F. (2004) *FEBS Lett.* **562**, 11-15
23. Richter, K. and Buchner, J. (2001) *J. Cell Physiol* **188**, 281-290
24. Young, J. C., Moarefi, I., and Hartl, F. U. (2001) *J. Cell Biol.* **154**, 267-273
25. Nemoto, T., Sato, N., Iwanari, H., Yamashita, H., and Takagi, T. (1997) *J. Biol. Chem.* **272**, 26179-26187
26. Felts, S. J., Owen, B. A., Nguyen, P., Trepel, J., Donner, D. B., and Toft, D. O. (2000) *J. Biol. Chem.* **275**, 3305-3312
27. Grammatikakis, N., Vultur, A., Ramana, C. V., Siganou, A., Schweinfest, C. W., Watson, D. K., and Raptis, L. (2002) *J. Biol. Chem.* **277**, 8312-8320
28. Moore, S. K., Kozak, C., Robinson, E. A., Ullrich, S. J., and Appella, E. (1989) *J. Biol. Chem.* **264**, 5343-5351
29. Rebbe, N. F., Ware, J., Bertina, R. M., Modrich, P., and Stafford, D. W. (1987) *Gene* **53**, 235-245
30. Ullrich, S. J., Moore, S. K., and Appella, E. (1989) *J. Biol. Chem.* **264**, 6810-6816
31. Shen, Y., Liu, J., Wang, X., Cheng, X., Wang, Y., and Wu, N. (1997) *FEBS Lett.* **413**, 92-98
32. Zhang, S. L., Yu, J., Cheng, X. K., Ding, L., Heng, F. Y., Wu, N. H., and Shen, Y. F. (1999) *FEBS Lett.* **444**, 130-135
33. Bharadwaj, S., Ali, A., and Ovsenek, N. (1999) *Mol. Cell Biol.* **19**, 8033-8041
34. Morimoto, R. I. (1998) *Genes Dev.* **12**, 3788-3796
35. Shi, Y., Mosser, D. D., and Morimoto, R. I. (1998) *Genes Dev.* **12**, 654-666

36. Minami, Y., Kawasaki, H., Miyata, Y., Suzuki, K., and Yahara, I. (1991) *J. Biol. Chem.* **266**, 10099-10103
37. Pratt, W. B. (1997) *Annu. Rev. Pharmacol. Toxicol.* **37**, 297-326
38. Prodromou, C., Roe, S. M., O'Brien, R., Ladbury, J. E., Piper, P. W., and Pearl, L. H. (1997) *Cell* **90**, 65-75
39. Buchner, J. (1999) *Trends Biochem. Sci.* **24**, 136-141
40. Maruya, M., Sameshima, M., Nemoto, T., and Yahara, I. (1999) *J. Mol. Biol.* **285**, 903-907
41. Mayer, M. P. and Bukau, B. (1999) *Curr. Biol.* **9**, R322-R325
42. Owen, B. A., Sullivan, W. P., Felts, S. J., and Toft, D. O. (2002) *J. Biol. Chem.* **277**, 7086-7091
43. Soti, C., Racz, A., and Csermely, P. (2002) *J. Biol. Chem.* **277**, 7066-7075
44. Richter, K. and Buchner, J. (2006) *Cell* **127**, 251-253
45. Richter, K., Moser, S., Hagn, F., Friedrich, R., Hainzl, O., Heller, M., Schlee, S., Kessler, H., Reinstein, J., and Buchner, J. (2006) *J. Biol. Chem.* **281**, 11301-11311
46. Wandinger, S. K., Richter, K., and Buchner, J. (2008) *J. Biol. Chem.* **283**, 18473-18477
47. Richter, K., Soroka, J., Skalniak, L., Leskovar, A., Hessling, M., Reinstein, J., and Buchner, J. (2008) *J. Biol. Chem.* **283**, 17757-17765
48. Schulte, T. W., Akinaga, S., Soga, S., Sullivan, W., Stensgard, B., Toft, D., and Neckers, L. M. (1998) *Cell Stress Chaperones*. **3**, 100-108
49. Smith, D. F., Whitesell, L., Nair, S. C., Chen, S., Prapapanich, V., and Rimerman, R. A. (1995) *Mol. Cell Biol.* **15**, 6804-6812
50. Onuoha, S. C., Mukund, S. R., Coulstock, E. T., Sengerova, B., Shaw, J., McLaughlin, S. H., and Jackson, S. E. (2007) *J. Mol. Biol.* **372**, 287-297
51. Csermely, P., Schnaider, T., Soti, C., Prohaszka, Z., and Nardai, G. (1998) *Pharmacol. Ther.* **79**, 129-168
52. Neckers, L. (2002) *Trends Mol. Med.* **8**, S55-S61
53. Xu, W. and Neckers, L. (2007) *Clin. Cancer Res.* **13**, 1625-1629

54. Carreras, C. W., Schirmer, A., Zhong, Z., and Santi, D. V. (2003) *Anal. Biochem.* **317**, 40-46
55. Kamal, A., Thao, L., Sensintaffar, J., Zhang, L., Boehm, M. F., Fritz, L. C., and Burrows, F. J. (2003) *Nature* **425**, 407-410
56. Powers, M. V. and Workman, P. (2007) *FEBS Lett.* **581**, 3758-3769
57. Powers, M. V. and Workman, P. (2006) *Endocr. Relat Cancer* **13 Suppl 1**, S125-S135
58. Sharp, S. Y., Boxall, K., Rowlands, M., Prodromou, C., Roe, S. M., Maloney, A., Powers, M., Clarke, P. A., Box, G., Sanderson, S., Patterson, L., Matthews, T. P., Cheung, K. M., Ball, K., Hayes, A., Raynaud, F., Marais, R., Pearl, L., Eccles, S., Aherne, W., McDonald, E., and Workman, P. (2007) *Cancer Res.* **67**, 2206-2216
59. Schulte, T. W., Akinaga, S., Murakata, T., Agatsuma, T., Sugimoto, S., Nakano, H., Lee, Y. S., Simen, B. B., Argon, Y., Felts, S., Toft, D. O., Neckers, L. M., and Sharma, S. V. (1999) *Mol. Endocrinol.* **13**, 1435-1448
60. Rowlands, M. G., Newbatt, Y. M., Prodromou, C., Pearl, L. H., Workman, P., and Aherne, W. (2004) *Anal. Biochem.* **327**, 176-183
61. Richter, K., Hendershot, L. M., and Freeman, B. C. (2007) *Nat. Struct. Mol. Biol.* **14**, 90-94
62. Storti, S., Vittorini, S., Iascone, M. R., Sacchelli, M., Baroni, A., Luisi, V. S., Crucean, A., Vanini, V., Biagini, A., and Clerico, A. (2003) *Cell Stress Chaperones*. **8**, 18-25
63. Fleming, I., Bauersachs, J., and Busse, R. (1997) *J. Vasc. Res.* **34**, 165-174
64. Fleming, I. and Busse, R. (1999) *Cardiovasc. Res.* **43**, 532-541
65. Fleming, I. and Busse, R. (1999) *J. Mol. Cell Cardiol.* **31**, 5-14
66. Sessa, W. C. (2005) *Mem. Inst. Oswaldo Cruz* **100 Suppl 1**, 15-18
67. Sessa, W. C. (2004) *J. Cell Sci.* **117**, 2427-2429
68. Garcia-Cardena, G., Fan, R., Shah, V., Sorrentino, R., Cirino, G., Papapetropoulos, A., and Sessa, W. C. (1998) *Nature* **392**, 821-824
69. Fulton, D., Gratton, J. P., McCabe, T. J., Fontana, J., Fujio, Y., Walsh, K., Franke, T. F., Papapetropoulos, A., and Sessa, W. C. (1999) *Nature* **399**, 597-601

70. Garcia-Cardena, G., Fan, R., Stern, D. F., Liu, J., and Sessa, W. C. (1996) *J. Biol. Chem.* **271**, 27237-27240
71. Gratton, J. P., Fontana, J., O'Connor, D. S., Garcia-Cardena, G., McCabe, T. J., and Sessa, W. C. (2000) *J. Biol. Chem.* **275**, 22268-22272
72. Papapetropoulos, A., Fulton, D., Lin, M. I., Fontana, J., McCabe, T. J., Zoellner, S., Garcia-Cardena, G., Zhou, Z., Gratton, J. P., and Sessa, W. C. (2004) *Mol. Pharmacol.* **65**, 407-415
73. Griffin, T. M., Valdez, T. V., and Mestril, R. (2004) *Am. J. Physiol Heart Circ. Physiol* **287**, H1081-H1088
74. Harris, M. B., Blackstone, M. A., Ju, H., Venema, V. J., and Venema, R. C. (2003) *Am. J. Physiol Heart Circ. Physiol* **285**, H333-H340
75. Takahashi, S. and Mendelsohn, M. E. (2003) *J. Biol. Chem.* **278**, 9339-9344
76. Fleming, I., Fisslthaler, B., Dimmeler, S., Kemp, B. E., and Busse, R. (2001) *Circ. Res.* **88**, E68-E75
77. Lin, M. I., Fulton, D., Babbitt, R., Fleming, I., Busse, R., Pritchard, K. A., Jr., and Sessa, W. C. (2003) *J. Biol. Chem.* **278**, 44719-44726
78. Fulton, D., Church, J. E., Ruan, L., Li, C., Sood, S. G., Kemp, B. E., Jennings, I. G., and Venema, R. C. (2005) *J. Biol. Chem.* **280**, 35943-35952
79. Boo, Y. C., Hwang, J., Sykes, M., Michell, B. J., Kemp, B. E., Lum, H., and Jo, H. (2002) *Am. J. Physiol Heart Circ. Physiol* **283**, H1819-H1828
80. Boo, Y. C., Sorescu, G., Boyd, N., Shiojima, I., Walsh, K., Du, J., and Jo, H. (2002) *J. Biol. Chem.* **277**, 3388-3396
81. Boo, Y. C., Sorescu, G. P., Bauer, P. M., Fulton, D., Kemp, B. E., Harrison, D. G., Sessa, W. C., and Jo, H. (2003) *Free Radic. Biol. Med.* **35**, 729-741
82. Boo, Y. C., Kim, H. J., Song, H., Fulton, D., Sessa, W., and Jo, H. (2006) *Free Radic. Biol. Med.* **41**, 144-153
83. Takahashi, S. and Mendelsohn, M. E. (2003) *J. Biol. Chem.* **278**, 30821-30827
84. Pritchard, K. A., Jr., Ackerman, A. W., Gross, E. R., Stepp, D. W., Shi, Y., Fontana, J. T., Baker, J. E., and Sessa, W. C. (2001) *J. Biol. Chem.* **276**, 17621-17624
85. Xu, H., Shi, Y., Wang, J., Jones, D., Weilrauch, D., Ying, R., Wakim, B., and Pritchard, K. A., Jr. (2007) *J. Biol. Chem.* **282**, 37567-37574

86. Xu, H. and Pritchard, K. A., Jr. (2008) *Arterioscler. Thromb. Vasc. Biol.* **28**, 1580-1581
87. Venema, R. C., Venema, V. J., Ju, H., Harris, M. B., Snead, C., Jilling, T., Dimitropoulou, C., Maragoudakis, M. E., and Catravas, J. D. (2003) *Am. J. Physiol Heart Circ. Physiol* **285**, H669-H678
88. Yetik-Anacak, G., Xia, T., Dimitropoulou, C., Venema, R. C., and Catravas, J. D. (2006) *Am J Physiol Heart Circ. Physiol*
89. Duval, M., Le, B. F., Huot, J., and Gratton, J. P. (2007) *Mol. Biol. Cell* **18**, 4659-4668
90. Matsubara, O., Kasuga, T., Marumo, F., Itoh, H., and Tashima, Y. (1990) *Kidney Int.* **38**, 830-834
91. Ramirez, V., Uribe, N., Garcia-Torres, R., Castro, C., Rubio, J., Gamba, G., and Bobadilla, N. A. (2004) *Cell Stress Chaperones* **9**, 198-206
92. Masilamani, S., Kim, G. H., Mitchell, C., Wade, J. B., and Knepper, M. A. (1999) *J Clin. Invest* **104**, R19-R23
93. Masilamani, S., Wang, X., Kim, G. H., Brooks, H., Nielsen, J., Nielsen, S., Nakamura, K., Stokes, J. B., and Knepper, M. A. (2002) *Am J Physiol Renal Physiol* **283**, F648-F657
94. Wang, X. Y., Masilamani, S., Nielsen, J., Kwon, T. H., Brooks, H. L., Nielsen, S., and Knepper, M. A. (2001) *J. Clin. Invest* **108**, 215-222
95. Couette, B., Jalaguier, S., Hellal-Levy, C., Lupo, B., Fagart, J., Auzou, G., and Rafestin-Oblin, M. E. (1998) *Mol. Endocrinol.* **12**, 855-863
96. Tumlin, J. A., Lea, J. P., Swanson, C. E., Smith, C. L., Edge, S. S., and Someren, J. S. (1997) *J. Clin. Invest* **99**, 1217-1223
97. Ortiz, P. A., Hong, N. J., and Garvin, J. L. (2001) *Am J Physiol Renal Physiol* **281**, F819-F825
98. Ortiz, P. A., Hong, N. J., and Garvin, J. L. (2004) *Am. J. Physiol Renal Physiol*
99. Ortiz, P. A., Hong, N. J., and Garvin, J. L. (2004) *Am. J. Physiol Renal Physiol*
100. Jeon, U. S., Kim, J. A., Sheen, M. R., and Kwon, H. M. (2006) *Acta Physiol (Oxf)* **187**, 241-247

101. Jeon, U. S., Han, K. H., Park, S. H., Lee, S. D., Sheen, M. R., Jung, J. Y., Kim, W. Y., Sands, J. M., Kim, J., and Kwon, H. M. (2007) *Am. J. Physiol Renal Physiol* **293**, F408-F415
102. Sheen, M. R., Kim, J. A., Lim, S. W., Jung, J. Y., Han, K. H., Jeon, U. S., Park, S. H., Kim, J., and Kwon, H. M. (2008) *Kidney Int.*
103. Chen, Y., Schnetz, M. P., Irarrazabal, C. E., Shen, R. F., Williams, C. K., Burg, M. B., and Ferraris, J. D. (2007) *Am. J. Physiol Renal Physiol* **292**, F981-F992
104. Somji, S., Ann, S. M., Garrett, S. H., Gurel, V., Todd, J. H., and Sens, D. A. (2002) *Toxicol. Lett.* **133**, 241-254
105. Ohtani, H., Wakui, H., Komatsuda, A., Satoh, K., Miura, A. B., Itoh, H., and Tashima, Y. (1995) *Lab Invest* **72**, 161-165
106. Satoh, K., Wakui, H., Komatsuda, A., Nakamoto, Y., Miura, A. B., Itoh, H., and Tashima, Y. (1994) *Ren Fail.* **16**, 313-323
107. Komatsuda, A., Wakuil, H., Imai, H., Itoh, H., Yasuda, T., and Miura, A. B. (1999) *Ren Fail.* **21**, 113-117
108. Perez-Rojas, J. M., Blanco, J. A., Gamba, G., and Bobadilla, N. A. (2005) *Kidney Int.* **68**, 1888-1893
109. Pereira, P., Ardenghi, P., de Souza, M. M., Choi, H., Moletta, B., and Izquierdo, I. (2001) *Behav. Pharmacol.* **12**, 299-302
110. Davidson D.W. and Sackner M.A. (1963) *J. Lab. Clin. Med.* **62**, 351-356
111. Perez-Rojas, J., Blanco, J. A., Cruz, C., Trujillo, J., Vaidya, V. S., Uribe, N., Bonventre, J. V., Gamba, G., and Bobadilla, N. A. (2006) *Am. J. Physiol Renal Physiol*
112. Vaidya, V. S., Ramirez, V., Ichimura, T., Bobadilla, N. A., and Bonventre, J. V. (2006) *Am. J. Physiol Renal Physiol* **290**, F517-F529
113. Livak, K. J. and Schmittgen, T. D. (2001) *Methods* **25**, 402-408
114. Cai, S., Khoo, J., Mussa, S., Alp, N. J., and Channon, K. M. (2005) *Diabetologia* **48**, 1933-1940
115. Klatt, P., Schmidt, K., Lehner, D., Glatter, O., Bachinger, H. P., and Mayer, B. (1995) *EMBO J.* **14**, 3687-3695
116. Li, C., Ruan, L., Sood, S. G., Papapetropoulos, A., Fulton, D., and Venema, R. C. (2007) *Vascul. Pharmacol.* **47**, 257-264

117. Kupatt, C., Dessim, C., Hinkel, R., Raake, P., Daneau, G., Bouzin, C., Boekstegers, P., and Feron, O. (2004) *Arterioscler. Thromb. Vasc. Biol.* **24**, 1435-1441
118. Fleming, I. and Busse, R. (2003) *Am. J. Physiol Regul. Integr. Comp Physiol* **284**, R1-12
119. Whitsett, J., Martasek, P., Zhao, H., Schauer, D. W., Hatakeyama, K., Kalyanaraman, B., and Vasquez-Vivar, J. (2006) *Free Radic. Biol. Med.* **40**, 2056-2068
120. Wilcox, C. S., Deng, X., and Welch, W. J. (1998) *Am. J. Physiol* **274**, R1588-R1593
121. Ortiz, P. A. and Garvin, J. L. (2002) *Am. J. Physiol Renal Physiol* **282**, F777-F784
122. Song, Y., Zweier, J. L., and Xia, Y. (2001) *Biochem. J.* **355**, 357-360
123. Bender, A. T., Silverstein, A. M., Demady, D. R., Kanelakis, K. C., Noguchi, S., Pratt, W. B., and Osawa, Y. (1999) *J. Biol. Chem.* **274**, 1472-1478
124. Fontana, J., Fulton, D., Chen, Y., Fairchild, T. A., McCabe, T. J., Fujita, N., Tsuruo, T., and Sessa, W. C. (2002) *Circ. Res.* **90**, 866-873
125. Lei, H., Venkatakrishnan, A., Yu, S., and Kazlauskas, A. (2007) *J. Biol. Chem.* **282**, 9364-9371
126. Frossard, J. L., Quadri, R., Hadengue, A., Morel, P., and Pastor, C. M. (2006) *World J Gastroenterol.* **12**, 228-233
127. Cheng,J.; Ou,J.S.; Singh,H.; Falck,J.R.; Narsimhaswamy,D.; Pritchard,K.A.,Jr.; Schwartzman,M.L. (2008) Am.J.Physiol Heart Circ.Physiol. **294** (2); H 1018-H1026.
128. Miao,R.Q.; Fontana,J.; Fulton,D.; Lin,M.I.; Harrison,K.D.; Sessa,W.C. (2008). *Arterioscler.Thromb.Vasc.Biol.* **28** (1); 105-111.
- 129 Marletta, Michael A. (1994). *Cell.* **78**, 927-930.
- 130 Kone, B., Kuncewicz, T., Zhang, W., and Yu, Z. (2003) *Am J Physiol Renal Physiol.* **285**, F178-F190.

Upregulation and intrarenal redistribution of heat shock proteins 90 α and 90 β by low-sodium diet in the rat

Victoria Ramírez, Norma Uribe, Romeo García-Torres, Clementina Castro, Julieta Rubio, Gerardo Gamba, and Norma A. Bobadilla

Molecular Physiology Unit, Department of Genomic Medicine and Environmental Toxicology, Instituto de Investigaciones Biomédicas, Universidad Nacional Autónoma de México and Departments of Nephrology and Pathology, Instituto Nacional de Ciencias Médicas y Nutrición, Salvador Zubirán, Mexico City, 14000 Mexico

Abstract Two genes encoding isoforms heat shock protein (Hsp) 90 α and Hsp90 β constitute the Hsp90 subfamily. In addition to their role in regulating mineralocorticoid and glucocorticoid receptors, these proteins have been associated with nitric oxide production. However, little is known regarding Hsp90 isoform expression and regulation in kidney. In this study we characterized the expression and localization of Hsp90 isoforms and evaluated the influence of low-sodium intake on their expression and distribution in kidney by using reverse transcription–polymerase chain reaction, Western blot, and immunohistochemistry techniques. We found that Hsp90 α and Hsp90 β were expressed abundantly in both the renal cortex and the medulla; however, Hsp90 isoform expression was higher in the medulla than in the cortex. Immunohistochemistry of Hsp90 α and Hsp90 β showed intense staining in the apical membrane of proximal and distal tubules. In the outer cortex these proteins were localized intracytosolically, whereas in the inner renal medulla they were restricted mainly to the basolateral membrane. Expression of Hsp90 α and Hsp90 β was upregulated in the renal cortex during sodium restriction. In addition, both proteins exhibited redistribution from the cytoplasm to the basolateral side in thick ascending limb cells when rats were fed with a low-salt diet. Our results showed that Hsp90 α and Hsp90 β were expressed abundantly in renal tissue. Expression and localization patterns under normal and salt-restricted intake were different between the cortex and the medulla, suggesting that these proteins may be involved in different processes along the nephron. Hsp90 α and Hsp90 β upregulation induced by a low-sodium diet together with redistribution in thick ascending limb cells suggests that Hsp90 plays a role in the modulation of sodium reabsorption under these circumstances.

INTRODUCTION

The heat shock protein (Hsp) family is formed by several genes that encode for proteins with molecular mass between 10 and 170 kDa (Jäättelä 1999). In the majority of eukaryotic cells, 3 classes of Hsps—Hsp90, Hsp70, and small Hsp—are synthesized abundantly. Specifically, the 90-kDa subfamily is constituted of 2 genes known as

Hsp90 α and Hsp90 β in humans (Hsp86 and Hsp84 in mouse) (Rebbe et al 1987; Moore et al 1989). Hsp90 influences the activity and stability of a wide range of client proteins that function as key regulators in cellular growth, differentiation, and death pathways. Among the >100 known Hsp90 protein clients are found steroid receptors; transcription factors; tyrosine kinases; G-protein subunits; and neuronal, inducible, and endothelial nitric oxide synthases (García-Cerdeña et al 1998; Bender et al 1999; Yoshida and Xia 2003).

In the kidney the best-characterized Hsp90 function is the interaction of this protein with the mineralocorticoid receptor. Hsp90 together with other factors and cochaperones forms a heterocomplex that binds to the mineral-

Received 2 February 2004; Revised 22 March 2004; Accepted 31 March 2004.

Correspondence to: Norma A. Bobadilla, Unidad de Fisiología Molecular, Vasco de Quiroga No. 15, Tlalpan, 14000 Mexico City, Mexico, Tel: 525 54852676; Fax: 525 56550382; E-mail: nab@biomedicas.unam.mx; nbobadillas@sni.conacyt.mx.

ocorticoid receptor (Couette et al 1996, 1998). The presence of Hsp90 in the complex seems to facilitate anchoring of unbound receptors to cytoskeleton and maintains the hormone-binding protein in a high-affinity conformation (Pratt 1993). In other words, association with Hsp90 stabilizes the mineralocorticoid receptor in its hormone-binding form. Then, binding of aldosterone to the receptor releases the Hsp heterocomplex, and the new receptor-aldosterone complex migrates to the nucleus and binds deoxyribonucleic acid (DNA), harboring the appropriated responsive elements in several genes.

One of the major regulators of Na⁺ excretion is aldosterone, and its effects are mediated by mineralocorticoid receptors. Transcriptional activation of these receptors in distal tubule epithelial cells (Tumlin 1997) triggers a series of events that stimulate Na⁺ retention by the kidney, including increased expression and activation of epithelial Na⁺ channel subunits (Masilamani et al 1999), which mediates apical Na⁺ entry across collecting duct principal cells and an abundance of thiazide-sensitive Na-Cl co-transporter in distal tubule (Velázquez et al 1996; Kim et al 1998). Because Hsp90 is required for proper conformation of the mineralocorticoid receptor before its binding to aldosterone, it is possible that it plays a role in regulating the effects of aldosterone. Moreover, it has been shown that some aldosterone effects in the collecting duct, such as activation of calcineurin, are mediated by the released Hsp heterocomplex rather than by the aldosterone-receptor complex (Tumlin et al 1997). In addition to the potential role of Hsp90 in aldosterone response, angiotensin II has been postulated as an inductor of Hsp70 and Hsp25, as well as of HO-1 expression, in the renal cortex (Aizawa et al 2000; Ishisaka et al 2002). However, no studies to date have addressed whether angiotensin II also modulates expression of Hsp90 isoforms.

Although some studies have evaluated the intrarenal expression of Hsp family members (Hsp32, Hsp25, Hsp60, Hsp70/72, Hsp73, and α B-crystallin) (Muller et al 1996; Aizawa et al 2000; Smoyer et al 2000), little attention has been paid to Hsp90 α and Hsp90 β expression in renal tissue. Thus, in the present study we assessed and characterized the expression and localization of both Hsp90 isoforms in rat kidney. Because of the potential relevance of Hsp90 isoforms as mediators of aldosterone function, we also analyzed the expression and distribution of Hsp90 in kidney of rats treated with a low-salt diet as a physiologic approach to activate the renin-angiotensin-aldosterone system (RAAS).

We observed that Hsp90 α and Hsp90 β are abundantly expressed in the renal cortex and the medulla. Both isoforms are expressed along the nephron, showing specific cellular patterns depending on the nephron segment analyzed. In addition, a low-sodium diet (LSD) was associated with upregulation of Hsp90 isoform expression in

the renal cortex and redistribution of both isoforms within thick ascending limb cells.

MATERIALS AND METHODS

Male Wistar rats weighing 300–350 g were used in the study. All procedures followed were in accordance with our institutional guidelines. Two groups of 22 rats were studied. Rats maintained for 21 days on a normal diet served as the control group (N), and rats fed with an LSD (0.02%), as the experimental group. At the end of the study, rats were placed in metabolic cages for 24-hour urine collection to assess urine osmolarity and sodium excretion. In addition, blood samples were taken to evaluate serum aldosterone levels. Aldosterone and sodium were determined by radioimmunoassay and with a NOVA4 electrolyte analyzer (NOVA Biomedical, Waltham, MA, USA), respectively.

Eighteen rats of each group were anesthetized by intraperitoneal injection of sodium pentobarbital (30 mg/kg), and their kidneys were macroscopically divided into renal cortex and medulla, frozen in liquid nitrogen, and maintained at -80°C until use. Total ribonucleic acid (RNA) was isolated individually from the renal cortex and medulla from 6 rats of each group according to the guanidine isothiocyanate–cesium chloride method, as we have reported previously (Bobadilla et al 1997, 1998). Integrity of isolated total RNA was examined by 1% agarose gel electrophoresis, and RNA concentration was determined by ultraviolet (UV) light absorbance at 260 nm (Beckman DU640, Brea, CA, USA). To avoid genomic DNA contamination, all RNA samples were treated with RNase-free DNase I.

Primer sequences to amplify Hsp90 α and Hsp90 β and glyceraldehyde phosphate dehydrogenase (GADPH) as a housekeeping gene were custom obtained (Invitrogen, Carlsbad, CA, USA) (Rocco et al 1992; Tang et al 1995). Sense primer for Hsp90 α was 5' ACA AGC ACA TAT GGC TGG ACA GCA 3', and antisense primer was 5' TTC AGT TAC AGC AGC ACT GGTATC 3', whereas sense primer for Hsp90 β was 5' ACC AGC ACC TAC GGC TGG ACA GCC 3', and antisense primer was 5' GAT CTC ATC AGG AAC TGC AGC ATT 3'. To verify Hsp90 isoform amplification, single bands of 320 base pairs (bp) for Hsp90 α and 318 bp for Hsp90 β were obtained and resolved in 1.5% agarose gels. Polymerase chain reaction (PCR) products were observed with ethidium bromide, gel was purified (Qiagen, Hilden, Germany), and the products were automatically sequenced (I PRISM 310, Perkin-Elmer, Wellesley, MA, USA).

Relative quantitation of Hsp90 α and Hsp90 β

Relative messenger RNA (mRNA) levels of Hsp90 α and Hsp90 β were assessed in renal cortex and medulla by

semiquantitative reverse transcription (RT)-PCR, as we have described previously (Bobadilla et al 1997, 1998, 1999; Feria et al 2003). In brief, RT was carried out with Moloney murine leukemia virus reverse transcriptase (Invitrogen), using 2.5 µg of total RNA from each renal cortex and each renal medulla. Then, one-tenth of individual RT samples of each group were used for each amplification in 20-µL-final volume reactions containing 1× PCR buffer, 0.1 mM of each deoxynucleoside triphosphate, 0.2 µCi of [α^{32} P]-deoxycytidine triphosphate (~3000 Ci/mmol, 9.25 MBq, 250 µCi), 10 µM of each primer, and 1 unit of *Taq* DNA polymerase (Invitrogen). Complementary DNA (cDNA) amplification was carried out in a thermal cycler (M.J. Research, Watertown, MA, USA) with the following profile: denaturation for 1 minute at 94°C; annealing for 1 minute at 57°C, and a 1-minute extension step at 72°C. GADPH was coamplified simultaneously in each reaction. Genomic DNA contamination was checked by running samples through PCR procedure without adding RT.

Amplification kinetics was performed according to our standard procedure (Bobadilla et al 1997, 1998, 1999; Feria et al 2003). To analyze PCR products, half of each reaction was electrophoresed in 5% acrylamide gel. Bands were ethidium bromide stained and observed under UV light, cut out, suspended in 1 mL of scintillation cocktail (Ecolume, ICN, Aurora, OH, USA), and counted by liquid scintillation (Beckman LS6500, Fullerton, CA, USA). The amount of radioactivity recovered from excised bands was plotted on a log scale against the number of cycles. To semiquantify each Hsp90 isoform, all reactions were performed individually from each cortex or medulla in duplicate during the exponential phase.

Protein extraction and Western blot analysis

Proteins were extracted into 2 separate pools per group. Each pool was obtained from 6 different cortices or 6 medullas by homogenization using a Kinematica polytron homogenizer (Switzerland) in 4 volumes of lysis buffer (225 mM mannitol, 75 mM sucrose, 0.1 mM ethylenediamine-tetraacetic acid [pH 7.0], and 0.5 mM 3-(N-morpholino)propanesulfonic acid [pH 7.0], containing 5 mM benzamidine and 5 mM dithiothreitol). Homogenates were centrifuged at 4000 × g for 4 minutes at 4°C to remove tissue debris without precipitating plasma membrane fragments. Protein concentrations were assessed in duplicate using Bio-Rad DC protein assay (Bio-Rad, Hercules, CA, USA).

Protein samples containing 50 µg of total protein in 10 µL loading buffer (6% sodium dodecyl sulfate [SDS], 15% glycerol, 150 mM Tris, bromophenol blue 3%, β-mercaptoethanol 2%, pH 7.6) were denatured by boiling for 5 minutes and were electrophoresed by SDS-polyacryl-

amide gel electrophoresis (PAGE). Proteins were transferred onto polyvinyl difluoride membrane (Amersham Pharmacia Biotech, Piscataway, NJ, USA) for 2 hours at 400 mA. Prestained rainbow markers (Amersham) were used as molecular mass standards. Nonspecific binding sites were blocked for 30 minutes at 37°C in Tris-buffered saline containing 0.1% Tween-20 (TBS-T) and 5% nonfat dry milk. Thereafter, membrane was incubated with primary antibody anti-Hsp90 1:1000 (Transduction Laboratories, Lexington, KY, USA) for 30 minutes at 37°C. Membranes were washed for 60 minutes with TBS-T changed every 15 minutes. Membranes were incubated with secondary antibody horseradish peroxidase (HRP)-conjugated goat antimouse IgG 1:80 000 (Transduction Laboratories) for 30 minutes at 37°C and washed again. Proteins were detected by using an enhanced chemiluminescence kit (Amersham Pharmacia Biotech) and autoradiography according to the manufacturer's recommendations. Bands were scanned for densitometric analysis.

Immunohistochemistry

In 4 rats from each group, kidneys were perfused with phosphate buffer through a femoral catheter at pressure corresponding to the mean arterial pressure of each animal. After blanching of the kidney, the perfusate was replaced by 10% freshly prepared buffered formalin, and perfusion was continued until fixation was completed. Tissue samples were embedded in paraffin, and kidney sections were cut to 3-µm thickness. Antigen retrieval for Hsp90α, Hsp90β, and Na⁺K⁻2Cl cotransporter detection was carried out by microwave heating in citrate buffer (0.01 M, pH 5.4) before adding HRP-conjugated reagents; endogenous peroxidase activity was blocked by 10 µg *d*-biotin/mL H₂O₂ solution. Then, slides were incubated for 1 hour with ready-to-use rabbit polyclonal antibodies against Hsp90α or Hsp90β (neomarkers distributed by Lab Vision Corporation, Fremont, CA, USA) and against renal-specific Na⁺K⁻2Cl cotransporter (generously provided by Mark Knepper). Slides were washed and incubated with biotinylated secondary antibody, and staining was completed using 3'3-diaminobenzidine tetrahydrochloride as chromogen (DAKO Liquid DAB+, DAKO Corp., Carpinteria, CA, USA), followed by counterstaining with Meyer hematoxylin. Tissue slides of N and LSD groups were processed simultaneously under similar conditions.

Statistical analysis

Significance was defined as 2-tailed *P* < 0.05, and results are presented as mean ± standard error of mean. Hsp90 isoform expression is shown as the ratio between Hsp90

Table 1 Effect of low-sodium diet (LSD) on body weight (BW), urinary sodium excretion (UNaV), fractional excretion of sodium (FENa), urinary osmolarity (UOsm), and serum aldosterone

Group	BW (g)	UNaV (meq/24 h)	FENa (%)	UOsm (mM)	Aldosterone (pg/mL)
N (normal diet)	281.0 ± 11.7	0.61 ± 0.130	0.236 ± 0.05	622.0 ± 87.1	97.6 ± 25.7
LSD	299.4 ± 4.1	0.03 ± 0.002*	0.005 ± 0.002*	257.7 ± 47.2*	1592.5 ± 268*

* P < 0.05 vs rats fed with normal salt diet.

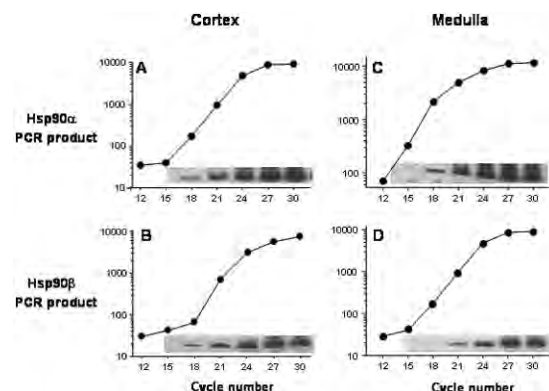


Fig 1. Polymerase chain reaction (PCR) amplification kinetics for Hsp90 α and Hsp90 β in renal tissue. (A,C) Hsp90 α PCR product during different number of cycles in renal cortex and medulla total ribonucleic acid (RNA), respectively. (B,D) Hsp90 β amplification kinetics from renal cortex and medulla total RNA, respectively. Plots are expressed as log scale of counts per minute from complementary deoxyribonucleic acid bands cut from acrylamide gels. Insets show autoradiography of the same PCR products stained with ethidium bromide.

and GADPH PCR product. Differences among groups were analyzed by an unpaired *t*-test.

RESULTS

Physiologic parameters from animals studied are shown in Table 1. Rats fed with an LSD had similar body weight to rats fed with a normal diet. As expected, the LSD group presented a significant reduction of urinary excretion of sodium, fractional excretion of sodium, and osmolarity. This reduction in sodium excretion was accompanied by an important elevation of serum aldosterone, a result of the well-known activation of the RAAS during sodium restriction, as extensively reported by other authors (Tarjan et al 1980; Rubattu et al 1994; Jo et al 1996).

Expression and localization of Hsp90 α and Hsp90 β

A PCR fragment of both Hsp90 α and Hsp90 β was amplified from cortex and renal medulla total RNA using specific primers. Both PCR products were sequenced. The degree of identity between rat Hsp90 α and that of mouse and human was 95.1 and 91.5%, respectively, and for Hsp90 β it was 92.5 and 85.6%, respectively (GenBank accession Nos. AY027778 and AY027779). Thus, amplified

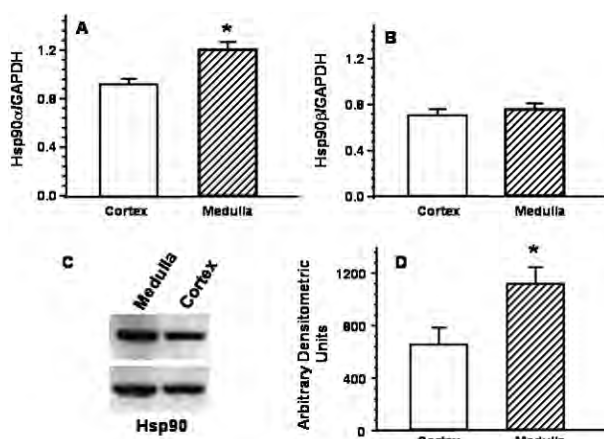


Fig 2. Messenger ribonucleic acid (mRNA) levels of Hsp90 α and Hsp90 β and Hsp90 protein expression. White bands represent results obtained in cortex, and hatched bands indicate results obtained in renal medulla. (A,B) mRNA levels of Hsp90 α and Hsp90 β , respectively, assessed by semiquantitative reverse transcription–polymerase chain reaction and expressed as the ratio of Hsp90 to glyceraldehyde phosphate dehydrogenase. (C) Western blot analyses showing Hsp90 protein expression in renal cortex and medulla from normal rats. Western blot was carried out using 2 different cortex and medulla pools. (D) Densitometric analysis of equal amounts of protein. *P < 0.05 vs renal cortex.

bands corresponded to rat orthologs of Hsp90 α and Hsp90 β .

Amplification kinetics

Amplification kinetics for Hsp90 α and Hsp90 β cDNA from renal cortex and medulla total RNA are depicted in Figure 1. Two phases are clearly distinguished in each curve: the exponential and plateau phases. To evaluate the amount of expression of each Hsp90 isoform, we chose the midpoint of the exponential phase. As shown in Figure 1, amplification kinetics for Hsp90 α exhibited the exponential phase between 15 and 24 cycles in cortex and between 12 and 24 in renal medulla, whereas exponential phase for Hsp90 β was between 18 and 24 cycles in renal cortex and between 15 and 24 cycles in renal medulla. To routinely amplify and semiquantify Hsp90 isoforms, we chose 20 cycles, except for medullary Hsp90 α amplification, in which we used 18 cycles. Similar analysis was performed for GADPH (data not shown).

Hsp90 α and Hsp90 β RT-PCR and Hsp90 Western blot analysis

Figure 2 depicts Hsp90 α and Hsp90 β mRNA levels expressed as the ratio between each isoform-amplified product over GADPH from renal cortex and medulla total RNA. Semiquantitative RT-PCR analysis showed that Hsp90 α was more abundant in the renal medulla than in the renal cortex (1.21 ± 0.06 and 0.93 ± 0.04 , respectively; $P = 0.001$) (Fig 2A). In contrast, similar levels of Hsp90 β were observed between medulla and cortex (0.71 ± 0.05 and 0.75 ± 0.05 , respectively; $P = \text{not significant}$) (Fig 2B). Greater expression of Hsp90 α in renal medulla was more apparent at the protein level (Fig 2C) because densitometric analysis from 2 different protein pools extracted from 6 normal cortices and 6 medullas revealed that Hsp90 band intensity in the medulla was higher than in the cortex (Fig 2D).

Hsp90 α and Hsp90 β immunohistochemical analysis

To evaluate whether Hsp90 α and Hsp90 β were expressed differently along the nephron, immunohistochemistry was performed to localize these proteins in renal tissue. In the glomeruli of normal rats, Hsp90 α and Hsp90 β staining was seen mainly in the glomerular capillaries, mesangial cells, and Bowman epithelia (as marked by the asterisk, arrowhead, and arrow, respectively, in Fig 3 B,C). In the proximal tubule, immunostaining for Hsp90 α and Hsp90 β was observed in the cytosol of the tubular epithelium (as marked by the asterisk in Fig 3 E,F, respectively). Interestingly, strong immunoreactivity was also detected in the proximal brush border membrane (indicated by short arrows), whereas no immunoreactivity was present in the basolateral side. In distal tubules a similar pattern was observed; the apical membrane showed more intense staining as compared with cytosol staining. In contrast, in cortical collecting ducts, Hsp90 isoforms principally exhibited intracytosolic distribution (figure not shown).

In the outer renal medulla, Hsp90 α and Hsp90 β were predominantly detected intracytosically in the thick limb of Henle loop cells (Fig 3 H,I). Immunoreactivity for Hsp90 isoforms in the outer renal medulla was stronger than in the renal cortex and in the inner medulla sections. Interestingly, Hsp90 protein immunoreactivity observed in the outer medulla nearly disappeared from the cytosol of inner medullary tubular cells, to be localized predominantly in the basolateral epithelium (see arrows in Fig 3 K,L). In addition, strong positive staining of Hsp90 α and Hsp90 β was observed in the renal pelvis, in particular in dome-shaped and basal cells (marked with an asterisk in Fig 3 N,O). In contrast to the inner medulla, Hsp90 α and Hsp90 β were detected in the cytosol of collecting duct

cells of the papilla tip (as indicated by a double asterisk). In addition, Hsp90 α staining was also seen in interstitial cells and extracellular matrix (see arrowhead in Fig 3N), whereas faint Hsp90 β staining was detected in these regions (Fig 3O).

In addition, Hsp90 α staining was also seen in interstitial cells and extracellular matrix (see arrowhead in Fig 3N), whereas faint Hsp90 β staining was detected in these regions (Fig 3O).

Hsp90 α and Hsp90 β expression and localization with an LSD

Figure 4 A,B shows Hsp90 α and Hsp90 β mRNA levels in the renal cortex, respectively, from rats fed with an LSD as compared with normal rats. Hsp90 α mRNA levels were significantly more abundant in the LSD group than in the control group (2.6 ± 0.2 vs 1.7 ± 0.1 ; $P = 0.0005$) (Fig 4A). Similarly, Hsp90 β mRNA levels were greater in the LSD as compared with the N group (2.0 ± 0.2 vs 1.6 ± 0.1 ; $P = 0.017$) (Fig 4B). Upregulation of Hsp90 isoforms induced by low-sodium intake in the renal cortex was more apparent at the protein level. As shown in Figure 4C, Western blot analysis revealed that Hsp90 isoform densitometric value in the low-salt diet group was significantly higher than that observed in control rats (78.4 ± 1.2 AU vs 31.1 ± 3.5 AU; $P = 0.002$). Increase of Hsp90 α and Hsp90 β expression was observed only in the renal cortex.

In the renal medulla, Hsp90 α and Hsp90 β mRNA levels were not different between the LSD and N groups (Hsp90 α -GADPH ratio was 0.7 ± 0.1 in N and 0.9 ± 0.1 in the LSD group, whereas the Hsp90 β -GADPH ratio was 0.3 ± 0.03 in N and 0.5 ± 0.01 in the LSD group). Similarly, Hsp90 protein levels were not different in both groups studied (data not shown). However, although LSD induced no change in the amount of expression of Hsp90 proteins in the renal medulla, it was evident that sodium restriction was clearly associated with a change in Hsp90 α and Hsp90 β distribution of intracellular localization in thick ascending limb cells. As shown in Figure 5 A,B, Hsp90 α and Hsp90 β were localized in the cytosol of ascending limb cells of normal rats, whereas in LSD rats immunostaining was present mainly in the basolateral side of these cells (Fig 5 C,D). To corroborate basolateral Hsp90 redistribution in response to low-salt diet, nephron was stained with rabbit polyclonal antibody specific for Na $^+$ K $^+$ 2Cl $^-$ cotransporter (BSC1) because it has been extensively demonstrated that this cotransporter is exclusively expressed in the apical membrane of thick ascending limb (Kaplan et al 1996; Nielsen et al 1998; Mount et al 1999). Arrows in Figure 5E highlight immunostaining of apical membrane with anti-BSC1 antibody. A serial kidney section was used to colocalize

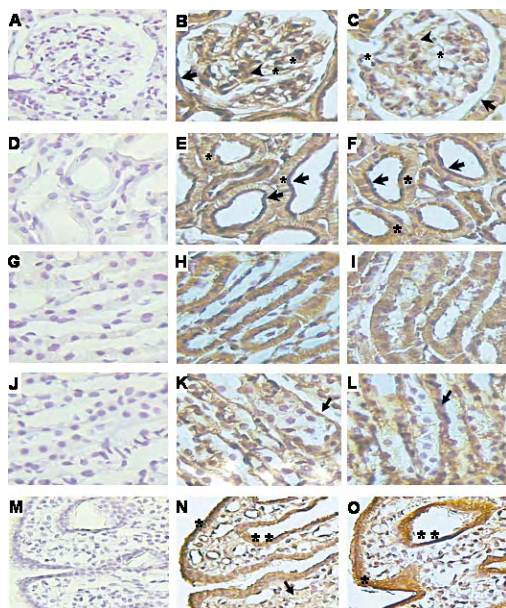


Fig 3. Immunohistochemistry of Hsp90 isoforms in renal cortex from rats fed with normal salt diet. (A,D,G,J,M) Negative immunostaining, (B,E,H,K,N) Hsp90 α immunoreactivity, (C,F,I,L,O) Hsp90 β immunoreactivity. (A–F) Renal cortex, (G–L) outer renal medulla, (J–L) inner renal medulla, (M–O) tip of papilla. In glomerulus, Hsp90 α and Hsp90 β immunoreactivity was observed in glomerular capillaries (see asterisk in B,C), mesangium (see arrowheads in B,C), and Bowman epithelium (see arrows in B,C). Under physiologic conditions, proximal and distal tubules were characterized by intense Hsp90 α and Hsp90 β staining in apical membrane (indicated by short arrows in E,F). Cytoplasm of proximal and distal tubules as well as cortical collecting ducts was diffusely stained (see asterisk in E,F). In outer medulla, staining of Hsp90 α and Hsp90 β was observed mainly in cytoplasm (H,I). In contrast, in inner medulla, reactivity was observed mainly in basolateral membrane (shown by arrows in K,L). In addition, immunostaining in outer medulla was more intense than in inner medulla and in renal cortex sections. In renal pelvis (N,O), intense Hsp90 α and Hsp90 β immunostaining was observed in epithelial lining of papilla (*) and in medullary collecting ducts (**). In addition, the arrow in (N) shows Hsp90 α reactivity in interstitial cells and extracellular matrix in tip of papilla, which was not observed for Hsp90 β . (A–L) Magnification 400 \times , (M–O) magnification 200 \times .

Hsp90 α in the same area. As shown in Figure 5F, immunostaining with anti-Hsp90 α antibody is positive in the opposite membrane to BSC1 immunoreactivity, indicating that Hsp90 α reactivity is located in the basolateral membrane. Thus, these observations suggest that with a low-salt diet, Hsp90 proteins in thick ascending limbs migrate from the cytosol to the basolateral membrane.

DISCUSSION

In the present study we assessed Hsp90 α and Hsp90 β expression in normal rat kidney and the effect of low-salt diet during 21 days. We observed that expression of both Hsp90 isoforms was higher in medulla than in renal cortex in normal rats. Immunohistochemical analysis revealed that Hsp90 α and Hsp90 β were similarly distrib-

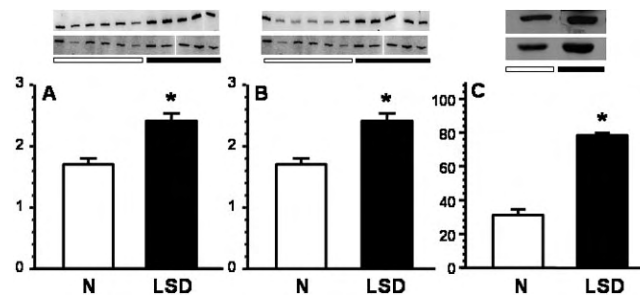


Fig 4. Upregulation of Hsp90 induced by low-sodium intake in renal cortex. (A,B) Semiquantitative reverse transcriptase polymerase chain reaction (RT-PCR) analysis of Hsp90 α and Hsp90 β and (C) Hsp90 Western blot analysis. (A,B) Upper autoradiographies represent Hsp90 α and Hsp90 β and lower glyceraldehyde phosphate dehydrogenase (GADPH) RT-PCR products obtained from individual cortices from N (white bars) and LSD groups (black bars). Graphs depict average and standard error of Hsp90 α -GADPH and Hsp90 β -GADPH ratios from each group. (C) Densitometric analysis of Western blot showing Hsp90 protein expression in renal cortex. Insets show immunoblots carried out using 2 different cortex pools. *P < 0.05 vs control group.

uted along the nephron, from glomerulus to papilla. Expression of Hsp90 isoforms, however, was upregulated by low-salt diet in renal cortex. In addition, sodium restriction resulted in the redistribution of both proteins within thick limb cells.

In renal cortex, Hsp90 α and Hsp90 β were expressed in glomerular capillaries, mesangial cells, and Bowman epithelia. Staining of Hsp90 α and Hsp90 β was also de-

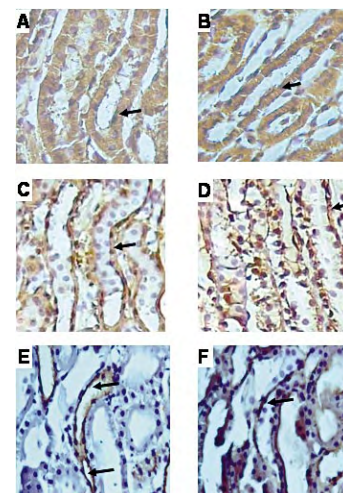


Fig 5. Redistribution of Hsp90 α and Hsp90 β in outer medulla in rats fed with an LSD. (A,C) Outer medulla Hsp90 α immunostaining in N and LSD groups, respectively. (B,D) Outer medulla Hsp90 β immunoreactivity in N and LSD, respectively. Magnification 400 \times . Sodium restriction during 21 days induced redistribution of both Hsp90 proteins in thick limb of Henle loop. Hsp90 proteins nearly disappeared from cytoplasm to be redistributed in basolateral side. (E,F) Serial kidney sections of rat fed with an LSD staining with Hsp90 α and Na $^{+}$ K $^{+}$ 2Cl $^{-}$ cotransporter antibodies. Arrows in (E) show apical localization of Na $^{+}$ K $^{+}$ 2Cl $^{-}$ cotransporter in ascending limb cells, whereas arrows in (F) show basolateral localization of Hsp90 α in these cells.

tectable in cytosol of proximal and distal epithelial cells, with strong immunoreactivity in apical membrane. Aufricht et al (1998) and Schober et al (1998) reported a similar pattern of expression for Hsp25 in proximal tubule, ie, predominant expression in apical side with less staining in cytoplasm or nucleus. In this study we also found that in outer medulla, Hsp90 α and Hsp90 β are mainly and abundantly located in the cytoplasm of thick limb cells, whereas in inner renal medulla, proteins were detected in the basolateral membrane of thin limb cells and collecting ducts. In addition, when collecting duct was near the renal pelvis, reactivity became more intense and was observed mainly in the cytoplasm of these cells.

It has been observed that Hsp90 expression in the rat proximal tubule is upregulated by nephrotoxic agents such as gentamicin or cisplatin (Beck et al 2000; Borkan and Gullans 2002). In addition, in human proximal tubule cells heat and arsenite induce expression of Hsp90 α and Hsp90 β , indicating that induction of Hsp90 may reduce renal damage during stress insults (Somji et al 2002). However, the physiologic role of constitutively expressed Hsp90 α and Hsp90 β proteins in kidney has never been addressed. Their intense expression pattern along the nephron suggests that these proteins are involved in several specific processes. Organized interactions between low-affinity mineralocorticoid receptor and Hsp90 heterocomplex are required to shape the mature receptor characterized by high hormone affinity (Borkan and Gullans 2002). In other words, in the absence of Hsp90 the affinity of mineralocorticoid receptor for aldosterone is very low. After binding of aldosterone to the high-affinity receptor, Hsp90 complex dissociates. Subsequently, aldosterone-receptor complex is translocated into the nucleus and binds to DNA steroid-responsive elements (Couette et al 1996, 1998). Thus, activation of mineralocorticoid receptor initiates a series of events that include sodium retention. In addition, it has been suggested that some aldosterone effects are mediated by the liberated Hsp90 heterocomplex rather than by the aldosterone-receptor complex (Tumlin et al 1997). Thus, a very interesting potential role for Hsp90 isoforms in renal physiology is modulation of the effects of aldosterone in kidney. In the present study we evaluated activation of the RAAS system induced by LSD on expression and localization of Hsp90 α and Hsp90 β in kidney. We observed that sodium restriction induced upregulation of Hsp90 α and Hsp90 β mRNA levels in the renal cortex, an effect more apparent at the protein level (Fig 4). It is possible, then, that increased Hsp90 expression serves to enhance response to aldosterone by switching more mineralocorticoid receptors to their high-affinity conformation. To test this hypothesis, it will be necessary to prevent association between Hsp90 and the mineralocorticoid receptor. However, compounds that possess this effect—such

as geldanamycin—also prevent interaction of Hsp90 with other proteins such as nitric oxide synthases, resulting in modification of renal hemodynamics, which by itself alters sodium reabsorption rates.

Aizawa et al (2000) and Ishizaka et al (2002) reported that angiotensin II was able to induce Hsp70, Hsp25, and HO-1 expression, particularly in the renal cortex. These studies suggest that angiotensin II could also be responsible for increasing expression of Hsp90 isoforms with a low-salt diet. Another possibility, however, is that aldosterone itself could induce expression of these proteins. Further studies will be necessary to determine the mechanism by which an LSD induces cortical Hsp90 isoform upregulation.

Another potential role of the Hsp90 subfamily is regulation of renal vascular tone and sodium excretion by the well-known positive effect of Hsp90 on nitric oxide generated by endothelial nitric oxide synthase (eNOS). García-Cardeña et al (1998) observed that interaction between Hsp90 and eNOS in human umbilical vein and bovine lung endothelial cells enhanced production of nitric oxide by eNOS. In addition, Shah et al (1999) showed that interaction between Hsp90 and eNOS participated in regulating vasomotor function in mesenteric vessels; in addition, they demonstrated that excessive nitric oxide production in experimental portal hypertension was mediated in part by enhanced Hsp90-eNOS interaction. On the other hand, recent evidence shows that uncoupling of eNOS and Hsp90 results in increased eNOS-dependent superoxide generation (Pritchard et al 2001). In kidney, preliminary data (Carmines et al 2002) showed that uncoupling between Hsp90 and eNOS with geldanamycin reduced renal afferent arteriolar diameter, suggesting that interaction between Hsp90 and eNOS is required to maintain appropriate afferent tone.

Ortiz et al (2001) showed that nitric oxide production by eNOS in thick ascending limb resulted in reduction of salt reabsorption due to inhibition of Na-K-2Cl cotransporter. They also observed that increased tubular flow in isolated and perfused thick ascending limbs was associated with trafficking of eNOS to the apical membrane and that eNOS migrated together with Hsp90 (Ortiz et al 2002), suggesting that to reduce Na-K-2Cl cotransporter function, the eNOS-Hsp90 complex migrated to the apical membrane. In this regard, one of the most intriguing observations in the present study is that LSD was associated with redistribution of Hsp90 isoforms from the cytoplasm to the basolateral membrane in the thick limb of Henle loop. Thus, in a condition under which salt reabsorption in the thick ascending limb is enhanced, Hsp90 migrates to the basolateral membrane. Because a recent study revealed that Hsp90 stabilizes Na⁺-K⁺-ATPase within cells (Bidmon et al 2002), it is possible that migration of Hsp90 to the basolateral membrane during low-

salt diet not only resulted in preventing Hsp90-eNOS inhibition of Na-K-2Cl cotransporter but also in increasing the number or activity of basolateral Na⁺-K⁺-ATPase by Hsp90 chaperone activity. Additional studies will be necessary to provide insight into the role of Hsp90 in regulating the activity of renal cotransporters.

ACKNOWLEDGMENTS

Part of this work was presented at the 35th Meeting of the American Society of Nephrology, Philadelphia, PA, USA, 2002. This work was supported by research grants G34511M and 40182 (to N.A.B.) from the Mexican Council of Science and Technology (CONACYT) and by grant DGAPA IN208602-3 (to N.A.B. and G.G.) from the National Autonomous University of Mexico (UNAM). We thank Norma Vázquez for her technical assistance and Cristina Cruz for aldosterone measurements.

REFERENCES

- Aizawa T, Ishizaka N, Taguchi J, Nagai R, Mori I, Tang SS, Ingelfinger JR, Ohno M. 2000. Heme oxygenase-1 is upregulated in the kidney of angiotensin II-induced hypertensive rats: possible role in renoprotection. *Hypertension* 35: 800–806.
- Aufrecht C, Ardito T, Thulin G, Kashgarian M, Siegel NJ, Van Why SK. 1998. Heat-shock protein 25 induction and redistribution during actin reorganization after renal ischemia. *Am J Physiol Renal Physiol* 274: F215–F222.
- Beck FX, Neuhofer W, Muller E. 2000. Molecular chaperones in the kidney: distribution, putative roles, and regulation. *Am J Physiol Renal Physiol* 279: F203–F215.
- Bender AT, Silverstein AM, Demady DR, Kanelakis KC, Noguchi S, Pratt WB, Osawa Y. 1999. Neuronal nitric-oxide synthase is regulated by the Hsp90-based chaperone system *in vivo*. *J Biol Chem* 274: 1472–1478.
- Bidmon B, Endemann M, Muller T, Arbeiter K, Herkner K, Aufrecht C. 2002. HSP-25 and HSP-90 stabilize Na,K-ATPase in cytoskeletal fractions of ischemic rat renal cortex. *Kidney Int* 62: 1620–1627.
- Bobadilla NA, Herrera JP, Merino A, Gamba G. 1997. Semi-quantitative PCR: a tool to study low abundance messages in the kidney. *Arch Med Res* 28: 55–60.
- Bobadilla NA, Gamba G, Tapia E, García-Torres R, Bolio A, López-Zetina P, Herrera-Acosta J. 1998. Role of NO in cyclosporin nephrotoxicity: effects of chronic NO inhibition and NO synthases gene expression. *Am J Physiol Renal Physiol* 274: F791–F798.
- Bobadilla NA, Tapia E, Jiménez F, et al. 1999. Dexamethasone increases eNOS gene expression and prevents renal vasoconstriction induced by cyclosporin. *Am J Physiol Renal Physiol* 277: F464–F471.
- Borkan SC, Gullans SR. 2002. Molecular chaperones in the kidney. *Annu Rev Physiol* 64: 503–527.
- Carmines PK, Fallet RW, Roscow J, Sasser JM, Pollock JS. 2002. Renal cortical Hsp90 and its impact on NOS activity and afferent arteriolar tone are diminished in diabetes mellitus. *J Am Soc Nephrol* 13: 532A.
- Couette B, Fagart J, Jalaguier S, Lomber M, Souque A, Rafestin-Oblin ME. 1996. Ligand-induced conformational change in the human mineralocorticoid receptor occurs within its hetero-oligomeric structure. *Biochem J* 315(Pt 2): 421–427.
- Couette B, Jalaguier S, Hellal-Levy C, Lupo B, Fagart J, Auzou G, Rafestin-Oblin ME. 1998. Folding requirements of the ligand-binding domain of the human mineralocorticoid receptor. *Mol Endocrinol* 12: 855–863.
- Feria I, Pichardo I, Juárez P, et al. 2003. Therapeutic benefit of spironolactone in experimental chronic cyclosporine A nephrotoxicity. *Kidney Int* 63: 43–52.
- García-Cerdeña G, Fan R, Shah V, Sorrentino R, Cirino G, Papapetropoulos A, Sessa WC. 1998. Dynamic activation of endothelial nitric oxide synthase by Hsp90. *Nature* 392: 821–824.
- Ishizaka N, Aizawa T, Ohno M, et al. 2002. Regulation and localization of HSP70 and HSP25 in the kidney of rats undergoing long-term administration of angiotensin II. *Hypertension* 39: 122–128.
- Jäättelä M. 1999. Heat shock proteins as cellular lifeguards. *Ann Med* 31: 261–271.
- Jo H, Yang EK, Lee WJ, Park KY, Kim HJ, Park JS. 1996. Gene expression of central and peripheral renin-angiotensin system components upon dietary sodium intake in rats. *Regul Pept* 67: 115–121.
- Kaplan MR, Plotkin MD, Lee WS, Xu ZC, Lytton J, Hebert SC. 1996. Apical localization of the Na-K-Cl cotransporter, rBSC1, on rat thick ascending limbs. *Kidney Int* 49: 40–47.
- Kim GH, Masilamani S, Turner R, Mitchell C, Wade JB, Knepper MA. 1998. The thiazide-sensitive Na-Cl cotransporter is an aldosterone-induced protein. *Proc Natl Acad Sci U S A* 95: 14552–14557.
- Masilamani S, Kim GH, Mitchell C, Wade JB, Knepper MA. 1999. Aldosterone-mediated regulation of ENaC alpha, beta, and gamma subunit proteins in rat kidney. *J Clin Invest* 104: R19–R23.
- Moore SK, Kozak C, Robinson EA, Ullrich SJ, Appella E. 1989. Murine 86- and 84-kDa heat shock proteins, cDNA sequences, chromosome assignments, and evolutionary origins. *J Biol Chem* 264: 5343–5351.
- Mount DB, Baekgaard A, Hall AE, Plata C, Xu J, Beier DR, Gamba G, Hebert SC. 1999. Isoforms of the Na-K-2Cl cotransporter in murine TAL I. Molecular characterization and intrarenal localization. *Am J Physiol Renal Physiol* 276: F347–F358.
- Muller E, Neuhofer W, Ohno A, Rucker S, Thurau K, Beck FX. 1996. Heat shock proteins HSP25, HSP60, HSP72, HSP73 in iso-osmotic cortex and hyperosmotic medulla of rat kidney. *Pflugers Arch* 431: 608–617.
- Nielsen S, Maunsbach AB, Ecelbarger CA, Knepper MA. 1998. Ultrastructural localization of Na-K-2Cl cotransporter in thick ascending limb and macula densa of rat kidney. *Am J Physiol Renal Physiol* 275: F885–F893.
- Ortiz PA, Hong NJ, Garvin JL. 2001. NO decreases thick ascending limb chloride absorption by reducing Na(+)-K(+)-2Cl(−) cotransporter activity. *Am J Physiol Renal Physiol* 281: F819–F825.
- Ortiz PA, Hong NJ, Garvin JL. 2004. Liminal flow induces eNOS activation and translocation in the rat thick ascending limb II: role of PI3 kinase and Hsp90. *Am J Physiol Renal Physiol*, in press.
- Pratt WB. 1993. The role of heat shock proteins in regulating the function, folding, and trafficking of the glucocorticoid receptor. *J Biol Chem* 268: 21455–21458.
- Pritchard KA Jr, Ackerman AW, Gross ER, Stepp DW, Shi Y, Fontana JT, Baker JE, Sessa WC. 2001. Heat shock protein 90 mediates the balance of nitric oxide and superoxide anion from endothelial nitric-oxide synthase. *J Biol Chem* 276: 17621–17624.
- Rebbe NF, Ware J, Bertina RM, Modrich P, Stafford DW. 1987. Nu-

- cleotide sequence of a cDNA for a member of the human 90-kDa heat-shock protein family. *Gene* 53: 235–245.
- Rocco MV, Neilson EG, Hoyer JR, Ziyadeh FN. 1992. Attenuated expression of epithelial cell adhesion molecules in murine polycystic kidney disease. *Am J Physiol Renal Physiol* 262: F679–F686.
- Rubattu S, Enea I, Ganten D, et al. 1994. Enhanced adrenal renin and aldosterone biosynthesis during sodium restriction in TGR (mREN2)27. *Am J Physiol* 267: E515–E520.
- Schober A, Burger-Kentischer A, Muller E, Beck FX. 1998. Effect of ischemia on localization of heat shock protein 25 in kidney. *Kidney Int Suppl* 67: S174–S176.
- Shah V, Wiest R, García-Cerdeña G, Cadelina G, Groszmann RJ, Sessa WC. 1999. Hsp90 regulation of endothelial nitric oxide synthase contributes to vascular control in portal hypertension. *Am J Physiol* 277: G463–G468.
- Smoyer WE, Ransom R, Harris RC, Welsh MJ, Lutsch G, Benndorf R. 2000. Ischemic acute renal failure induces differential expression of small heat shock proteins. *J Am Soc Nephrol* 11: 211–221.
- Somji S, Ann SM, Garrett SH, Gurel V, Todd JH, Sens DA. 2002. Expression of hsp 90 in the human kidney and in proximal tubule cells exposed to heat, sodium arsenite and cadmium chloride. *Toxicol Lett* 133: 241–254.
- Tang PZ, Gannon MJ, Andrew A, Miller D. 1995. Evidence for oestrogenic regulation of heat shock protein expression in human endometrium and steroid-responsive cell lines. *Eur J Endocrinol* 133: 598–605.
- Tarjan E, Spat A, Balla T, Szekely A. 1980. Role of the renin-angiotensin system in the adaptation of aldosterone biosynthesis to sodium restriction in the rat. *Acta Endocrinol (Copenh)* 94: 381–388.
- Tumlin JA, Lea JP, Swanson CE, Smith CL, Edge SS, Someren JS. 1997. Aldosterone and dexamethasone stimulate calcineurin activity through a transcription-independent mechanism involving steroid receptor-associated heat shock proteins. *J Clin Invest* 99: 1217–1223.
- Velázquez H, Bartiss A, Bernstein P, Ellison DH. 1996. Adrenal steroids stimulate thiazide-sensitive NaCl transport by rat renal distal tubules. *Am J Physiol Renal Physiol* 270: F211–F219.
- Yoshida M, Xia Y. 2003. Heat shock protein 90 as an endogenous protein enhancer of inducible nitric-oxide synthase. *J Biol Chem* 278: 36953–36958.

Victoria Ramírez, Juan M. Mejía-Vilet, Damián Hernández, Gerardo Gamba and Norma A. Bobadilla

Am J Physiol Renal Physiol 295:1044-1051, 2008. First published Jul 30, 2008;
doi:10.1152/ajprenal.90278.2008

You might find this additional information useful...

This article cites 33 articles, 15 of which you can access free at:

<http://ajprenal.physiology.org/cgi/content/full/295/4/F1044#BIBL>

Updated information and services including high-resolution figures, can be found at:

<http://ajprenal.physiology.org/cgi/content/full/295/4/F1044>

Additional material and information about *AJP - Renal Physiology* can be found at:

<http://www.the-aps.org/publications/ajprenal>

This information is current as of October 9, 2008 .

Radicicol, a heat shock protein 90 inhibitor, reduces glomerular filtration rate

Victoria Ramírez, Juan M. Mejía-Vilet, Damián Hernández, Gerardo Gamba, and Norma A. Bobadilla

Molecular Physiology Unit, Instituto de Investigaciones Biomédicas, Universidad Nacional Autónoma de México and Instituto Nacional de Ciencias Médicas y Nutrición Salvador Zubirán, Mexico City, Mexico

Submitted 29 April 2008; accepted in final form 24 July 2008

Ramírez V, Mejía-Vilet JM, Hernández D, Gamba G, Bobadilla NA. Radicicol, a heat shock protein 90 inhibitor, reduces glomerular filtration rate. *Am J Physiol Renal Physiol* 295: F1044–F1051, 2008. First published July 30, 2008; doi:10.1152/ajprenal.90278.2008.—The heat shock protein subfamily of 90 kDa (HSP90) is composed of five isoforms. The more abundant proteins of this subfamily are cytosolic isoforms known as HSP90 α and HSP90 β . More than 100 client proteins have been found to be regulated by HSP90. Several studies have shown that HSP90 regulates nitric oxide synthesis that is dependent on endothelial nitric oxide synthase (eNOS). Because eNOS regulates renal vascular tone and glomerular filtration rate (GFR), the present study was designed to evaluate the effect of acute HSP90 inhibition with radicicol on GFR and the eNOS pathway. Twenty male Wistar rats were divided into two groups: control vehicle animals and radicicol-infused animals ($25 \mu\text{g} \cdot \text{ml}^{-1} \cdot \text{min}^{-1}$). Basal levels were taken before experimental measurements. Mean arterial pressure and renal blood flow (RBF) were recorded, as well as GFR, urinary nitrite and nitrate excretion ($\text{UNO}_2/\text{NO}_3\text{V}$). Additionally, we evaluated eNOS expression, Ser1177 and Thr495 eNOS phosphorylation levels, the eNOS dimer-to-monomer ratio, as well as oxidative stress by assessing renal lipoperoxidation and urinary isoprostanate $F_{2\alpha}$ and hydrogen peroxide. HSP90 inhibition with radicicol produced a fall in RBF and GFR that was associated with a significant reduction of $\text{UNO}_2/\text{NO}_3\text{V}$. The effects of radicicol were in part mediated by a significant decrease in eNOS phosphorylation and in the eNOS dimer-to-monomer ratio. Our findings suggest that GFR is in part maintained by HSP90-eNOS interaction.

renal blood flow; heat shock protein 90 isoforms

THE HEAT SHOCK PROTEIN (HSP) subfamily of 90 kDa is one of the most abundant proteins of eukaryotic cells, comprising 1–2% of total protein under nonstress conditions (30). Five isoforms of HSP90 have been identified, which differ in their cellular localization and abundance. In particular, HSP90 α and HSP90 β , the major cytoplasmic isoforms, share ~85% sequence identity at protein level. Their main structure encompasses an NH₂-terminal ATPase domain, followed by a charged domain, a client protein binding domain, and a COOH-terminal dimerization domain (26). The ATP binding site is the major target for HSP90 inhibitors, of which geldanamycin, 17-allylamino-17-demethoxy-geldanamycin, and radicicol are the most used because of their high specificity for HSP90 inhibition. These compounds interfere with ATP binding to HSP90, preventing the formation of the mature complex that results in the proteasome-dependent degradation of associated proteins (26).

HSP90 has been shown to interact with and stabilize >100 different client proteins (for a full list see <http://www.picard.ch/downloads/Hsp90interactors>), including several kinases, transcriptional factors, hormone receptors, antiapoptotic proteins, and, of particular interest for cardiovascular and renal physiology, endothelial nitric oxide synthase (eNOS) (5).

Recent studies have emphasized the physiological role of HSP90 in regulating vascular tone. eNOS is the primary source of nitric oxide (NO) that produces vasorelaxation. It has been demonstrated that HSP90-eNOS coupling increases the activity of this enzyme, with greater NO production as a result. On the contrary, not only is HSP90-eNOS uncoupling associated with reduction of NO synthesis but it also turns eNOS into a superoxide generator (10, 24, 34). These studies strongly suggest that the dual role of eNOS in vascular physiology is modulated by its interaction with HSP90. Despite the growing evidence that this interaction is relevant for vascular physiology, little to nothing is known about the role that HSP90 plays in renal physiology. In this regard, we previously (27) characterized the expression pattern of HSP90 α and HSP90 β along the nephron, observing that both proteins are expressed in glomerular capillaries, mesangial cells, and Bowman epithelia and along tubular epithelium. Although it is well known that eNOS is highly expressed in renal vascular endothelial cells, and that renal blood flow (RBF) and glomerular filtration rate (GFR) are regulated by eNOS-dependent NO production, it is unknown to what extent RBF and GFR depend on HSP90-regulated eNOS activity. Here we show that HSP90 inhibition with radicicol results in a significant reduction of RBF and GFR that is associated with decreased NO generation. These findings suggest that HSP90 is an important regulator of renal function.

MATERIALS AND METHODS

Twenty male Wistar rats weighing 300–320 g each and fed with a standard chow diet were divided into two groups: control rats and rats in which HSP90 was acutely inhibited by radicicol infusion (see below). All experiments were performed in a control period and a vehicle or radicicol infusion period. Animal procedures were in accordance with our institutional guidelines for animal care. All experiments involving animals were conducted in accordance with the *Guide for the Care and Use of Laboratory Animals* (National Academy Press, Washington DC, 1996) and were approved by Institutional Animal Care and Use Committee of the National University of Mexico.

Functional studies. The day of the experiment, rats were anesthetized with an intraperitoneal injection of pentobarbital sodium (30 mg/kg) and placed on a homeothermic table to maintain core body temperature at 37°C. The trachea, jugular vein, and femoral artery were cannulated with polyethylene tubing (PE-240 and PE-50). The bladder was also cannulated with PE-90. During surgery, rats were

Address for reprint requests and other correspondence: N. A. Bobadilla, Unidad de Fisiología Molecular, Vasco de Quiroga No. 15, Tlalpan, 14000 Mexico City, Mexico (e-mail: nab@biomedicas.unam.mx, nabs@quetzal.innsz.mx).

The costs of publication of this article were defrayed in part by the payment of page charges. The article must therefore be hereby marked “advertisement” in accordance with 18 U.S.C. Section 1734 solely to indicate this fact.

maintained under euvolemic conditions by infusion of 10 ml/kg body wt isotonic rat plasma, followed by an infusion of 5% low-calorie commercial sugar (METCO, Mexico City, Mexico) at 1.6 ml/h as a marker of GFR. We previously showed (23) that this compound has enough sensitivity to measure GFR under normal and pathophysiological conditions to a similar extent as the standard measurement using polyfructosan. All experiments were performed in two stages. In the first stage, after an appropriate equilibrium period of 60 min urine was drained from the bladder by gravity. Care was taken to avoid dead space in the bladder while urine was collected over a period of 30–60 min. Blood samples were taken at the beginning and end of each urine collection period and replaced with blood from a donor rat. An ultrasound transit-time flow probe (1RB, Transonic, Ithaca, NY) was placed around the left renal artery and filled with ultrasonic coupling gel (HR Lubricating Jelly, Carter-Wallace, New York, NY) for recording RBF. Mean arterial pressure (MAP) was monitored throughout the experiment with a pressure transducer (model p23 db, Gould) and recorded on a polygraph (Grass Instruments, Quincy, MA). After basal measurements, the second stage began. In addition to low-calorie sugar infusion, one-half of the rats received an infusion of 10% DMSO and 10% ethanol in saline solution as a vehicle. The other half received an infusion of the HSP90 inhibitor radicicol (25 µg/kg; 10% DMSO and 10% ethanol in saline solution) (22). After 45 min of equilibrium, all measurements of GFR, RBF, urine flow, and MAP were repeated. At the end of the experiment, both kidneys were removed and quickly frozen for biochemical and molecular studies. To confirm our results with low-calorie commercial sugar, an additional group of six rats was included in which renal function before and after radicicol was evaluated by using 5% polyfructosan as a gold standard GFR marker (Inutest, Laevosan, Linz, Austria).

Low-calorie sugar concentrations in urine and plasma were determined by the technique of Davidson and Sackner (8) for determining GFR. Low-calorie sugar clearance was calculated by standard formula as we previously reported (23).

Urinary nitrites and nitrate excretion. The end products of NO, nitrites and nitrates (NO_2^- and NO_3^-), were estimated in 30-min urine samples by reducing NO_3^- to NO_2^- with nitrate reductase (Roche) and β -adenine nicotinamide (β -NADPH, Sigma), followed by nitrite quantification with the Griess reagent, as we (21) and others (6) previously reported.

Renal lipoperoxidation. Malondialdehyde (MDA), a measure of lipid peroxidation, was assayed in the form of thiobarbituric acid-reactive substances (TBARS) as previously described (20). Briefly, after homogenization of the renal tissue, the reaction was performed in a 0.8% aqueous solution of thiobarbituric acid in 15% TCA and heated at 95°C for 45 min. TBARS were quantified with an extinction coefficient of $1.56 \times 10^5 \text{ M}^{-1}/\text{cm}^{-1}$ and expressed as nanomoles of TBARS per milligram of protein. The tissue protein was estimated with the Bradford method.

Urinary hydrogen peroxide and isoprostan F_{2α} assays. The amount of hydrogen peroxide (H_2O_2) in urine was determined with an Amplex Red Hydrogen Peroxide/Peroxidase Assay Kit (Invitrogen) according to manufacturer's instructions. Briefly, the assay was performed with a standard curve of H_2O_2 1–10 µM. A 50-µl volume of each urine or standard was placed in a microplate, 50 µl of Amplex red reagent-horseradish peroxidase (HRP) was then added, and the samples were incubated for 30 min at room temperature and protected from light. The plate was read at 560 nm. The H_2O_2 concentration in the samples was expressed as nanomoles per milliliter.

The concentration of isoprostan F_{2α} (8-iso-PGF_{2α}) were determined in urine samples with a urinary 8-iso-PGF_{2α} ELISA assay from Northwest (Vancouver, WA) according to the manufacturer's instructions. Briefly, 100 µl of each sample or standard was placed in wells that contained the anti-8-iso-PGF_{2α} antibody, and 100 µl of 15-isoprostan F2T HRP enzyme conjugate was added. Then 200 µl of 3'3'5'-tetramethyl benzidine substrate was added to the wells and incubated again; the reaction was stopped by addition of 50 µl of 3 M H_2SO_4 , and

the wells were read at 450 nm. The isoprostan F_{2α} concentration was reported as nanograms per milliliter.

RNA isolation and real-time PCR. The renal cortex was isolated from both kidneys and snap frozen in liquid nitrogen. Total RNA was isolated from each kidney with the TRIzol method (Invitrogen) and checked for integrity by 1% agarose gel electrophoresis. To avoid DNA contamination, all total RNA samples were treated with DNase (Invitrogen). Reverse transcription (RT) was carried out with 2.5 µg of total RNA and 200 U of Moloney murine leukemia virus reverse transcriptase (Invitrogen). The mRNA levels of HSP90α and HSP90β as well as eNOS were quantified by real-time PCR on the ABI Prism 7300 Sequence Detection System (TaqMan, ABI, Foster City, CA). Primers and probes for HSP90α and eNOS were ordered as kits: Rn00822023-g1 and Rn02132634-s1 (Assays-on-Demand, ABI) and HSP90BRAT-X (Assay-on-Design, ABI) for HSP90β. As an endogenous control, we used eukaryotic 18S rRNA (predesigned assay reagent Applied by ABI, external run). Relative quantification of HSP90α, HSP90β, and eNOS gene expression was performed with the comparative threshold cycle (C_T) method (18).

Western blot analysis. Total renal proteins were isolated from six different cortices of each group and homogenized separately in lysis buffer [50 mM HEPES pH 7.4, 250 mM NaCl, 5 mM EDTA, 0.1% NP-40, and Complete protease inhibitor (Roche)]. Protein samples containing 50 µg of total protein were resolved by 7.5% SDS-PAGE, semidried, and electroblotted onto polyvinylidene difluoride membranes (Amersham). eNOS protein (Abcam, Cambridge, MA) or HSP90α transfected HEK cells were loaded as positive controls. Membranes were then blocked first with 0.1% blotting grade blocker nonfat dry milk (Bio-Rad) and incubated in 5% blotting grade blocker nonfat dry milk with their respective specific antibodies as detailed below. The lower part of the membranes was incubated with a goat anti-actin antibody (1:5,000 dilution) overnight at 4°C (Santa Cruz Biotechnology, Santa Barbara, CA). The upper membranes were incubated with polyclonal anti-rabbit HSP84 (HSP90β, Abcam), polyclonal anti-rabbit HSP86 (HSP90α, Abcam), anti-rabbit eNOS (Cell Signaling Technology), polyclonal anti-rabbit phosphorylated eNOS-S1177 (Cell Signaling Technology), or polyclonal anti-rabbit phospho-eNOST495 antibodies (Cell Signaling Technology). Membranes were then incubated with the secondary antibody HRP-conjugated rat anti-rabbit IgG (Alpha Diagnostics, San Antonio, TX). Proteins were detected with an enhanced chemiluminescence kit (Amersham) and autoradiography, following the manufacturer's recommendations.

The eNOS dimer-to-monomer ratio was evaluated by Western blot in nondenatured proteins isolated from cortices of both vehicle- and radicicol-infused animals as previously reported (4, 14). Nonboiled samples containing 50 µg of total protein were resolved in a 6% SDS-PAGE at 4°C. Proteins were transferred to a polyvinylidene difluoride membrane, and Western blot analysis for eNOS was performed as described above. The bands were scanned for densitometric analysis.

Statistical analysis. Results are presented as means \pm SE. Differences between control and experimental periods in the same group were tested by paired *t*-test. Significant differences among the groups were tested by ANOVA with Bonferroni's correction for multiple comparisons. Statistical significance was defined when the *P* value was <0.05 .

RESULTS

We evaluated the role of HSP90 in regulating renal function by acutely inhibiting HSP90 in rats with radicicol. Renal function was evaluated in each animal in two steps: during normal euvolemic conditions and during vehicle or radicicol infusion. All animals had similar body weight (control animals 303 ± 3.1 g, radicicol-infused animals 309 ± 2.8 g). Radicicol infusion produced a significant reduction in RBF, from 8.6 ± 1.1 to 5.6 ± 0.3 ml/min (*P* = 0.01), which represents a

decrease of 35%. In contrast, left RBF did not change during vehicle infusion in the control group (Fig. 1B). Furthermore, HSP90 inhibition was also associated with a significant reduction in GFR (Fig. 1C). Thus GFR decreased from 2.0 ± 0.2 ml/min during the basal period to 1.2 ± 0.2 ml/min during the radicicol infusion ($P = 0.002$), representing a 40% reduction in renal function. As expected, GFR was not modified by vehicle infusion in the control group. Although we previously demonstrated that low-calorie sugar is a sensitive and accurate GFR marker, we confirmed our previous findings in a group of rats in which a gold standard Inutest was infused to evaluate GFR in the absence and in the presence of radicicol. Similar to our observations with low-calorie sugar, radicicol infusion produced a similar extent of reduction in RBF from 8.7 ± 0.5 to 5.6 ± 0.3 ml/min ($P = 0.002$) and in GFR from 1.9 ± 0.5 to 1.3 ± 0.4 ml/min ($P = 0.001$). The results obtained with both GFR markers suggest that HSP90 inhibition produces renal vasoconstriction that is responsible for GFR reduction. Since MAP was monitored throughout the experiment, we observed that during basal period both groups had similar MAP, which vehicle infusion did not modify (Fig. 1A). In contrast, radicicol infusion produced a slight but significant reduction in MAP values compared with the basal period. Accordingly, MAP in the basal period was 117 ± 3.8 mmHg and decreased to 102 ± 8.5 mmHg during HSP90 inhibition ($P = 0.004$). This reduction represents a fall of 12.9%, which remains, however, within a renal autoregulatory range that cannot explain the fall in 35% fall in GFR. Interestingly, this systemic effect of radicicol was the opposite of what would be expected as a consequence of uncoupling eNOS and HSP90. It is not known, however, whether all vascular beds are similarly sensitive to the uncoupling effect of radicicol. Because kidneys have a higher blood flow than many other organs, it is possible that their sensitivity to vasoactive factors would be greater.

It has been shown that HSP90 inhibitors, such as radicicol or geldanamycin, may induce the overexpression of HSP90 by releasing heat shock factor 1 (HSF1), which is responsible for transcriptional activation of the heat shock genes (3, 11). Although this effect is observed after several hours of HSP90 inhibition, we first evaluated whether the expression of

HSP90 α and HSP90 β remained unaltered after acute HSP90 inhibition. Radicicol did not modify HSP90 α and HSP90 β mRNA levels in renal cortex compared with the expression observed in vehicle-infused animals (Fig. 2, A and B). Accordingly, no differences were found in HSP90 α and HSP90 β protein levels between groups (Fig. 2, C and D).

To investigate whether renal vasoconstriction induced by HSP90 inhibition by radicicol was mediated by either reduced NO availability or increased generation of reactive oxygen species, we evaluated urinary nitrite and nitrate excretion (UNO₂/NO₃V), renal lipoperoxidation, and the amount of isoprostan F_{2 α} and hydrogen peroxide in the urine. As shown in Fig. 3A, radicicol infusion produced a significant decrease in urinary NO metabolites by 58%. This effect was not observed in the animals that received vehicle infusion. At the end of the experiment, renal lipoperoxidation was measured in the cortex and medulla separately (Fig. 3B). In contrast to the effect on NO metabolite excretion, HSP90 inhibition did not modify MDA values compared with those in vehicle-infused animals. In addition, greater lipoperoxidation levels were observed in the medulla than in the cortex in both groups. These findings could be expected because of the higher hypoxia in the medullary region. To confirm the absence of change in oxidative stress rate, more specific assays, such as isoprostanes and hydrogen peroxide, were used. Figure 3, C and D, show that HSP90 inhibition did not modify urinary hydrogen peroxide and isoprostan F_{2 α} , respectively, confirming our observations at the tissue level. Together, these results suggest that the observed GFR reduction induced by acute radicicol infusion was, in part, mediated by a decrease in NO generation rather than an increase in oxidative stress.

To evaluate whether NO reduction by radicicol was mediated by changes in eNOS expression and phosphorylation, we evaluated renal eNOS mRNA and protein levels by real-time PCR and Western blot. We also evaluated Ser1177 and Thr497 eNOS phosphorylation in the renal cortex of vehicle- and radicicol-infused animals by using phospho-specific antibodies against each site. We found that eNOS mRNA levels were not modified by either vehicle or radicicol infusion (Fig. 4A). Similar results were observed when eNOS protein levels were

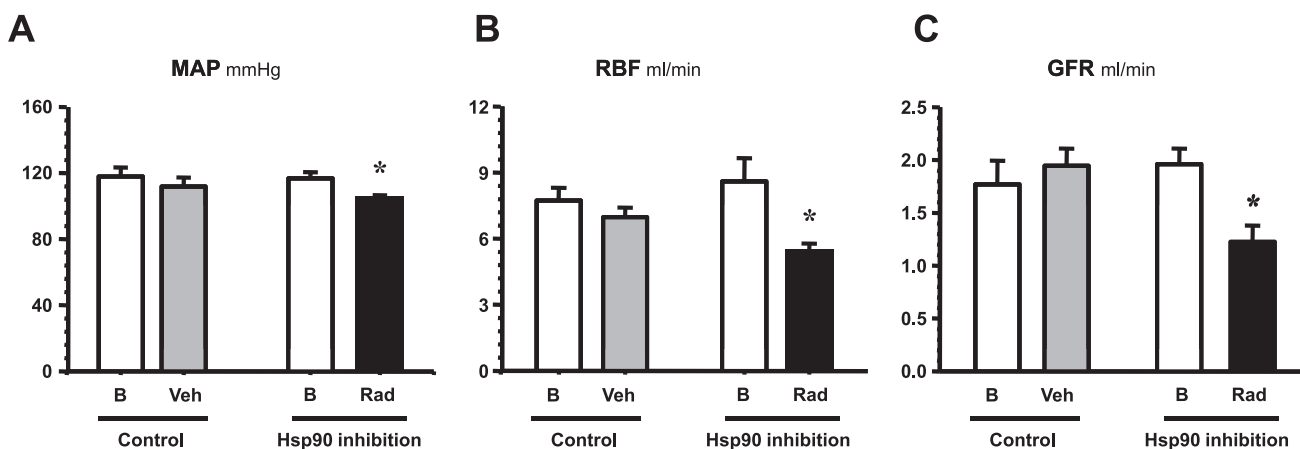


Fig. 1. Effect of heat shock protein (HSP)90 inhibition on renal function. A: mean arterial blood pressure (MAP). B: mean renal blood flow (RBFI) recorded by a renal artery ultrasonic probe. C: mean glomerular filtration rate (GFR) evaluated with a GFR marker. Open bars, basal (B) period before vehicle or radicicol infusion; gray bars, vehicle (Veh) infusion period; filled bars, radicicol (Rad) infusion period. Statistical differences between basal and experimental periods were tested by paired *t*-test; * $P < 0.05$.

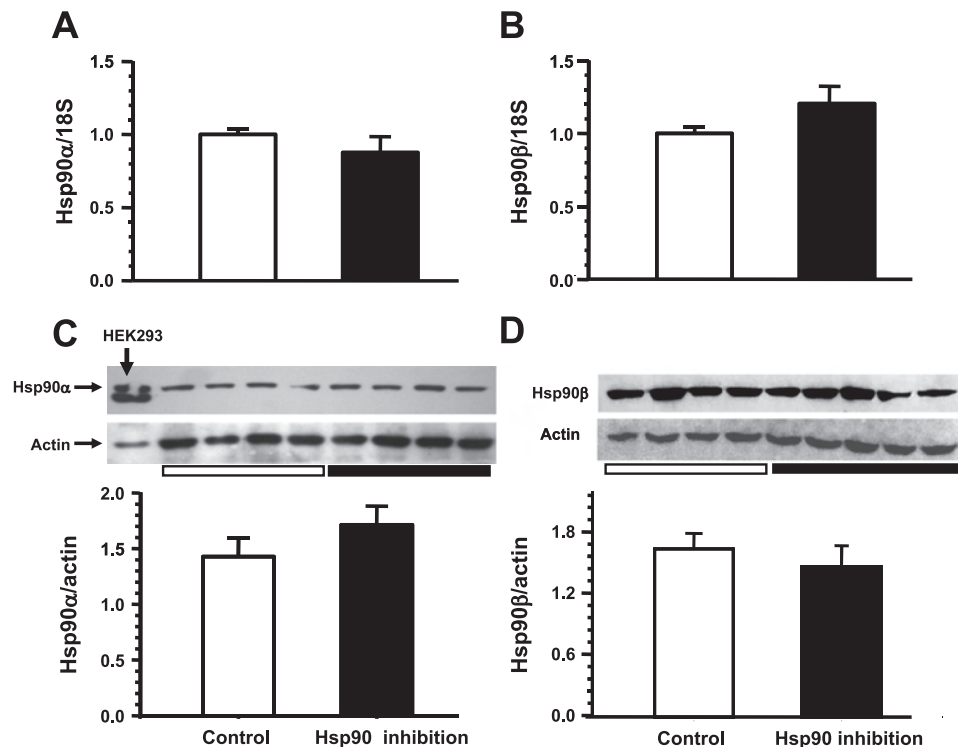


Fig. 2. Effect of acute radicicol infusion on renal HSP90 α and HSP90 β expression. *A* and *B* show real-time RT-PCR analysis of HSP90 α and HSP90 β , respectively, normalized by 18S in control (open bars) and acute radicicol-infused (filled bars) rats. HSP90 α and HSP90 β protein levels were also assessed by Western blot analysis. *C* and *D*: mean optical density ratio between each HSP90 and actin. Proteins extracted from human embryonic kidney cells (HEK293) transfected with HSP90 α were included as positive control. Insets, representative digitalized images of HSP90 α and HSP90 β and their respective actins.

assessed, as represented by Western blot and densitometry analysis (Fig. 4*B*). In contrast, a significant increase in eNOS phosphorylation at Thr495 was observed. The immunodetection signal of eNOS phosphorylated at Thr495 was increased in rats infused with radicicol (Fig. 4*C*). The mean ratio of eNOS phosphorylated at Thr495 to actin during HSP90 inhibition was 0.78 ± 0.12 compared with 0.47 ± 0.18 in vehicle-infused animals ($P < 0.02$). In contrast, radicicol infusion did not produce any effect on Ser1177 eNOS phosphorylation (Fig. 4*D*). The mean ratio of eNOS phosphorylated at S1177 to actin was similar in vehicle- and radicicol-infused rats (0.59 ± 0.14 and 0.57 ± 0.13 , respectively). Since eNOS expression levels did not change by radicicol infusion, the ratios of pThr495-eNOS/eNOS and pS1177-eNOS/eNOS.

It has also been demonstrated that eNOS activation requires the formation of its dimeric form since monomers exhibit significantly lower activity (1, 15). In this study, we also evaluated whether HSP90 inhibition modified the ratio of the monomeric vs. the dimeric state of eNOS. We observed that HSP90 inhibition was associated with a significant increase in monomeric eNOS together with a reduction in the dimeric form when proteins were analyzed under nondenatured conditions (Fig. 5*A*). This was confirmed by densitometric analysis of the bands corresponding to dimeric and monomeric eNOS forms in the renal cortex (Fig. 5, *B* and *C*). As a result, the ratio between the dimeric and monomeric forms was significantly reduced, from 1.74 ± 0.32 in vehicle-infused rats to 0.33 ± 0.07 in radicicol-infused rats (Fig. 5*D*; $P < 0.05$).

DISCUSSION

In this study, we have shown that infusion of the HSP90 inhibitor radicicol produced a significant decrease in RBF and GFR, which was associated with a decrease in the excretion of

NO metabolites in the urine. Reduction in NO synthesis seems to be a consequence of an increase in inactivating eNOS phosphorylation and the concomitant increase in eNOS monomerization. Thus our results suggest that HSP90 is an important modulator of GFR by favoring the renal NO/eNOS system.

Molecular chaperones can assist in the folding and maintenance of newly translated proteins, activate proteins through promoting their phosphorylation or protein-protein interactions, and also lead to degradation of misfolded and destabilized proteins. Indeed, HSP90 is a key member of this machinery. It plays a central role in cellular signaling since it is essential for maintaining the activity of several signaling proteins, including steroid hormone receptors and enzymes such as eNOS.

Previous studies have shown that the association of HSP90 with eNOS plays a key role in the generation of NO through several mechanisms, including enhancing eNOS enzymatic activity, modulating the release of NO vs. superoxide by eNOS, assisting with the intracellular trafficking of eNOS, and helping to activate eNOS by dissociating it from caveolin-1 (16). Furthermore, HSP90 has been proposed to facilitate the calcineurin-dependent dephosphorylation of the Thr495 site of eNOS, which contributes to enzyme activity (16). In this study, we found that the acute infusion of radicicol, an HSP90 inhibitor, produced decreases in RBF and GFR that were associated with a significant decrease in the urinary excretion of NO metabolites ($\text{UNO}_2/\text{NO}_3\text{V}$), suggesting that eNOS-HSP90 uncoupling resulted in reduced NO synthesis that, in turn, promoted renal vasoconstriction. In support of this observation, recent findings by Xu et al. (34) demonstrated that disruption of the eNOS-HSP90 complex with decoy peptides that block the interaction between HSP90 and eNOS inhibited eNOS-dependent NO generation and reduced acetylcholine-

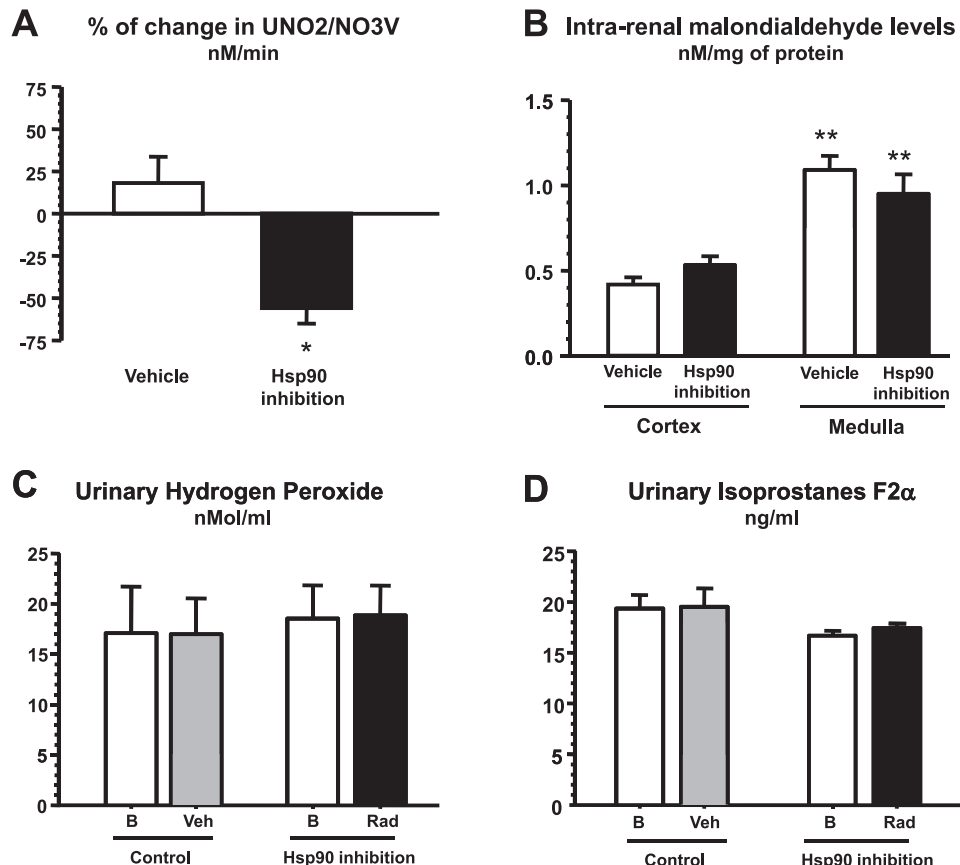


Fig. 3. Effect of HSP90 inhibition on nitric oxide (NO) metabolite excretion and oxidative stress. *A*: % change in urinary nitrite and nitrate excretion (UNO₂/NO₃V) after vehicle (open bars) and HSP90 inhibition with radicicol (filled bars). *B*: malondialdehyde levels quantified in renal cortex and medulla homogenates. Open bars, vehicle control group; filled bars, radicicol-infused group. *C* and *D*: urinary hydrogen peroxide (*C*) and isoprostane F₂ α (*D*) levels quantified in vehicle control group during basal period and vehicle infusion (open and gray bars, respectively). These determinations were also assayed in the rats before and during HSP90 inhibition (open and filled bars, respectively). Statistical differences between groups were tested by unpaired *t*-test and between the renal cortex and medulla by paired *t*-test. **P* < 0.05 vs. vehicle control group, ***P* < 0.05 vs. renal cortex.

induced vasodilation in mouse facialis arteries. In addition, it has been shown that inhibition of HSP90 not only decreases stimulated NO synthesis but also increases superoxide anion generation, which has been shown to be dependent on eNOS (10, 24, 34). These reports indicated that inhibiting eNOS-HSP90 coupling shifts the product of eNOS from NO to O₂⁻. In this regard, we observed that acute HSP90 inhibition was associated with decreased NO synthesis rather than increased oxidative stress that was measured by renal lipoperoxidation and urinary H₂O₂ and isoprostanes F₂ α , suggesting that renal vasoconstriction was in part due to the reduction of NO availability, although other pathways regulated by HSP90 might be involved, considering that several proteins are regulated by HSP90. In this regard, it has been shown that HSP90 also activates neuronal nitric oxide synthase (nNOS) (2, 29). NO derived from nNOS, present in macula densa cells, might regulate glomerular blood flow and GFR by modulating afferent arteriolar vascular tone (for review, see Ref. 33); thus it is also plausible that HSP90 inhibition could inactivate nNOS and this effect could be also involved in the observed reduction of GFR. Further experiments with specific nNOS inhibitors or nNOS-null mice will be required to clarify this issue. However, in the present study we observed several changes in eNOS-NO pathway, suggesting that at least part of the radicicol effect must be due to its effect on eNOS.

To investigate the mechanism by which HSP90 inhibition produced a decrease in NO metabolites, we evaluated eNOS phosphorylation and dimerization. Several putative eNOS phosphorylation sites have been reported. The most studied are the Ser1177 site, which activates eNOS, and the Thr495 site, which

inactivates it. This threonine residue is found in the calcium-calmodulin (CaM) binding domain and interferes with CaM binding, resulting in the inactivation of eNOS (19, 31). In this regard, coupling of HSP90 and eNOS is associated with enhanced Ser1177 phosphorylation by Akt (32), whereas uncoupling of eNOS-HSP90 promotes Thr495 phosphorylation by protein kinase C (19). In this study, we observed that radicicol infusion did not alter Ser1177 phosphorylation but was able to increase Thr495 phosphorylation without changing eNOS protein levels. This finding suggests that reduced NO synthesis by HSP90 inhibition is at least due to reduction of eNOS activity that follows augmented Thr495 phosphorylation.

Not only is activation of eNOS dependent on phosphorylation state by upstream kinases, but it is also determined by its conformational state (13). It is known that NO is produced by eNOS when it is conformed as a homodimer. This conformation creates high-affinity binding sites for the NOS substrate L-arginine, enabling electron transfer from the reductase domain of one NOS monomer to the oxygenase domain of the other monomer (28). Interestingly, we observed that acute infusion of radicicol produced a significant reduction of the dimer-to-monomer ratio due to an increase in eNOS monomers. This observation suggests that, in addition to eNOS phosphorylation at the Thr497 site, inhibition of HSP90 with radicicol reduces NO production by preventing the formation of eNOS homodimers.

The physiological relevance of eNOS-HSP90 uncoupling has been recently attested in experimental models of disease, such as diabetes mellitus, arterial hypertension, and liver cirrhosis. Diabetes is characterized by NO deficiency. Lei et al. (17) demon-

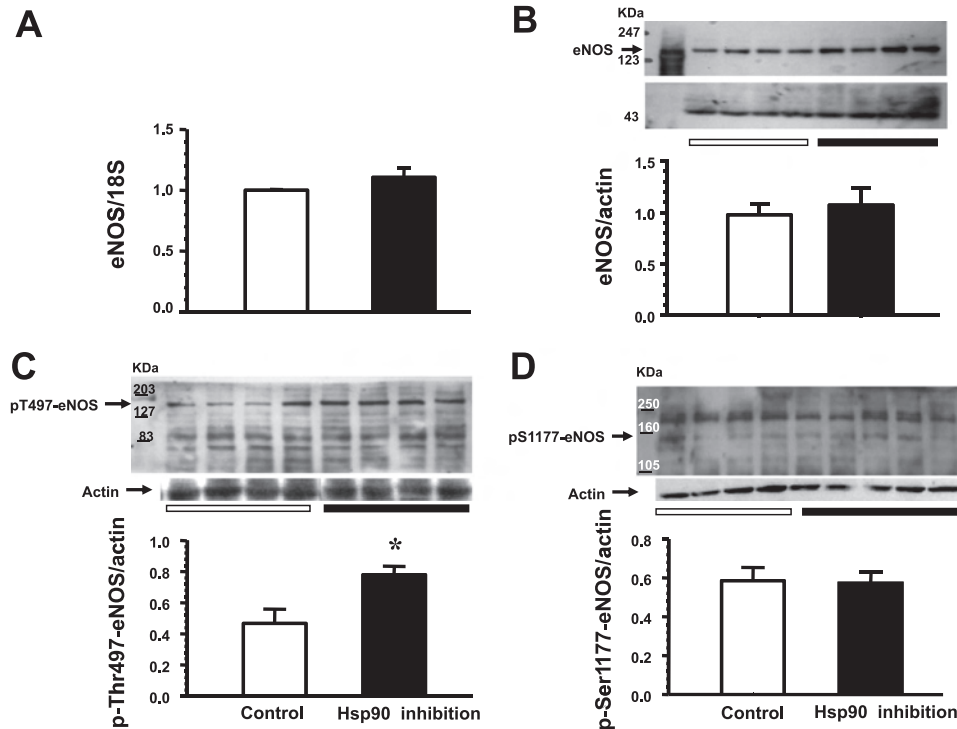


Fig. 4. Effect of radicicol administration on endothelial nitric oxide synthase (eNOS) expression and eNOS phosphorylation was evaluated by real time RT-PCR and Western blot analysis using specific eNOS and phosphorylated eNOS antibodies. *A* and *B*: eNOS/18S mRNA (*A*) and eNOS/actin protein (*B*) levels were not altered by radicicol infusion (filled bars), compared with vehicle-treated rats (open bars). First lane, eNOS purified protein as positive control. *C*: in contrast, eNOS phosphorylation in the threonine 497 site (pT497-eNOS) was significantly increased during HSP90 inhibition. *D*: eNOS phosphorylation in the serine 1177 site (pS1177-eNOS) was not altered by radicicol infusion. *B–D*: mean optical density of each Western blot assessed. Protein markers were loaded in each assay as described in MATERIALS AND METHODS. Insets, representative digitalized images of Western blot analysis. Statistical differences between groups were tested by unpaired *t*-test; **P* < 0.05.

strated that, in streptozotocin-induced diabetic rats, high levels of glucose increased phosphorylation of HSP90 α in a cAMP-protein kinase A-dependent manner, an effect that was associated with translocation of HSP90 α to the aortic endothelium membrane. The consequence of this translocation was the reduction of NO synthesis due to eNOS-HSP90 uncoupling.

The arterial hypertension that occurs during pregnancy known as preeclampsia is, in part, mediated by an increase in endothelial oxidative stress in maternal vasculature. To explain the mechanism, Gu et al. (12) demonstrated that HSP90 protein expression was significantly decreased in endothelial cells from preeclamptic women, which corre-

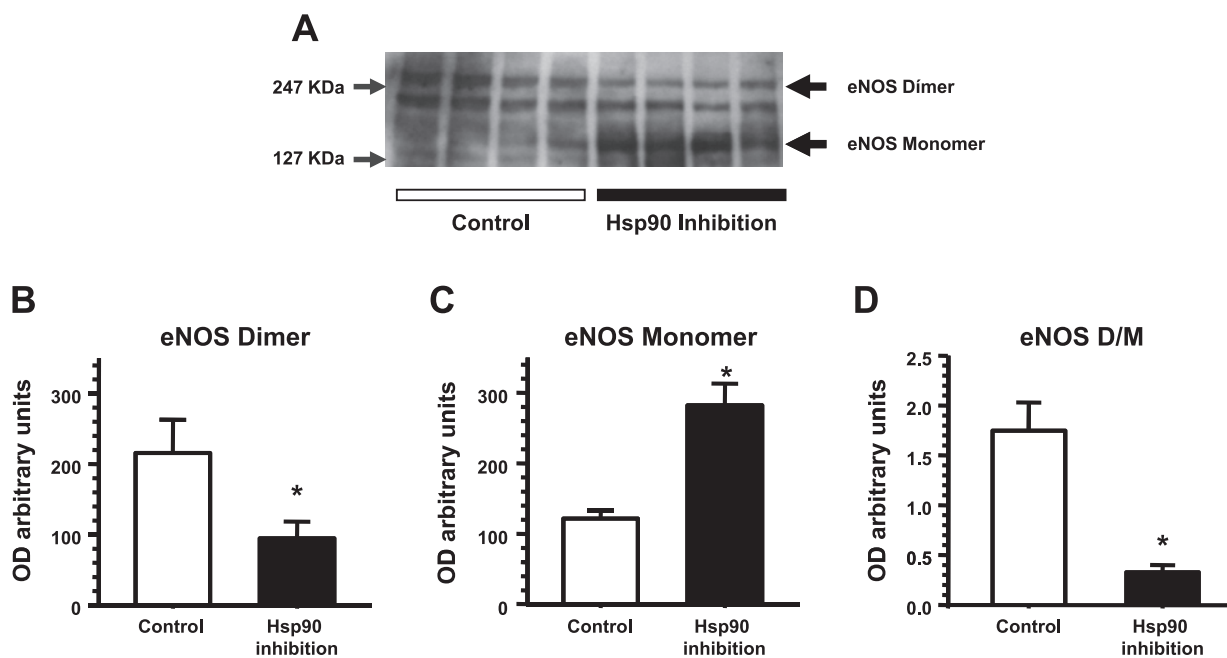


Fig. 5. Effect of HSP90 inhibition on the expression of eNOS protein dimer/monomer. *A*: representative image of a Western blot analysis of nondenatured proteins isolated from cortices of vehicle control and radicicol-treated rats. *B–D*: dimeric eNOS (*B*), monomeric eNOS (*C*), and eNOS dimer-to-monomer ratio (D/M; *D*) in vehicle (open bars) and radicicol-infused (filled bars) animals. Statistical differences between groups were tested by unpaired *t*-test; **P* < 0.05. OD, optical density.

lated with greater superoxide generation. In addition, a more recent study reported that hypertension and endothelial dysfunction induced by increased production of 20-hydroxyeicosatetraenoic acid (20-HETE), a major vasoconstrictor eicosanoid in the microcirculation, were in part due to eNOS-HSP90 uncoupling (7).

Finally, another pathophysiological role for eNOS-HSP90 coupling/uncoupling was observed in rats with hepatopulmonary syndrome, a complication of cirrhosis that is characterized by overproduction of NO in lungs and NO deficiency in the liver. In an elegant study, Frossard et al. (9) showed an opposite regulation of eNOS by HSP90 since greater NO synthesis in the lungs was associated with elevated eNOS and HSP90 interaction, whereas the contrary effect was observed in liver homogenates, in which NO production was decreased. Thus lesser NO production in the liver was attributed to eNOS-HSP90 uncoupling together with enhanced association of eNOS to the caveolin. Together, these studies indicate that HSP90-eNOS coupling/uncoupling ratio may play a major role in several pathophysiological conditions. Thus it will be interesting to study the role that HSP90-eNOS coupling/uncoupling could play in the progression of kidney diseases, such as diabetic or hypertensive nephropathy, in which renal vascular dysfunction plays a major role.

ACKNOWLEDGMENTS

We thank Rosalba Pérez for technical assistance and all members of the Molecular Physiology Unit for enthusiastic comments.

Part of this work was presented at Experimental Biology 2006, San Francisco, CA.

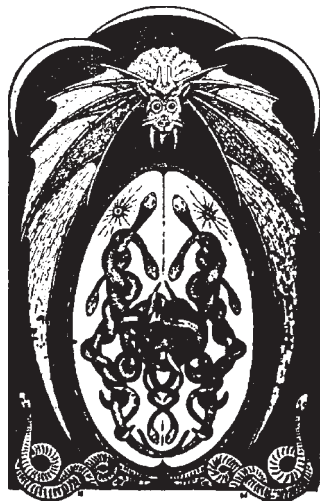
GRANTS

This work was supported by Grants IN228206-3 of the National University of Mexico and 48483 of the Mexican Council of Science and Technology to N. A. Bobadilla.

REFERENCES

- Antoniades C, Shirodaria C, Warrick N, Cai S, de Bono J, Lee J, Leeson P, Neubauer S, Ratnatunga C, Pillai R, Refsum H, Channon KM. 5-Methyltetrahydrofolate rapidly improves endothelial function and decreases superoxide production in human vessels: effects on vascular tetrahydrobiopterin availability and endothelial nitric oxide synthase coupling. *Circulation* 114: 1193–1201, 2006.
- Bender AT, Silverstein AM, Demady DR, Kanelakis KC, Noguchi S, Pratt WB, Osawa Y. Neuronal nitric-oxide synthase is regulated by the Hsp90-based chaperone system in vivo. *J Biol Chem* 274: 1472–1478, 1999.
- Bharadwaj S, Ali A, Ovsenek N. Multiple components of the HSP90 chaperone complex function in regulation of heat shock factor 1 in vivo. *Mol Cell Biol* 19: 8033–8041, 1999.
- Cai S, Khoo J, Musso S, Alp NJ, Channon KM. Endothelial nitric oxide synthase dysfunction in diabetic mice: importance of tetrahydrobiopterin in eNOS dimerisation. *Diabetologia* 48: 1933–1940, 2005.
- Caplan AJ, Jackson S, Smith D. Hsp90 reaches new heights. *EMBO Rep* 4: 126–130, 2003.
- Chatterjee PK, Patel NS, Kvale EO, Cuzzocrea S, Brown PA, Stewart KN, Mota-Filipe H, Thiemermann C. Inhibition of inducible nitric oxide synthase reduces renal ischemia/reperfusion injury. *Kidney Int* 61: 862–871, 2002.
- Cheng J, Ou JS, Singh H, Falck JR, Narsimhaswamy D, Pritchard KA, Schwartzman ML. 20-Hydroxyeicosatetraenoic acid causes endothelial dysfunction via eNOS uncoupling. *Am J Physiol Heart Circ Physiol* 294: H1018–H1026, 2008.
- Davidson DW, Sackner MA. Simplification of the anthrone method for the determination of inulin in clearance studies. *J Lab Clin Med* 62: 351–356, 1963.
- Frossard JL, Schiffer E, Cikirkcioglu B, Bourquin J, Morel DR, Pastor CM. Opposite regulation of endothelial NO synthase by HSP90 and caveolin in liver and lungs of rats with hepatopulmonary syndrome. *Am J Physiol Gastrointest Liver Physiol* 293: G864–G870, 2007.
- Garcia-Cardena G, Fan R, Shah V, Sorrentino R, Cirino G, Papapetropoulos A, Sessa WC. Dynamic activation of endothelial nitric oxide synthase by Hsp90. *Nature* 392: 821–824, 1998.
- Griffin TM, Valdez TV, Mestril R. Radicicol activates heat shock protein expression and cardioprotection in neonatal rat cardiomyocytes. *Am J Physiol Heart Circ Physiol* 287: H1081–H1088, 2004.
- Gu Y, Lewis DF, Zhang Y, Groome LJ, Wang Y. Increased superoxide generation and decreased stress protein Hsp90 expression in human umbilical cord vein endothelial cells (HUVECs) from pregnancies complicated by preeclampsia. *Hypertens Pregnancy* 25: 169–182, 2006.
- Hellermann GR, Solomonson LP. Calmodulin promotes dimerization of the oxygenase domain of human endothelial nitric-oxide synthase. *J Biol Chem* 272: 12030–12034, 1997.
- Clatt P, Schmidt K, Lehner D, Glatter O, Bachinger HP, Mayer B. Structural analysis of porcine brain nitric oxide synthase reveals a role for tetrahydrobiopterin and L-arginine in the formation of an SDS-resistant dimer. *EMBO J* 14: 3687–3695, 1995.
- Komers R, Schutzer WE, Reed JF, Lindsley JN, Oyama TT, Buck DC, Mader SL, Anderson S. Altered endothelial nitric oxide synthase targeting and conformation and caveolin-1 expression in the diabetic kidney. *Diabetes* 55: 1651–1659, 2006.
- Kupatt C, Dassy C, Hinkel R, Raake P, Daneau G, Bouzin C, Bocksteges P, Feron O. Heat shock protein 90 transfection reduces ischemia-reperfusion-induced myocardial dysfunction via reciprocal endothelial NO synthase serine 1177 phosphorylation and threonine 495 dephosphorylation. *Arterioscler Thromb Vasc Biol* 24: 1435–1441, 2004.
- Lei H, Venkatakrishnan A, Yu S, Kazlauskas A. Protein kinase A-dependent translocation of Hsp90alpha impairs endothelial nitric-oxide synthase activity in high glucose and diabetes. *J Biol Chem* 282: 9364–9371, 2007.
- Livak KJ, Schmittgen TD. Analysis of relative gene expression data using real-time quantitative PCR and the $2^{-\Delta\Delta CT}$ method. *Methods* 25: 402–408, 2001.
- Matsubara M, Hayashi N, Jing T, Titani K. Regulation of endothelial nitric oxide synthase by protein kinase C. *J Biochem (Tokyo)* 133: 773–781, 2003.
- Mejia-Vilet JM, Ramirez V, Cruz C, Uribe N, Gamba G, Bobadilla NA. Renal ischemia-reperfusion injury is prevented by the mineralocorticoid receptor blocker spironolactone. *Am J Physiol Renal Physiol* 293: F78–F86, 2007.
- Munoz-Fuentes RM, Vargas F, Bobadilla NA. Assay validation for determining nitrates and nitrites in biological fluids. *Rev Invest Clin* 55: 670–676, 2003.
- Pereira P, Ardenghi P, de Souza MM, Choi H, Moletta B, Izquierdo I. Effects of infusions of the tyrosine kinase inhibitor radicicol into the hippocampus on short- and long-term memory of the inhibitory avoidance task. *Behav Pharmacol* 12: 299–302, 2001.
- Perez-Rojas JM, Blanco JA, Gamba G, Bobadilla NA. Low calorie commercial sugar is a sensitive marker of glomerular filtration rate. *Kidney Int* 68: 1888–1893, 2005.
- Pritchard KA Jr, Ackerman AW, Gross ER, Stepp DW, Shi Y, Fontana JT, Baker JE, Sessa WC. Heat shock protein 90 mediates the balance of nitric oxide and superoxide anion from endothelial nitric-oxide synthase. *J Biol Chem* 276: 17621–17624, 2001.
- Prodromou C, Pearl LH. Structure and functional relationships of Hsp90. *Curr Cancer Drug Targets* 3: 301–323, 2003.
- Ramirez V, Uribe N, Garcia-Torres R, Castro C, Rubio J, Gamba G, Bobadilla NA. Upregulation and intrarenal redistribution of heat shock proteins 90alpha and 90beta by low-sodium diet in the rat. *Cell Stress Chaperones* 9: 198–206, 2004.
- Sagami I, Daff S, Shimizu T. Intra-subunit and inter-subunit electron transfer in neuronal nitric-oxide synthase: effect of calmodulin on heterodimer catalysis. *J Biol Chem* 276: 30036–30042, 2001.
- Song Y, Zweier JL, Xia Y. Determination of the enhancing action of HSP90 on neuronal nitric oxide synthase by EPR spectroscopy. *Am J Physiol Cell Physiol* 281: C1819–C1824, 2001.

30. Soti C, Nagy E, Giricz Z, Vigh L, Csermely P, Ferdinand P. Heat shock proteins as emerging therapeutic targets. *Br J Pharmacol* 146: 769–780, 2005.
31. Sugimoto M, Nakayama M, Goto TM, Amano M, Komori K, Kaibuchi K. Rho-kinase phosphorylates eNOS at threonine 495 in endothelial cells. *Biochem Biophys Res Commun* 361: 462–467, 2007.
32. Takahashi S, Mendelsohn ME. Synergistic activation of endothelial nitric-oxide synthase (eNOS) by HSP90 and Akt: calcium-independent eNOS activation involves formation of an HSP90-Akt-CaM-bound eNOS complex. *J Biol Chem* 278: 30821–30827, 2003.
33. Tojo A, Onozato ML, Fujita T. Role of macula densa neuronal nitric oxide synthase in renal diseases. *Med Mol Morphol* 39: 2–7, 2006.
34. Xu H, Shi Y, Wang J, Jones D, Weilrauch D, Ying R, Wakim B, Pritchard KA Jr. A heat shock protein 90 binding domain in endothelial nitric-oxide synthase influences enzyme function. *J Biol Chem* 282: 37567–37574, 2007.



ARTÍCULO DE REVISIÓN

Significado funcional de las proteínas de choque térmico de 90 kDa

Carlo César Cortés-González,* Victoria Ramírez-González,* Ana Carolina Ariza,* Norma A. Bobadilla*

* Unidad de Fisiología Molecular, Instituto de Investigaciones Biomédicas,
Universidad Nacional Autónoma de México e Instituto Nacional de Ciencias Médicas y Nutrición Salvador Zubirán.

Functional significance of heat shock protein 90

ABSTRACT

The heat shock protein 90 kDa (Hsp90) subfamily is constituted by five isoforms, among them Hsp90 α and Hsp90 β are the more abundant cytosolic proteins. These two proteins are molecular chaperons that participate in numerous cellular processes, through interacting with more than 100 proteins known as client proteins of Hsp90. These client proteins include: transcriptional factors, kinase proteins and other proteins that participate in transcriptional and transductional regulation such as steroid hormone receptors and nitric oxide synthases. This review offers a retrospective in the recent information about molecular and cellular functions of Hsp90 in the vascular physiology. In addition, the studies that evaluate Hsp90 role in the renal physiology and pathophysiology are discussed. Finally, the molecular tools developed to manipulate the Hsp90 expression in vitro and in vivo, through its inhibition or over-expression are reviewed. All these studies together have allowed increasing our knowledge regarding the role of Hsp90 during normal and pathophysiological conditions.

Key words. Vascular physiology. Endothelial nitric oxide synthase. Nitric oxide. Superoxide anion. Renal pathophysiology.

INTRODUCCIÓN

Existen diferentes condiciones y factores externos que pueden desequilibrar la homeostasis como lo son: cambios en la temperatura, osmolaridad, pH, entre otros. De tal forma que cada célula está constantemente expuesta a diversas condiciones de estrés que se acentúan durante procesos fisiopatológicos. Ante estas condiciones, las células desarrollaron un mecanismo evolutivo para detectar, monitorear y responder a cambios extremos del

RESUMEN

La subfamilia de proteínas de choque térmico de 90 kDa (Hsp90) está compuesta por cinco isoformas, dentro de las cuales las dos isoformas citosólicas más abundantes se conocen como la Hsp90 α y la Hsp90 β . Estas proteínas son conocidas como chaperonas moleculares y regulan diferentes procesos celulares a través de interactuar con más de 100 proteínas conocidas como proteínas cliente de Hsp90. Dentro de las proteínas cliente destacan: factores de transcripción, proteínas cinasas y proteínas que participan en la regulación transcripcional y trasduccional de señales, tales como el receptor de hormonas esteroideas y las sintetasas de óxido nítrico. Esta revisión ofrece una retrospectiva sobre el avance en el conocimiento de las funciones celulares y moleculares de Hsp90 en la fisiología vascular. También se describen los estudios que han intentado esclarecer la participación de Hsp90 en la fisiología y la fisiopatología renal. Al mismo tiempo, se revisan las herramientas moleculares alternativas que se han desarrollado con el fin de manipular la expresión de Hsp90 *in vitro* e *in vivo*, mediante su inhibición o su sobre-expresión, lo que ha permitido incrementar nuestro conocimiento sobre esta subfamilia de proteínas en condiciones normales y durante procesos fisiopatológicos.

Palabras clave. Fisiología vascular. Sintasa de óxido nítrico endotelial. Óxido nítrico. Anión superóxido. Fisiopatología renal.

medio ambiente con el fin de mantener la homeostasis celular.¹⁻⁴

En situaciones de estrés celular, la síntesis proteica se ve afectada dando lugar a proteínas mal plegadas o con una conformación inadecuada, lo que puede propiciar la formación de agregados proteicos no funcionales y comprometer la viabilidad celular. En estas condiciones se activa la transcripción de genes que principalmente está dirigida hacia proteínas reparadoras conocidas como proteínas de choque térmico (Hsp), lo que inicia la reparación

proteica y la activación de vías de señalización que permiten una mejor adaptación al estado de estrés en el que se encuentra la célula.⁴

En la década de los sesenta, Ritossa, *et al.*⁵ demostraron por primera vez la presencia de las proteínas de choque térmico en las glándulas salivales de *Drosophila melanogaster*. En este estudio, se observó que un incremento súbito en la temperatura aumentaba la expresión de una familia de genes, que más tarde se denominó como proteínas de estrés. Durante los siguientes años, se demostró que esta respuesta al estrés se encuentra conservada desde las bacterias hasta los mamíferos. A partir de este momento se abrió un campo nuevo de estudio para la caracterización de las Hsp y de los procesos celulares en los que intervienen estas proteínas.

LAS PROTEÍNAS DE CHOQUE TÉRMICO

Las proteínas de choque térmico pertenecen a una familia multigénica con un peso molecular que varía entre los 10 y los 150 kDa. Se han clasificado de acuerdo a su peso molecular en seis subfamilias: la Hsp de 100-110 kDa, la de 90 kDa, la de 70 kDa, la de 60 kDa, la de 40 kDa y la subfamilia de Hsp's con peso molecular de 18-30 kDa.^{6,7} Estas proteínas se encuentran tanto en organismos procariontes como eucariontes y presentan una alta homología a nivel de secuencia nucleotídica y de aminoácidos. Se encuentran principalmente en el citosol y su principal función es mantener la homeostasis celular y evitar el daño proteotóxico. Durante condiciones adversas la expresión de algunas subfamilias de Hsp aumenta con el fin de reparar las proteínas dañadas. En este proceso, las Hsp pueden ensamblar correctamente a las proteínas parcialmente dañadas y degradar a las que fueron dañadas irreversiblemente.

PROTEÍNAS DE CHOQUE TÉRMICO DE 90 KDA (Hsp90)

Una de las subfamilias más abundantes son las proteínas de choque térmico de 90 kDa, objeto de nuestra revisión. Las Hsp90 comprenden de 1 a 2% de la proteína citosólica total y su expresión puede llegar a aumentar hasta 15% en condiciones de estrés celular. Hasta el momento, se han descrito cinco isoformas de Hsp90: la Grp94, la Hsp90N, la TRAP1, la Hsp90 α y la Hsp90 β que se diferencian básicamente por su localización intracelular. La Hsp90 α y la Hsp90 β se encuentran en el citosol, a diferencia de las otras isoformas que se encuentran asociadas a organelos. Estas dos isoformas com-

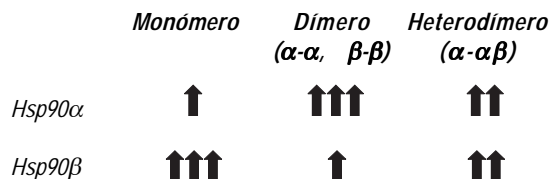
prenden 80% de esta subfamilia y son las encargadas de modular la mayoría de sus acciones intracelulares.^{8,9}

La Hsp90 α y la Hsp90 β mantienen hasta 85% de identidad a nivel de proteína. En condiciones fisiológicas, la proporción de Hsp90 α es menor en comparación con Hsp90 β , ya que mientras la primera constituye 40% de la proteína total citosólica de Hsp90, la segunda conforma 60%.¹⁰ Ambas isoformas pueden encontrarse en forma monomérica, dimérica o heterodimérica, como se ilustra en la figura 1A. La Hsp90 α se encuentra en mayor proporción en forma dimérica, mientras que la Hsp90 β principalmente en forma monomérica. Es importante mencionar que la conformación dimérica de Hsp90 es la forma funcional.¹¹

El gene para Hsp90 α consta de 10 exones que codifican para un transcripto de 5.3 Kb, lo que da lugar a una proteína de 733 aminoácidos con un peso molecular de 86 kDa. A pesar de que el gene de Hsp90 β consta de 11 exones y el transcripto es de 6.8 Kb, la proteína resultante es más pequeña, formada por 726 aminoácidos con un peso molecular de 84 kDa.² Los genes que codifican para estas proteínas se localizan en distintos cromosomas dentro del genoma. El primer exón en ambas isoformas no se traduce, pero aún se desconoce la razón de esta omisión en la transcripción. Se ha observado que la región promotora juega un papel importante en las diferencias de expresión de cada una de las isoformas, por lo que se ha propuesto que son reguladas de manera diferente. Esto se apoya por el hecho de que Hsp90 α contiene cinco elementos de respuesta a estrés térmico (HSE) en la región promotora, mientras que Hsp90 β sólo contiene dos, lo que podría explicar por qué Hsp90 α es conocida como la isoforma inducible.^{12,13}

La figura 1B muestra la estructura general de la Hsp90 α y de la Hsp90 β en donde se puede apreciar que es similar para ambas isoformas y que está compuesta principalmente por un dominio carboxilo terminal (C-terminal), un dominio medio, un dominio de carga y un dominio amino terminal (N-terminal). El dominio C-terminal, junto con el dominio medio, son importantes para la dimerización de Hsp90, siendo el estado dimérico crítico para su activación. En el dominio de carga abundan aminoácidos con carga negativa (de ahí su nombre) y hasta la fecha no se conoce su función. El dominio medio es el responsable de la actividad de chaperona de las Hsp90, debido a que está implicado en la unión a diversas proteínas. Finalmente, el dominio N-terminal es el encargado de la unión e hidrólisis de ATP y es el sitio de unión a algunos fármacos como la geldanamici-

A



B

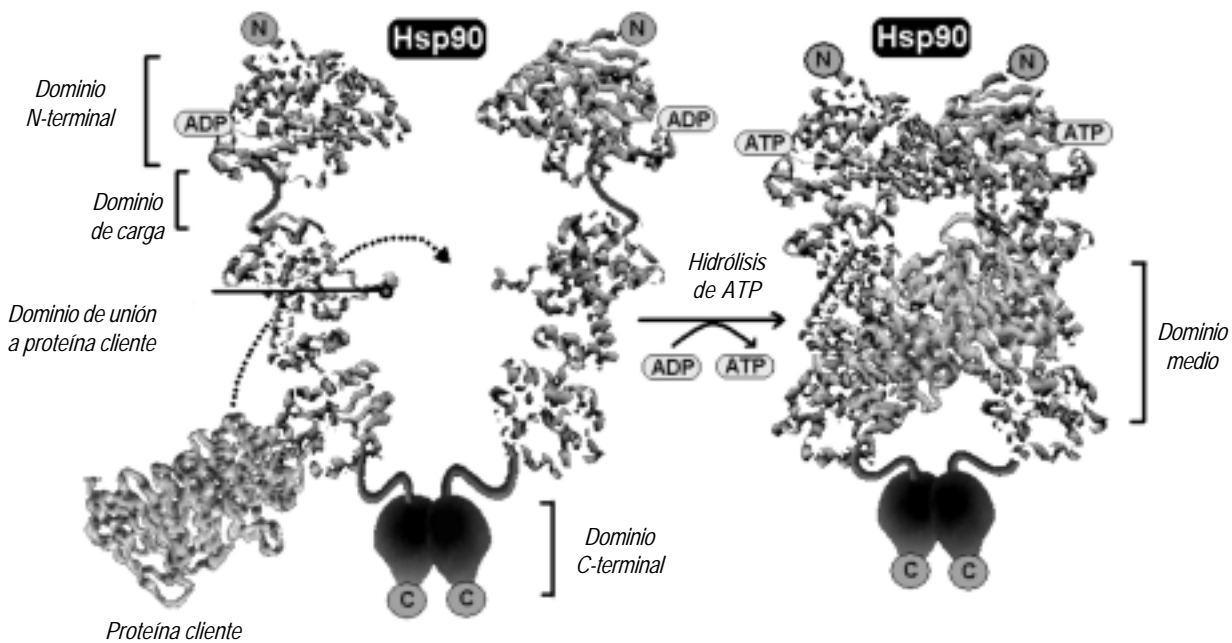


Figura 1. A. Comparación de la conformación y abundancia citoplásmica entre la Hsp90 α y la Hsp90 β en condiciones normales. B. Estructura general de la subfamilia de las Hsp90 α y Hsp90 β . La estructura está compuesta por cuatro dominios: dominio N-terminal, dominio de carga, dominio medio y dominio C-terminal, así como la unión con sus proteínas cliente, siendo este paso dependiente de la hidrólisis de ATP. (Modificada del sitio: www.ulyssse.u-bordeaux.fr/atelier/lkramer/biocell_diffusion/gbb.cel.fa.107.b3/content/access.htm).

na (GA) y el radicicol (RA) que inhiben la actividad de chaperona de las Hsp90.¹⁴⁻¹⁷

PRINCIPALES FUNCIONES CELULARES DE Hsp90

La función celular más estudiada y conocida de las Hsp90 es que actúan como moduladoras alostéricas de varias proteínas denominadas “proteínas cliente de Hsp90”, lo que les confiere su función como chaperonas moleculares. En la última década, la lista de proteínas cliente de Hsp90 ha aumentado sustancialmente y en ella se encuentran (<http://www.picard.ch/downloads/Hsp90interactors>): factores transcripcionales,^{18,19} proteínas cinasas²⁰⁻²² y proteínas que participan en la regulación transcripcional y trasduccional de señales, tales como el re-

ceptor de hormonas esteroideas^{23,24} y las sintetasas de óxido nítrico.²⁵⁻²⁸ Asimismo, recientemente se describió que la Hsp90 α también puede prolongar la vida media de sus proteínas cliente, a través de estabilizar y prevenir la degradación proteosómica de las proteínas a las que se une.²⁹

Dentro de las principales funciones celulares de Hsp90 se encuentran:

1. Asistir en el plegamiento de proteínas inmaduras, lo que proporciona la conformación adecuada y evita la agregación proteica.
2. Favorecer la translocación de sus proteínas cliente a organelos o a las membranas celular y nuclear.
3. Activar a las proteínas cliente a través de facilitar su fosforilación y/o dimerización.

- Degradar proteínas dañadas irreversiblemente mediante ubiquitinación.³⁰
- Mediar procesos anti-apoptóticos, a través de inhibir algunas vías que llevan a la muerte celular programada, como lo es la inhibición de la activación de caspasa 3 y 9, así como de inhibir al activador de la caspasa derivado de la mitocondria conocido como SMAC/DIABLO (second mitochondria-derived activator of caspase-direct IAP binding protein with low pI).³¹
- Participar en el desarrollo y diferenciación celular, mediante la regulación del ciclo celular.³²

MECANISMOS DE REGULACIÓN E INDUCCIÓN DE LAS Hsp90

En condiciones normales, la inducción de las Hsp90 se inicia con la liberación del factor de respuesta a estrés térmico (HSF1), que comúnmente se encuentra asociado a Hsp90 en el citosol. Una vez liberado, el HSF1 se transloca al núcleo en donde se une a elementos de respuesta a estrés térmico (HSE), dando lugar a la activación de la transcripción de proteínas de choque térmico, la aparición de nuevos mensajeros de Hsp90 y el subsecuente aumento en la expresión de estas proteínas.³³ A su vez, las Hsp90 son reguladas por proteínas cinasas y/o fosfatasas.^{6,34} A este respecto, se conoce que Hsp90 β contiene cinco sitios potenciales de fosforilación por la familia de proteínas cinasas PKA, mientras que Hsp90 α sólo contiene tres. Asimismo, se ha reportado que Hsp90 es regulada de forma positiva por la proteína fosfatasa PP1, la cual favorece la maduración de sus proteínas cliente, previniendo la hiperfosforilación de Hsp90.³⁵

Hsp90 EN LA FISIOLOGÍA VASCULAR

En 1998 García-Cardeña, *et al.*²⁵ mostraron por primera vez que Hsp90 es capaz de interactuar con la sintasa de óxido nítrico endotelial (eNOS). La trascendencia de este hallazgo en la fisiología vascular fue demostrada por el hecho de que esta interacción activa a eNOS, lo que produce un aumento en la generación de óxido nítrico (NO), que es un compuesto vasodilatador que regula el tono vascular y la presión arterial. En este estudio también se demostró que el desacople entre eNOS y Hsp90, que fue inducido por un inhibidor selectivo de Hsp90, produjo vasoconstricción en los anillos de aorta aislados, lo que se asoció con una reducción de los niveles de GMPc, el segundo mensajero de óxido nítrico. Años más tarde, Pritchard, *et al.*³⁶ confirmaron que el desacople entre

eNOS y Hsp90 reducía la síntesis de NO, pero además demostraron que eNOS en ausencia de Hsp90 era capaz de sintetizar al anión superóxido (O_2^-). El impacto de la activación de eNOS por Hsp90 en condiciones fisiopatológicas fue documentado por Kuppatt, *et al.*³⁷ quienes reportaron que la sobre-expresión de Hsp90 mediante transfección *in vivo* reduce el daño cardiovascular inducido por isquemia/reperfusión cardiaca. La inducción de la expresión de Hsp90 en los cardiomocitos promovió una mayor asociación de eNOS a Hsp90, aumentó la fosforilación activante de eNOS por Akt (S1177) y redujo la fosforilación inactivante de eNOS (T497), por lo que la protección conferida resultó en un aumento en la formación de NO. Estos estudios apoyan la idea de que el efecto dual que parece ejercer eNOS en la generación de los radicales de NO y del O_2^- en la fisiología vascular es regulado por Hsp90.

Otra evidencia que muestra la participación de Hsp90 en la regulación de la actividad de eNOS se ha observado durante la angiogénesis. Durante este proceso, el factor de crecimiento del endotelio vascular (VEGF) ejerce sus efectos angiogénicos a través de la activación de eNOS. En esta vía, se ha documentado que el VEGF induce la asociación temprana de Ca^{2+} con la calmodulina, lo que promueve la liberación de eNOS de la caveolina I, la cual mantiene a eNOS unida a la membrana en un estado inactivo. El complejo Ca^{2+} /calmodulina también promueve la asociación entre eNOS y Hsp90, donde finalmente Hsp90 recluta a la proteína cinasa B/Akt para mediar la activación de eNOS, a través de su fosforilación en el residuo de la serina 1177 con la consecuente mayor síntesis de NO.³⁸ Lo anterior establece una secuencia crítica temporal en la vía de la angiogénesis mediada por NO, en donde la señalización por VEGF activa la vía eNOS-Hsp90-Akt. En apoyo a esto, Sun, *et al.*³⁹ reportaron que Hsp90 no sólo activa la fosforilación de eNOS vía Akt, sino que también regula la transcripción génica y la estabilidad de eNOS.

Estudios recientes han mostrado que las estatinas poseen acciones protectoras adicionales a su propiedad hipocolesterolemianta. En este contexto y de forma interesante, se ha demostrado que las estatinas regulan en forma indirecta la activación de Hsp90, aumentando su fosforilación en los residuos de tiroxina,⁴⁰ lo que promueve una mayor síntesis de NO y neovascularización mediada por eNOS y Akt.³⁸

El efecto de Hsp90 en la vía de eNOS/NO no sólo radica en la activación de esta enzima, sino también se ha demostrado que Hsp90 estabiliza a la guanilato ciclase (GCs) que es una proteína clave en la señalización del NO. Esto fue demostrado en

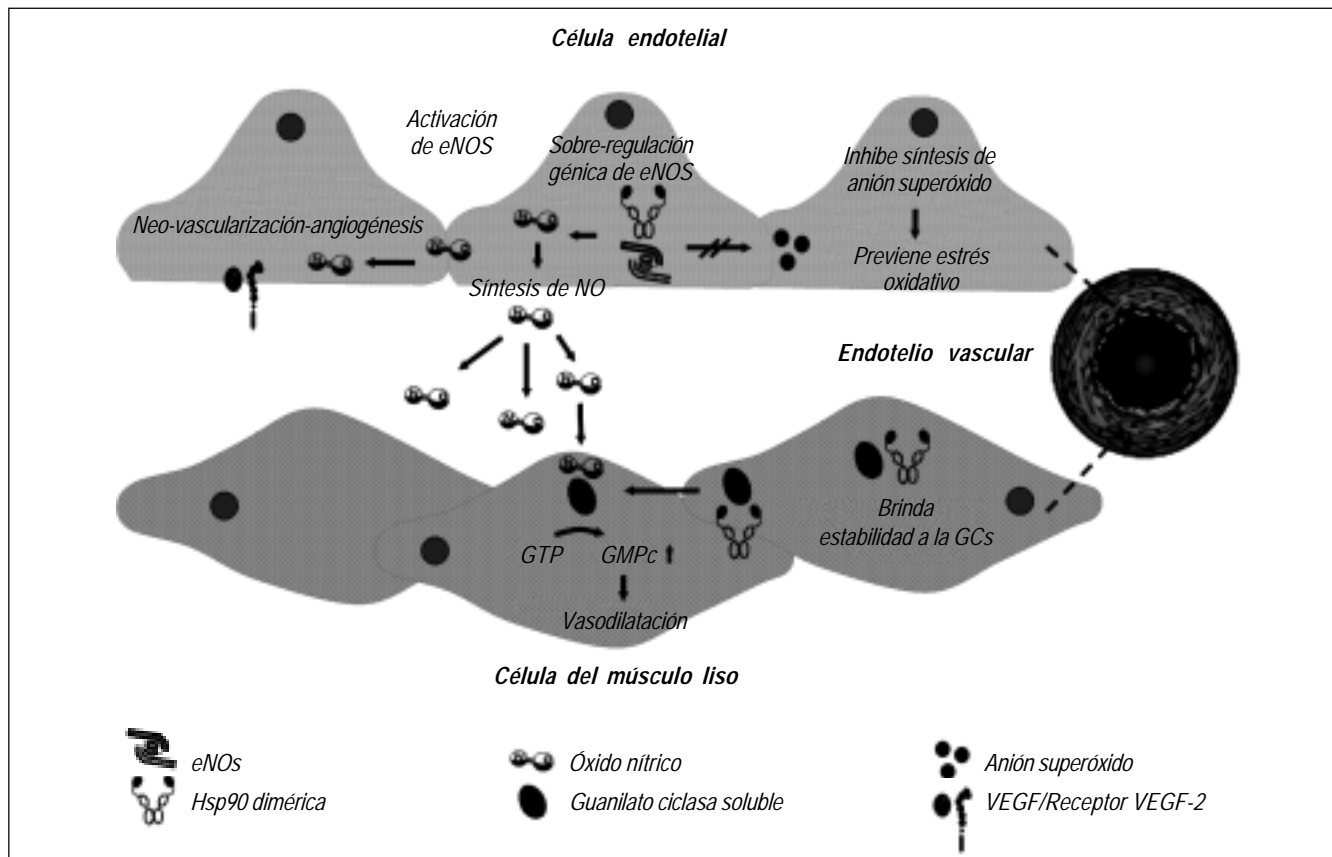


Figura 2. Significado fisiológico vascular de la Hsp90 y las vías que regula para el mantenimiento del tono vascular y angiogénesis.

condiciones de citotoxicidad por grandes cantidades de NO, donde el daño endotelial se asoció con una reducción en la estabilidad de la GCs por Hsp90.⁴¹

La relevancia del desacople entre eNOS y Hsp90 ha sido también documentada en procesos fisiopatológicos, como la diabetes mellitus que se caracteriza por una deficiencia en la biodisponibilidad de NO. Estudios recientes conducidos *in vitro* e *in vivo* demostraron que concentraciones elevadas de glucosa en el medio del cultivo celular y en un modelo de diabetes tipo I en la rata, la Hsp90 α es fosforilada en la treonina 89 por la proteína cinasa A (PKA) dependiente de AMPc, lo que induce su translocación hacia el exterior de las células endoteliales y reduce la actividad de eNOS y, por lo tanto, la producción de NO. Este fenómeno es revertido cuando se previene la translocación de Hsp90, lo cual se consiguió por un cambio en la treonina 89 por alanina de la Hsp90 α , evitando así que PKA pueda fosforilar a Hsp90 y transportarla a la membrana.⁴²

Lo anterior sugiere que Hsp90 puede ser un nuevo blanco terapéutico para prevenir el daño endote-

rial observado en diversas enfermedades en las cuales se requiera aumentar la producción de NO, o bien, prevenir o favorecer la formación de vasos sanguíneos *de novo*. Los efectos de Hsp90 en la fisiología vascular se resumen en la figura 2.

Hsp90 EN PROCESOS NEOPLÁSICOS

A diferencia de los tratamientos iniciales que fueron usados en la terapia anti-cáncer en los que se utilizaban agentes citotóxicos, la tendencia actual se ha enfocado en blancos terapéuticos que participen en las vías de señalización que conllevan a la enfermedad. Estudios recientes han mostrado que la sobre-expresión de Hsp90 juega un papel fundamental en la adaptación, proliferación y supervivencia de las células tumorales. Es por esta razón, que la inhibición de Hsp90 se ha considerado como una maniobra terapéutica para evitar o reducir la carcinogénesis. Como se detalla en la figura 3, la importancia de Hsp90 radica en promover la estabilidad y la actividad de pro-oncogenes y de oncogenes, dentro de los cuales destacan: ERBB2, el factor de creci-

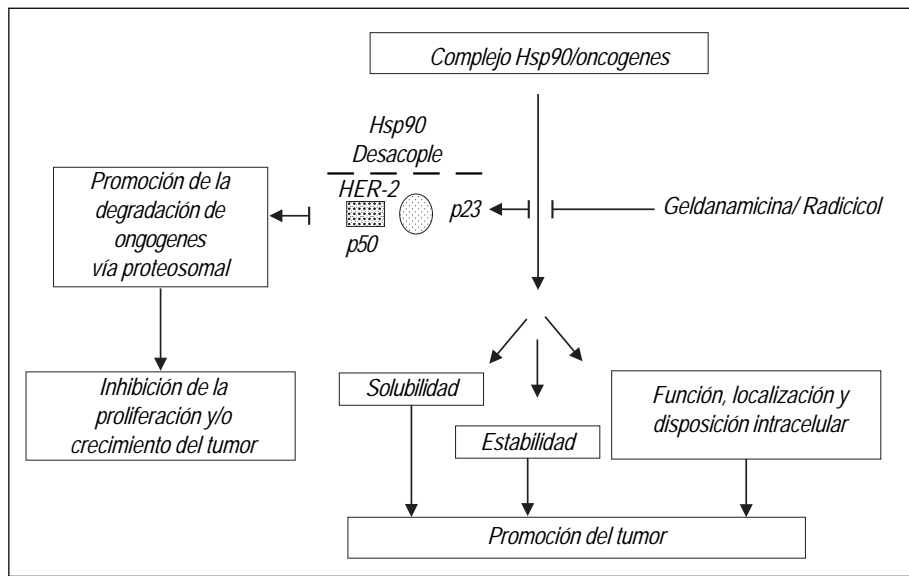


Figura 3. Modelo que describe el efecto citoprotector y anti-tumoral de los inhibidores de Hsp90, geldanamicina y radicicol, como blancos terapéuticos en el tratamiento contra el cáncer.

miento epidermal humano (HER-2), la proteína cinasa B/Akt, la cinasa dependiente de ciclina (CDK4), el gene supresor de tumor (p53) y el factor inducible por hipoxia (HIF1).⁴³⁻⁴⁶

Si bien la geldanamicina fue el primer inhibidor de Hsp90 utilizado en la clínica con buenos resultados sobre la reducción del crecimiento tumoral, la razón de la declinación en su uso se debió a la hepatotoxicidad reportada. Actualmente existen diferentes moléculas inhibidoras de Hsp90 dentro de los cuales se encuentran análogos de la geldanamicina, tales como el 17-alilamino-17-dimetoxigeldanamicina (17-AAG), que se utilizan solos o en combinación con agentes quimioterapéuticos en el tratamiento contra el cáncer. El uso terapéutico de 17-AAG se encuentra actualmente en fase clínica II.⁴³

Hsp90 EN LA FISIOLOGÍA RENAL

A pesar de la implicación de las proteínas de choque térmico de 90 kDa en múltiples procesos celulares, poco se conoce del papel que juegan en la fisiología y fisiopatología renal. En 1990, Matsubara, *et al.*⁴⁷ desarrollaron un anticuerpo dirigido contra Hsp90 de la rata y observaron la presencia de inmunotinción en el citoplasma de las células de los túbulos proximales y distales de la corteza renal. Sin embargo, se desconocía cuál isoforma de Hsp90 se expresaba en el riñón y menos aún el patrón de expresión de cada isoforma. Por lo tanto, en un trabajo reciente de nuestro laboratorio caracterizamos la expresión y localización de la Hsp90 α y de la Hsp90 β en la nefrona.⁴⁸ Primero nos dimos a la ta-

rea de evaluar la expresión de cada isoforma y encontramos que los niveles de RNAm y de proteína fueron más abundantes en la medula renal que en la corteza. El análisis de inmunohistoquímica mostró que la Hsp90 α y la Hsp90 β se localizaban desde el glomérulo hasta la punta de la papila y que el patrón de expresión fue muy similar entre ambas isoformas. Específicamente, observamos que en la corteza la Hsp90 α y la Hsp90 β se localizan en los capilares glomerulares, en las células mesangiales y en la cápsula de Bowman. También se detectó la presencia de ambas proteínas en el citoplasma de células epiteliales de los túbulos proximales y distales, con una importante inmunotinción en la membrana apical. La presencia de Hsp90 en el borde en cepillo del túbulo proximal no parece ser exclusiva de la subfamilia de Hsp90, ya que en dos trabajos anteriores al nuestro, Aufrich, *et al.*⁴⁹ y Schober, *et al.*⁵⁰ observaron el mismo patrón de localización para la Hsp25, que fue su presencia en el glomérulo y en menor proporción en la vasculatura con una fuerte inmunotinción en la membrana apical de las células del túbulo proximal y una ligera inmunotinción en el citoplasma y núcleo de este epitelio. En este estudio también observamos que en la medula externa, la Hsp90 α y la Hsp90 β están localizadas en el citoplasma de las células del asa gruesa ascendente de Henle, mientras que en la medula interna estas proteínas se localizaron principalmente en la membrana basolateral de las células del asa delgada de Henle, en los túbulos colectores y en la pelvis renal.⁴⁸ La distribución y la expresión específica de la Hsp90 α y de la Hsp90 β observada a lo largo de la nefrona, su-

gieren que estas proteínas podrían estar involucradas en la regulación de la filtración glomerular, así como en la reabsorción y la secreción tubular, funciones características de la nefrona.

Dentro de las funciones de Hsp90 en la fisiología renal, la más conocida, es su participación en la estabilización, activación y translocación del receptor de mineralocorticoide, a través de formar un heterocomplejo con Hsp70, Hip (p48), Hop (p56) y Hsp40. Una vez que la aldosterona se une al complejo receptor mineralocorticoide/Hsp90/cochaperonas, el complejo hormona/receptor es trasladado al núcleo donde se une a los elementos de respuesta a aldosterona, lo que a su vez activa la transcripción de diversos genes que responden a esta hormona como lo son: el canal epitelial de sodio (ENaC), el cotransportador de sodio-cloro (NCC), el canal de potasio (ROMK) y la bomba Na-K ATPasa,⁵¹⁻⁵³ con lo que la aldosterona ejerce su acción clásica que es promover la reabsorción de sodio y la excreción de potasio.

Además del papel de Hsp90 en la reabsorción de sodio en el túbulos distal y colector, Ortiz, *et al.*⁵⁴ mostraron que esta proteína también está implicada en regular la actividad del cotransportador de $\text{Na}^+ \text{K}^+:2\text{Cl}^-$ en el asa de Henle. Estos autores observaron que cuando eNOS está en el citoplasma de estas células epiteliales, el NO producido por esta isoforma inhibe al cotransportador, pero cuando eNOS se transloca a la membrana basolateral y no produce NO, esto activa al cotransportador. Interesantemente, también demostraron que Hsp90 es la responsable de transportar a eNOS, ya que cuando incubaron las asas de Henle aisladas y perfundidas con geldanamicina se evitó que eNOS fuera trasladada a la membrana basolateral y por lo tanto la actividad del cotransportador se redujo.⁵⁵ Estos resultados sugieren que Hsp90 participa también en la reabsorción de sodio en el asa de Henle.

Otra función recientemente descrita de Hsp90 es su participación en la adaptación a la hiperosmolaridad. La osmolaridad de la medula renal es de cuatro a cinco veces mayor que la encontrada en la corteza y en otros tejidos y está continuamente expuesta a cambios en la concentración de osmolitos que son finamente sensados por una proteína conocida como TonEBP (Tonicity-responsive Enhancer Binding Protein), la cual pertenece a la familia de factores nucleares NFAT (por sus siglas en inglés: Nuclear Factor of Activated T cell). El TonEBP protege a las células epiteliales del estrés hiperosmótico activando la transcripción de genes como: el cotransportador $\text{Na}^+/\text{mio-inositol}$, el cotransportador $\text{Na}^+/\text{Cl}^-/\beta\text{etaina}$, $\text{Na}^+/\text{Cl}^-/\text{taurina}$ y aldosa reductasa. A este res-

pecto, Chen, *et al.*⁵⁶ utilizando células embrionarias de epitelio renal de humano (HEK-293) transfectadas con TonEBP, mostraron por co-inmunoprecipitación que este factor forma un complejo con proteínas de estrés, dentro de las cuales destacan primordialmente la Hsp90 α y la Hsp90 β . En condiciones de hiperosmolaridad, la inhibición de Hsp90 por geldanamicina disminuyó tanto la expresión de TonEBP, como su actividad transcripcional. Estos resultados sugieren que en la medula renal, la citoprotección necesaria frente al estrés producido por hiperosmolaridad es mediada por Hsp90.

Los estudios realizados hasta el momento sobre el papel fisiológico de Hsp90 son muy escasos y menos aún se conoce el papel específico de Hsp90 α y de Hsp90 β . De forma general podemos resumir que Hsp90 participa en la regulación de la reabsorción de sodio y en reducir el estrés osmótico en la medula renal. Asimismo, estudios muy recientes de nuestro laboratorio sugieren que Hsp90 está implicada también en el mantenimiento de la función renal. Considerando que el NO producido por eNOS en el endotelio de los capilares glomerulares regula el tono vascular renal y la filtración glomerular, hemos observado que la inhibición de Hsp90 produce vasoconstricción renal y disminución de la filtración glomerular, lo que se asocia con una reducción en la producción de NO, que resultó por cambios en la fosforilación y en la dimerización de eNOS.⁵⁷

Hsp90 EN LA FISIOPATOLOGÍA RENAL

En cuanto a condiciones fisiopatológicas renales, se ha encontrado que la intoxicación con metales pesados como mercurio, zinc, cobalto, hierro y arsénico, así como fármacos nefrotóxicos, como gentamicina y cisplatino producen un aumento de la expresión de Hsp90 en los túbulos renales, principalmente en el segmento S3 del túbulos proximal.⁵⁸ Aunado a esto, Morita, *et al.*⁵⁹ demostraron mediante Western blot e inmunohistoquímica un aumento en la expresión de la Hsp73 y la Hsp90 después de 60 min de isquemia renal unilateral en la rata. En otro estudio, se observó que la inducción de estas proteínas, durante el daño renal por isquemia/reperfusión, se localizó en el túbulos proximal y en células de asa de Henle, comprobando que el aumento de estas proteínas persiste en la regiones de regeneración celular.⁶⁰ De manera similar, Komatsuda, *et al.*⁶¹ reportaron un caso clínico de un paciente con insuficiencia renal aguda, oliguria e hipertensión severa, en donde la biopsia renal reveló un aumento en la expresión de Hsp90 en el citoplasma de

las células del segmento S3 del túbulo proximal en la etapa de recuperación y regeneración tubular.

En la fisiopatología de la isquemia renal, el daño tubular observado se asocia con una pérdida de la polaridad de la membrana celular de las células del epitelio tubular. A este respecto Bidmon, *et al.*,⁶² usando el modelo de isquemia bilateral en la rata, mostraron mediante análisis de Western blot que la bomba de sodio potasio ATPasa se relocaliza de la membrana basolateral al citoplasma y que es indispensable la presencia de Hsp90 para trasladar y estabilizar a la bomba del citoplasma hacia la membrana basolateral y con ello nuevamente restaurar la polaridad de la membrana celular.

CONCLUSIONES

La evidencia descrita hasta el momento muestra que Hsp90 participa en diversas funciones en el tejido renal, dentro de las que destacan:

- Regular la reabsorción de sodio, a través de estabilizar y activar al receptor de mineralocorticoïdes y regular la actividad del cotransportador $\text{Na}^+ \text{K}^+ : 2\text{Cl}^-$.
- Mantener el gradiente electroquímico, al estabilizar la bomba de sodio potasio ATPasa.
- Regular la producción de NO mediante la interacción con eNOS y favorecer su activación por Akt.

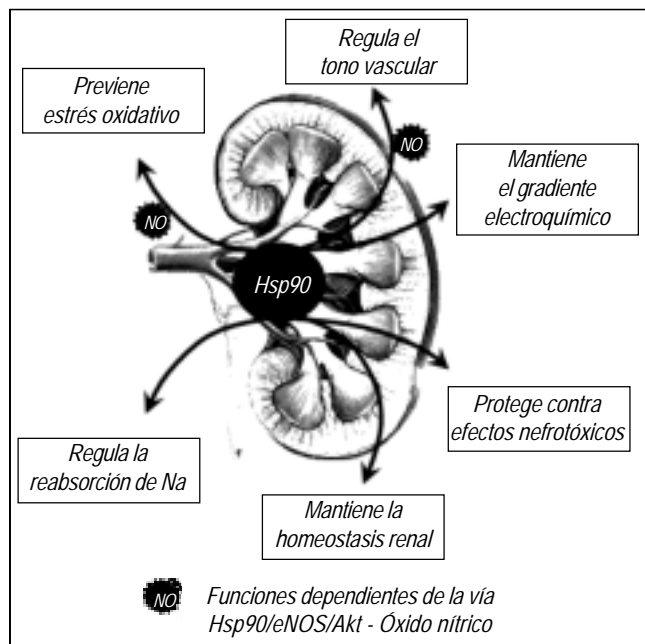


Figura 4. Un esquema de la participación de Hsp90 en procesos que regulan la fisiología renal.

- Sin menospreciar su principal función de chaperona que consiste en estabilizar o aumentar la actividad de diversas proteínas que parecen conservar la homeostasis renal, como se muestra en la figura 4.

Sin embargo, se requieren más estudios que permitan dilucidar la función individual de Hsp90 α y de Hsp90 β en diversas vías de señalización, no sólo en la fisiología renal, sino también en diversas condiciones fisiopatológicas que hasta ahora no han sido exploradas.

AGRADECIMIENTOS

Se reconoce la entusiasta participación y colaboración de los miembros de la Unidad de Fisiología Molecular. Los trabajos citados de nuestro laboratorio fueron apoyados por el Consejo Nacional de Ciencia y Tecnología (208602-3) y por la Universidad Nacional Autónoma de México (DGAPA IN228206). Carlo César Cortés-González y Victoria Ramírez-González son alumnos de posgrado y becarios del Consejo Nacional de Ciencia y Tecnología.

REFERENCIAS

1. Morimoto RI. Regulation of the Heat Shock Transcriptional Response: Cross Talk between a Family of Heat Shock Factors, Molecular Chaperones, and Negative Regulators. *Genes Dev* 1998; 12: 3788-96.
2. Csermely P, Schnaider T, Soti C, et al. The 90-KDa Molecular Chaperone Family: Structure, Function, and Clinical Applications. A Comprehensive Review. *Pharmacol Ther* 1998; 79: 129-68.
3. Csermely P, Soti C, Blatch GL. Chaperones as Parts of Cellular Networks. *Adv Exp Med Biol* 2007; 594: 55-63.
4. Sangster TA, Bahrami A, Wilczek A, et al. Phenotypic Diversity and Altered Environmental Plasticity in *Arabidopsis Thaliana* with Reduced Hsp90 Levels. *Plos ONE* 2007; 2: E648.
5. Ritossa FA. New Puffing Pattern Induced by Temperature Shock and DNP in *Drosophila*. *Experientia* 1962; 18: 571-3.
6. Richter K, Buchner J. Hsp90: Chaperoning Signal Transduction. *J Cell Physiol* 2001; 188: 281-90.
7. Sreedhar AS, Kalmar E, Csermely P, et al. Hsp90 Isoforms: Functions, Expression and Clinical Importance. *FEBS Lett* 2004; 562: 11-15.
8. Lindquist S, Craig EA. The Heat-Shock Proteins. *Annu Rev Genet* 1988; 22: 631-77.
9. Welch WJ. The Role of Heat-Shock Proteins as Molecular Chaperones. *Curr Opin Cell Biol* 1991; 3: 1033-8.
10. Gupta RS. Phylogenetic Analysis of the 90 Kd Heat Shock Family of Protein Sequences and an Examination of the Relationship Among Animals, Plants, and Fungi Species. *Mol Biol Evol* 1995; 12: 1063-73.
11. Minami Y, Kawasaki H, Miyata Y, et al. Analysis of Native Forms and Isoform Compositions of the Mouse 90-KDa Heat Shock Protein, HSP90. *J Biol Chem* 1991; 266: 10099-103.
12. Zhang SL, Yu J, Cheng XK, et al. Regulation of Human Hsp90alpha Gene Expression. *FEBS Lett* 1999; 444: 130-5.

13. Shen Y, Liu J, Wang X, et al. Essential Role of the First Intron in the Transcription of Hsp90beta Gene. *FEBS Lett* 1997; 413: 92-8.
14. Prodromou C, Roe SM, O'Brien R, et al. Identification and Structural Characterization of the ATP/ADP-Binding Site in the Hsp90 Molecular Chaperone. *Cell* 1997; 90: 65-75.
15. Waza M, Adachi H, Katsuno M, et al. 17-AAG, an Hsp90 Inhibitor, Ameliorates Polyglutamine-Mediated Motor Neuron Degeneration. *Nat Med* 2005; 11: 1088-95.
16. Wei Q, Xia Y. Roles of 3-Phosphoinositide-Dependent Kinase 1 in the Regulation of Endothelial Nitric-Oxide Synthase Phosphorylation and Function by Heat Shock Protein 90. *J Biol Chem* 2005; 280: 18081-6.
17. Ou J, Fontana JT, Ou Z, et al. Heat Shock Protein 90 and Tyrosine Kinase Regulate Enos NO[•] Generation But Not NO[•] Bioactivity. *Am J Physiol Heart Circ Physiol* 2004; 286: H561-H569.
18. Xu W, Yu F, Yan M, et al. Geldanamycin, a Heat Shock Protein 90-Binding Agent, Disrupts Stat5 Activation in IL-2-Stimulated Cells. *J Cell Physiol* 2004; 198: 188-96.
19. Zou J, Guo Y, Guettouche T, et al. Repression of Heat Shock Transcription Factor HSF1 Activation by HSP90 (HSP90 Complex) that Forms a Stress-Sensitive Complex with HSF1. *Cell* 1998; 94: 471-80.
20. Buchner J. Hsp90 & Co. - A Holding for Folding. *Trends Biochem Sci* 1999; 24: 136-41.
21. Caplan AJ. Hsp90's Secrets Unfold: New Insights from Structural and Functional Studies. *Trends Cell Biol* 1999; 9: 262-8.
22. Mayer MP, Bukau B. Molecular Chaperones: The Busy Life of Hsp90. *Curr Biol* 1999; 9: R322-R325.
23. Cadepond F, Schweizer-Groyer G, Segard-Maurel I, et al. Heat Shock Protein 90 as a Critical Factor in Maintaining Glucocorticosteroid Receptor in a Nonfunctional State. *J Biol Chem* 1991; 266: 5834-41.
24. Pratt WB, Toft DO. Regulation of Signaling Protein Function and Trafficking by the Hsp90/Hsp70-Based Chaperone Machinery. *Exp Biol Med (Maywood)* 2003; 228: 111-33.
25. Garcia-Cardenas G, Fan R, Shah V, et al. Dynamic Activation of Endothelial Nitric Oxide Synthase by Hsp90. *Nature* 1998; 392: 821-4.
26. Balligand JL. Heat Shock Protein 90 in Endothelial Nitric Oxide Synthase Signaling: Following the Lead(Er)? *Circ Res* 2002; 90: 838-41.
27. Bender AT, Silverstein AM, Demady DR, et al. Neuronal Nitric-Oxide Synthase Is Regulated by the Hsp90-Based Chaperone System In Vivo. *J Biol Chem* 1999; 274: 1472-8.
28. Yoshida M, Xia Y. Heat Shock Protein 90 as an Endogenous Protein Enhancer of Inducible Nitric-Oxide Synthase. *J Biol Chem* 2003; 278: 36953-8.
29. Lu C, Chen D, Zhang Z, et al. Heat Shock Protein 90 Regulates the Stability of C-Jun in HEK293 Cells. *Mol Cells* 2007; 24: 210-14.
30. Zhang L, Nephew KP, Gallagher PJ. Regulation of Death-Associated Protein Kinase. Stabilization by HSP90 Heterocomplexes. *J Biol Chem* 2007; 282: 11795-804.
31. Jiang B, Xiao W, Shi Y, et al. Heat Shock Pretreatment Inhibited the Release of Smac/DIABLO from Mitochondria and Apoptosis Induced by Hydrogen Peroxide in Cardiomyocytes and C2C12 Myogenic Cells. *Cell Stress Chaperones* 2005; 10: 252-62.
32. Sangster TA, Queitsch C, Lindquist S. Hsp90 and Chromatin: Where Is the Link? *Cell Cycle* 2003; 2: 166-8.
33. Soti C, Pal C, Papp B, et al. Molecular Chaperones as Regulatory Elements of Cellular Networks. *Curr Opin Cell Biol* 2005; 17: 210-5.
34. Sud N, Sharma S, Wiseman DA, et al. Nitric Oxide and Superoxide Generation from Endothelial NOS: Modulation by HSP90. *Am J Physiol Lung Cell Mol Physiol* 2007; 293: L1444-L1453.
35. Wandinger SK, Suhre MH, Wegele H, et al. The Phosphatase Ppt1 Is a Dedicated Regulator of the Molecular Chaperone Hsp90. *EMBO J* 2006; 25: 367-76.
36. Pritchard KA Jr, Ackerman AW, Gross ER, et al. Heat Shock Protein 90 Mediates the Balance of Nitric Oxide and Superoxide Anion from Endothelial Nitric-Oxide Synthase. *J Biol Chem* 2001; 276: 17621-4.
37. Kupatt C, Dessy C, Hinkel R, et al. Heat Shock Protein 90 Transfection Reduces Ischemia-Reperfusion-Induced Myocardial Dysfunction Via Reciprocal Endothelial NO Synthase Serine 1177 Phosphorylation and Threonine 495 Dephosphorylation. *Arterioscler Thromb Vasc Biol* 2004; 24: 1435-41.
38. Brouet A, Sonveaux P, Dessy C, et al. Hsp90 Ensures the Transition from the Early Ca²⁺-Dependent to the Late Phosphorylation-Dependent Activation of the Endothelial Nitric-Oxide Synthase in Vascular Endothelial Growth Factor-Exposed Endothelial Cells. *J Biol Chem* 2001; 276: 32663-9.
39. Sun J, Liao JK. Induction of Angiogenesis by Heat Shock Protein 90 Mediated by Protein Kinase Akt and Endothelial Nitric Oxide Synthase. *Arterioscler Thromb Vasc Biol* 2004; 24: 2238-44.
40. Brouet A, Sonveaux P, Dessy C, et al. Hsp90 and Caveolin Are Key Targets for the Proangiogenic Nitric Oxide- Mediated Effects of Statins. *Circ Res* 2001; 89: 866-73.
41. Antonova G, Lichtenbeld H, Xia T, et al. Functional Significance of Hsp90 Complexes with NOS and Sgc in Endothelial Cells. *Clin Hemorheol Microcirc* 2007; 37: 19-35.
42. Lei H, Venkatakrishnan A, Yu S, et al. Protein Kinase A-Dependent Translocation of Hsp90 Alpha Impairs Endothelial Nitric-Oxide Synthase Activity in High Glucose and Diabetes. *J Biol Chem* 2007; 282: 9364-71.
43. Tsutsumi S, Neckers L. Extracellular Heat Shock Protein 90: A Role for a Molecular Chaperone in Cell Motility and Cancer Metastasis. *Cancer Sci* 2007; 98: 1536-9.
44. Neckers L. Heat Shock Protein 90: The Cancer Chaperone. *J Biosci* 2007; 32: 517-30.
45. Xu W, Neckers L. Targeting the Molecular Chaperone Heat Shock Protein 90 Provides a Multifaceted Effect on Diverse Cell Signaling Pathways of Cancer Cells. *Clin Cancer Res* 2007; 13: 1625-9.
46. Bagatell R, Whitesell L. Altered Hsp90 Function in Cancer: A Unique Therapeutic Opportunity. *Mol Cancer Ther* 2004; 3: 1021-30.
47. Matsubara O, Kasuga T, Marumo F, et al. Localization of 90-Kda Heat Shock Protein in the Kidney. *Kidney Int* 1990; 38: 830-4.
48. Ramirez V, Uribe N, Garcia-Torres R, et al. Upregulation and Intrarenal Redistribution of Heat Shock Proteins 90alpha And 90beta by Low-Sodium Diet In the Rat. *Cell Stress Chaperones* 2004; 9: 198-206.
49. Aufrecht C, Ardito T, Thulin G, et al. Heat-Shock Protein 25 Induction and Redistribution During Actin Reorganization after Renal Ischemia. *Am J Physiol* 1998; 274: F215-F222.
50. Schober A, Burger-Kentischer A, Muller E, et al. Effect of Ischemia on Localization of Heat Shock Protein 25 in Kidney. *Kidney Int Suppl* 1998; 67: S174-S176.
51. Kim GH, Masilamani S, Turner R, et al. The Thiazide-Sensitive Na-Cl Cotransporter Is an Aldosterone-Induced Protein. *Proc Natl Acad Sci USA* 1998; 95: 14552-7.
52. Masilamani S, Kim GH, Mitchell C, et al. Aldosterone-Mediated Regulation of Ena Alpha, Beta, and Gamma Subunit Proteins in Rat Kidney. *J Clin Invest* 1999; 104: R19-R23.
53. Seok JH, Hong JH, Jeon JR, et al. Aldosterone Directly Induces Na, K-Atpase Alpha 1-Subunit Mrna in the Renal Cortex of Rat. *Biochem Mol Biol Int* 1999; 47: 251-4.
54. Ortiz PA, Hong NJ, Garvin JL. Luminal Flow Induces Enos Activation and Translocation in the Rat Thick Ascending Limb. *Am J Physiol Renal Physiol* 2004; 287: F274-F280.

55. Ortiz PA, Hong NJ, Garvin JL. Luminal Flow Induces Enos Activation and Translocation in the Rat Thick Ascending Limb. II. Role of PI3-Kinase and Hsp90. *Am J Physiol Renal Physiol* 2004; 287: F281-F288.
56. Chen Y, Schnetz MP, Irarrazabal CE, et al. Proteomic Identification of Proteins Associated with the Osmoregulatory Transcription Factor Tonebp/OREBP: Functional Effects of Hsp90 and PARP-1. *Am J Physiol Renal Physiol* 2007; 292: F981-F92.
57. Ramírez V, Mejía-Vilet JM, Hernández D, Gamba G, Bobadilla NA. Radicicol, a heat shock protein 90 (Hsp90) inhibitor reduces glomerular filtration rate. *Am J Physiol* (En prensa).
58. Borkan SC, Gullans SR. Molecular Chaperones in the Kidney. *Annu Rev Physiol* 2002; 64: 503-27.
59. Morita K, Wakui H, Komatsuda A, et al. Induction of Heat-Shock Proteins HSP73 and HSP90 in Rat Kidneys after Ischemia. *Ren Fail* 1995; 17: 405-19.
60. Wakui H, Komatsuda A, Miura AB. Heat-Shock Proteins in Animal Models for Acute Renal Failure. *Ren Fail* 1995; 17: 641-9.
61. Komatsuda A, Wakui H, Imai H, et al. Expression of 90-KDa Heat Shock Protein within Regenerative Tubular Cells in a Patient with Acute Oliguric Renal Failure Due to Malignant Hypertension. *Ren Fail* 1999; 21: 113-7.
62. Bidmon B, Endemann M, Muller T, et al. HSP-25 and HSP-90 Stabilize Na,K-ATPase in Cytoskeletal Fractions of Ischemic Rat Renal Cortex. *Kidney Int* 2002; 62: 1620-7.

Reimpresos:

Dra. Norma A. Bobadilla

Unidad de Fisiología Molecular
 Instituto de Investigaciones Biomédicas,
 Universidad Nacional Autónoma de México
 Instituto Nacional de Ciencias Médicas
 y Nutrición Salvador Zubirán
 Vasco de Quiroga No. 15, Tlalpan
 Col. Sección XVI
 14080, México, D.F.
 Tel.: 525-485-2676, fax: 525-655-0382
 Correo electrónico: nab@biomedicas.unam.mx
 nabs@quetzal.innsz.mx

*Recibido el 19 de febrero de 2008.
 Aceptado el 21 de julio de 2008.*

Therapeutic benefit of spironolactone in experimental chronic cyclosporine A nephrotoxicity

**IRIS FERIA, ISRAEL PICHARDO, PATRICIA JUÁREZ, VICTORIA RAMÍREZ, MARCO A. GONZÁLEZ,
NORMA URIBE, ROMEO GARCÍA-TORRES, FERNANDO LÓPEZ-CASILLAS, GERARDO GAMBA,
and NORMA A. BOBADILLA**

Molecular Physiology Unit, Instituto de Investigaciones Biomédicas, UNAM; Departments of Nephrology and Pathology, Instituto Nacional de Ciencias Médicas y Nutrición Salvador Zubirán; and Instituto de Fisiología Celular, Universidad Nacional Autónoma de México, Mexico City, Mexico

Therapeutic benefit of spironolactone in experimental chronic cyclosporine A nephrotoxicity.

Background. Cyclosporine A (CsA) is an immunosuppressive drug used to prevent tissue allograft rejection. However, its long-term utilization is limited due to chronic nephrotoxicity for which no prevention is available. This study evaluated the effect of spironolactone on renal functional and structural alterations induced by CsA, and assessed whether the protective effect was associated with a reduction of transforming growth factor- β (TGF- β) and the change of extracellular matrix protein mRNA level.

Methods. Male Wistar rats fed with low sodium diet were divided in four treatment groups: vehicle, CsA (30 mg/kg), spironolactone (20 mg/kg), or CsA+spironolactone. After 21 days, creatinine clearance (C_{Cr}), blood CsA, arteriolopathy in renal tissue, and TGF- β , collagen I, collagen IV, fibronectin, and epidermal growth factor (EGF) mRNA levels in renal cortex were determined.

Results. CsA reduced the C_{Cr} and up-regulated TGF- β , collagen I and fibronectin mRNA expression with a significant development of arteriolopathy, and reduced EGF mRNA levels. In contrast, spironolactone administration prevented the fall in renal function and TGF- β , collagen I, and fibronectin up-regulation, together with a reduction of arteriolopathy and tubulointerstitial fibrosis.

Conclusion. Our data show that aldosterone plays an important role as a mediator of renal injury induced by CsA. Thus, mineralocorticoid receptor blockade may be a potential strategy to prevent CsA nephrotoxicity.

Long-term cyclosporine (CsA) immunosuppressive therapy in allograft recipients and in patients with autoimmune diseases has been limited due to the concomitant development of chronic nephrotoxicity [1], which

Key words: aldosterone, arteriolopathy, interstitial fibrosis, TGF- β , renal function, low sodium diet, mineralocorticoid therapy.

Received for publication January 22, 2002
and in revised form July 17, 2002

Accepted for publication August 12, 2002

© 2003 by the International Society of Nephrology

is characterized by derangement of renal function and architecture. Renal dysfunction seems to be the result of enhanced vasoconstrictor factors release, particularly due to increased endothelin production and to the activation of the renin-angiotensin-aldosterone system (RAAS) [2–5], while the structural damage, such as arteriolopathy and tubulointerstitial fibrosis, appears to be the consequence of several mechanisms including hypoxia, free radical production and up-regulation of transforming growth factor- β 1 (TGF β 1) synthesis [6–11]. The increase in this profibrotic cytokine, TGF- β 1, results in the activation of extracellular matrix protein synthesis, such as collagen I and fibronectin [10, 12] as well as an increase in the renal apoptosis index [7, 13, 14], which are known to be associated with the development of kidney injury. In addition, it has been shown recently that epidermal growth factor (EGF), which mediates regeneration in tubular cells after renal damage, is significantly reduced during chronic CsA nephrotoxicity [14]. Thus, the reduction in EGF might contribute to enhance the structural changes observed in this condition.

Considerable attention has been directed to angiotensin II (Ang II) as a mediator of renal damage progression observed in several nephropathies, including chronic CsA toxicity. As a consequence, a therapeutic advantage has been observed with the use of angiotensin-converting enzyme (ACE) inhibitors or Ang II receptor antagonists to retard the progression rate of renal failure in the clinical setting, including the chronic nephropathy associated with diabetes mellitus [15–17]. Although aldosterone is part of the renin-angiotensin-aldosterone axis, little attention has been addressed to this mineralocorticoid as a potential key molecule mediating renal damage. Recent studies suggest that aldosterone could play an important role in the progression of renal disease. Continuous infusion of aldosterone in normal rats induced up-regulation of TGF- β mRNA in the kidney (abstract;

Juknevicius et al, *J Am Soc Nephrol* 11:622A, 2000) and the inhibition of aldosterone actions with the aldosterone receptor blocker, spironolactone, reduced renal damage without lowering blood pressure in both the renal ablation model and the stroke-prone spontaneously hypertensive rat [18–20]. Hostetter et al speculated that the mechanism by which mineralocorticoids promote renal injury in these models could be explained by the up-regulation of TGF- β 1 induced by aldosterone [21]. In this regard, the structural injury that is observed in the chronic CsA nephropathy model in the rat (induced by administration of CsA in animals fed a low salt diet) has been associated with an increase in TGF- β 1 expression [9, 10], which can be partially abrogated by the concomitant administration of the Ang II receptor antagonist losartan [9]. However, because losartan administration also will result in a reduction of aldosterone release, it is unknown if the protective effect of losartan is due to blockade of the Ang II receptors in the kidney, by the reduction of aldosterone secretion, or by a combination of both mechanisms.

Our present study used a model of chronic CsA nephrotoxicity and showed that spironolactone administration effectively prevented renal dysfunction and up-regulation of TGF- β 1 and extracellular matrix proteins mRNA, and reduced the structural damage induced by CsA. These data suggest that aldosterone is a key molecule in the pathogenesis of chronic CsA nephropathy.

METHODS

The present study utilized the chronic CsA nephrotoxicity model in the rat that is produced by the administration of CsA and a low sodium diet. Four groups of twelve male Wistar rats, weighing 350 g and fed with low salt diet (0.02%), were included in the study. Group I (V) animals received 0.1 mL SC of olive oil as the vehicle every 24 hours. Group II (CsA) rats were treated with a daily dose of CsA 30 mg/kg SC. Group III (SPIRO) received 20 mg/kg/day of spironolactone by gastric gavage, and group IV comprised rats treated with CsA+SPIRO. All animals were treated during 21 days. The V and SPIRO groups were pair-fed with the CsA and CsA+SPIRO groups, respectively.

Functional studies

Systolic blood pressure was measured by a non-invasive tail cuff method at the end of the experimental protocol (Model 179, IITC Life Science, Woodland Hills, CA, USA). All animals were placed in metabolic cages and urine that was spontaneously voided during every 24 hours was collected. Serum and urine creatinine concentration were measured with an autoanalyzer (Technicon RA-1000; Bayer Co. Tarrytown, NY, USA). Renal creatinine clearances were calculated by the standard formula $C_{Cr} = U \cdot V/P$, where U is the concentration in

urine, V is the urine flow rate and P is plasma concentration. In all studied groups urinary protein excretion was determined using the trichloroacetic acid (TCA) turbidimetric method [22], and serum aldosterone and potassium levels were determined by radioimmunoassay (RIA) and with a NOVA4 electrolyte analyzer (NOVA Biomedical, Waltham, MA, USA), respectively. Blood CsA concentration also was determined by monoclonal radioimmunoassay kit (TDx/TDxFLx; Abbott Laboratories, Abbot Park, IL, USA) in groups receiving CsA.

Kidneys were obtained from six rats of each group for histological study. Rats were anesthetized by intraperitoneal injection of sodium pentobarbital and their kidneys were excised, macroscopically divided into renal cortex and medulla, frozen in liquid nitrogen, and kept at -80°C until used.

Histological studies

Before renal cortex separation, one half of the left kidney was taken and fixed in alcoholic Bouin's solution for light microscopy studies. After an appropriate dehydration, kidney slices were embedded in paraffin, sectioned at 3 μ , and periodic acid-Schiff (PAS), Van Gieson and trichromic stains were performed. Arteriolopathy percentage was determined by counting at least 100 afferent arterioles showing the characteristic lesion of this model. Arteriolopathy was counted as present or non-present (dichotomic variable). Thus, the results are expressed as the percentage of affected arterioles over total number of arterioles. The degree of tubulointerstitial fibrosis was evaluated by morphometry. For this purpose, ten subcortical periglomerular fields per Van Gieson stained section (magnification, $\times 200$) were randomly selected in kidneys from the different groups. The images were recorded and the affected areas were delimited and semiquantified using the Leica processing and analysis system Ltd., (Leica Imaging System Ltd., Cambridge, UK). Finally, the proportion of fibrosis was calculated dividing the interstitial fibrosis by total area. The histological analysis was performed without knowing the group at which each kidney belonged.

Molecular studies

RNA isolation. Total RNA was isolated from each renal cortex or medulla following the guanidine isothiocyanate-cesium chloride method [23]. Integrity of isolated total RNA was examined by 1% agarose gel electrophoresis and RNA concentration was determined by UV-light absorbance at 260 nm (Beckman DU640, Brea, CA, USA).

Northern blot analysis. Aliquots of 20 μ g of total RNA from each renal cortex sample were separated by 0.9% agarose/formaldehyde gel electrophoresis and transferred to a nylon membrane (Biotrans; ICN, East Hills, NY, USA), and fixed by UV cross linking (Stratalinker; Stratagene, La Jolla, CA, USA). The probes used were TGF- β 1,

collagen alpha I chain and collagen alpha IV chain obtained from mouse, as well as fibronectin and glyceraldehyde-3-phosphate dehydrogenase (GADPH) from rat. Labeling of cDNA probes was done using the Random Primer Labeling Kit (Boehringer, Mannheim, Germany) and [$\alpha^{32}\text{P}$]-dCTP (Amersham, Little Chalfont, Buckinghamshire, UK) accordingly to the manufacturer's instructions. Hybridization was performed overnight at 42°C in 5 × standard sodium citrate (SSC), 50 mmol/L sodium phosphate (pH 6.8), 50% formamide, 5 × Denharts solution, 0.1% sodium dodecyl sulfate (SDS), and 250 µg/mL of Torula yeast total RNA. Membranes were washed three times for 10 minutes at room temperature in 2 × SSC, 0.1% SDS, and twice for 45 minutes at 68°C in 0.1 × SSC, 0.1% SDS. Autoradiographs were scanned and the hybridization bands were measured by densitometric analysis.

Semiquantitative RT-PCR. The relative level of EGF and GAPDH mRNA expression was assessed in the renal cortex by semiquantitative reverse transcription-polymerase chain reaction (RT-PCR), as previously described [24, 25]. Briefly, primer sequences [26, 27] were custom obtained from Invitrogen (Gaithersburg, MD, USA).

Reverse transcription (RT) was carried out using 10 µg of total RNA from the renal cortex of each rat. RT was performed at 37°C for 60 minutes in a total volume of 20 µL using 200 U of the Moloney murine leukemia virus reverse transcriptase (Invitrogen), 100 pmol of random hexamers (Invitrogen), 0.5 mmol/L of each dNTP (Sigma Chemical Co., St. Louis MO, USA), and 1× RT buffer [75 mmol/L KCl; 50 mmol/L Tris-HCl; 3 mmol/L MgCl₂; 10 mmol/L dithiothreitol (DTT), pH 8.3]. One tenth of the RT from each individual sample was used for EGF, and GAPDH amplification in 20 µL final volume reactions containing 0.2 µCi of [$\alpha^{32}\text{P}$]-dCTP (~3000 Ci/mmol, 9.25 MBq, 250 µCi). PCR cycles were performed in a DNA thermal cycler (M.J. Research, Watertown, MA, USA). The control gene was amplified simultaneously in each reaction. Amplification kinetics for EGF and the housekeeping gene GAPDH in renal cortex total RNA, and the optimal number of cycles for each primer pair were assessed as we previously reported [24, 25]. To analyze the PCR products, one-half of each reaction was electrophoresed in a 5% acrylamide gel. Bands were ethidium bromide stained and visualized under UV light, cut out, suspended in 1 mL of scintillation cocktail (Ecolume; ICN, Aurora, OH, USA), and counted by liquid scintillation (Beckman LS6500). All reactions were performed individually from each cortex total RNA in duplicate. Genomic DNA contamination was checked by treating all RNA samples with RNase-free DNAse I and by carrying samples through PCR procedure without adding reverse transcriptase.

Statistical analysis

The results are presented as mean ± SEM. The significance of the differences between groups was tested by analysis of variance (ANOVA) comparison using Bonferroni's correction for multiple comparisons. Statistical significance was defined as two-tailed $P < 0.05$.

RESULTS

Physiological and functional studies

All treatments were well tolerated by all rats along the study. The CsA and CsA+SPIRO groups lost body weight gradually over 21 days of treatment. Mean body weights for these groups were 355.4 ± 6.2 and 353.6 ± 1.68 g, respectively, at the beginning of the experiment and 276.2 ± 4.1 and 294.0 ± 7.4 g, respectively, at the end. In contrast, the V and V+SPIRO groups that were pair-fed showed a slight gain in body weight during the study. The initial body weights were 358.5 ± 4.2 and 356.3 ± 6.0 g, respectively, and final body weights were 384.75 ± 5.8 and 369.1 ± 7.1 g, respectively.

Figure 1 depicts the most important physiological parameters that were evaluated in control and experimental groups. After 21 days, systolic blood pressure (SBP) was measured. As has been previously reported by several authors [7, 12, 14, 28], CsA administration in this experimental model is not associated with hypertension. SBP in the control group was 125.5 ± 3.4 whereas it was 132.6 ± 8.6 mm Hg in CsA treated rats ($P = \text{NS}$). Spironolactone also had no effect in SBP (123.5 ± 3.1 mm Hg). Thus, all of the rats studied were normotensive. As shown in Figure 1B, the amount of proteins in urine was not different among the groups, and although the proteinuria levels were less in CsA treated rats, as reported previously [12], this difference was not statistically different. In order to evaluate the effect of cyclosporine and spironolactone on the well known increase in serum potassium levels produced by these compounds, serum potassium was determined in all four groups. As Figure 1C shows, CsA administration resulted in hyperkalemia since the serum potassium in this group was 4.3 ± 0.3 mEq/L, which is significantly different to the control group (3.4 ± 0.2 mEq/L, $P < 0.05$). Serum potassium in the CsA+SPIRO group was 4.4 ± 0.2 mEq/L. Thus, spironolactone administration had no further effect on serum potassium levels. Finally, it is well known that a low sodium diet activates aldosterone production. Figure 1D shows a significant increase in aldosterone levels in all of the groups studied. Although values were slightly higher in rats receiving spironolactone, the differences were not significant.

To evaluate the effect of aldosterone inhibition with spironolactone on renal function, creatinine clearance (C_{Cr}), as an index of glomerular filtration rate, was mea-

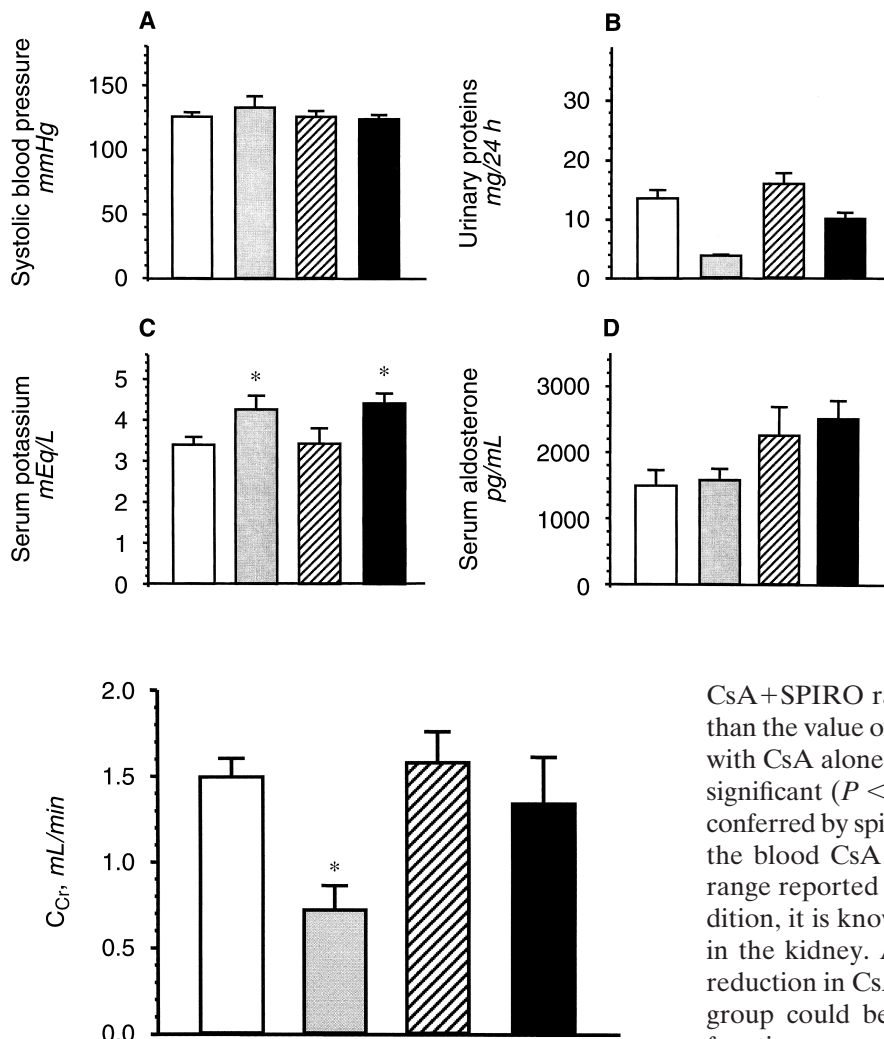


Fig. 1. (A) Systolic blood pressure, (B) urinary protein excretion, (C) serum potassium, and (D) serum aldosterone levels in the vehicle group (□), CsA treated animals (▨), SPIRO group (▨) and CsA+SPIRO treated rats (▨). * $P < 0.05$ vs. V, SPIRO. Although not shown, serum aldosterone levels in rat fed with normal salt diet are around 100 pg/mL.

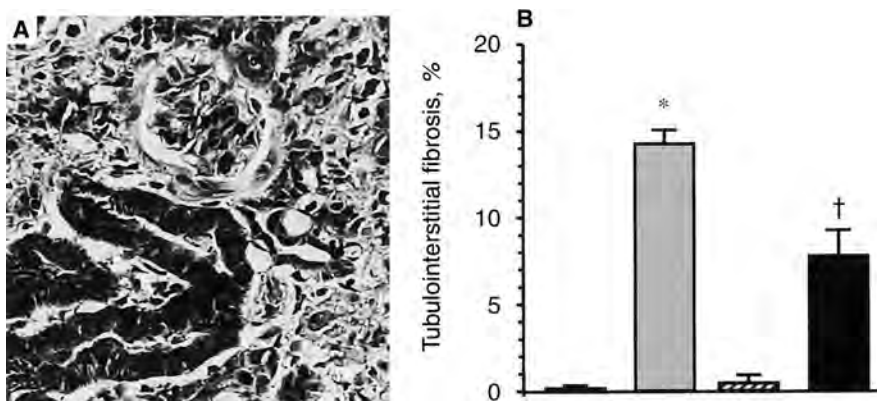
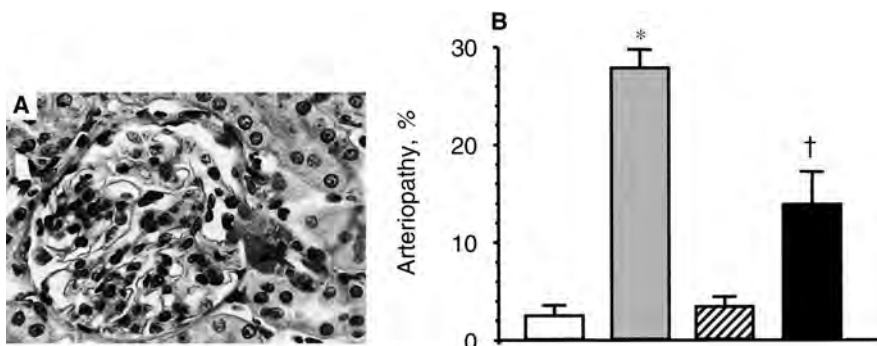
Fig. 2. Glomerular filtration rate estimated by creatinine clearance in vehicle group (□), animals treated with CsA during 21 days with 30 mg/kg (▨), SPIRO group (▨) and CsA+SPIRO treated rats (▨) maintaining on low sodium diet, * $P < 0.05$ vs. V, SPIRO, and CsA+SPIRO groups.

sured at the end of the 21 days of treatment in the four groups of rats. As shown in Figure 2, the administration of CsA resulted in a significant reduction in the glomerular filtration rate, from 1.49 ± 0.1 mL/min in the V group to 0.72 ± 0.1 mL/min in CsA group, whereas inhibition of aldosterone with spironolactone in the V+SPIRO group had no effect on this parameter (1.58 ± 0.2 mL/min). Interestingly, spironolactone administration prevented the fall in renal function induced by CsA treatment, since the C_{Cr} in the CsA+SPIRO treated rats was 1.34 ± 0.3 mL/min. This C_{Cr} value was not statistically different from values observed in V and V+SPIRO control groups. To differentiate if the protective effect of spironolactone was related to a decrease in CsA blood levels, we assessed the CsA concentration in blood from CsA and CsA+SPIRO groups. The value observed in

CsA+SPIRO rats of 3594 ± 133 ng/mL was 14% lower than the value of 4199 ± 99 ng/mL obtained in rats treated with CsA alone. Although the reduction was statistically significant ($P < 0.05$), it does not explain the protection conferred by spironolactone in CsA-treated animals, since the blood CsA concentration was still within the toxic range reported by other investigators [10, 11, 14]. In addition, it is known that one tenth of CsA is metabolized in the kidney. Accordingly, it is feasible that the small reduction in CsA blood levels observed in CsA+SPIRO group could be secondary to the restoration of renal function.

Histological studies

To establish if aldosterone receptor blockade with spironolactone also reduces or prevents the structural damage induced by CsA administration, the degree of afferent arteriolopathy and tubulointerstitial fibrosis was quantified. The percentage of arteriolopathy was obtained by counting at least 100 preglomerular afferent arterioles in each rat. A representative light microscopy image of the characteristic arteriolar lesion of CsA nephropathy is shown in Figure 3A. This alteration was mainly located in the preglomerular afferent arteriole and extended several microns upstream, consisting of an enlargement of the smooth muscle cells and resulting in a partial or total narrowing of the arteriolar lumen. The affected cell cytoplasm showed eosinophilic, PAS positive, homogeneous or granular degeneration. Endothelial cells looked prominent and perivascular cells seemed proliferated. The percentage of afferent arterioles showing this kind of lesion is shown in Figure 3B. As we previously reported [29], in the control group treated with vehicle alone, a few afferent arterioles were shown



to have arteriolopathy (2.6%), possibly as a result of activation of the RAAS system induced by a low sodium diet. This low frequency of arteriolopathy was similar in the SPIRO group. In contrast, as expected, in the chronic CsA group, arteriolar lesion was present in as much as 28% of glomeruli, whereas this percentage of arteriolopathy was reduced to 14% in the CsA+SPIRO group.

The photomicrograph presented in Figure 4A is a representative example of the tubulointerstitial fibrosis observed in CsA sodium-depleted animals. The morphometric analysis is shown in Figure 4B. As expected, significant tubulointerstitial fibrosis was observed in the group receiving CsA. In contrast, spironolactone was able to reduce this alteration. These observations suggest that at least part of the CsA-induced arteriolar and tubulointerstitial lesions are mediated by aldosterone, and demonstrates that spironolactone not only prevents the negative effects of CsA at the functional, but also at the structural level.

Molecular studies

To begin to understand the mechanisms by which spironolactone protects the kidney from CsA toxicity, we evaluated the gene expression level of extracellular matrix proteins that are known to be involved in the pathogenesis of chronic renal injury. The autoradiographs of

the Northern blot analysis of total RNA from renal cortex using specific probes for TGF- β , collagen I, collagen IV, and fibronectin are shown in Figure 5, together with the Northern blot analysis of the housekeeping gene GAPDH that was used to control each experiment. The densitometric analysis of TGF- β 1 is shown in Figure 6. In contrast to vehicle-treated animals, CsA administration in sodium-depleted rats produced a marked increase in TGF- β 1 mRNA levels. The TGF- β /GAPDH ratio was 1.1 ± 0.1 in the vehicle group and 4.5 ± 0.5 in the CsA group ($P < 0.01$). The administration of aldosterone antagonist spironolactone had no effect on TGF- β 1 mRNA expression, since the TGF- β /GAPDH ratio in the SPIRO group was 1.6 ± 0.1 . In contrast, in CsA+SPIRO group the TGF- β /GAPDH ratio was 2.0 ± 0.4 . This value was significantly lower than the expression observed in the CsA group (2.0 ± 0.4 vs. 4.5 ± 0.5 , $P < 0.05$), but not different to the value observed in the SPIRO group (2.0 ± 0.4 vs. 1.6 ± 0.1 , $P = \text{NS}$). Accordingly, spironolactone administration prevented the TGF- β 1 up-regulation induced by CsA.

The effects of CsA and spironolactone on the expression of extracellular matrix proteins such as collagen I, collagen IV, and fibronectin mRNAs in renal cortex are shown in Figure 7. Chronic CsA nephrotoxicity was associated with a fivefold up-regulation of collagen I. The ratio

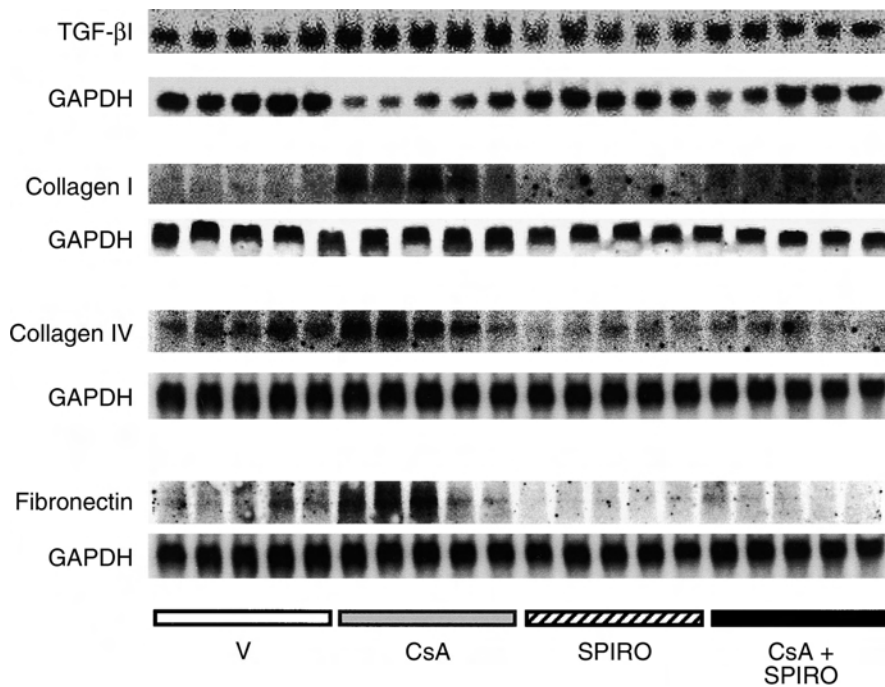


Fig. 5. Northern blot analysis of mRNA from renal cortex of the four study groups using specific probes for TGF- β 1, collagen I, collagen IV, fibronectin and GAPDH. Each lane was loaded with 20 μ g of total RNA from a different rat, corresponding to each group as stated.

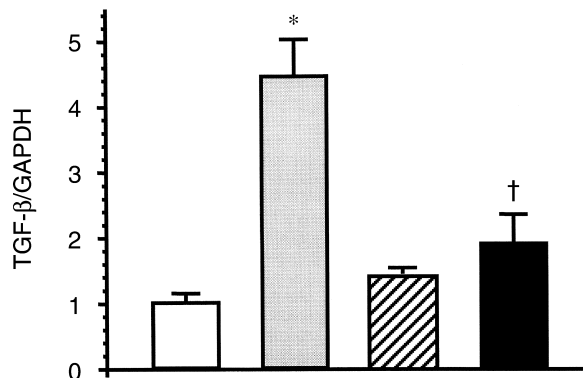


Fig. 6. TGF- β 1 mRNA levels in renal cortex are represented as the ratio between TGF- β 1 and GAPDH bands densitometry in vehicle group (□), CsA-treated animals (▨), SPIRO group (▨) and CsA+SPIRO treated rats (■). * $P < 0.05$ vs. V, SPIRO and CsA+SPIRO groups and † $P < 0.05$ vs. CsA group.

of collagen I/GAPDH in the CsA group was 3.8 ± 0.9 , whereas in the V group it was 0.6 ± 0.05 , $P < 0.01$. This up-regulation of collagen I induced by CsA was abrogated by spironolactone, since the ratio in CsA+SPIRO group was 1.6 ± 0.3 . A similar observation was obtained in the analysis of fibronectin mRNA expression that is shown in Figure 7B. The ratio of fibronectin/GAPDH increased in CsA treated rats and this up-regulation was prevented by spironolactone. The values of the ratio between collagen IV and GAPDH are shown in Figure 7C. The expression of collagen IV in the CsA group was increased, but the difference with the V group did not reach

significance with ANOVA for multiple comparisons (V group 0.36 ± 0.01 vs. CsA group 0.51 ± 0.07 , $t = 2.77$, $P > 0.05$). However, the ratio of collagen IV/GAPDH observed in the CsA+SPIRO group (0.18 ± 0.03) was significantly lower than the ratio in the CsA treated group (0.51 ± 0.07 , $t = 6.1$, $P < 0.01$). Thus, CsA induced up-regulation of extracellular matrix proteins mRNA in renal cortex, and this effect of CsA was prevented when spironolactone was simultaneously administered.

It has been suggested previously that down-regulation of the EGF contributes to the structural damage induced by toxic agents, including CsA [14, 30], since EGF is a potent mitogenic agent and its expression has been associated with renal repair following ischemic injury. Thus, we analyzed the effect of CsA and spironolactone on the EGF mRNA levels in renal cortex following a semi-quantitative RT-PCR strategy. The upper panel of Figure 8 shows the PCR products obtained for each rat and the lower panel shows the mean ratio between EGF and GAPDH of each group. CsA treatment induced a significant reduction in the expression of EGF as compared to the V group (1.5 ± 0.1 vs. 3.9 ± 0.1 , respectively, $P < 0.01$). Interestingly, spironolactone alone also induced a slight decrease in EGF mRNA levels (3.0 ± 0.1 SPIRO, $P < 0.05$ vs. V group). However, when spironolactone was administered with CsA, the ratio of EGF/GAPDH was 2.2 ± 0.3 . This value was significantly higher than the value observed in the CsA group, suggesting that spironolactone partially reversed the down-regulation of EGF induced by chronic CsA toxicity.

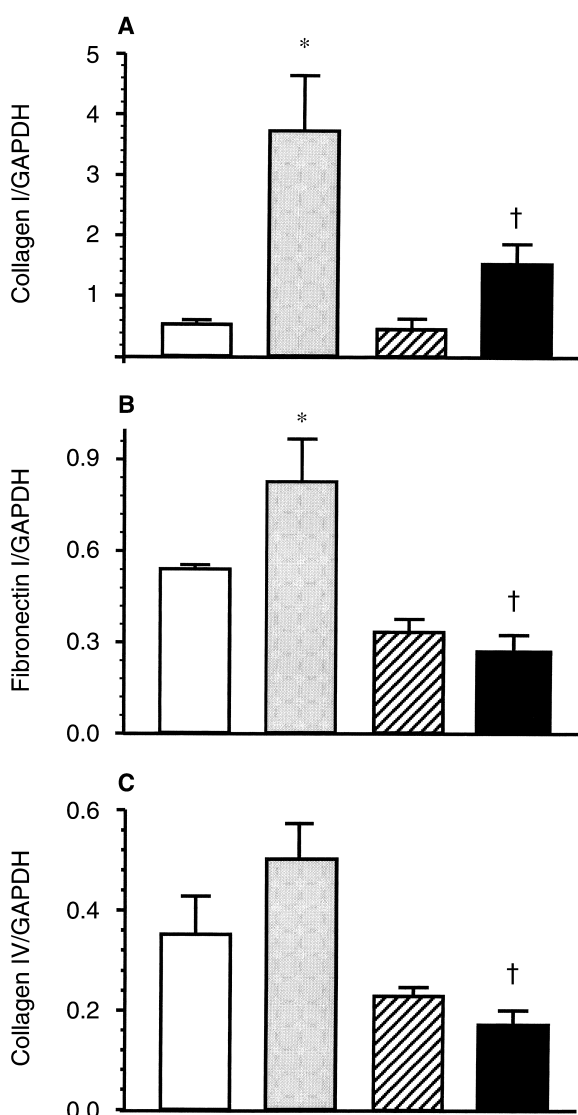


Fig. 7. Effects of CsA and SPIRO on the expression of extracellular matrix proteins. (A) Collagen I, (B) fibronectin and (C) collagen IV in vehicle group (□), CsA-treated animals (■), SPIRO group (▨) and CsA+SPIRO treated rats (■). *P < 0.05 vs. V, SPIRO and CsA+SPIRO groups and †P < 0.05 vs. CsA-treated rats.

DISCUSSION

Using a model of chronic CsA nephrotoxicity in the rat, our present study shows that aldosterone receptor blockade with spironolactone effectively prevents the fall in renal function, as well as reduces the arteriolopathy and tubulointerstitial fibrosis induced by CsA. The protective effect of spironolactone was associated with prevention of the CsA-induced up-regulation of TGF- β , collagen I, collagen IV, and fibronectin, and partial restoration of CsA-inducing down-regulation of EGF mRNA levels in renal cortex.

A chronic CsA nephrotoxicity model induced by CsA administration in rats fed with a low salt diet is characterized by renal failure accompanied by severe renal vaso-

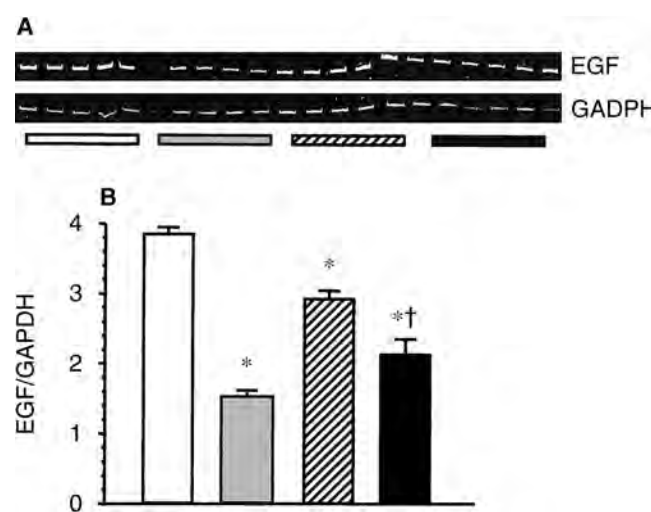


Fig. 8. Epidermal growth factor mRNA levels in renal cortex assessed by RT-PCR. (A) An acrylamide gel showing EGF and GAPDH amplification bands for all of the study groups. Each lane was loaded with 10 μ L of the RT-PCR reaction from different animals. (B) Graphic representation of the mean ratio between EGF and GAPDH for the Vehicle group (□), CsA-treated animals (■), SPIRO group (▨) and CsA+SPIRO treated rats (■). *P < 0.05 vs. V and †P < 0.05 vs. CsA group.

constriction, which is due at least in part to activation of the renin-angiotensin-aldosterone system (RAAS). Our data show that C_{cr} of the rats treated with spironolactone and CsA was similar to the vehicle-treated animals and significantly higher than the C_{cr} observed in the CsA group (Fig. 2). Therefore, aldosterone receptor blockade completely prevented the decrease in glomerular filtration rate induced by CsA. It is unlikely that this spironolactone-conferred protection was due to the effect of this diuretic agent on the blood pressure levels, since this model is not associated with the development of hypertension. SBP was similar among all of the study groups. It is also unlikely that protection conferred by spironolactone was secondary to the small reduction on CsA blood levels observed in the CsA+SPIRO group. It has been shown that CsA levels above 1000 pg/mL are enough to produce renal damage [10, 11, 14]. In addition, because it is known that one tenth of CsA is metabolized in the kidney, the small reduction in CsA blood levels observed in CsA+SPIRO group was probably secondary to the restoration of renal function.

This beneficial effect of spironolactone was associated with a significant reduction of arteriolopathy and tubulointerstitial fibrosis, which is the structural hallmark of CsA injury in the kidney. Several therapeutic agents such as endothelin [31] and angiotensin inhibitors [9, 14, 31], vascular endothelial growth factor (VEGF) [28], polysulphate pentosan [29] and L-arginine [32, 33] have been investigated as possible tools to reduce chronic CsA nephrotoxicity. However, most of these treatments have not effectively reduced both functional and structural

changes induced by CsA in the kidney. Although administration of losartan [9, 14], VEGF [28], and polysulfate pentosan [29] partially prevented the structural damage induced by CsA, these agents did not improve the renal dysfunction during chronic CsA nephrotoxicity.

The mechanism for arteriolopathy and chronic renal damage to the kidney induced by CsA is unknown and, thus, the mechanism of protection by spironolactone is not clear. Acute experimental CsA nephrotoxicity is directly related to renal vasoconstriction and this form of nephrotoxicity can be completely prevented by co-administration of dexamethasone [34], arginine [35, 36], or glycine [6] as well as enalapril and spironolactone [4]. Thomson et al [4] and Iacona et al [37] observed that spironolactone improved renal function during acute CsA nephrotoxicity in the rat. In contrast, chronic CsA toxicity not only involves renal injury due to hypoxia, but also is due to up-regulation of TGF- β and extracellular matrix proteins [9, 10] as well as an increase in apoptosis [7]. Interestingly, Viera et al have shown up-regulation of TGF- β expression within the afferent arterioles, suggesting that this cytokine not only mediates interstitial lesions, but also might be a mediator of hypertrophy observed in juxtaglomerular arterioles [11]. Shihab et al showed that chronic CsA toxicity in the rat is associated with up-regulation of TGF- β expression, and that this effect could be prevented by Ang II blockade, either with the enzyme converting inhibitor enalapril or the angiotensin II receptor antagonist losartan [9]. The use of these compounds, however, did not prevent renal dysfunction, suggesting that up-regulation of TGF- β during CsA toxicity is independent of renal hemodynamics, and is mediated, at least in part, directly by Ang II. With our current data, however, we propose that CsA-induced overexpression of TGF- β is not mediated by Ang II. Instead, it is mediated by aldosterone, since it can be completely prevented by spironolactone (Fig. 6). In this regard, preliminary evidence shows that aldosterone infusion in normal rats increased TGF- β mRNA levels in the kidney (abstract; Juknevicius et al, *J Am Soc Nephrol* 11:622A, 2000). The chronic model for CsA toxicity is produced in rats that are fed with low salt diet. Hence, the activity of the renin-angiotensin system is enhanced and this also includes the increased release of aldosterone. Therefore, the beneficial effect of losartan or enalapril on TGF- β expression observed by Shihab et al [9] is probably the result of decreasing aldosterone release that is expected to occur when angiotensin blockers are used. In contrast to Shihab et al, we observed that spironolactone not only prevented the increase in the expression of TGF- β in the renal cortex, but also the functional and structural damage induced by CsA. Thus, spironolactone appears to be a helpful agent that effectively offers a therapeutic benefit in chronic CsA nephrotoxicity in the rat.

Increased attention has arisen on aldosterone as a potentially important mediator of chronic heart failure and renal disease. The use of spironolactone improves the survival rate in patients with chronic heart disease [38]. Moreover, studies in two different experimental models of renal disease, one due to hypertension and the other due to renal ablation, has shown that aldosterone infusion abrogates the renal protection conferred by Ang II inhibition either with ACE inhibitors, or Ang II receptor antagonists. In the model of severe hypertension in stroke-prone spontaneously hypertensive rats that were fed with high salt diet, Rocha et al observed that glomerular and vascular lesions were prevented with spironolactone or captopril, and the effect of captopril was reversed when rats were treated with aldosterone [19, 20]. In the renal ablation model, Greene, Kren and Hostetter provided evidence that aldosterone contributes to the development of hypertension and renal injury [18]. In these rats with 5/6 nephrectomy, losartan and enalapril reduces proteinuria and nephrosclerosis, but the protection conferred by these agents was completely avoided when aldosterone was re-infused to maintain levels comparable to untreated rats with reduced renal mass. In addition, selective blockade of aldosterone with eplerenone reduced proteinuria and glomerulosclerosis in L-NAME hypertensive rats [39]. Thus, aldosterone seems to play an important role in the progression of renal diseases. In this regard, recently it has been suggested that patients with diabetic nephropathy and already treated with enalapril may obtain further benefit by adding spironolactone to their daily treatment [40].

The exact mechanisms by which spironolactone protects the kidney from CsA toxicity are not clear from our current data and further studies will be necessary to clarify this issue. However, our observation that renal function was completely restored by spironolactone administration in CsA-treated rats suggests that, in addition to its effect on TGF- β expression, aldosterone blockade counterbalances the renal vasoconstriction induced by CsA. Although the mechanisms for this effect remain to be elucidated, it has been proposed that aldosterone modulates the vascular tone [41], possibly through increased vasoconstrictive effects of catecholamines [42], impaired vasodilation in response to acetylcholine [43], up-regulation of β -adrenergic and Ang II receptors [44–46], and a direct aldosterone effect, which could be mediated by non-genomic mechanisms [41]. The fact that arginine administration also prevented renal dysfunction and partially reversed the structural injury during chronic CsA toxicity [10] suggests that the possible vasodilatory action of spironolactone administration is responsible, at least in part, for the renal protection observed in our study.

Epidermal growth factor (EGF) is a 53-amino acid polypeptide that is known to be important as mediator of renal repair following injury. Recently, Yang et al showed

that chronic CsA nephrotoxicity is associated with a reduction of EGF protein levels in the kidney, which correlates with the degree of fibrosis and apoptosis [14]. Because these effects were reversed with losartan administration, the authors proposed that Ang II is the principal mediator of tubular injury through its effect on EGF. The present study confirms a down-regulation of EGF mRNA levels in the renal cortex of CsA treated rats. We also observed partial restoration of EGF expression when spironolactone was concomitantly administered with CsA. Thus, our data together with observations by Yang et al [14] show that blockade of either Ang II or aldosterone partially abrogates the EGF down-regulation observed in CsA-treated animals, and that this effect was associated with a significant reduction of tubulointerstitial damage.

In conclusion, our findings show that aldosterone plays a key role in producing functional and structural changes associated with CsA nephrotoxicity, and points to mineralocorticoid blockade as a potential treatment for reducing renal toxicity induced by CsA.

ACKNOWLEDGMENTS

This study was supported by research grant No. 28668 to Norma A. Bobadilla from the Mexican Council of Science and Technology (CONACYT). Part of this work was presented at the 2002 Experimental Biology Meeting, New Orleans, LA. We thank Mr. Cristina Cruz and Mr. Cesar Juárez for aldosterone measurements.

Reprint requests to Norma A. Bobadilla, Ph.D., Unidad de Fisiología Molecular, Vasco de Quiroga No. 15, Tlalpan, 14000, México City, México. E-mail: nbobadillas@sni.conacyt.mx

REFERENCES

- KOPP JB, KLOTMAN PE: Cellular and molecular mechanisms of cyclosporin nephrotoxicity. *J Am Soc Nephrol* 1:162–179, 1990
- KON V, SUGIURA M, INAGAMI T, et al: Role of endothelin in cyclosporine-induced glomerular dysfunction. *Kidney Int* 37:1487–1491, 1990
- PERICO N, DADAN J, REMUZZI G: Endothelin mediates the renal vasoconstriction induced by cyclosporine in the rat. *J Am Soc Nephrol* 1:76–83, 1990
- THOMSON AW, McAULEY FT, WHITING PH, SIMPSON JG: Angiotensin-converting enzyme inhibition or aldosterone antagonism reduces cyclosporine nephrotoxicity in the rat. *Transplant Proc* 19:1242–1243, 1987
- PERICO N, BENIGNI A, ZOJA C, et al: Functional significance of exaggerated renal thromboxane A2 synthesis induced by cyclosporin A. *Am J Physiol* 251:F581–F587, 1986
- ZHONG Z, ARTEEL GE, CONNOR HD, et al: Cyclosporin A increases hypoxia and free radical production in rat kidneys: Prevention by dietary glycine. *Am J Physiol* 275:F595–F604, 1998
- THOMAS SE, ANDOH TF, PICHLER RH, et al: Accelerated apoptosis characterizes cyclosporine-associated interstitial fibrosis. *Kidney Int* 53:897–908, 1998
- AMORE A, EMANCIPATOR SN, CIRINA P, et al: Nitric oxide mediates cyclosporine-induced apoptosis in cultured renal cells. *Kidney Int* 57:1549–1559, 2000
- SHIHAB FS, BENNETT WM, TANNER AM, ANDOH TF: Angiotensin II blockade decreases TGF-beta1 and matrix proteins in cyclosporine nephropathy. *Kidney Int* 52:660–673, 1997
- SHIHAB FS, YI H, BENNETT WM, ANDOH TF: Effect of nitric oxide modulation on TGF-beta1 and matrix proteins in chronic cyclosporine nephrotoxicity. *Kidney Int* 58:1174–1185, 2000
- VIEIRA JM JR, NORONHA IL, MALHEIROS DM, BURDMANN EA: Cyclosporine-induced interstitial fibrosis and arteriolar TGF-beta expression with preserved renal blood flow. *Transplantation* 68:1746–1753, 1999
- YOUNG BA, BURDMANN EA, JOHNSON RJ, et al: Cellular proliferation and macrophage influx precede interstitial fibrosis in cyclosporine nephrotoxicity. *Kidney Int* 48:439–448, 1995
- ORTIZ A, LORZ C, CATALAN M, et al: Cyclosporine A induces apoptosis in murine tubular epithelial cells: Role of caspases. *Kidney Int* 54(Suppl 68):S25–S29, 1998
- YANG CW, AHN HJ, KIM WY, et al: Influence of the renin-angiotensin system on epidermal growth factor expression in normal and cyclosporine-treated rat kidney. *Kidney Int* 60:847–857, 2001
- LEWIS EJ, HUNSICKER LG, BAIN RP, ROHDE RD: The effect of angiotensin-converting-enzyme inhibition on diabetic nephropathy. The Collaborative Study Group. *N Engl J Med* 329:1456–1462, 1993
- LEWIS EJ, HUNSICKER LG, CLARKE WR, et al: Renoprotective effect of the angiotensin-receptor antagonist irbesartan in patients with nephropathy due to type 2 diabetes. *N Engl J Med* 345:851–860, 2001
- BRENNER BM, COOPER ME, DE ZEEUW D, et al: Effects of losartan on renal and cardiovascular outcomes in patients with type 2 diabetes and nephropathy. *N Engl J Med* 345:861–869, 2001
- GREENE EL, KREN S, HOSTETTER TH: Role of aldosterone in the remnant kidney model in the rat. *J Clin Invest* 98:1063–1068, 1996
- ROCHA R, CHANDER PN, KHANNA K, et al: Mineralocorticoid blockade reduces vascular injury in stroke-prone hypertensive rats. *Hypertension* 31:451–458, 1998
- ROCHA R, CHANDER PN, ZUCKERMAN A, STIER CT JR: Role of aldosterone in renal vascular injury in stroke-prone hypertensive rats. *Hypertension* 33:232–237, 1999
- HOSTETTER TH, ROSENBERG ME, IBRAHIM HN, JUKNEVICIUS I: Aldosterone in renal disease. *Curr Opin Nephrol Hypertens* 10:105–110, 2001
- HENRY RJ, SOBEL CH, SEGALOVE M: Turbidimetric determination of proteins with sulfoasalic acid and tricholoroacetic acid. *Proc Soc Exp Biol Med* 92:748–751, 1956
- SAMBROOK J, FRITSCH EF, MANIATIS T: *Molecular Cloning. A Laboratory Manual*. Cold Spring Harbor, Cold Spring Harbor Laboratory Press, 1989, pp 7–7.15
- BOBADILLA NA, GAMBA G, TAPIA E, et al: Role of NO in cyclosporin nephrotoxicity: Effects of chronic NO inhibition and NO synthases gene expression. *Am J Physiol* 274:F791–F798, 1998
- BOBADILLA NA, HERRERA JP, MERINO A, GAMBA G: Semi-quantitative PCR: A tool to study low abundance messages in the kidney. *Arch Med Res* 28:55–60, 1997
- DORRANCE AM, OSBORN HL, GREKIN R, WEBB RC: Spironolactone reduces cerebral infarct size and EGF-receptor mRNA in stroke-prone rats. *Am J Physiol Regul Integr Comp Physiol* 281:R944–R950, 2001
- ROCCO MV, NEILSON EG, HOYER JR, ZIYADEH FN: Attenuated expression of epithelial cell adhesion molecules in murine polycystic kidney disease. *Am J Physiol* 262:F679–F686, 1992
- KANG DH, KIM YG, ANDOH TF, et al: Post-cyclosporine-mediated hypertension and nephropathy: amelioration by vascular endothelial growth factor. *Am J Physiol Renal Physiol* 280:F727–F736, 2001
- SCHWEDLER SB, BOBADILLA N, STRIKER LJ, et al: Pentosan polysulfate treatment reduces cyclosporine-induced nephropathy in salt-depleted rats. *Transplantation* 68:1583–1588, 1999
- HARRIS RC: Potential physiologic roles for epidermal growth factor in the kidney. *Am J Kidney Dis* 17:627–630, 1991
- KON V, HUNLEY TE, FOGO A: Combined antagonism of endothelin A/B receptors links endothelin to vasoconstriction whereas angiotensin II effects fibrosis. Studies in chronic cyclosporine nephrotoxicity in rats. *Transplantation* 60:89–95, 1995
- ANDOH TF, GARDNER MP, BENNETT WM: Protective effects of dietary L-arginine supplementation on chronic cyclosporine nephrotoxicity. *Transplantation* 64:1236–1240, 1997
- YANG CW, KIM YS, KIM J, et al: Oral supplementation of L-arginine prevents chronic cyclosporine nephrotoxicity in rats. *Exp Nephrol* 6:50–56, 1998

34. BOBADILLA NA, TAPIA E, JIMÉNEZ F, et al: Dexamethasone increases eNOS gene expression and prevents renal vasoconstriction induced by cyclosporin. *Am J Physiol* 277:F464–F471, 1999
35. DE NICOLA L, THOMSON SC, WEAD LM, et al: Arginine feeding modifies cyclosporine nephrotoxicity in rats. *J Clin Invest* 92:1859–1865, 1993
36. AMORE A, GIANOGLIO B, GHIGO D, et al: A possible role for nitric oxide in modulating the functional cyclosporine toxicity by arginine. *Kidney Int* 47:1507–1514, 1995
37. IACONA A, ROSSETTI A, FILINGERI V, et al: Reduced nephrotoxicity and hepatotoxicity in cyclosporin A therapy by enalapril and spironolactone in rats. *Drugs Exp Clin Res* 17:501–506, 1991
38. PITT B, ZANNAD F, REMME WJ, et al: The effect of spironolactone on morbidity and mortality in patients with severe heart failure. Randomized Aldactone Evaluation Study Investigators. *N Engl J Med* 341:709–717, 1999
39. ROCHA R, STIER CT JR, KIFOR I, et al: Aldosterone: A mediator of myocardial necrosis and renal arteriopathy. *Endocrinology* 141:3871–3878, 2000
40. CHRYSOSTOMOU A, BECKER G: Spironolactone in addition to ACE inhibition to reduce proteinuria in patients with chronic renal disease. *N Engl J Med* 345:925–926, 2001
41. NGARMUKOS C, GREKIN RJ: Nontraditional aspects of aldosterone physiology. *Am J Physiol Endocrinol Metab* 281:E1122–E1127, 2001
42. WANG W, MCCLAIN JM, ZUCKER IH: Aldosterone reduces baroreceptor discharge in the dog. *Hypertension* 19:270–277, 1992
43. TADDEI S, VIRDIS A, MATTEI P, SALVETTI A: Vasodilation to acetylcholine in primary and secondary forms of human hypertension. *Hypertension* 21:929–933, 1993
44. JAZAYERI A, MEYER WJ III: Mineralocorticoid-induced increase in beta-adrenergic receptors of cultured rat arterial smooth muscle cells. *J Steroid Biochem* 33:987–991, 1989
45. SCHIFFRIN EL, FRANKS DJ, GUTKOWSKA J: Effect of aldosterone on vascular angiotensin II receptors in the rat. *Can J Physiol Pharmacol* 63:1522–1527, 1985
46. SCHIFFRIN EL, GUTKOWSKA J, GENEST J: Effect of angiotensin II and deoxycorticosterone infusion on vascular angiotensin II receptors in rats. *Am J Physiol* 246:H608–H614, 1984

Joyce Trujillo, Victoria Ramírez, Jazmín Pérez, Ivan Torre-Villalvazo, Nimbe Torres, Armando R. Tovar, Rosa M. Muñoz, Norma Uribe, Gerardo Gamba and Norma A. Bobadilla

Am J Physiol Renal Physiol 288:108-116, 2005. First published Aug 24, 2004;
doi:10.1152/ajprenal.00077.2004

You might find this additional information useful...

This article cites 64 articles, 26 of which you can access free at:

<http://ajprenal.physiology.org/cgi/content/full/288/1/F108#BIBL>

This article has been cited by 2 other HighWire hosted articles:

Cardiovascular consequences of life-long exposure to dietary isoflavones in the rat

G. Douglas, J. A. Armitage, P. D. Taylor, J. R. Lawson, G. E. Mann and L. Poston
J. Physiol., March 1, 2006; 571 (2): 477-487.

[\[Abstract\]](#) [\[Full Text\]](#) [\[PDF\]](#)

Renocortical mRNA expression of vasoactive factors during spironolactone protective effect in chronic cyclosporine nephrotoxicity

J. M. Perez-Rojas, S. Derive, J. A. Blanco, C. Cruz, L. M. de la Maza, G. Gamba and N. A. Bobadilla

Am J Physiol Renal Physiol, November 1, 2005; 289 (5): F1020-F1030.

[\[Abstract\]](#) [\[Full Text\]](#) [\[PDF\]](#)

Updated information and services including high-resolution figures, can be found at:

<http://ajprenal.physiology.org/cgi/content/full/288/1/F108>

Additional material and information about **AJP - Renal Physiology** can be found at:

<http://www.the-aps.org/publications/ajprenal>

This information is current as of October 22, 2007 .

Renal protection by a soy diet in obese Zucker rats is associated with restoration of nitric oxide generation

Joyce Trujillo,^{1,2} Victoria Ramírez,^{1,2} Jazmín Pérez,^{1,2} Iván Torre-Villalvazo,³ Nimbe Torres,³ Armando R. Tovar,³ Rosa M. Muñoz,⁴ Norma Uribe,⁵ Gerardo Gamba,^{1,2} and Norma A. Bobadilla^{1,2}

¹Molecular Physiology Unit, Instituto de Investigaciones Biomédicas, Universidad Nacional Autónoma de México,

Departments of ²Nephrology, ³Physiology of Nutrition, ⁴Gastroenterology, and ⁵Pathology, Instituto Nacional de Ciencias Médicas y Nutrición Salvador Zubirán, Mexico City, Mexico

Submitted 10 March 2004; accepted in final form 18 August 2004

Trujillo, Joyce, Victoria Ramírez, Jazmín Pérez, Iván Torre-Villalvazo, Nimbe Torres, Armando R. Tovar, Rosa M. Muñoz, Norma Uribe, Gerardo Gamba, and Norma A. Bobadilla. Renal protection by a soy diet in obese Zucker rats is associated with restoration of nitric oxide generation. *Am J Physiol Renal Physiol* 288: F108–F116, 2005. First published August 24, 2004; doi:10.1152/ajprenal.00077.2004.—The obese Zucker rat is a valuable model for studying kidney disease associated with obesity and diabetes. Previous studies have shown that substitution of animal protein with soy ameliorates the progression of renal disease. To explore the participation of nitric oxide (NO) and caveolin-1 in this protective effect, we evaluated proteinuria, creatinine clearance, renal structural lesions, nitrates and nitrites urinary excretion ($\text{UNO}_2^-/\text{NO}_3^- \text{V}$), and mRNA and protein levels of neuronal NO synthase (nNOS), endothelial NOS (eNOS), and caveolin-1 in lean and fatty Zucker rats fed with 20% casein or soy protein diet. After 160 days of feeding with casein, fatty Zucker rats developed renal insufficiency, progressive proteinuria, and renal structural lesions; these alterations were associated with an important fall of $\text{UNO}_2^-/\text{NO}_3^- \text{V}$, changes in nNOS and eNOS mRNA levels, together with increased amount of eNOS and caveolin-1 present in plasma membrane proteins of the kidney. In fatty Zucker rats fed with soy, we observed that soy diet improved renal function, $\text{UNO}_2^-/\text{NO}_3^- \text{V}$, and proteinuria and reduced glomerulosclerosis, tubular dilation, interstitial fibrosis, and extracapillary proliferation. Renal protection was associated with reduction of caveolin-1 and eNOS in renal plasma membrane proteins. In conclusion, our results suggest that renal protective effect of soy protein appears to be mediated by improvement of NO generation and pointed out to caveolin-1 overexpression as a potential pathophysiological mechanism in renal disease.

plasma membrane proteins; endothelial nitric oxide synthase; nitrates and nitrates excretion

SEVERAL RISK FACTORS ASSOCIATED with an increased rate of progression in renal disease have been informed, including African-American race, male sex, hypertension, obesity, diabetes, hyperlipidemia, smoking, high-protein intake, phosphate retention, and metabolic acidosis (36). Although obesity is often associated with diabetes and hypertension, which are two of the most common risk factors for the development of end-stage renal disease (ESRD), it has been suggested that obesity per se is an independent risk factor (22). Massive obesity has been shown to produce nephrotic syndrome (56, 58), and it has been reported that proteinuria and segmental glomerulosclerosis can be present in obese patients, even in the

absence of diabetes (59). In addition, a large-scale study including 6,818 renal biopsies from 1986 to 2000 revealed a 10-fold increase in renal lesion, such as glomerulomegaly and focal segmental glomerulosclerosis, which were associated with obesity. Increased frequency of obesity-related glomerulopathy over the studied time ran in parallel with the increased prevalence of obesity within general population (33).

Mediators involved in obesity-induced renal injury are poorly understood. Available information comes from studies performed in rats and dogs fed with high-fat diet (23, 25) and from fatty Zucker rat (17, 31, 34, 38, 41, 49), an animal model of genetic obesity that results from inactivating mutation in leptin receptor gene. Homozygous Zucker rats (*fa/fa*) exhibit most of the metabolic picture seen in human obesity, including hypercholesterolemia, hypertriglyceridemia, hyperinsulinemia, and proteinuria. These animals also develop glomerular hypertension, hypertrophy, and sclerosis (6, 17, 31, 49) and often die due to ESRD (31). The mechanism by which renal disease is produced in obese Zucker rats is largely unknown, but it has been shown that consumption of plant-derived proteins retards the development and progression of renal disease in humans and in several animal models of disease (9, 27, 30, 46, 52, 61). Maddox et al. (39) observed that soy protein diet reduces plasma cholesterol levels, urinary protein excretion, and the rate of progression of glomerular injury in obese Zucker rat. The mechanisms by which soy protein conferred renal protection, however, were not established, but it has been suggested that could be related to the high content of phytoestrogens in soybean products, compared with animal sources of protein (54). Isoflavones (the most common phytoestrogens in soy plant) have been shown to possess antiproliferative and antioxidant properties (51, 57) and to act as weak estrogens (40) by blocking transcription of growth factor- β_1 (35) and by inhibiting activation of transcription factors such as nuclear factor- κB and activator protein-1 (62, 63).

A number of recent studies showed that nitric oxide (NO) synthesis is reduced in chronic renal disease in both humans and animals (2, 48, 55, 60). Therefore, it has been suggested that an impaired NO synthetic pathway could have a key role in mediating the complex renal hemodynamic and nonhemodynamic mechanisms associated with the progression of renal disease (for a review, see Ref. 44). In this regard, Frisbee and Stepp (16) informed that obese Zucker rats exhibit a considerable impairment of endothelium-dependent vasodilatation in

Address for reprint requests and other correspondence: N. A. Bobadilla, Unidad de Fisiología Molecular, Vasco de Quiroga No. 15, Tlalpan 14000, México City, Mexico (E-mail: nab@biomedicas.unam.mx).

The costs of publication of this article were defrayed in part by the payment of page charges. The article must therefore be hereby marked “advertisement” in accordance with 18 U.S.C. Section 1734 solely to indicate this fact.

skeletal muscle arterioles, raising the possibility that NO deficiency could contribute to progression of renal disease in this animal model. Caveolin-1, the resident integral membrane protein of caveolae, is upregulated in bovine aortic endothelial cells exposed to serum of hypercholesterolemic patients (12), and several lines of evidence demonstrate that, by interacting with endothelial NO synthase (eNOS), caveolin-1 inhibits the activity of this enzyme (19, 20, 32), thus reducing NO production. In addition, it is known that soy protein has a higher L-arginine content, the precursor of NO. Taking all this information together, we reasoned that one of the possible mechanisms by which soy diet confers renal protection in Zucker rats could be related to improvement of NO generation. Here, we show that renal protection conferred by soy protein diet in Zucker rats is associated with increase in NO metabolites excretion rate, changes in expression pattern of NO synthases, and reduction of caveolin-1 expression within the kidney.

MATERIALS AND METHODS

Twenty-four lean (*Fa/Fa*) and 40 obese (*fa/fa*) Zucker rats were obtained at 5 wk of age (Harlan, Indianapolis, IN) and randomly divided into four groups: lean and obese Zucker rats fed ad libitum with 20% casein protein, constituting *Fa/Fa+cas* and *fa/fa+cas* groups, respectively. The other two groups of lean and obese Zucker rats were fed with 20% soy protein, forming *Fa/Fa+soy* and *fa/fa+soy* groups, respectively. Body weight and food intake were recorded every day. Rats were placed in metabolic cages every 30 days at 22°C with 12:12-h light-dark cycle and free access to water and thereafter were anesthetized with carbon dioxide and killed by decapitation. Obese rats were studied at 30, 60, 90, 120, and 160 days, whereas lean rats at 90, 120, and 160 days. All procedures followed were in accordance with our institutional guidelines.

Functional studies. Individual 24-h urine samples were collected by placing animals in metabolic cages. Urinary protein excretion was measured by TCA turbidimetric method (26). Serum and urine creatinine concentration were measured with an autoanalyzer (Technicon RA-1000, Bayer, Tarrytown, NY), and renal creatinine clearance was calculated by the standard formula $C = U^*V/P$, where U is the concentration in urine, V is urine flow rate, and P is the plasma concentration. The end products of NO, nitrites, and nitrates (NO_2^- and NO_3^-) were estimated in 24-h urine samples by reducing NO_3^- to NO_2^- using nitrate reductase (Roche) and β -adene nicotinamide (β -NADPH, Sigma), followed by nitrites quantification with the Griess reagent, as we and others previously reported (8, 43).

Serum insulin was determined by RIA with rat insulin kit (Linco Research, St. Charles, MO). The sensitivity for rat insulin assay was 0.1 ng/ml, and the intra- and interassay coefficients of variation were <5 and <5%, respectively. Immune complexes were counted with cobra II gamma counter (Packard Instrument, Menden, CT). Serum cholesterol and tryglicerides were measured enzymatically according to the manufacturer's instructions (Lakeside Diagnostics).

RNA isolation. Total RNA was isolated from cortices or medullas of each group following guanidine isothiocyanate-cesium chloride method (47). The integrity of isolated total RNA was examined by 1% agarose gel electrophoresis, and RNA concentration was determined by UV light absorbance at 260 nm (Beckman DU640, Brea, CA).

RT-PCR. Relative level of NOS and caveolin mRNA expression was assessed in renal cortex and medulla by semiquantitative RT-PCR, as previously described (3, 4). Briefly, all primer sequences were custom obtained from GIBCO BRL (Gaithersburg, MD). Sense nNOS primers were 5'-GAACCCCCAAGACCATCC-3' and antisense 3'-GGCTTTGCTCCCACAGTT-5', which amplified a fragment of 308 bp, bases 692 to 999 (3); sense inducible (i)NOS primers were 5'-GTG TTC CAC CAG GAG ATG TTG-3' and antisense 5'-CTC CTG CCC ACT GAG TTC GTC-3', which amplified a

fragment of 570 bp, bases 1407 to 1977 (42); sense eNOS primers were 5'-CCG GAA ATT CGA ATA CCA GCC TGA TCC ATG GAA-3' and antisense 5'-GCC GGA TCC TCC AGG AGG GTG TCC ACC GCA TG-3', which amplified a fragment of 614 bp, base 2456 to 3069 (1), and caveolin-1 sense primers were 5'-ATG TCT GGG GGT AAA TAC GT-3' and antisense: 5'-CCT TCT GGT TCC GCA ATC AC-3', which amplified a fragment of 230 bp, bases 1 to 230 (50). To evaluate or reduce nonspecific effects of experimental treatment and to semiquantify NOS isoforms or cavelin-1 expression, we amplified a fragment of GAPDH, using primers previously described (3). Genomic DNA contamination was checked by treating all RNA samples with DNase and by carrying samples through PCR procedure without adding reverse transcriptase.

RT was carried out using 2.5 μg of total RNA from renal cortices or medullas. Before RT reaction, total RNA was heated at 65°C for 10 min. RT was performed at 37°C for 60 min in a total volume of 20 μl using 200 U of the Moloney murine leukemia virus reverse transcriptase (GIBCO BRL), 100 pmol of random hexamers (GIBCO BRL), 0.5 mM of each dNTP (Sigma, St. Louis, MO), and 1× RT buffer (75 mM KCl, 50 mM Tris·HCl, 3 mM MgCl₂, 10 mM DTT, pH 8.3). Samples were heated at 95°C for 5 min to inactivate the reverse transcriptase and diluted to 40 μl with PCR grade water. One-tenth of RT individual samples of each group was used for each NOS isoform or GAPDH amplification in 20- μl final volume reactions containing 1× PCR buffer (10 mM Tris·HCl, 1.5 mM MgCl₂, 50 mM KCl, pH 8.3), 0.1 mM of each dNTP, 0.2 μCi of [$\alpha^{32}\text{P}$]-dCTP (~3,000 Ci/mmol, 9.25 MBq, 250 μCi), 10 μM of each primer, and one unit of *Taq* DNA polymerase (GIBCO, BRL). Samples were overlaid with 30 μl of mineral oil and PCR cycles were performed in a DNA thermal cycler (M.J. Research, Watertown, MA), with the following profile: denaturation 1 min at 94°C; annealing 1 min at 55°C for nNOS, iNOS, and caveolin, 58°C for eNOS primers; and 1 min extension step at 72°C. Last cycle was followed by a final extension step of 5 min at 72°C. Control gene was coamplified simultaneously in each reaction.

Amplification kinetics were performed following our standard procedure (3–5, 11). To analyze PCR products, one-half of each reaction was electrophoresed in a 5% acrylamide gel. Bands were ethidium bromide stained and visualized under UV light, cut out, suspended in 1 ml of scintillation cocktail (Ecolume, ICN, Aurora, OH), and counted by liquid scintillation (Beckman LS6500, Fullerton, CA). The amount of radioactivity recovered from the excised bands was plotted in a log scale against the number of cycles. To semiquantify each NOS isoform, caveolin, and the control gene, all reactions were performed at least by quadruplicate.

Western blot analysis. Plasma membrane proteins from pooled renal cortices or medullas were isolated by homogenization in sucrose buffer (0.32 M sucrose, 5 mM Tris·HCl, pH 7.5, 2 mM EDTA). Homogenates were centrifuged at 3,000 g, supernatants were then centrifuged at 20,000 g, and final supernatants were centrifuged at 100,000 g. Each pellet was resuspended in a buffer containing 5 mM Tris·HCl (pH 7.5) and 2 mM EDTA. For nNOS detection, total proteins were also extracted from pooled cortices or medullas by homogenization in four volumes of lysis buffer (225 mM mannitol, 75 mM sucrose, 0.1 mM EDTA, pH 7.0; 0.5 mM MOPS, pH 7.0, containing 5 mM benzamidine and 5 mM DTT). Homogenates were centrifuged at 4,000 g for 4 min at 4°C to remove tissue debris without precipitating plasma membrane fragments. Protein concentrations were assessed in duplicate using Bio-Rad DC Protein assay (Bio-Rad, Hercules, CA). Protein samples containing 70 μg of total protein or 50 μg of plasma membrane proteins in 10 μl loading buffer (6% SDS, 15% glycerol, 150 mM Tris, 3% bromophenol blue, 2% β -mercaptoethanol, pH 7.6) were resolved by SDS-PAGE, semidried, and electroblotted onto polyvinylidene difluoride membranes (Bio-Rad). Thereafter, membranes were cut and the lower part was incubated with a rabbit caveolin-1 antibody 1:500 (Abcam, Lexington, KY) overnight at 4°C, whereas the upper membrane was incubated with a

Table 1. Physiological parameters in lean and obese Zucker rats at the end of the study

Group	Mean Food Intake, g	Body Weight, g	Left Kidney Weight, g	Cholesterol, mg/dl	Triglycerides, mg/dl	Insulin, mg/dl
Fa/Fa+cas	24.2±3.3	480±20	1.3±0.1	98±13	126±9	2.2±0.5
Fa/Fa+soy	24.2±3.3	440±16*	1.3±0.1	67±5*	78±5*	1.4±0.3
fa/fa+cas	22.4±1.0	592±48*	2.4±0.2*	575±66*	814±116*	7.5±3.1*
fa/fa+soy	21.2±1.3	708±45†	1.6±0.03†	180±31†	458±42†	6.4±0.9*

Values are means ± SE. *P < 0.05 vs. Fa/Fa+cas. †P < 0.05 vs. fa/fa+cas. Cas, casein.

goat actin antibody 1:2,500 (Santa Cruz Biotechnology, Santa Barbara, CA). Additional membranes containing total proteins or plasma membrane proteins were also incubated with rabbit nNOS polyclonal antibody 1:500 (Cayman Chemical, Ann Arbor, MI) and monoclonal eNOS antibody 1:250 (Zymed Laboratories, San Francisco, CA), respectively. Thereafter, membranes were washed three times for 30 min with TBS-T. For caveolin and nNOS detection, each membrane was incubated with the secondary antibody AP-conjugated goat anti-rabbit IgG 1:2,500 (Bio-Rad) for 60 min at 37°C and washed again. For eNOS detection, membranes were incubated with a secondary antibody AP-conjugated goat anti-mouse IgG 1:3,000 (Bio-Rad) for 60 min at 37°C and washed again. Whereas for actin detection, membranes were incubated with a secondary antibody donkey anti-goat IgG-HRP (Santa Cruz Biotechnology). Proteins were detected by using an enhanced chemiluminescence kit (Bio-Rad) and autoradiography, following the manufacturer's recommendations. Bands were scanned for densitometric analysis.

Histological studies. Before renal cortex and medulla separation, one-half of the left kidney was taken and fixed in formalin-phosphate buffer for light microscopy studies. After appropriate dehydration, kidney slices were embedded in paraffin, sectioned at 3 µm, and periodic acid-Schiff (PAS), eosin-hematoxilin, and trichromic stains were performed. Focal and global glomeruloesclerosis as well as extracapillary proliferation were counted in at least 150 glomeruli. Tubular atrophy and dilation were evaluated in ~300 tubules. The degree of tubulointerstitial fibrosis was evaluated by morphometry as we previously reported (11). For this purpose, 10 subcortical periglomerular fields per Masson-stained section (magnification ×200) were randomly selected in kidneys from the different groups. The images were recorded, and the affected areas were delimited and semiquantified using Leica processing and analysis system (Leica Imaging System, Cambridge, UK). Finally, the proportion of fibrosis was calculated dividing the interstitial fibrosis by total area per field excluding the luminal tubular area. The histological analysis was performed without knowing the group at which each kidney belonged.

Statistical analysis. Comparison among the groups for continuous data was made by using ANOVA. When ANOVA showed a statistically significant difference, a group-by-group comparison was performed using a *t*-test with a Bonferroni's correction for multiple comparisons.

RESULTS

Physiological parameters of the four groups of Zucker rats at the end of the study are presented in Table 1. As expected, body weight in obese rats was significantly elevated compared with that in lean controls. At the end of the study, obese rats fed with casein protein diet gained significantly less weight than rats fed with soy probably due to their physical deterioration. Kidney weight was also higher in obese rats compared with lean rats. The obese rats fed with soy (fa/fa+soy) appeared to have less renal hypertrophy than fa/fa+cas group, given their significantly lower kidney weights. This difference remained significant when kidney/body weight ratio was calculated: the ratio in fa/fa+cas vs. fa/fa+soy was 0.42 ± 0.07 and 0.23 ±

0.01 g/100 g body wt, respectively. Obese rats developed hypercholesterolemia, hypertriglyceridemia, and hyperinsulinemia compared with lean controls. Whereas in obese soy-feeding rats, cholesterol and tryglicerides serum levels were significantly lower than fa/fa+cas, without changes in insulin serum levels, confirming hypolipidemic effect of soy diet.

Figure 1 shows urinary protein excretion and creatinine clearance in lean and obese rats fed with casein or soy diet along the study. No differences in urinary protein excretion were observed in lean rats during the period of the study, which remained within normal values (Fig. 1A). In contrast, a significant progressive increase in proteinuria was observed in fa/fa+cas group throughout the study. Abnormal urinary protein excretion began at day 60, at which the average value was 70.9 ± 7.8 mg/24 h and at the end of the study proteinuria in this group was 280.5 ± 83.6 mg/24 h. Interestingly, soy protein intake was associated with a significant reduction in proteinuria levels in obese rats, because at the day 60, average value was 25.0 ± 8.0 mg/24 h and at day 160, the value was 92.8 ± 39.4 mg/24 h. These differences were statistically significant compared with fa/fa+cas group.

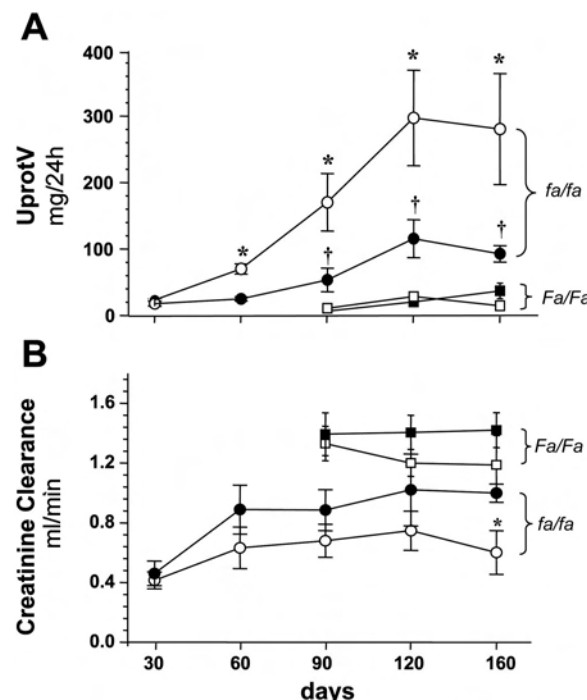


Fig. 1. A: creatinine clearance. B: urinary protein excretion measured every 30 days along the study of lean + casein (□, Fa/Fa+cas), lean + soy Fa/Fa+soy (■), Zucker + casein (○, fa/fa+cas), and Zucker + soy (●, fa/fa+soy) groups. *P < 0.05 all groups.

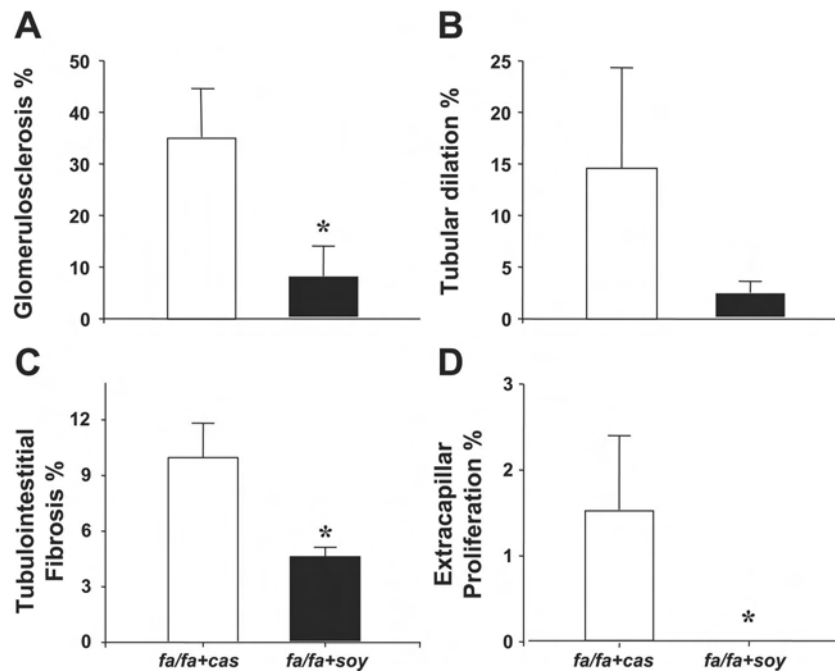


Fig. 2. Renal histological alterations in fatty Zucker rats after 160 days of feeding with casein (open bars) or soy diet (solid bars). Glomerulosclerosis (A) and extracapillary proliferation percentage (D) were calculated from at least 150 observed glomeruli, whereas tubular dilation percentage (B) was obtained from 300 examined tubules. Finally, the percentage of fibrosis (C) was calculated dividing the interstitial fibrosis by total area from 10 fields per Masson stained. *P < 0.05 vs. fa/fa+cas.

As shown in Fig. 1B, creatinine clearance in obese rats tended to be lower than control animals, but the difference was less evident in those rats fed with soy protein. Because at 160 days obese rats fed with casein had lesser body weight than soy animals, creatinine clearance was corrected by considering body weight of each animal. Glomerular filtration rate per 100 g of body weight in Fa/Fa+cas and Fa/Fa+soy was 0.26 ± 0.01 and $0.34 \pm 0.02 \text{ ml} \cdot \text{min}^{-1} \cdot 100 \text{ g}^{-1}$ ($P = 0.06$), respectively, and in fa/fa+cas and fa/fa+soy was 0.04 ± 0.02 and $0.11 \pm 0.02 \text{ ml} \cdot \text{min}^{-1} \cdot 100 \text{ g}^{-1}$ ($P = 0.03$), respectively. Although creatinine clearance in fa/fa+soy was not completely

normalized at the end of the study, a soy protective effect was clearly observed in this group, when it was compared with fa/fa+cas group.

Figure 2 shows the quantification of the most important lesions observed in fatty Zucker rats, and representative images are shown in Fig. 3. Fatty Zucker rats fed with casein exhibited the characteristic renal histological picture of this model that is segmental glomerulosclerosis, tubular dilation and atrophy, cast formation, and tubulointerstitial fibrosis. In fa/fa+cas group, percentage of glomerulosclerosis, tubular dilation, and tubulointerstitial fibrosis was 33.0 ± 11.8 ,

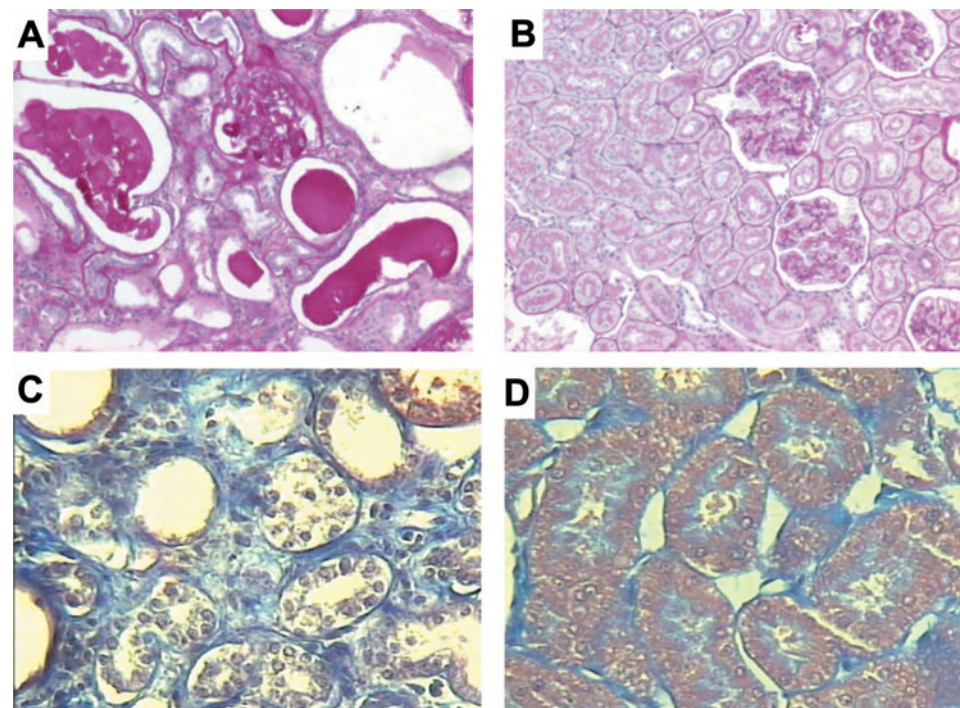


Fig. 3. Representative renal light microscopic findings of fatty Zucker rats after 160 days that were fed with casein or soy protein diet. Kidney slides were stained with periodic acid-Schiff, showing greater focal glomerulosclerosis and tubular dilation in fa/fa+cas (A) than fa/fa+soy (B) group (magnification $\times 100$). Also, tubulointerstitial fibrosis (C) and extracapillary proliferation (D) were more prominent in fa/fa+cas than fa/fa+soy group (Masson stain $\times 200$).

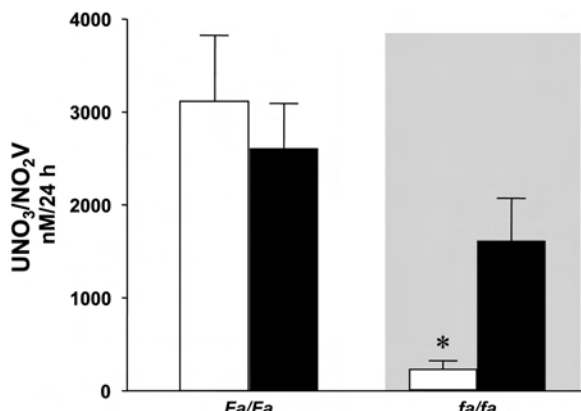


Fig. 4. Urinary nitrates and nitrites excretion ($\text{UNO}_3/\text{NO}_2\text{V}$) in lean and obese Zucker rats. Open bars represent animals fed with casein and solid bars represent rats fed with soy diet during 160 days. * $P < 0.05$ vs. all groups.

14.7 ± 9.8 , and $10 \pm 1.9\%$, respectively. All structural changes observed in obese rats were significantly reduced by soy protein diet. In *fa/fa+soy* group, mean percentage value of glomerulosclerosis, tubular dilation, and tubulointerstitial fibrosis were 8.3 ± 5.8 , 2.5 ± 1.1 , and 4.6 ± 0.5 , respectively. Thus our results indicate that the consumption of soy diet by obese Zucker rats reduces structural and functional changes.

To characterize the soy-protective effect on NO synthesis, end NO metabolites were quantified in urine. Urinary nitrates and nitrates excretion ($\text{UNO}_2/\text{NO}_3\text{V}$) is shown in Fig. 4 in lean and obese Zucker rats at 160 days after feeding with casein or soy protein diets. In lean Zucker rats, soy feeding had no effect on end NO metabolites excretion. In contrast, *fa/fa+cas* rats exhibited a significant reduction in $\text{UNO}_3/\text{NO}_2\text{V}$. Mean value was $238 \pm 77 \text{ nM}/24 \text{ h}$ in *fa/fa+cas* group vs. $3,114 \pm 702$

$\text{nM}/24 \text{ h}$ in *Fa/Fa+cas* ($P < 0.004$); however, the reduction observed in $\text{UNO}_3/\text{NO}_2\text{V}$ in *fa/fa+cas* rats was restored by soy protein intake, because average excretion in *fa/fa+soy* group was $1,615 \pm 456 \text{ nM}/24 \text{ h}$, a value that is significantly higher to that observed in *fa/fa+cas* group.

To explore if soy-induced renal protection is related to changes in intrarenal expression of NOS, neuronal (n)NOS and eNOS mRNA and protein levels were evaluated by semiquantitative RT-PCR and Western blot analysis, respectively (Figs. 5 and 6). Figure 5, left, shows that in renal cortex, soy protein diet in lean rats did not produce changes in eNOS or nNOS mRNA levels compared with rats fed with casein. In contrast, cortical nNOS mRNA level was upregulated in obese rats fed with casein, an effect that was reverted in *fa/fa+soy* group, together with a significant increase of eNOS expression in renal cortex. As shown in Fig. 5, right, eNOS mRNA in medulla was downregulated in *fa/fa+cas* rats, whereas soy protein was associated with a significant increase of eNOS in both lean and obese animals. No changes in medulla nNOS mRNA levels among all groups were observed.

Western blotting was used to assess protein expression of these enzymes. Actin was used as control protein to normalize each sample. Figure 6 shows the abundance of eNOS in plasma membrane proteins extracted from renal cortex (A) and medulla (B). Figure 6, top insets, are representative images of eNOS immunoblot. The eNOS protein level was similar in lean rats fed with casein or soy protein diet. In contrast, in *fa/fa+cas* group, there was a significant increase by threefold of eNOS in plasma membrane proteins from renal cortex; this effect was not observed in the medulla. As expected, nNOS was not detected in membrane proteins fraction (data not shown); thus total proteins were used to analyze nNOS expression. No difference in cortical nNOS expression was observed in lean and obese rats, regardless the source of protein; how-

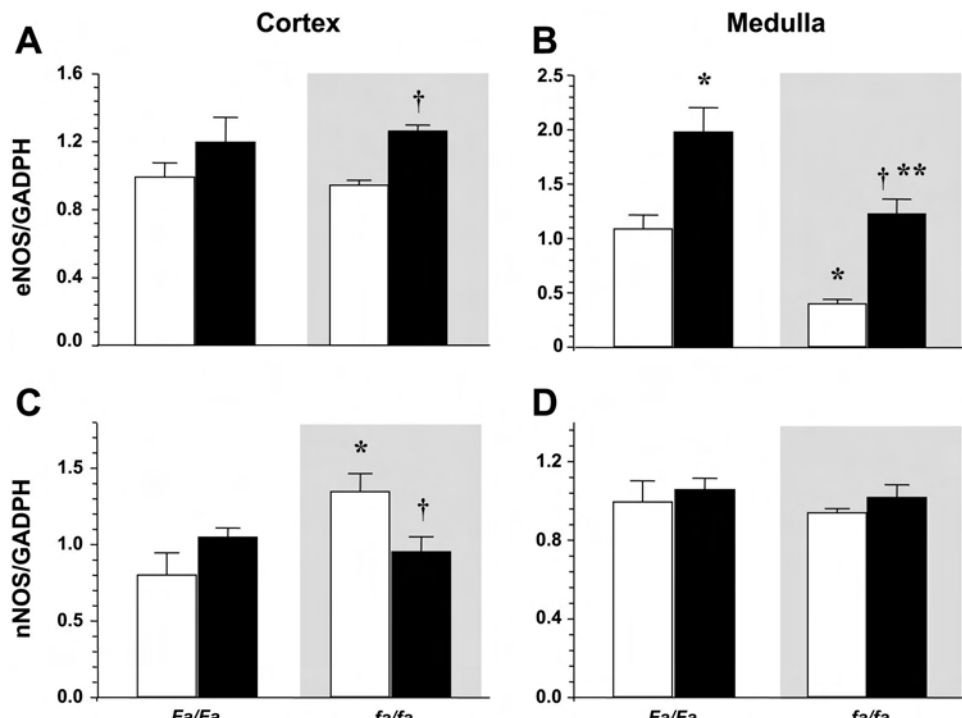


Fig. 5. mRNA levels of endothelial nitric oxide synthase (eNOS) and neuronal NOS (nNOS) in renal cortex (A and C) and medulla (B and D) of lean (*Fa/Fa*) and obese (*fa/fa*) Zucker rats at the end of the study, as stated. Open bars represent casein and solid bars represent soy diet-fed rats. Values were normalized by housekeeping gene expression. * $P < 0.05$ vs. *Fa/Fa+cas*. † $P < 0.05$ vs. *fa/fa+cas*. ** $P < 0.05$ *Fa/Fa+soy* group.

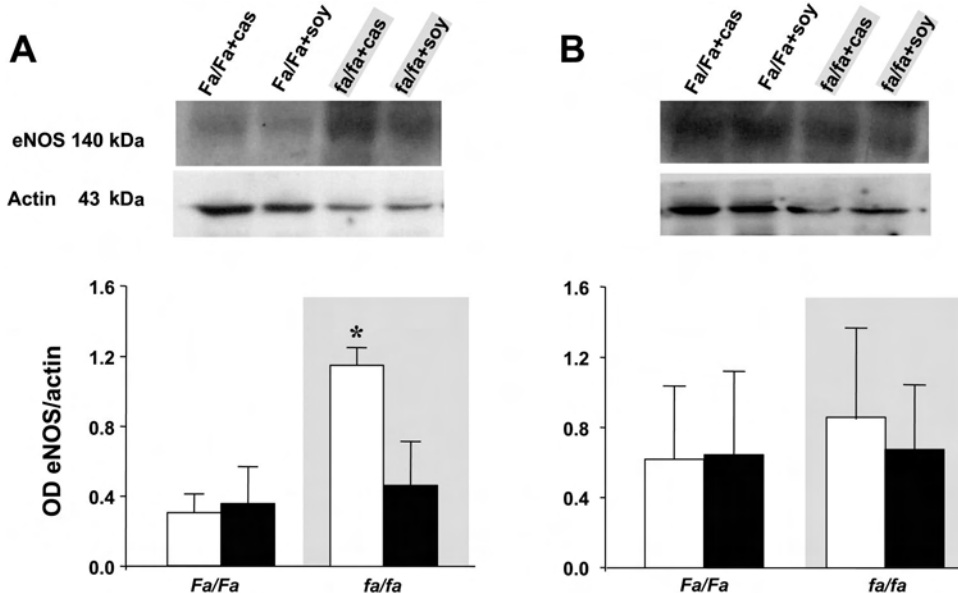


Fig. 6. Inactive form of eNOS protein was assessed by Western blot analysis in proteins isolated from renal cortex plasma membrane (A) and medulla (B) in lean and obese Zucker rats. Insets: representative images of eNOS and actin immunoblot. Charts represent optical density ratio between eNOS and actin. Open bars correspond to rats fed with casein and solid bars correspond to rats fed with soy. *P < 0.05 vs. all groups.

ever, an increase in medulla nNOS protein was observed in *fa/fa+cas* compared with *Fa/Fa+cas* group (1.8 ± 0.2 vs. 0.8 ± 0.1 , respectively), effect that was abrogated when rats were fed with soy diet (1.0 ± 0.1 ; data not shown).

Because it is known that eNOS activity is modulated by caveolin-1, level of expression of this protein was evaluated in renal cortex and medulla. As shown in Fig. 7, in renal cortex *Fa/Fa+cas* and *Fa/Fa+soy* groups exhibited similar caveolin-1 mRNA levels. Caveolin-1/GAPDH ratio was 1.45 ± 0.10 and 1.25 ± 0.18 , respectively. In contrast, *fa/fa+cas* group was associated with a significant caveolin-1 upregulation by almost twofold (2.60 ± 0.33 , $P = 0.008$ vs. *Fa/Fa+cas*). Intriguingly, soy protein intake in obese rats prevented this upregulation, because caveolin-1/GAPDH ratio was 1.33 ± 0.08 ($P = 0.004$). In renal medulla, similar results were observed. Casein-fed obese Zucker rats had higher caveolin-1 mRNA level than lean rats fed with casein: 2.29 ± 0.32 vs. 1.04 ± 0.04 , respectively ($P < 0.005$). This effect was prevented by soy protein diet, because the value in *fa/fa+soy* group was 1.39 ± 0.05 . In addition, caveolin-1 protein levels were assayed in plasma membrane proteins obtained from rat renal cortex and medulla by using Western blot analysis (Fig. 8). Western blot analysis confirmed our findings at mRNA level, caveolin-1 protein in isolated plasma membranes from renal cortex was significantly higher in *fa/fa+cas* than *Fa/Fa+cas* rats and the increase of these protein was normal-

ized when rats were fed with soy protein diet (*fa/fa+soy* group). A similar pattern was observed in renal medulla; however, the difference did not reach statistical significance.

DISCUSSION

In the present study, we observed that obese Zucker rats fed with casein developed a progressive renal disease characterized by proteinuria and glomeruloesclerosis that were associated with hypercholesterolemia, hypertriglyceridemia, and hyperinsulinemia. Renal progressive disease, as well as the increase in cholesterol and triglycerides levels, was significantly ameliorated when the obese Zucker rats were fed with soy instead of casein protein diet. These observations are consistent with a previous report (39), but little is known about the mechanism of the renal soy-protective effect. In this regard, hypertension seems not to be responsible for renal damage in this animal model, because Maddox et al. (39) observed that fatty Zucker rats exhibited only a slight increase in systolic blood pressure that cannot explain the development and progression of renal disease. Moreover, arterial pressure was not modified when rats were fed with soy. Data from this study revealed that soy diet conferring renal protection is associated with restoration of NO production.

A number of recent studies showed that NO synthesis is reduced in chronic renal disease in both humans and animals

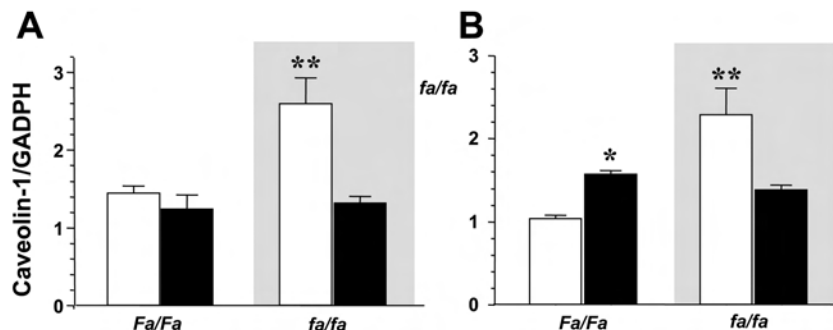


Fig. 7. Caveolin-1 mRNA levels in renal cortex (A) and medulla (B) of lean and obese Zucker rats. The open bars represent the ratio of caveolin-1 and housekeeping gene of rats fed with casein, whereas solid bars are rats fed with soy diet. *P < 0.05 vs. *Fa/Fa+cas*. **P < 0.05 vs. all groups.

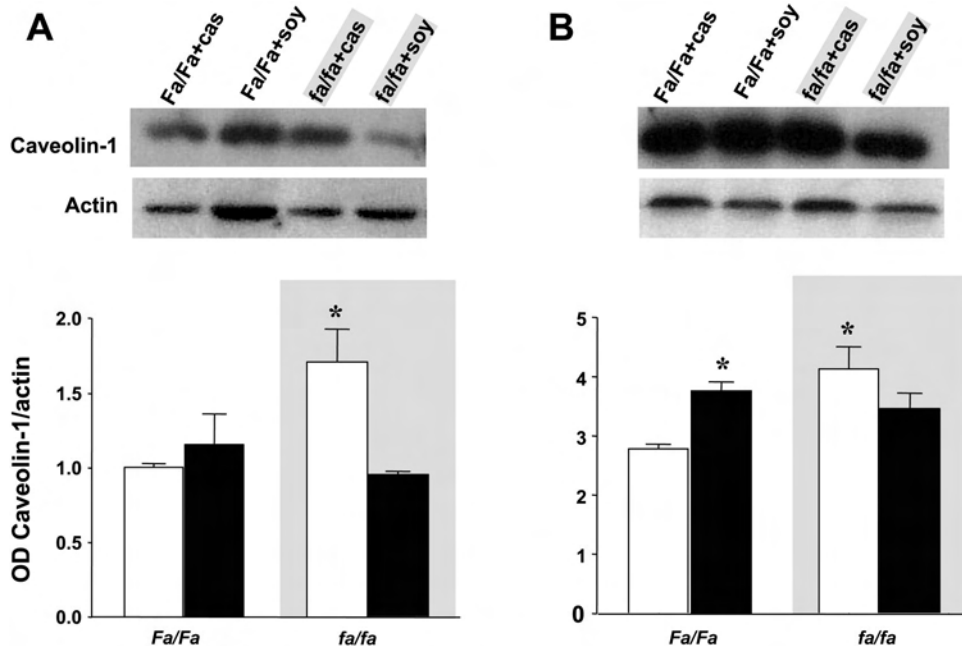


Fig. 8. Caveolin-1 Western blot analysis. Top insets: representative autoradiographs of caveolin-1 and actin from plasma membrane proteins extracted from renal cortex and medulla in lean and obese Zucker rats. Graphic representation of optical density showing the ratio between caveolin-1 and actin in renal cortex (A) and medulla (B). Open bars represent rats fed with casein and solid bars represent rats fed with soy. * $P < 0.05$ vs. Fa/Fa+cas.

(2, 48, 55, 60), suggesting that availability of NO in kidney is an important factor in defining the rate of progression injury in renal disorders. To explore the role of NO in renal protection conferred by soy protein diet, we evaluated the expression pattern of nNOS and eNOS in renal cortex and medulla, as well as NO metabolites excretion. We observed that both nNOS and eNOS expression pattern in obese rats fed with casein (*fa/fa+cas*) was different to that observed in lean animals fed with the same diet. At mRNA levels, there was an upregulation of nNOS in cortex and a downregulation of eNOS in medulla, these changes were normalized by soy diet. At protein level, *fa/fa+cas* group presented a significant increase of nNOS in total proteins from renal medulla. Physiological significance of this observation is unclear because the role of nNOS in renal medulla is unknown. However, upregulation of nNOS was prevented in obese rats fed with soy diet. Interestingly, *fa/fa+cas* group had a greater amount of eNOS in membrane proteins fraction, an effect that was also reverted in *fa/fa+soy* rats. Although eNOS expression was higher in *fa/fa+cas* group, it is unlikely that eNOS in this animal model is active because most of this enzyme was located in plasma membrane, a location in which it is known that association with caveolin-1 precludes its activity. In addition to these findings, we observed an unexpected small, but significant, increase in caveolin-1 mRNA and protein expression in renal medulla from lean animals fed with soy. Because the physiological role of caveolin-1 in renal medulla is not known, interpretation of this finding is difficult. Interestingly, a recent study demonstrated that caveolin-1 knockout mouse develops hypercalciuria and urolithiasis, suggesting that caveolin-1 is a critical determinant of urinary calcium homeostasis (7).

Supporting that changes in the NO synthetic pathway are altered in the fatty Zucker rats and that it is corrected by soy diet, we found that $\text{NO}_2^-/\text{NO}_3^-$ urinary excretion in *fa/fa+cas* rats was considerably depressed and soy protein intake was associated with restoration of NO systemic production. In addition, recent studies showed that obese Zucker strain has an

impairment in NO-mediated dilation of skeletal muscle arterioles, suggesting a deficient NO availability (16a, 24).

NO biosynthesis is tightly regulated by a variety of mechanisms ranging from transcriptional to posttranslational level (37). Recent studies indicate that some proteins directly interact with NOS-forming complexes that regulate NOS activity or spatial distribution in the cell. For instance, eNOS is regulated by proteins residing in or recruited to plasmalemmal caveolae of endothelial cells. Caveolins, the resident scaffolding proteins of caveolae, and calmodulin undergo reciprocal Ca^{2+} -dependent association and dissociation with eNOS in the caveolar membrane that inhibits (caveolins) and activates (calmodulin) eNOS activity (10, 13, 21, 32). Thus it has been suggested that association of eNOS to the caveolae through caveolin-1 maintains eNOS in its inactive form; on the contrary, the release of eNOS from caveolae is thought to facilitate the synthesis of NO (13, 21, 32). In support to this, it has been demonstrated that the mice with targeted disruption of caveolin-1 exhibit enhanced eNOS activity (10). Given the caveolin importance in regulating NO generation, we evaluated the expression of this protein. We observed that in normal lean rats, caveolin-1 is more abundant in medulla than in cortex plasma membrane proteins and that caveolin-1 mRNA and protein levels were significantly upregulated in cortex and medulla of fatty Zucker rats fed with casein, suggesting that increased expression of caveolin-1, together with greater amount of eNOS in plasma membrane, further decreases NO production in renal tissue. An interesting observation of this study is that soy protein diet significantly reduced caveolin-1 expression and eNOS abundance in plasma membranes in the kidney of these animals, suggesting that another mechanism by which soy diet improves NO generation is by decreasing the expression of caveolin-1, a natural inhibitor of NO synthesis (10, 13, 18, 21).

Several studies in humans and animals have revealed that soy protein intake ameliorates proteinuria and progression of renal disease (9, 27, 30, 39, 46, 52, 53, 61). There are several

possible mechanisms to explain this effect of soy. 1) Isoflavones. A component of soy that is believed to be involved in this protective effect is the isoflavones, by mechanisms that are still unclear, but include the following possibilities. Isoflavones comprise the most common class of phytoestrogens present mainly in soybean products. After ingestion, isoflavones are hydrolyzed in the intestine by bacterial β -glucosidases and converted to the bioactive aglycones: genistein and daidzein. Because isoflavones possess an important hypocholesterolemic effect observed in this study (Table 1), this is one of the mechanisms that have been suggested to be involved in renal protection induced by these compounds (34, 39, 46). Renoprotection also could result from antioxidant properties of isoflavones, which not only could avoid formation of free radicals (45) but also might result in enhancing NO availability (29). Finally, preliminary evidence suggests that diadzein directly downregulates caveolin-1 protein expression in rat aorta, which in turn was associated with twofold increase in NO metabolites (61a). 2) Amino acid content in soy protein. Although both soy and casein protein sources contain the same amount of total amino acids, there are differences in the proportion of certain residues. For instance, L-arginine, precursor of NO, is more abundant in soy than in casein protein (7.6 vs. 3.7%, respectively) and glycine, another residue that has been shown to produce vasodilation (28), is also more abundant in soy protein (4.2 vs. 1.8%, respectively). Therefore, soy-fed rats received a greater proportion of two residues that could be directly involved in vasodilatory processes. 3) Soy-induced hypocholesterolemia. It is possible that caveolin-1 downregulation results from hypocholesterolemic effect of soy diet, because Fielding and Fielding (15) postulated that caveolae behave as sensors of free cholesterol content of the cell and that depletion of caveolar cholesterol leads to downregulation of caveolin-1 at mRNA and protein levels (14). Moreover, Feron et al. (12) observed that exposure of bovine endothelial cells to serum from hypercholesterolemic patients resulted in upregulation of caveolin-1, an effect that was associated with an impairment of basal NO release, together with an increase in formation of inhibitory caveolin-eNOS complex; thus these studies suggest that cholesterol level regulates caveolin-1 expression.

In summary, our data show that nephropathy associated with obesity in the obese Zucker rat model could be reduced by feeding animals with soy, instead casein protein diet. The protective effect of soy diet was associated with reduction in cholesterol and triglyceride levels, as well as correction of a marked reduction in NO generation, that was associated with restoration of a normal pattern of NOS expression in the kidney and reduction of eNOS, together with a downregulation of caveolin-1 in plasma membrane proteins.

GRANTS

This work was supported by research Grants G34511M and CO1-40182A-1 from the Mexican Council of Science and Technology (Consejo Nacional de Ciencia y Tecnología) and Programa de Apoyo a Proyectos de Investigación y de Innovación Tecnológica IN208602-3 of National University of Mexico (to N. A. Bobadilla) and American Soybean Association. Part of this work was presented at the EB Meeting in San Diego, CA, 2003, and Washington, DC, 2004.

REFERENCES

- Abassi Z, Gurbanov K, Rubinstein I, Better OS, Hoffman A, and Winaver J. Regulation of intrarenal blood flow in experimental heart failure: role of endothelin and nitric oxide. *Am J Physiol Renal Physiol* 274: F766–F774, 1998.
- Aiello S, Noris M, Todeschini M, Zappella S, Foglieni C, Benigni A, Corna D, Zoja C, Cavallotti D, and Remuzzi G. Renal and systemic nitric oxide synthesis in rats with renal mass reduction. *Kidney Int* 52: 171–181, 1997.
- Bobadilla NA, Gamba G, Tapia E, Garcia-Torres R, Bolio A, Lopez-Zetina P, and Herrera-Acosta J. Role of NO in cyclosporin nephrotoxicity: effects of chronic NO inhibition and NO synthases gene expression. *Am J Physiol Renal Physiol* 274: F791–F798, 1998.
- Bobadilla NA, Herrera JP, Merino A, and Gamba G. Semiquantitative PCR: a tool to study low abundance messages in the kidney. *Arch Med Res* 28: 55–60, 1997.
- Bobadilla NA, Tapia E, Jimenez F, Sanchez-Lozada LG, Santamaría J, Monjardin A, Bolio A, Gamba G, and Herrera-Acosta J. Dexamethasone increases eNOS gene expression and prevents renal vasoconstriction induced by cyclosporin. *Am J Physiol Renal Physiol* 277: F464–F471, 1999.
- Bray GA. The Zucker-fatty rat: a review. *Fed Proc* 36: 148–153, 1977.
- Cao G, Yang G, Timme TL, Saika T, Truong LD, Satoh T, Goltssov A, Park SH, Men T, Kusaka N, Tian W, Ren C, Wang H, Kadmon D, Cai WW, Chinault AC, Boone TB, Bradley A, and Thompson TC. Disruption of the caveolin-1 gene impairs renal calcium reabsorption and leads to hypercalciuria and urolithiasis. *Am J Pathol* 162: 1241–1248, 2003.
- Chatterjee PK, Patel NS, Kvale EO, Cuzzocrea S, Brown PA, Stewart KN, Mota-Filipe H, and Thiemermann C. Inhibition of inducible nitric oxide synthase reduces renal ischemia/reperfusion injury. *Kidney Int* 61: 862–871, 2002.
- Djuric Z, Chen G, Doerge DR, Heilbrun LK, and Kucuk O. Effect of soy isoflavone supplementation on markers of oxidative stress in men and women. *Cancer Lett* 172: 1–6, 2001.
- Drab M, Verkade P, Elger M, Kasper M, Lohn M, Lauterbach B, Menne J, Lindschau C, Mende F, Luft FC, Schedl A, Haller H, and Kurzchalia TV. Loss of caveolae, vascular dysfunction, and pulmonary defects in caveolin-1 gene-disrupted mice. *Science* 293: 2449–2452, 2001.
- Feria I, Pichardo I, Juarez P, Ramirez V, Gonzalez MA, Uribe N, Garcia-Torres R, Lopez-Casillas F, Gamba G, and Bobadilla NA. Therapeutic benefit of spironolactone in experimental chronic cyclosporine A nephrotoxicity. *Kidney Int* 63: 43–52, 2003.
- Feron O, Dessy C, Moniotte S, Desager JP, and Balligand JL. Hypercholesterolemia decreases nitric oxide production by promoting the interaction of caveolin and endothelial nitric oxide synthase. *J Clin Invest* 103: 897–905, 1999.
- Feron O, Michel JB, Sase K, and Michel T. Dynamic regulation of endothelial nitric oxide synthase: complementary roles of dual acylation and caveolin interactions. *Biochemistry* 37: 193–200, 1998.
- Fielding CJ, Bist A, and Fielding PE. Caveolin mRNA levels are upregulated by free cholesterol and downregulated by oxysterols in fibroblast monolayers. *Proc Natl Acad Sci USA* 94: 3753–3758, 1997.
- Fielding PE and Fielding CJ. Intracellular transport of low density lipoprotein derived free cholesterol begins at clathrin-coated pits and terminates at cell surface caveolae. *Biochemistry* 35: 14932–14938, 1996.
- Frisbee JC and Stepp DW. Impaired NO-dependent dilation of skeletal muscle arterioles in hypertensive diabetic obese Zucker rats. *Am J Physiol Heart Circ Physiol* 281: H1304–H1311, 2001.
- Fulton J, Harris MB, Venema RC, and Stepp DW. Altered expression of endothelial NO synthase in the microcirculation of the obese Zucker rat (Abstract). *FASEB J* 17: 4861, 2003.
- Gades MD, Van Goor H, Kayser GA, Johnson PR, Horwitz BA, and Stern JS. Brief periods of hyperphagia cause renal injury in the obese Zucker rat. *Kidney Int* 56: 1779–1787, 1999.
- Garcia-Cardena G, Fan R, Stern DF, Liu J, and Sessa WC. Endothelial nitric oxide synthase is regulated by tyrosine phosphorylation and interacts with caveolin-1. *J Biol Chem* 271: 27237–27240, 1996.
- Garcia-Cardena G, Martasek P, Masters BS, Skidd PM, Couet J, Li S, Lisanti MP, and Sessa WC. Dissecting the interaction between nitric oxide synthase (NOS) and caveolin. Functional significance of the NOS caveolin binding domain in vivo. *J Biol Chem* 272: 25437–25440, 1997.

20. Garcia-Cardena G, Oh P, Liu J, Schnitzer JE, and Sessa WC. Targeting of nitric oxide synthase to endothelial cell caveolae via palmitoylation: implications for nitric oxide signaling. *Proc Natl Acad Sci USA* 93: 6448–6453, 1996.
21. Gratton JP, Fontana J, O'Connor DS, Garcia-Cardena G, McCabe TJ, and Sessa WC. Reconstitution of an endothelial nitric oxide synthase (eNOS), hsp90, and caveolin-1 complex in vitro. Evidence that hsp90 facilitates calmodulin stimulated displacement of eNOS from caveolin-1. *J Biol Chem* 275: 22268–22272, 2000.
22. Hall JE. The kidney, hypertension, and obesity. *Hypertension* 41: 625–633, 2003.
23. Hattori M, Nikolic-Paterson DJ, Miyazaki K, Isbel NM, Lan HY, Atkins RC, Kawaguchi H, and Ito K. Mechanisms of glomerular macrophage infiltration in lipid-induced renal injury. *Kidney Int Suppl* 71: S47–S50, 1999.
24. Hayashi K, Kanda T, Homma K, Tokuyama H, Okubo K, Takamatsu I, Tatematsu S, Kumagai H, and Saruta T. Altered renal microvascular response in Zucker obese rats. *Metabolism* 51: 1553–1561, 2002.
25. Henegar JR, Bigler SA, Henegar LK, Tyagi SC, and Hall JE. Functional and structural changes in the kidney in the early stages of obesity. *J Am Soc Nephrol* 12: 1211–1217, 2001.
26. Henry RJ, Sobel CH, and Segalove M. Turbidimetric determination of proteins with sulfoasalicylic and trichloroacetic acid. *Proc Soc Exp Biol Med* 92: 748–751, 1956.
27. Hermansen K, Sondergaard M, Hoie L, Carstensen M, and Brock B. Beneficial effects of a soy-based dietary supplement on lipid levels and cardiovascular risk markers in type 2 diabetic subjects. *Diabetes Care* 24: 228–233, 2001.
28. Herrera-Acosta J, Tapia E, Bobadilla NA, Romero L, Cermenio JL, Alvarado JA, and Gabbai FB. Evaluating hyperfiltration with glycine in hypertensive rats with renal ablation. *Hypertension* 11: I33–I37, 1988.
29. Hwang J, Wang J, Morazzoni P, Hodis HN, and Sevanian A. The phytoestrogen equal increases nitric oxide availability by inhibiting superoxide production: an antioxidant mechanism for cell-mediated LDL modification. *Free Radic Biol Med* 34: 1271–1282, 2003.
30. Jibani MM, Bloodworth LL, Foden E, Griffiths KD, and Galpin OP. Predominantly vegetarian diet in patients with incipient and early clinical diabetic nephropathy: effects on albumin excretion rate and nutritional status. *Diabet Med* 8: 949–953, 1991.
31. Johnson PR, Stern JS, Horwitz BA, Harris RE Jr, and Greene SF. Longevity in obese and lean male and female rats of the Zucker strain: prevention of hyperphagia. *Am J Clin Nutr* 66: 890–903, 1997.
32. Ju H, Zou R, Venema VJ, and Venema RC. Direct interaction of endothelial nitric oxide synthase and caveolin-1 inhibits synthase activity. *J Biol Chem* 272: 18522–18525, 1997.
33. Kambham N, Markowitz GS, Valeri AM, Lin J, and D'Agati VD. Obesity-related glomerulopathy: an emerging epidemic. *Kidney Int* 59: 1498–1509, 2001.
34. Kasiske BL, O'Donnell MP, Cleary MP, and Keane WF. Treatment of hyperlipidemia reduces glomerular injury in obese Zucker rats. *Kidney Int* 33: 667–672, 1988.
35. Kim H, Peterson TG, and Barnes S. Mechanisms of action of the soy isoflavone genistein: emerging role for its effects via transforming growth factor- β signaling pathways. *Am J Clin Nutr* 68: 1418S–1425S, 1998.
36. Klahr S and Morrissey J. Progression of chronic renal disease. *Am J Kidney Dis* 41: S3–S7, 2003.
37. Kone BC, Kuncewicz T, Zhang W, and Yu ZY. Protein interactions with nitric oxide synthases: controlling the right time, the right place, and the right amount of nitric oxide. *Am J Physiol Renal Physiol* 285: F178–F190, 2003.
38. Maddox DA, Alavi FK, Santella RN, and Zawada ET Jr. Prevention of obesity-linked renal disease: age-dependent effects of dietary food restriction. *Kidney Int* 62: 208–219, 2002.
39. Maddox DA, Alavi FK, Silbernick EM, and Zawada ET. Protective effects of a soy diet in preventing obesity-linked renal disease. *Kidney Int* 61: 96–104, 2002.
40. Martin PM, Horwitz KB, Ryan DS, and McGuire WL. Phytoestrogen interaction with estrogen receptors in human breast cancer cells. *Endocrinology* 103: 1860–1867, 1978.
41. Matsuda S, Arai T, Iwata K, Oka M, and Nagase M. A high-fat diet aggravates tubulointerstitial but not glomerular lesions in obese Zucker rats. *Kidney Int Suppl* 71: S150–S152, 1999.
42. Morrissey JJ, McCracken R, Kaneto H, Vehaskari M, Montani D, and Klahr S. Location of an inducible nitric oxide synthase mRNA in the normal kidney. *Kidney Int* 45: 998–1005, 1994.
43. Munoz-Fuentes RM, Vargas F, and Bobadilla NA. Assay validation for determining nitrates and nitrites in biological fluids. *Rev Invest Clin* 55: 670–676, 2003.
44. Noris M and Remuzzi G. Physiology and pathophysiology of nitric oxide in chronic renal disease. *Proc Assoc Am Physicians* 111: 602–610, 1999.
45. Pedraza-Chaverri J, Barrera D, Hernandez-Pando R, Medina-Campos ON, Cruz C, Murguia F, Juarez-Nicolas C, Correa-Rotter R, Torres N, and Tovar AR. Soy protein diet ameliorates renal nitrotyrosine formation and chronic nephropathy induced by puromycin aminonucleoside. *Life Sci* 74: 987–999, 2004.
46. Sakemi T, Ikeda Y, and Shimazu K. Effect of soy protein added to casein diet on the development of glomerular injury in spontaneous hypercholesterolemic male Imai rats. *Am J Nephrol* 22: 548–554, 2002.
47. Sambrook J, Fritsch EF, and Maniatis T. *Molecular Cloning: A Laboratory Manual*. New York: Cold Spring Harbor Laboratory, 1989.
48. Schmidt RJ and Baylis C. Total nitric oxide production is low in patients with chronic renal disease. *Kidney Int* 58: 1261–1266, 2000.
49. Schmitz PG, O'Donnell MP, Kasiske BL, Katz SA, and Keane WF. Renal injury in obese Zucker rats: glomerular hemodynamic alterations and effects of enalapril. *Am J Physiol Renal Fluid Electrolyte Physiol* 263: F496–F502, 1992.
50. Tamai O, Oka N, Kikuchi T, Koda Y, Soejima M, Wada Y, Fujisawa M, Tamaki K, Kawachi H, Shimizu F, Kimura H, Imaizumi T, and Okuda S. Caveolae in mesangial cells and caveolin expression in mesangial proliferative glomerulonephritis. *Kidney Int* 59: 471–480, 2001.
51. Tham DM, Gardner CD, and Haskell WL. Clinical review 97: potential health benefits of dietary phytoestrogens: a review of the clinical, epidemiological, and mechanistic evidence. *J Clin Endocrinol Metab* 83: 2223–2235, 1998.
52. Tomobe K, Philbrick DJ, Ogborn MR, Takahashi H, and Holub BJ. Effect of dietary soy protein and genistein on disease progression in mice with polycystic kidney disease. *Am J Kidney Dis* 31: 55–61, 1998.
53. Tovar AR, Murguia F, Cruz C, Hernandez-Pando R, Aguilar-Salinas CA, Pedraza-Chaverri J, Correa-Rotter R, and Torres N. A soy protein diet alters hepatic lipid metabolism gene expression and reduces serum lipids and renal fibrogenic cytokines in rats with chronic nephrotic syndrome. *J Nutr* 132: 2562–2569, 2002.
54. Velasquez MT and Bhathena SJ. Dietary phytoestrogens: a possible role in renal disease protection. *Am J Kidney Dis* 37: 1056–1068, 2001.
55. Wagner L, Riggleman A, Erdely A, Couser W, and Baylis C. Reduced nitric oxide synthase activity in rats with chronic renal disease due to glomerulonephritis. *Kidney Int* 62: 532–536, 2002.
56. Warne RA and Kempson RL. The nephrotic syndrome in massive obesity: a study by light, immunofluorescence, and electron microscopy. *Arch Pathol Lab Med* 102: 431–438, 1978.
57. Wei H, Bowen R, Cai Q, Barnes S, and Wang Y. Antioxidant and antipromotional effects of the soybean isoflavone genistein. *Proc Soc Exp Biol Med* 208: 124–130, 1995.
58. Weisinger JR, Kempson RL, Eldridge FL, and Swenson RS. The nephrotic syndrome: a complication of massive obesity. *Ann Intern Med* 81: 440–447, 1974.
59. Wesson DE, Kurtzman NA, and Frommer JP. Massive obesity and nephrotic proteinuria with a normal renal biopsy. *Nephron* 40: 235–237, 1985.
60. Wever R, Boer P, Hijmering M, Stroes E, Verhaar M, Kastelein J, Versluis K, Lagerwerf F, van Rijn H, Koomans H, and Rabelink T. Nitric oxide production is reduced in patients with chronic renal failure. *Arterioscler Thromb Vasc Biol* 19: 1168–1172, 1999.
61. Williams AJ and Walls J. Metabolic consequences of differing protein diets in experimental renal disease. *Eur J Clin Invest* 17: 117–122, 1987.
- 61a. Woodman L and Boujaoude M. The isoflavone daidzein enhances nitric oxide synthesis by decreasing expression of caveolin-1 and increasing expression of calmodulin (Abstract). *FASEB J* 17: 5015, 2003.
62. Zhu Y, Lin JH, Liao HL, Friedli O Jr, Verna L, Marten NW, Straus DS, and Stemerman MB. LDL induces transcription factor activator protein-1 in human endothelial cells. *Arterioscler Thromb Vasc Biol* 18: 473–480, 1998.
63. Zhu Y, Lin JH, Liao HL, Verna L, and Stemerman MB. Activation of ICAM-1 promoter by lysophosphatidylcholine: possible involvement of protein tyrosine kinases. *Biochim Biophys Acta* 1345: 93–98, 1997.

Vishal S. Vaidya, Victoria Ramirez, Takaharu Ichimura, Norma A. Bobadilla and Joseph V. Bonventre

Am J Physiol Renal Physiol 290:517-529, 2006. First published Sep 20, 2005;
doi:10.1152/ajprenal.00291.2005

You might find this additional information useful...

This article cites 41 articles, 18 of which you can access free at:

<http://ajprenal.physiology.org/cgi/content/full/290/2/F517#BIBL>

This article has been cited by 8 other HighWire hosted articles, the first 5 are:

The Utility of a Rodent Model in Detecting Pediatric Drug-Induced Nephrotoxicity

P. Espandiar, J. Zhang, B. A. Rosenzweig, V. S. Vaidya, J. Sun, L. Schnackenberg, E. H. Herman, A. Knapton, J. V. Bonventre, R. D. Beger, K. L. Thompson and J. Hanig
Toxicol. Sci., October 1, 2007; 99 (2): 637-648.

[Abstract] [Full Text] [PDF]

Shedding of the Urinary Biomarker Kidney Injury Molecule-1 (KIM-1) Is Regulated by MAP Kinases and Juxtamembrane Region

Z. Zhang, B. D. Humphreys and J. V. Bonventre
J. Am. Soc. Nephrol., October 1, 2007; 18 (10): 2704-2714.

[Abstract] [Full Text] [PDF]

Increased susceptibility of aging kidney to ischemic injury: identification of candidate genes changed during aging, but corrected by caloric restriction

G. Chen, E. A. Bridenbaugh, A. D. Akintola, J. M. Catania, V. S. Vaidya, J. V. Bonventre, A. C. Dearman, H. W. Sampson, D. C. Zawieja, R. C. Burghardt and A. R. Parrish
Am J Physiol Renal Physiol, October 1, 2007; 293 (4): F1272-F1281.

[Abstract] [Full Text] [PDF]

Urinary N-Acetyl-beta-(D)-Glucosaminidase Activity and Kidney Injury Molecule-1 Level Are Associated with Adverse Outcomes in Acute Renal Failure

O. Liangos, M. C. Perianayagam, V. S. Vaidya, W. K. Han, R. Wald, H. Tighiouart, R. W. MacKinnon, L. Li, V. S. Balakrishnan, B. J.G. Pereira, J. V. Bonventre and B. L. Jaber
J. Am. Soc. Nephrol., March 1, 2007; 18 (3): 904-912.

[Abstract] [Full Text] [PDF]

Mineralocorticoid receptor blockade confers renoprotection in preexisting chronic cyclosporine nephrotoxicity

J. Perez-Rojas, J. A. Blanco, C. Cruz, J. Trujillo, V. S. Vaidya, N. Uribe, J. V. Bonventre, G. Gamba and N. A. Bobadilla
Am J Physiol Renal Physiol, January 1, 2007; 292 (1): F131-F139.

[Abstract] [Full Text] [PDF]

Updated information and services including high-resolution figures, can be found at:

<http://ajprenal.physiology.org/cgi/content/full/290/2/F517>

Additional material and information about *AJP - Renal Physiology* can be found at:

<http://www.the-aps.org/publications/ajprenal>

This information is current as of October 22, 2007 .

Urinary kidney injury molecule-1: a sensitive quantitative biomarker for early detection of kidney tubular injury

Vishal S. Vaidya,¹ Victoria Ramirez,² Takaharu Ichimura,¹
Norma A. Bobadilla,² and Joseph V. Bonventre¹

¹Renal Division, Department of Medicine, Brigham and Women's Hospital, Harvard Medical School, Boston, Massachusetts; and ²Molecular Physiology Unit, Instituto de Investigaciones Biomédicas, Universidad Nacional Autónoma de México and Instituto Nacional de Ciencias Médicas y Nutrición Salvador Zubirán, Mexico City, Mexico

Submitted 15 July 2005; accepted in final form 13 September 2005

Vaidya, Vishal S., Victoria Ramirez, Takaharu Ichimura, Norma A. Bobadilla, and Joseph V. Bonventre. Urinary kidney injury molecule-1: a sensitive quantitative biomarker for early detection of kidney tubular injury. *Am J Physiol Renal Physiol* 290: F517–F529, 2006. First published September 20, 2005; doi:10.1152/ajprenal.00291.2005.—Sensitive and specific biomarkers are needed to detect early kidney injury. The objective of the present work was to develop a sensitive quantitative urinary test to identify renal injury in the rodent to facilitate early assessment of pathophysiological influences and drug toxicity. Two mouse monoclonal antibodies were made against the purified ectodomain of kidney injury molecule-1 (Kim-1), and these were used to construct a sandwich Kim-1 ELISA. The assay range of this ELISA was 50 pg/ml to 5 ng/ml, with inter- and intra-assay variability of <10%. Urine samples were collected from rats treated with one of three doses of cisplatin (2.5, 5, or 7.5 mg/kg). At one day after each of the doses, there was an approximately three- to fivefold increase in the urine Kim-1 ectodomain, whereas other routinely used biomarkers measured in this study [plasma creatinine, blood urea nitrogen (BUN), urinary *N*-acetyl-β-glucosaminidase (NAG), glycosuria, proteinuria] lacked the sensitivity to show any sign of renal damage at this time point. When rats were subjected to increasing periods (10, 20, 30, or 45 min) of bilateral ischemia, there was an increasing amount of urinary Kim-1 detected. After only 10 min of bilateral ischemia, Kim-1 levels on day 1 were 10-fold higher (5 ng/ml) than control levels, whereas plasma creatinine and BUN were not increased and there was no glycosuria, increased proteinuria, or increased urinary NAG levels. Thus urinary Kim-1 levels serve as a noninvasive, rapid, sensitive, reproducible, and potentially high-throughput method to detect early kidney injury in pathophysiological studies and in preclinical drug development studies for risk-benefit profiling of pharmaceutical agents.

biomarkers; nephrotoxicity; enzyme-linked immunosorbent assay; cisplatin; ischemia; acute renal failure

ALTHOUGH THERE HAS BEEN a significant progress in understanding the biochemical and molecular mechanisms of ischemic or toxic forms of acute kidney injury (AKI) in animal models, translation of these findings to therapeutics useful in clinical practice remains challenging (13, 38). One of the predominant reasons for the slow translation of the results from bench to bedside, especially in the treatment of existing AKI, is the absence of reliable biomarkers of injury in animal and human studies (36, 39). The Food and Drug Administration's critical path initiative has reinforced the need for additional biomarkers to predict drug toxicity in preclinical studies. These biomarkers can act as surrogate endpoints and/or aid in making

efficacious and cost-saving decisions including terminating drug development more quickly (39a). Easily quantifiable and sensitive biomarkers can be influential in every phase of therapeutics, from drug discovery and preclinical evaluation through each phase of clinical trials and into postmarketing studies.

Routinely used measures of renal function, such as levels of blood urea nitrogen (BUN) and serum creatinine, increase significantly only after substantial kidney injury occurs and then with a time delay (15). In drug development, minimizing nephrotoxicity is highly desirable. Insensitivity of tests affects the evaluation of toxicity in preclinical studies by allowing drug candidates, which have low but nevertheless important nephrotoxic side effects in animals, to pass the preclinical safety criteria only to be found to be clinically nephrotoxic in humans at great costs to patients. The kidney is one of the primary sites of drug toxicity. Despite this, the tests available to detect toxicity and early ischemic renal injury are either invasive and difficult to quantitate or noninvasive, nonspecific, and insensitive. Acute kidney failure is a common disease and is associated with a high mortality rate (5, 38). It has been recognized that better biomarkers for kidney injury are needed both for animal studies and for use in humans where early detection of kidney injury will influence therapy and potentially morbidity and mortality.

Urine has been examined as a source for biomarkers given its easy availability and reduced complexity when compared with serum. Many urinary proteins such as α- and π-glutathione-S-transferases (α- and π-GST; see Ref. 7), neutrophil gelatinase-associated lipocalin (NGAL; see Ref. 24), cysteine-rich protein 61 (CYR-61; see Refs. 26), interleukin (IL)-18 (28), clusterin (2), F-actin (34), *N*-acetyl-β-D-glucosaminidase (NAG; see Ref. 42), etc., have been evaluated as noninvasive indicators of renal injury. However, problems with reliable use of these proteins to identify and monitor kidney injury includes instability in the urine, modification due to physicochemical properties of the urine, delayed appearance, inconsistency of upregulation with different models of nephrotoxicity, absence of sustained elevation throughout the time course of renal injury to monitor progression and regression of injury, and lack of a high-throughput detection method.

We have cloned a potential biomarker for AKI named kidney injury molecule-1 (Kim-1; see Ref. 16). Kim-1 is a type 1 transmembrane protein that is not detectable in normal

Address for reprint requests and other correspondence: J. V. Bonventre, Renal Division, Brigham and Women's Hospital, Harvard Medical School, 4 Blackfan Circle, Harvard Institutes of Medicine, Rm. 550, Boston, MA 02115 (e-mail: joseph_bonventre@hms.harvard.edu).

The costs of publication of this article were defrayed in part by the payment of page charges. The article must therefore be hereby marked "advertisement" in accordance with 18 U.S.C. Section 1734 solely to indicate this fact.

kidney tissue but is expressed at very high levels in dedifferentiated proximal tubule epithelial cells in human and rodent kidneys after ischemic or toxic injury (12, 16). The Kim-1 ectodomain is stable in the urine for prolonged periods of time and can be detected in the kidney and urine in a number of nephrotoxic models in animals (1, 17) and in humans with AKI (13). Although we have previously developed a sensitive ELISA assay to measure human KIM-1 in the urine (12), this unfortunately does not detect either rat or mouse Kim-1.

The present study was designed to develop, evaluate, and validate a high-throughput detection method for quantitating Kim-1 in rat urine and to test the sensitivity of this assay to detect kidney injury before changes in other tests used routinely to detect kidney injury. The test was applied and validated in two well-established and widely used mechanistically distinct animal models of renal injury: cisplatin-induced nephrotoxicity and bilateral renal ischemia-reperfusion (I/R; see Ref. 32).

MATERIALS AND METHODS

Animals

Male Sprague-Dawley rats (275–300 g) were purchased from Charles River laboratories (Wilmington, MA), and male Wistar rats (275–300 g) were purchased from Harlan (Indianapolis, IN). Rats were maintained in central animal facilities in Boston and Mexico City under conditions of $21 \pm 1^\circ\text{C}$ and 50–80% relative humidity at all times in a 12:12-h light-dark cycle over wood chips free of any known chemical contaminants. The rats were fed with commercial rodent chow (Teklad rodent diet no. 7012), given water ad libitum, and acclimated for 1 wk before use. All animal maintenance and treatment protocols were in compliance with the *Guide for Care and Use of Laboratory Animals* as adopted and promulgated by the United States National Institutes of Health and were approved by our Institutional Animal Care and Use Committees.

Cisplatin-Induced Nephrotoxicity Studies

Male Sprague-Dawley rats were administered 2.5, 5, or 7.5 mg cisplatin/kg intraperitoneally in 0.9% saline or the same volume of vehicle as controls ($n = 4$ /dose for each time point). Animals were euthanized by an overdose of pentobarbital sodium (200 mg/kg ip) at days 1, 2, 3, 4, or 5. Blood was collected from the dorsal aorta in heparinized tubes for measurement of BUN and creatinine. One kidney was perfused via the left ventricle with PBS and then with paraformaldehyde lysine periodate (PLP) for 10 min for histology and immunostaining, as described below. The other kidney pedicle was clamped before PLP perfusion, and that kidney was snap-frozen for immunoblotting and RNA extraction. Another set of rats ($n = 10$ /dose for each time point) was kept in Nalgene rat metabolic cages (Fisher) before and subsequent to administration of cisplatin. Urine was collected daily for 5 days and stored in aliquots at -80°C . Urine was centrifuged at 6,000 g for 15 min, and the supernatant was used to measure creatinine, glucose, protein, NAG, and Kim-1 as described below.

Tissue Collection, Preparation, and Histology

Kidneys from control and treated rats at various time points were perfused via the left ventricle with PBS at 37°C and then with PLP for 10 min (17, 30). The right contralateral pedicle-clamped unfixed kidney, to be used for biochemical analyses, was removed immediately after perfusion was started. After an initial 10- to 15-min period of perfusion fixation, the left kidney was removed, washed with ice-cold normal saline (0.9% NaCl), and cut sagittally into two halves. One half of the left kidney was kept in the PLP fixative overnight at

4°C , rinsed with PBS, and kept in PBS containing 0.2% sodium azide at 4°C before cryosectioning. Pieces of fixed kidneys were equilibrated for at least 1 h at room temperature in PBS containing 30% sucrose, embedded in optimum cutting temperature medium, frozen in liquid nitrogen, and cryosectioned (5 μm). Sections on glass slides were kept in -20°C until further processing. The other half was fixed with 10% phosphate-buffered formaldehyde for 48 h. The tissues were then transferred to 70% ethyl alcohol, processed, and embedded in paraffin wax. Kidney sections (5 μm) were stained with hematoxylin and eosin for histological examination under a light microscope. The kidney harvested for biochemical analysis was washed with PBS, hemisected, and snap-frozen in liquid nitrogen; tissue was stored at -70°C .

Renal I/R Studies

Twenty-five male Wistar rats weighing ~ 300 g were anesthetized with an intraperitoneal injection of pentobarbital sodium (30 mg/kg) and placed on a homeothermic table to maintain core body temperature at 37°C , by means of a rectal probe attached to a temperature regulator that was in turn attached to a homeothermic blanket. A midline laparotomy was made, renal pedicles were isolated, and bilateral renal ischemia was induced by clamping the renal pedicles for 0, 10, 20, 30, or 45 min. Reperfusion commenced when the clips were removed. Occlusion was verified visually by change in the color of the kidneys to a paler shade and reperfusion by a blush.

After reperfusion (2 h), the rats were placed in metabolic cages at 22°C with a 12:12-h light-dark cycle and allowed free access to water. Individual 24-h urine samples were collected.

Renal Functional Parameters

In the cisplatin studies, plasma and urine creatinine concentrations were measured using a Beckman Creatinine Analyzer II. BUN was spectrophotometrically measured at 340 nm using a commercially available kit (catalog no. TR12421; ThermoTrace). Collected urine samples were centrifuged at 6,000 rpm for 15 min. Supernatants were collected and diluted 1:10 with deionized water. Diluted urine samples were used for analysis of creatinine. Urine glucose (catalog no. 1530–500; Thermo-DMA), protein (catalog no. TP0400; Sigma), and NAG (catalog no. 875406; Roche Diagnostics) were measured spectrophotometrically (41) according to the manufacturers' protocols.

In the I/R studies, urinary protein excretion was measured by the TCA turbidimetric method (14). Serum and urine creatinine concentration and BUN were measured with an autoanalyzer (Technicon RA-1000; Bayer, Tarrytown, NY), and renal creatinine clearance was calculated by the standard formula $C = (U \times V)/P$, where U is the concentration in urine, V is urine flow rate, and P is the plasma concentration.

RNA Isolation

Total RNA was isolated from cortices of each group using the guanidine isothiocyanate-cesium chloride method (33). Integrity of isolated total RNA was examined by 1% agarose gel electrophoresis, and RNA concentration was determined by ultraviolet light absorbance at 260 nm (model DU640; Beckman, Brea, CA).

Kim-1 Semiquantitative RT-PCR

Relative levels of Kim-1 and glyceraldehyde-3-phosphate dehydrogenase (GADPH) mRNA expression were assessed in renal cortex and medulla by semiquantitative RT-PCR, as previously described (4, 10). Briefly, primer sequences were custom made by GIBCO-BRL (Gaithersburg, MD). Kim-1 primers were designed from the rat Kim-1 sequence. The sense primer was 5'-CGGTGCCTGTGAGTAAATA-GAT-3' and antisense 3'-CTGGCCATGACACAAATAAGAC-5', which amplified a fragment of 418 bp, bases 1 to 418. To evaluate or reduce nonspecific effects of experimental treatment and to semiquan-

tify Kim-1 expression, we amplified a fragment of GAPDH using primers previously described (31). Genomic DNA contamination was checked by treating all RNA samples with DNase and by carrying samples through the PCR procedure without adding reverse transcriptase (RT).

RT was carried out using 2.5 µg total RNA from renal cortices. Before RT reaction, total RNA was heated at 65°C for 10 min. RT was performed at 37°C for 60 min in a total volume of 20 µl using 200 units of the Moloney murine leukemia virus RT (GIBCO-BRL), 100 pmol random hexamers (GIBCO-BRL), 0.5 mM of each dNTP (Sigma Chemical, St. Louis, MO), and 1× RT buffer (75 mM KCl, 50 mM Tris·HCl, 3 mM MgCl₂, and 10 mM dithiothreitol, pH 8.3). Samples were heated at 95°C for 5 min to inactivate the RT and diluted to 40 µl with PCR-grade water. One-tenth of RT individual samples of each group was used for Kim-1 or GAPDH amplification in 20 µl final volume reactions containing 1× PCR buffer (10 mM Tris·HCl, 1.5 mM MgCl₂, and 50 mM KCl, pH 8.3), 0.1 mM of each dNTP, 0.2 µCi [α -³²P]dCTP (~3,000 Ci/mmol, 9.25 MBq, 250 µCi), 10 µM of each primer, and 1 unit *Taq* DNA polymerase (GIBCO-BRL). Samples were overlaid with 30 µl mineral oil, and PCR cycles were performed in a DNA thermal cycler (Whatman; Biometra), with the following profile: denaturing for 1 min at 94°C, annealing for 1 min at 57°C, and 1 min extension step at 72°C. The last cycle was followed by a final extension step of 5 min at 72°C. The control gene was coamplified simultaneously in each reaction. The optimal number of cycles for each primer pair was determined through kinetic amplification following our standard procedure (4, 10). To routinely semiquantify Kim-1 and the control gene, 23 and 18 cycles were used. All reactions were performed individually from each total RNA isolated from each renal cortex. Genomic DNA contamination was checked by treating all RNA samples with RNase-free DNase I and by carrying samples through the PCR procedure without adding RT.

To analyze PCR products, one-half of each reaction was electrophoresed in a 5% acrylamide gel. Bands were ethidium bromide stained and visualized under ultraviolet light, cut out, suspended in 1 ml scintillation cocktail (Ecolume; ICN, Aurora, OH), and counted by liquid scintillation (model LS6500; Beckman, Fullerton, CA). Kim-1 mRNA levels are expressed as the ratio of the radioactivity amount recovered from the excised Kim-1 bands over the radioactivity of the respective gene control bands. The RT-PCR semiquantitative analysis was performed at least in quadruplicate.

Kim-1 Real-time PCR

PCR primers and 6-carboxyfluorescein (FAM) or VIC dye-labeled *TaqMan* minor groove binder (MGB) probes sets were selected from the Applied Biosystems Assays-on-demand product line and were specifically used to detect and quantify cDNA sequences without detecting genomic DNA. For Kim-1 and 18S rRNA expression analysis, FAM and VIC probes, respectively, have been designed (4331182 and 4319413E; Applied Biosystems). FAM and VIC were used as fluorescent reporter dyes and conjugated to 5' ends of probes to detect amplification products. The amount of FAM or VIC fluorescence in each reaction liberated by the exonuclease degradation of the *TaqMan* probe during PCR amplification was measured as a function of PCR cycle number using an ABI 7000 Prism (Applied Biosystems). PCR was carried out in 96-well plates on cDNA equivalent to 2.5 ng total RNA isolated individually from each renal cortex. Thermal cycling conditions were 10 min at 95°C followed with 40 cycles at 95°C for 1 min and 60°C for 1 min. Data were collected using the ABI PRISM 7000 SDS analytical thermal cycler (Applied Biosystems). Each individual sample was tested in triplicate to ensure statistical significance. The relative quantification of Kim-1 gene expression was performed using the comparative threshold cycle (C_t) method (21). The C_t value is defined as the point where a statistically significant increase in the fluorescence has occurred. The number of PCR cycles (C_t) required for the FAM and VIC intensities to exceed

a threshold just above background was calculated for the test and reference reactions. In all experiments, 18S rRNA was used as control. Results were analyzed in a relative quantification study by the ratio Kim-1/18S rRNA. Negative controls were included in the reaction plate.

Recombinant Rat Kim-1 Ectodomain Protein

The soluble form of rat Kim-1 was obtained as described earlier (3). Briefly, a construct [rat Kim-1 (mucin)-Ig] was made that encoded the extracellular domain of rat Kim-1 (residues 1–234) attached to the Fc portion of human IgG₁ hinge, calponin homology (CH2 + CH3) domains and cloned into an expression vector PEAG347, obtained from Biogen Idec. Transfected Chinese hamster ovary (CHO) cell lines expressing the fusion protein were selected, adapted in suspension with the hybridoma serum-free media (BD Biosciences), and grown in a cell factory (Fisher Scientific). The rat Kim-1-Fc protein was purified from the conditioned media by chromatography on a protein A-Sepharose column (Amersham Biosciences). In brief, the protein A-Sepharose column (2 × 20 cm) was equilibrated with 20 mM sodium phosphate and 0.15 M NaCl (pH 7). The conditioned media was applied, and the column was washed with the equilibration buffer. The column was eluted with 25 mM sodium phosphate and 0.1 M NaCl (pH 2.8). Fractions (1 ml) were collected in 1.5-ml Eppendorf tubes containing 50 µl neutralizing buffer (0.5 M sodium phosphate, pH 8.6). The concentration of each fraction was measured by a sandwich ELISA using rabbit anti-human-IgG-Fc as a trapping antibody and horseradish peroxidase (HRP)-labeled goat anti-human IgG-Fc as a secondary antibody. This was further confirmed by measuring the Kim-1 protein concentration using a protein assay reagent (Bio-Rad). Fractions of similar concentrations were combined and dialyzed [mol wt cut off (MWCO) = 30,000] against PBS overnight at 4°C and concentrated using 30,000 MWCO amicon centriplus centrifugal filters (Millipore).

Mouse Monoclonal Antibodies Against Rat Kim-1 Ectodomain

Mice were immunized with purified rat Kim-1-Fc protein to generate monoclonal antibodies using standard antibody production techniques by contract to Dr. Jun Hayashi's laboratory at the University of Maryland (Baltimore, MD). Eighteen hybridoma clones were selected that were positive for Kim-1-Fc and negative for human IgG-Fc. These clones were adapted in suspension with the serum-free hybridoma media (BD Biosciences) grown in 175-cm² tissue culture flasks. The monoclonal anti-rat Kim-1 ectodomain (MARKE) antibodies were purified from conditioned media using a protein G-Sepharose column (Amersham Biosciences). In brief, the protein G-Sepharose column (2 × 20 cm) was equilibrated with 20 mM sodium phosphate and 0.15 M NaCl (pH 7). The conditioned media was applied, and the column was washed with the equilibration buffer. The column was eluted with 100 mM glycine buffer and 0.1 M NaCl (pH 2.7). Fractions (1 ml) were collected in 1.5-ml Eppendorf tubes containing 50 µl neutralizing buffer (1 M Tris-Cl, pH 9). Absorbance of each fraction was measured in a quartz cuvette at 280 nm (absorbance of 1 = 0.8 mg/ml) using a spectrophotometer (Molecular Devices). Fractions of similar concentrations were combined and dialyzed against PBS overnight at 4°C and concentrated using amicon centriplus centrifugal filters with 30,000 MWCO (Millipore).

Rat Kim-1 Sandwich ELISA

Biotinylation of MARKE-1. One MARKE antibody (MARKE-Trap), at a concentration ~1.5 mg/ml, served as a trapping/primary antibody. The other MARKE antibody (concentration ~2.2 mg/ml) was biotinylated using the Pierce EZ-Link NHS-PEO₄-Biotin conjugating kit (Pierce) to act as a detecting/secondary antibody. The number of moles of biotin/mole of protein was determined to be six (corresponding to very high efficiency of biotinylation) using an

EZ-Biotin Quantitation Kit. The nonreacted and hydrolyzed biotinylation reagent was removed by dialyzing with PBS, pH 7, overnight at 4°C.

Construction of Kim-1 sandwich ELISA. The wells of an ELISA plate (MaxiSorp; Nunc, Naperville, IL) were coated with MARKE-Trap [overnight incubation at 4°C with 100 µl antibody and 10 µg/ml in coating buffer (0.1 M potassium phosphate buffer, pH 9)]. The plate was washed three times using a squirt bottle with wash solution (PBS-0.05% Tween, PBST). The wells were then blocked for 1 h at 37°C with a blocking solution (3% BSA/PBS with 0.02% sodium azide), and after the incubation period the plate was washed again three times with PBST. One hundred microliters of either standard rat Kim-1-Fc pure protein in serial dilutions (0–5 ng/ml) or urine samples from control and treated groups were added to the plate in duplicate, and the plate was incubated for 1.5 h at 37°C. All of the dilutions of Kim-1 standards, urine samples, MARKE-1, and HRP-conjugated streptavidin antibody were done in a sample diluent (2.38% HEPES, 0.6% NaCl, 1% BSA, and 0.1% Tween, pH 7.4). After three washes with PBST, biotinylated MARKE-1 antibody was added, followed by HRP-conjugated streptavidin. Color was developed by adding 3,3,5,5-tetramethyl benzidine substrate (Sigma), and the reaction was stopped after 15 min by adding 1 N HCl. The absorbance was measured at 450 nm using a plate reader (Molecular Devices). The urinary Kim-1 concentration was calculated based on the standard curve and expressed in absolute terms (ng/ml).

Evaluation of the Kim-1 ELISA. The performance characteristics of the Kim-1 ELISA were evaluated by measuring the sensitivity, assay range, specificity, reproducibility, recovery, dilutional linearity, and interference. The analytical recovery was determined by adding a known amount of 750 or 1,500 pg/ml recombinant Kim-1-Fc into vehicle-treated rat urine samples and quantitating the Kim-1 levels in these spiked samples. To assess the recovery of Kim-1 in urine from animals with kidney injury, a known amount of 750 or 1,500 pg/ml recombinant Kim-1-Fc was added to 5 mg cisplatin/kg treated rat urine samples containing 300–2,100 pg/ml Kim-1. This was done to verify that there was no interfering substance in the urine of animals with AKI and to demonstrate that cisplatin, which is in the urine of these animals, does not interfere with the assay (27). Dilutional linearity was evaluated in normal and cisplatin-treated rat urine to justify sample dilution to fit the concentrations of Kim-1 in the linear range of the standard curve (0–5,000 pg/ml). Cisplatin-treated rat urine samples containing 6, 8, 12, or 18 ng/ml (as measured by the Kim-1 ELISA) corresponding to medium and high concentration of Kim-1 were diluted 1:5, 1:10, 1:20 using sample diluent, and the Kim-1 levels were measured by ELISA.

Immunofluorescence Microscopy

Immunocytochemistry for Kim-1 was performed as previously described (17). Sections were thawed, washed with PBS, and blocked in 1.5% normal goat serum in PBS (blocking solution) for 30 min. Sections were then incubated for 1 h with the primary antibodies [MARKE-1, MARKE-2, and MARKE-Trap (5 µg/ml) diluted in the blocking solution]. The sections were washed with PBS and incubated with anti-mouse Cy3 conjugated (1:800 dilution; Jackson) in PBS for 30 min. At the final step, sections were washed with PBS and mounted with Vector Shield mounting reagent (Vector) containing 12.5 µg/ml DAPI to identify nuclei. As a negative control, the same concentration of mouse IgG (5 µg/ml) was used for the primary antibody.

Statistics

All results are expressed as means ± SE. Treatment means were compared with control means by ANOVA and subsequent Student's *t*-test. The level of significance was set at *P* < 0.05 in all cases.

RESULTS

Construction and Purification of Rat Kim-1 Ectodomain Fusion Protein

Rat Kim-1 maps to chromosome 10 (10q21) of the rat genome and is conserved across species with 77% identity to mouse Kim-1, 30% identity to chimpanzee, and 38% identity with human KIM-1. The protein structure of rat Kim-1 consists of a total of 307 amino acids (aa) with a signal peptide (1–21 aa), a highly conserved 6-cysteine-rich Ig-like domain (22–130), a serine-threonine- and proline-rich mucin domain containing several *N*- and *O*-linked glycosylation sites (131–235), a transmembrane domain (236–256), and a short cytoplasmic tail (257–307) containing a tyrosine kinase phosphorylation site from 291 to 297 aa (Fig. 1A). The Kim-1 ectodomain is shed from the proximal tubule after injury and has been detected by Western blot analysis in the urine of rats treated with nephrotoxicants (17). To quantitate the release of Kim-1 into the urine, monoclonal antibodies were generated that are specific to the ectodomain of rat Kim-1. A plasmid encoding a fusion protein of the rat Kim-1 ectodomain (1–234 aa) with the Fc portion of human IgG was generated (Fig. 1B), stably transfected into CHO cells, and purified from the conditioned media as described in MATERIALS AND METHODS. Three different batches of purified and dialyzed rat Kim-1-Fc were loaded on the gel, and the purity was assessed by Commassie staining (Fig. 1C) and Western blot analysis (Fig. 1D) using HRP-labeled anti-human IgG-Fc antibody. In the Commassie-stained blot, the strongest band was of the Kim-1-Fc protein at 85 kDa that corresponds to the predicted molecular weight of the glycosylated Kim-1 ectodomain (1–234 aa) fused to the Fc portion of human IgG. Similar results were obtained in the Western blot with only one band at 85 kDa in all three batches of purified Kim-1-Fc, attesting to its purity.

Monoclonal Antibodies and Evaluation of Performance Characteristics of the Kim-1 ELISA

To obtain highly specific MARKE antibodies, mouse monoclonal antibodies were generated against the pure recombinant Kim-1-Fc protein. The hybridoma cells were screened and selected in such a way that the conditioned media recognized Kim-1-Fc but did not recognize human IgG-Fc. Three such MARKE antibodies were purified using protein G-Sepharose, and the efficiency of three of these antibodies (MARKE-1, MARKE-2, and MARKE-Trap) to detect Kim-1-Fc was estimated by Western blot analysis (Fig. 2A). All three purified antibodies at the concentration of 1 µg/ml recognized 25 ng/lane of Kim-1-Fc without any nonspecific binding. This suggested that all three MARKEs were able to detect the denatured Kim-1-Fc protein. To further evaluate whether these antibodies would detect nondenatured three-dimensional Kim-1-Fc protein in a sandwich ELISA (Fig. 2B), MARKE-1 and -2 (2 µg/ml) were biotinylated to act as secondary antibodies, and MARKE-Trap (10 µg/ml) was used as a trapping antibody. Both MARKE-1 and -2 were able to detect Kim-1 when MARKE-Trap was used as a primary trapping antibody. When either MARKE-1 or -2 was used as the trapping antibody and the other as the detecting antibody, these two antibodies could not be made to effectively identify Kim-1, suggesting that they may be binding to the same or overlapping epitopes of Kim-1.

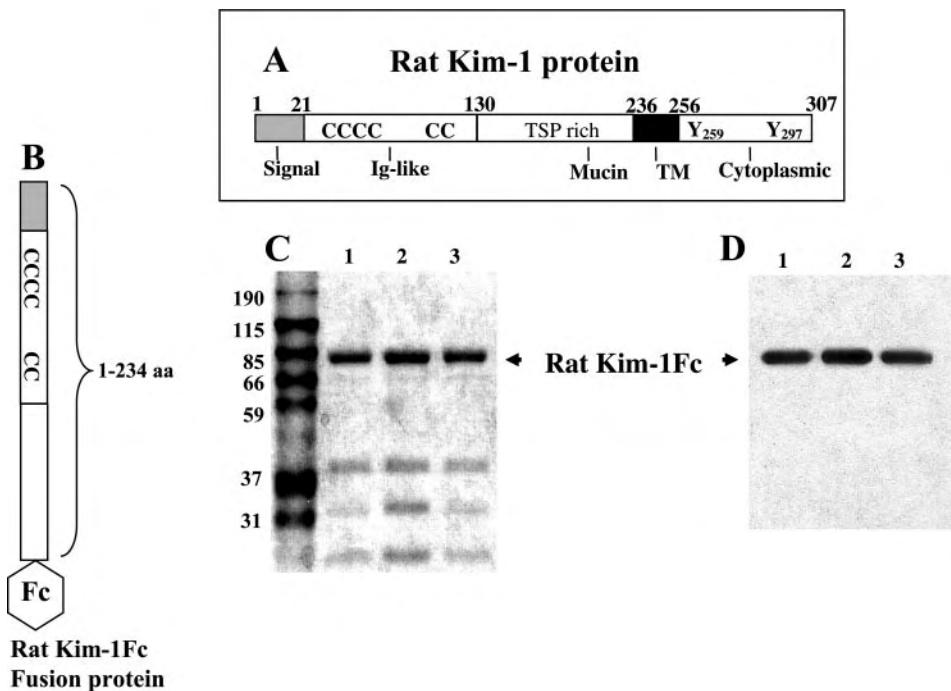


Fig. 1. Structure of kidney injury molecule-1 (Kim-1) and construction and purity of the rat Kim-1 ectodomain-Fc fusion protein. *A:* structure of rat Kim-1 protein consists of 307 amino acids (aa) with a signal peptide, Ig-like domain, mucin region, transmembrane domain (TM), and a short cytoplasmic tail with a tyrosine kinase phosphorylation site from 291–297 aa. *B:* Kim-1 ectodomain fusion protein was produced by creating an expression construct that encoded the extracellular domain of Kim-1 (1–234) fused to the Fc portion of human IgG1 as described in MATERIALS AND METHODS. Purity of the Kim-1-Fc fusion protein was assessed by PAGE of 3 different batches of purified and dialyzed Kim-1-Fc and detection by Commassie reagents (*C*) and Western blot (*D*) using horseradish peroxidase (HRP)-labeled anti-human IgG-Fc antibody. TSP, threonine, serine, proline; TM, transmembrane.

Thus a Kim-1 ELISA was constructed using MARKE-Trap as the primary antibody and MARKE-1 as a secondary antibody. The evaluation of the performance characteristics of the Kim-1 ELISA is as follows (Table 1).

Sensitivity (<39 pg/ml). A standard curve was generated using serial dilutions of Kim-1-Fc protein in sample diluent starting with 5,000 pg/ml (Fig. 2C). The sensitivity of this assay, or lower limit of detection (LLD), was defined as the lowest Kim-1-Fc concentration that could be differentiated from zero (assay blank/sample diluent) by Student's *t*-test. The LLD was 39 pg/ml sample diluent ($n = 5$; $P < 0.001$).

Assay range (0–5,000 pg/ml). The assay range was estimated by calculating the coefficient of variation (CV) of each standard constructing five independent standard curves. The CV obtained for each standard from 78.1 to 5,000 pg/ml sample diluent was <10%. The standard curve concentrations used for all the Kim-1 ELISAs were 5,000, 2,500, 1,250, 625, 312.5, 156.3, and 78.13 pg/ml.

Specificity. This ELISA is specific for the measurement of natural and recombinant rat Kim-1. It does not detect mouse and human KIM-1 (data not shown). It also does not detect human IgG-Fc or an irrelevant protein (C-RET, a protooncogene reported to be involved in sporadic papillary thyroid carcinoma) fused with human IgG (C-RETFc), attesting to the specificity of the antibodies to bind Kim-1.

Reproducibility. The precision profile was assessed by use of urine samples collected on days 1 and 2 after 5 mg cisplatin/kg that contained different concentrations of Kim-1 (732, 1,203, 1,692, 2,120, 2,630, and 4,250 pg/ml). Intra- and interassay CVs ranged from 2 to 4.9% ($n = 6$) and from 2.7 to 9.6% ($n = 3$ in 3 different plates), respectively (Fig. 2D).

Recovery. The analytical recovery was determined by adding 750 or 1,500 pg/ml recombinant Kim-1-Fc to vehicle-treated or 5 mg cisplatin/kg-treated rat urine samples containing 300–2,100 pg/ml Kim-1. Recoveries of Kim-1 ranged from 90 to 110%.

Dilution linearity. When cisplatin-treated rat urine samples containing 6, 8, 12, or 18 ng/ml corresponding to medium and high concentrations of Kim-1 were diluted 1:5, 1:10, and 1:20, each sample gave results close to linearity ($r = 0.95$ –0.99), confirming parallelism between the standards and the urine samples (data not shown).

Interference. Urine samples containing 732 or 2,630 pg/ml Kim-1 were supplemented with potentially interfering agents, including cisplatin and mercuric chloride, at various concentrations. We tested cisplatin, since we used it as a model nephrotoxicant in this study, and mercuric chloride to assess the ability of metals to potentially interfere with the Kim-1 ELISA. There was no significant interference from ascorbic acid (<56.8 mmol/l), albumin (<5 g/l), globin (<0.1 g/l), cisplatin (<5 mM), creatinine (<132.6 mmol/l), creatine (<38.1 mmol/l), mercuric chloride (<3 mM), urea (<1.0 mol/l), or sodium chloride (<0.5 mol/l), indicating that the estimation of Kim-1 was not affected by interference from a wide range of urinary constituents that are expected to be present in the urine after AKI.

Nephrotoxicity of Cisplatin as Measured by BUN, Plasma Creatinine, and Histopathology

We used a widely established and well-studied cisplatin-induced AKI model (1, 17, 18) to induce nephrotoxicity and to evaluate whether Kim-1 could serve as an early predictor of nephrotoxicity. Low (2.5 mg/kg), medium (5 mg/kg), or high (7.5 mg/kg) doses of cisplatin were administered intraperitoneally in 0.9% saline or the same volume of vehicle to male Sprague-Dawley rats. Because previously we had shown only mild changes in BUN, serum creatinine, and histopathology after a low dose of 2.5 mg cisplatin/kg (1, 17, 18), we only collected urine from this group. After 5 or 7.5 mg cisplatin/kg, BUN or plasma creatinine did not increase significantly until day 2 but increased ~4- and 10-fold, respectively, over base-

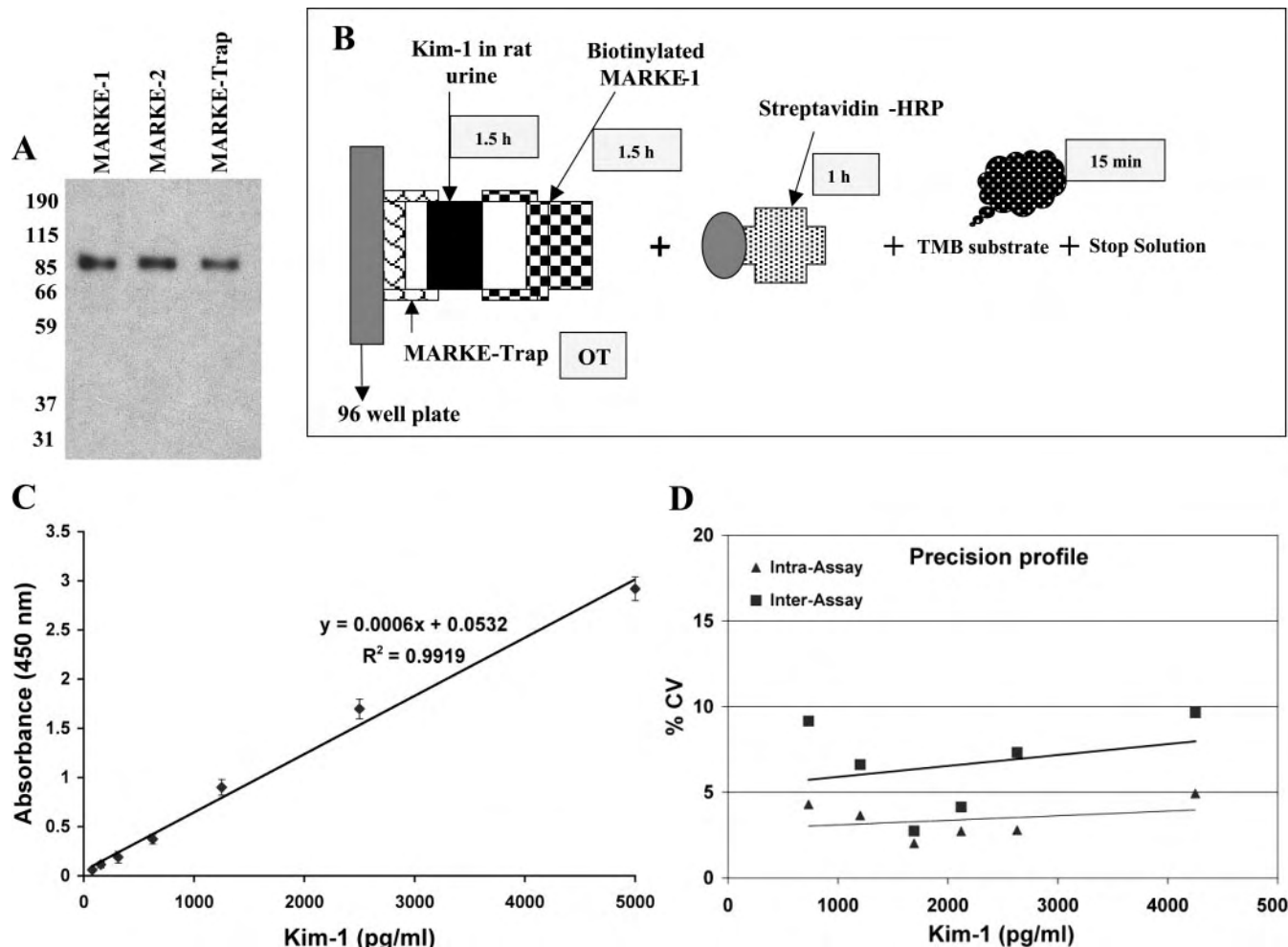


Fig. 2. Monoclonal antibodies to rat Kim-1, principle of Kim-1 ELISA, standard curve, and precision profile. *A*: monoclonal anti-rat Kim-1 ectodomain (MARKE)-1, MARKE-2, and MARKE-Trap detect Kim-1 ectodomain fusion protein by Western blot analysis. Purified Kim-1-Fc (25 ng/lane) was loaded on 3 different lanes for PAGE and transferred onto a polyvinylidene difluoride membrane that was then cut into 3 strips. Each strip was incubated with 1 μ g/ml of either MARKE-1, -2 or MARKE-Trap. Rabbit anti-mouse polyclonal antibody was used as a secondary antibody. *B*: Kim-1 ELISA is based on a typical sandwich ELISA assay protocol using 96-well plates coated with MARKE-Trap, which traps the Kim-1 antigen present in the urine. Biotinylated MARKE-1 is used as a secondary antibody, and this complex is colorimetrically detected using a spectrophotometer at 450 nm. *C*: typical standard curve using recombinant Kim-1 ectodomain fusion protein was made using serial dilutions from a 10 ng/ml stock concentration. The standard curves were repeated several times. The intra- and interassay variability was <5%; $R^2 = 0.99$ represents a very high correlation coefficient. The equation of the line ($y = 0.0006x + 0.0532$) can be used to calculate the unknown concentration of Kim-1 (x) by substituting the absorbance value (y). *D*: precision profile for Kim-1 ELISA. The intra-assay and interassay reproducibility of the Kim-1 ELISA was calculated by adding 5 different concentrations of Kim-1 (750, 1,000, 1,500, 2,000, and 2,500 pg/ml) to control urine samples. For the intra-assay variability, each sample was measured in $n = 6$ replicates within one plate. For the interassay variability, each sample was measured 3 times in three different plates. CV, coefficient of variation; OT, overnight; TMB, 3,3,5,5-tetramethylbenzidine.

line (*day 0*) on *day 3* (Fig. 3, *A* and *B*). BUN and creatinine further increased on *day 4* by 5- to 7-fold and 20-fold over baseline, respectively, reflecting significant renal dysfunction and kidney injury (Fig. 3, *A* and *B*). After 7.5 mg cisplatin/kg, 50% mortality was observed on *day 4*, whereas no mortality was observed with the 5 mg/kg dose until *day 5*. Histological examination of the kidney sections revealed no significant alterations on *day 1* after 5 (Fig. 3*D*) or 7.5 (Fig. 3*E*) mg cisplatin/kg compared with the controls (Fig. 3*C*). On *day 2* after either dose, there was some single cell necrosis, tubular dilation, and sloughing of cells in the lumen of the S_3 segment of proximal tubules into the outer stripe of the outer medulla (OSOM; Fig. 3, *F* and *G*). On *day 3* after either dose, there was significant proximal tubular necrosis, particularly in the S_3 segment, and intratubular casts were clearly seen (Fig. 3, *H* and

I). The inflammation, edema, tubular degeneration, dead cells, necrosis, and apoptosis were most severe in the 7.5-mg cisplatin/kg-treated group.

Urinary Kim-1 Levels Over Time in Response to Varying Doses of Cisplatin

Previous studies from our laboratory have shown Kim-1 protein levels to be upregulated in the kidney by immunocytochemistry and ectodomain shedding into the urine by immunoblot analysis from *day 1* to 6 after 10 mg cisplatin/kg in rats (17). We have previously lacked, however, a sensitive and high-throughput method of detecting Kim-1 in the urine. With the highly specific and sensitive ELISA we constructed to quantitate Kim-1, we found an approximate three- to fivefold

Table 1. Performance characteristics of Kim-1 ELISA

Parameter	Result
Sensitivity	Lowest limit of detection: 39 pg/ml
Assay range	78.1–5,000 pg/ml
Specificity	Does not cross-react with mouse or human KIM-1
Intra-assay variability	2–4.9%
Inter-assay variability	2.7–9.6%
Recovery	90–110%
Dilution linearity	1:5, 1:10, and 1:20
Interference	None identified

Kim-1, kidney injury molecule 1.

increase in urinary Kim-1 on day 1 after 2.5, 5, or 7.5 mg cisplatin/kg compared with the vehicle-treated controls (day 0). Urinary Kim-1 levels further increased to ~9- to 12-fold baseline on day 2 (Fig. 4). Kim-1 levels peaked on day 3 after administration of 7.5 mg cisplatin/kg, reaching ~26 ng/ml in the animals that subsequently succumbed (50%). The remaining 50% of the rats that survived this high dose had Kim-1 levels ~22 ng/ml on days 4 and 5. Kim-1 levels remained between 15 and 25 ng/ml for 2.5 and 5 mg cisplatin-treated groups from days 3 to 5, indicating a plateau in the excretion of Kim-1 associated with severe kidney injury. Thus there was a time-dependent progressive increase in Kim-1 after 2.5, 5, or 7.5 mg cisplatin/kg administration from day 0 to day 3 after which there was a plateau of urinary Kim-1 levels.

Immunocytochemical Localization of Kim-1 in the Kidney after 5 mg/kg Cisplatin Administration using Three Different Monoclonal Antibodies

As indicated previously, MARKE-Trap was used as a primary antibody, and biotinylated MARKE-1 or -2 was used as secondary antibody in the Kim-1 ELISA. We tested by immunocytochemistry the efficacy of these three monoclonal anti-Kim-1 ectodomain antibodies (including MARKE-2) to local-

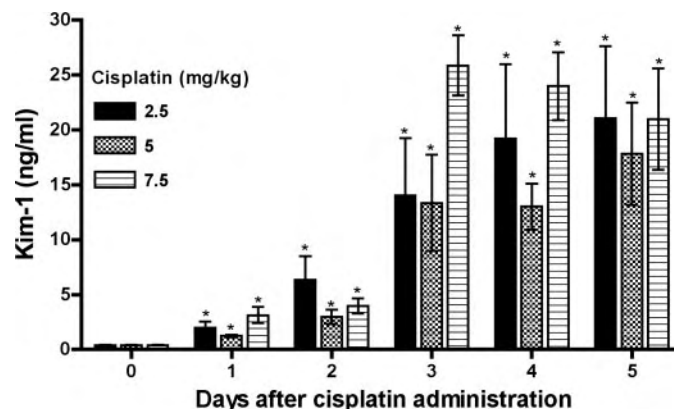


Fig. 4. Measurement of urinary Kim-1 by ELISA over time after cisplatin administration. Male Sprague-Dawley rats ($n = 10$ for each) were administered 2.5, 5, or 7.5 mg cisplatin/kg ip in 0.9% saline. Animals were kept in Nalgene rat metabolic cages overnight, and 12-h urine samples were collected in the morning from 0 to 5 days. Urine was centrifuged at 6,000 rpm for 15 min and stored in aliquots at -80°C for further analysis. Measurement of Kim-1 in the urine samples was performed by ELISA, as described in MATERIALS AND METHODS. Each sample was measured in triplicate diluted 1:5, 1:10, and 1:20 in sample diluent to fit in the linear range of the standard curve. The urinary Kim-1 content is expressed as ng/ml. * $P \leq 0.05$ compared with the value at time 0.

ize Kim-1 in tissue from animals treated with 5 mg/kg cisplatin (Fig. 5). With the use of the three MARKEs, there was no Kim-1 staining on day 0, indicating undetectable expression of Kim-1 under normal conditions (Fig. 5, A, E, and I). On day 1 after cisplatin, all three MARKEs showed a very similar pattern of positive Kim-1 staining in an apical membrane distribution in the OSOM in isolated epithelial cells of the S₃ segments of the proximal tubules (Fig. 5, B, F, and J). The expression significantly increased on day 3 after 5 mg cisplatin/kg administration, consistent with the high urinary Kim-1 levels (13.4 ± 4.4 ng/ml). Kim-1 was localized on the apical

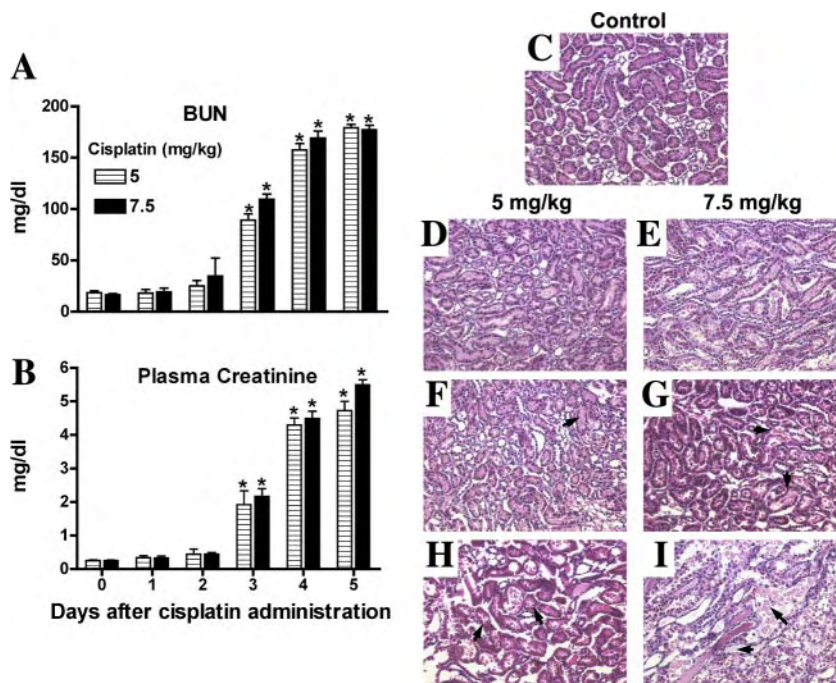


Fig. 3. Plasma blood urea nitrogen (BUN), creatinine, and renal histopathology over a time course after administration of 5 or 7.5 mg cisplatin/kg. Male Sprague-Dawley rats ($n = 4$) were administered 5 or 7.5 mg cisplatin/kg ip in 0.9% saline. Blood and kidney tissue were taken on days 0–5. Because the administration of 7.5 mg cisplatin/kg resulted in 50% mortality by day 4, 8 rats were treated in this group to get 4 survivors on day 4 and 5 each. BUN (A) and creatinine (B) were measured. * $P \leq 0.05$ compared with 0-h time point. C–I: representative photomicrographs of hematoxylin and eosin-stained kidney sections from respective treatment groups. C: vehicle-treated control; D, F, and H: days 1, 2, and 3, respectively, after 5 mg cisplatin/kg; E, G, and I: days 1, 2, and 3 after 7.5 mg cisplatin/kg, respectively. All fields were chosen from outer stripe of outer medulla (OSOM). Arrowheads indicate sloughing of cells, tubular dilation, and necrosis.

Days after 5 mg cisplatin/kg administration

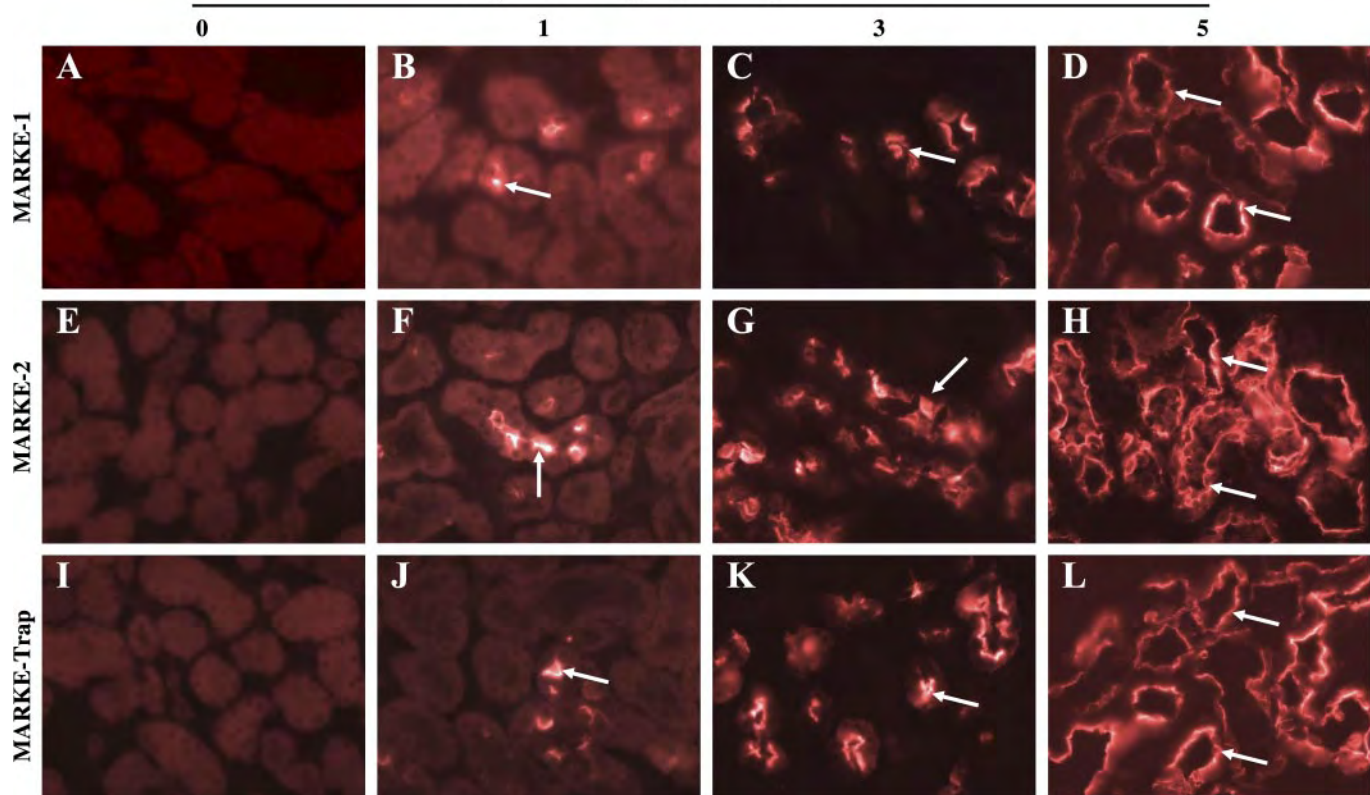


Fig. 5. Immunofluorescence staining to detect Kim-1 expression in the kidney after 5 mg cisplatin/kg administration using the MARKE antibodies. Purified and concentrated 5 μ g/ml MARKE-1 (*A–D*), MARKE-2 (*E–H*), or MARKE-Trap (*I–L*) were used for immunohistochemical localization of Kim-1 in the paraformaldehyde lysine periodate (PLP)-fixed frozen kidney sections from *day 0* to 5 after 5 mg cisplatin/kg administration, as described in MATERIALS AND METHODS. Arrows indicate the progressive increase of Kim-1 staining primarily on the apical membrane over time. No staining was observed on *day 0* or when using mouse IgG as a negative control (data not shown).

membranes of the injured tubules, which were dilated and also had protein casts. In some parts of the OSOM region, the Kim-1 staining pattern appeared diffusely cytoplasmic. On *day 5* after the 5 mg/kg dose, although the Kim-1 levels in the urine (17.8 ± 4.6 ng/ml) did not increase very dramatically from *day 3* (13.38 ± 4.37 ng/ml), there was a significantly greater Kim-1 protein expression in the kidneys as detected by all three MARKEs (Fig. 5, *D, H*, and *L*). The localization was apical and diffusely cytoplasmic but was much more widespread expressed throughout the injured region of the OSOM. Thus all three antibodies can very sensitively detect a progressive injury-dependent expression of denatured (Fig. 2*A*) or undenatured (Figs. 4 and 5) Kim-1 in the kidney after cisplatin nephrotoxicity.

Kim-1 as an Early Diagnostic Indicator of AKI After Cisplatin Nephrotoxicity

BUN, plasma creatinine, urinalysis, glycosuria, and proteinuria are currently the most widely used biomarkers for renal dysfunction and injury. In the urine samples collected on *days 0, 1*, and *2* from rats treated with 2.5, 5, or 7.5 mg cisplatin/kg glucose (Fig. 6*A*), protein (Fig. 6*B*) and NAG (Fig. 6*C*) were measured and compared with urinary Kim-1 (Fig. 6*D*) to evaluate the efficiency of Kim-1 as an early diagnostic indicator of kidney injury. In the 2.5 mg cisplatin/kg group, there was no significant increase in urine glucose (Fig. 6*A*), protein (Fig.

6*B*), or NAG (Fig. 6*C*) on *days 1* and *2*; however, by contrast, there was an ~5-fold increase in Kim-1 on *day 1* that further increased up to ~12-fold on *day 2* (Fig. 6*D*). Thus the concentrations of urinary Kim-1 were significantly higher on *days 1* and *2*, indicating renal injury when none of the conventionally used biomarkers of renal injury, including glycosuria, proteinuria, or urinary NAG levels, were able to predict this. Similarly, in the 5 and 7.5 mg cisplatin/kg groups, there were no significant differences in the urinary glucose, protein, NAG (Fig. 6, *A–C*), BUN (Fig. 6*E*), or plasma creatinine (Fig. 6*F*) values on *day 1*, but there was an approximate three- to fivefold increase in urinary Kim-1 levels, indicating significant renal injury as early as *day 1*. The ~7- to 10-fold increase in Kim-1 on *day 2* was accompanied by increases in glycosuria, proteinuria, and NAG values after 5 or 7.5 mg cisplatin/kg (Fig. 6, *A–D*). These results suggest that Kim-1 is a highly sensitive and early indicator of renal dysfunction useful for detection of even minor alterations in renal structural and functional integrity, as demonstrated by its significant upregulation on *day 1* after 2.5 mg/kg cisplatin.

Comparison of Kim-1 with other Biomarkers of Kidney Injury in Renal I/R Model

To generalize the effectiveness of Kim-1 as a sensitive and early diagnostic biomarker for AKI, we quantitated the Kim-1 ectodomain in the urine of male Wistar rats after different

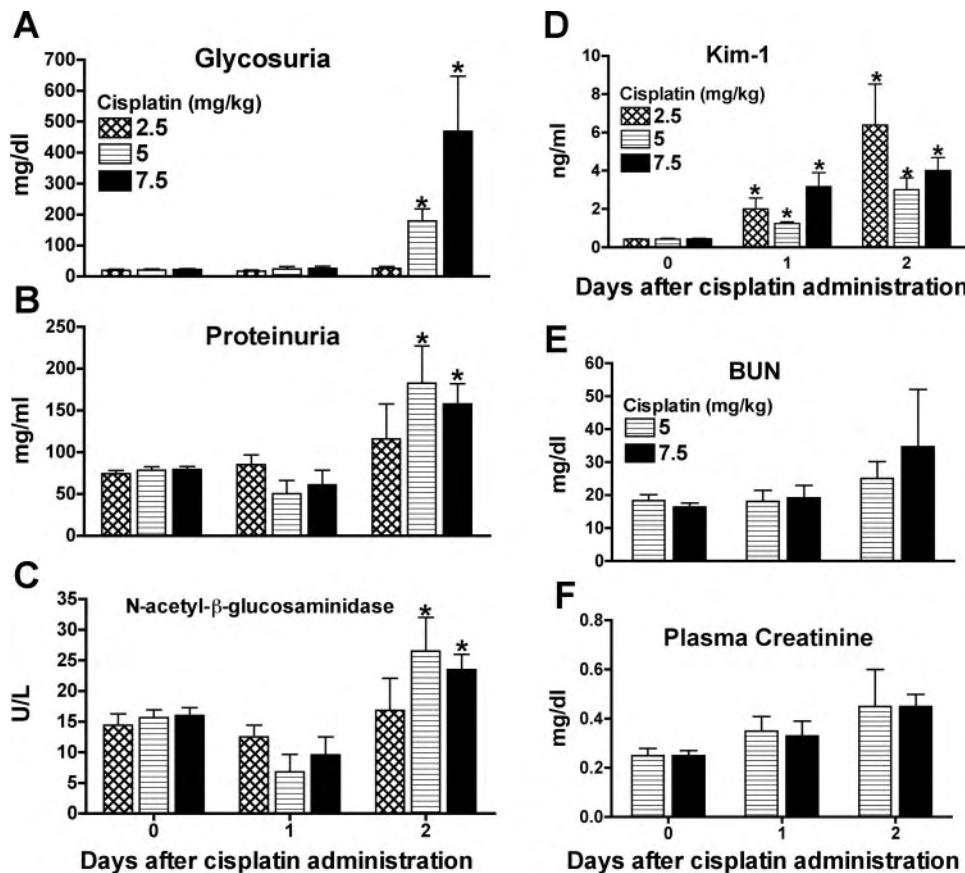


Fig. 6. Comparison of Kim-1 with routinely used biomarkers as an early diagnostic indicator of kidney injury. Urinary glucose (A), protein (B), and *N*-acetyl- β -glucosaminidase (C), and urine Kim-1 (D) were measured on days 0, 1, and 2 after 2.5, 5, or 7.5 mg cisplatin/kg administration. BUN (E) and plasma creatinine (F) were measured on these days after 5 and 7.5 mg/kg cisplatin administration. * $P \leq 0.05$ compared with value on day 0.

periods of bilateral I/R injury. There was no significant increase in BUN (Fig. 7A) or plasma creatinine (Fig. 7B) on day 1 after 10 or 20 min of bilateral I/R injury. By contrast, 1 day after 30 or 45 min bilateral I/R injury, BUN increased approx-

imately four- to fivefold, and plasma creatinine increased approximately five- to sixfold, indicating severe renal dysfunction. Twenty-four hours after 10 min of bilateral I/R injury, Kim-1 was fivefold higher (Fig. 7E) than sham-operated con-

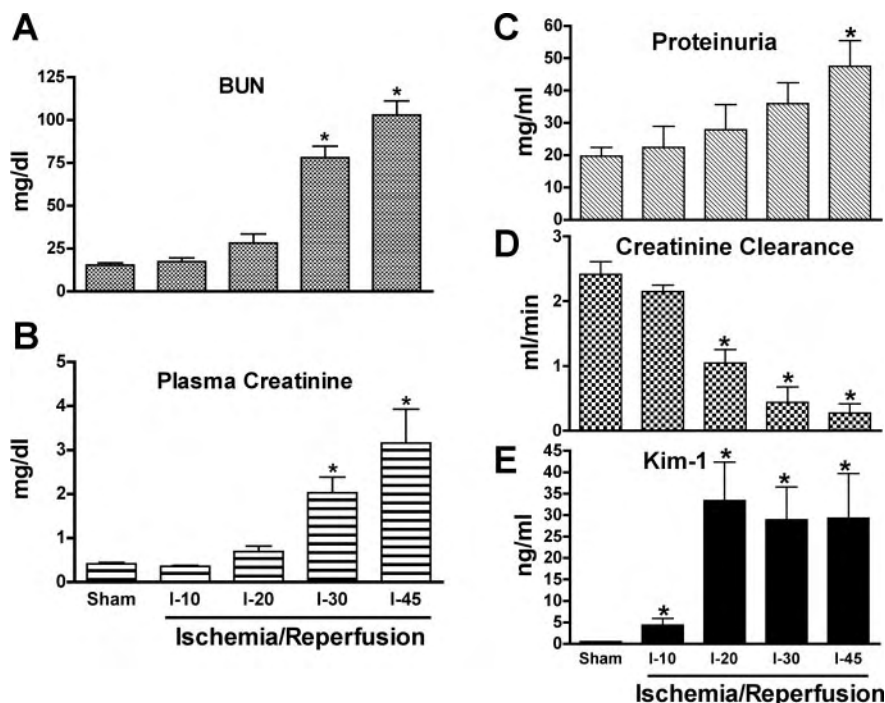


Fig. 7. Functional renal injury and urine Kim-1 levels after different times of renal ischemia. Male Wistar rats were subjected to 0 (sham), 10, 20, 30, or 45 min of bilateral ischemia by clamping the renal pedicles for the stipulated time and then removing the clamps and confirming reperfusion. After reperfusion (2 h), the rats were placed in metabolic cages, and urine, blood, and tissue were collected at 24 h. BUN (A) and plasma creatinine (B) concentrations were measured, and creatinine clearance (D) was calculated as per MATERIALS AND METHODS. Urine protein (C) and Kim-1 (E) concentrations were also measured. * $P \leq 0.05$ compared with value in sham-treated group.

trols, whereas there was no significant decrease in the creatinine clearance (Fig. 7D) nor an increase in proteinuria (Fig. 7C) with this length of ischemia. With 20 min bilateral I/R injury, there was a 50% reduction in creatinine clearance (Fig. 7D) with no significant change in proteinuria (Fig. 7C). Urine was collected for 24 h starting after initiation of reperfusion. Urinary Kim-1 was ~50-fold higher than controls in this collection (Fig. 7E). As seen previously in the cisplatin-induced nephrotoxicity model (Fig. 4), the urinary Kim-1 levels were quantitatively in the 25–35 ng/ml range in the 20, 30, or 45 min bilateral I/R groups after 24 h. Creatinine clearance decreased by 75 and 85%, respectively, after 30 or 45 min bilateral I/R (Fig. 7D), with a significant increase in proteinuria occurring only in the 45-min bilateral I/R group (Fig. 7C). Thus, in the bilateral I/R injury model, as in the cisplatin model, Kim-1 was a highly sensitive indicator of renal dysfunction, with fivefold higher Kim-1 levels in the 24-h collection of urine after 10-min bilateral I/R injury at a time when BUN, plasma creatinine, creatinine clearance, and urinary protein were unchanged from controls.

Renal I/R-Induced Injury-Dependent Changes in Kim-1 Gene Expression and its Correlation with Creatinine Clearance

To correlate Kim-1 gene expression with the degree of injury, Kim-1 mRNA was quantitated using semiquantitative

(Fig. 8, A and B) and quantitative (Fig. 8C) RT-PCR after different periods of bilateral I/R injury. In concordance with the urinary Kim-1 protein levels, which increased approximately fivefold after 10 min bilateral I/R injury, Kim-1 mRNA levels were also significantly upregulated at 24 h in this group (Fig. 8, A–C). With the use of quantitative real-time PCR, a much more sensitive measure of gene expression (Fig. 8C), Kim-1 mRNA was ~25-fold higher than controls after 10 min bilateral I/R injury at 24 h. There was an injury-dependent increase in Kim-1 mRNA, as seen in both semiquantitative and quantitative real-time PCR, with an ~160-, 280-, and 350-fold increase (Fig. 8C) in Kim-1 mRNA at 24 h after 20, 30, or 45 min bilateral I/R injury, respectively. These data complement the findings of an injury-dependent increase in Kim-1 protein expression (Fig. 5) after 5 mg/kg cisplatin. Collectively, these results indicate that both Kim-1 mRNA and protein expression increase as a function of injury. The correlation coefficient relating creatinine clearance as a parameter of renal function to Kim-1 mRNA levels was 0.732, with a statistical significance of $P < 0.0001$ (Fig. 8D).

DISCUSSION

We report the development of a quantitative assay for measuring Kim-1 in the rat urine as a biomarker for AKI and demonstrate that marked increases in urinary Kim-1 can be

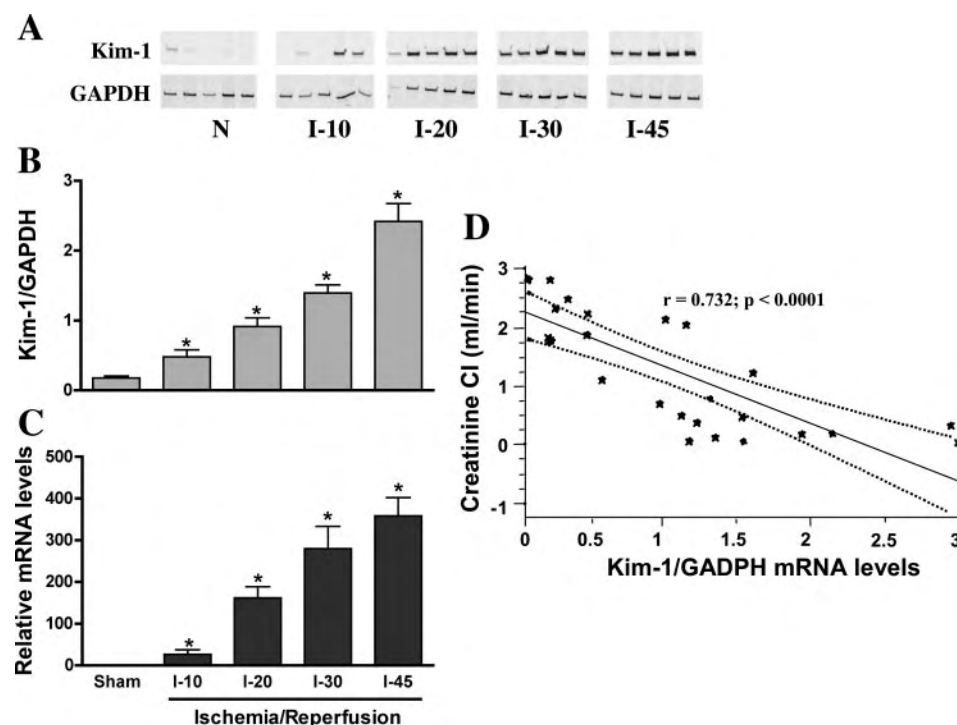


Fig. 8. Kim-1 mRNA levels in kidney after different periods of ischemia and correlation of Kim-1 mRNA in kidney with creatinine clearance. Kim-1 mRNA levels were measured by semiquantitative (A and B) and quantitative (C) real-time RT-PCR in renal cortex of rats at 24 h after 0, 10, 20, 30, and 45 min of bilateral ischemia [sham control (N), I-10, I-20, I-30, and I-45, respectively]. A: mRNA was isolated from renal cortex, and the RT-PCR products were separated on a 5% ethidium bromide acrylamide gel. *Top*, Kim-1 mRNA after different periods of renal ischemia. *Bottom*: renal glyceraldehyde-3-phosphate dehydrogenase (GAPDH) mRNA values, which were used as internal standard. B: Kim-1 mRNA level was semiquantitated by excising the bands from the ethidium bromide-stained gel and counted by liquid scintillation. The results are presented as the ratio of PCR products (cpm) of Kim-1 and GAPDH \pm SE. C: real-time PCR was carried out in 96-well plates on cDNA derived from 2.5 ng total RNA isolated individually from each renal cortex. The amount of fluorescence in each reaction liberated by the exonuclease degradation of the *TaqMan* probe during PCR amplification was measured as a function of the PCR cycle number using an ABI 7000 Prism (Applied Biosystems). Results are presented as relative Kim-1-to-18S rRNA ratios compared with the sham value. D: values of creatinine clearance (Cl) are plotted vs. Kim-1-to-GAPDH mRNA ratios. The r value of 0.732 indicates a high degree of correlation between creatinine clearance and Kim-1 mRNA expression with a significance of $P < 0.0001$. * $P \leq 0.05$ compared with value in the sham-treated group.

measured under conditions where changes in other standard indicators are not measurable. These results have direct implications for evaluation of nephrotoxicity in animals where sensitive and specific measures of toxicity have been elusive. Nephrotoxicity often is evaluated by reliance on serum creatinine levels, an insensitive measure of kidney injury, or histological analysis, which requires killing a large number of animals and is inherently difficult to quantitate. The Kim-1 assay is a very sensitive and robust system with minimal interference from other components of the diseased urine and is not affected by variation in physicochemical properties of the urine. The assay has a dynamic range from 0 to 5,000 pg/ml with the lowest limit of detection being <38 pg/ml and an inter- and intra-assay variability <10% (Fig. 2, C and D).

The performance characteristics of the developed ELISA are comparable to the commercially available ELISAs to measure cytokines in rat serum (e.g., tumor necrosis factor- α , IL-6) as markers of inflammation. Although an extensive performance characteristic evaluation has not been reported for the human KIM-1 ELISA, both the rat Kim-1 and human KIM-1 ELISAs are highly comparable in terms of sensitivity, inter- and intra-assay variability, and recovery (12). For the development of the rat Kim-1 ELISA, a panel of 18 mouse monoclonal antibodies was made against rat Kim-1-Fc fusion proteins from which three were purified, dialyzed, and concentrated to ~2.5 mg/ml. Two of these were used in the ELISA, and all three were used for immunocytochemistry. We found that just 500 ng/well MARKE-trap and 100 ng/well biotinylated MARKE-1 were sufficient to efficiently bind Kim-1 antigen in 100 μ l urine.

Investigators have relied on a set of tests to detect AKI in rodent models that include serum creatinine, BUN, urine volume, urinalysis (including pH, specific gravity, glycosuria, proteinuria), kidney weight (wet wt-to-dry wt ratio), and histopathology. A significant disadvantage of these tests is the time delay between injury and detection, making the tests insensitive and unreliable for diagnostic and prognostic measurements (36). Specific proteins excreted in the urine after injury to particular segments of the nephron can serve as biomarkers for assessing the site and severity of renal damage (44). Previously used biomarkers can be broadly classified into the following three categories (13): 1) enzymes: e.g., alanine aminopeptidase (AA), alkaline phosphatase (AP), γ -glutamyl-transpeptidase (γ -GT), NAG, cathepsin B, lysozyme, and lactate dehydrogenase (LDH); 2) low-molecular-weight proteins: e.g., β_2 -microglobulin, α_1 -microglobulins, and retinol-binding protein; and 3) kidney-derived antigens: e.g., α -GST, clusterin, CYR-61, NGAL, and F-actin. These biomarkers have been studied in various models of nephrotoxicity, but a number of disadvantages have been identified. AA, AP, and γ -GT are stable only for 4 h after urine collection, and urine samples have to be gel filtered to remove potentially interfering substances. β_2 -Microglobulin is unstable in acidic pH; therefore, the urine has to be neutralized immediately after collection (44). The α -GST assay requires that the urine be stored with a specific preservative. α -GST is localized to the proximal tubule and is readily and rapidly released in the urine when renal tubular injury occurs (40). NAG, a proximal tubular brush-border enzyme, is a sensitive and persistent indicator of renal proximal tubule injury, but some metals and other nephrotoxicants directly inhibit NAG activity and therefore in such cases NAG cannot be used as a biomarker (41, 43). Other markers

suffer from lack of specificity in measuring kidney injury. Serum, biliary, and urinary levels of γ -GT and LDH also increase after hepatic parenchymal injury (20). Elevation of urinary IL-6, IL-8, and IL-18 has been implicated as biomarkers for AKI, but these are also nonspecific since they are elevated with sepsis involving liver or lung in the absence of renal injury (8, 19, 28). Another problem with currently identified biomarkers is the onset of elevation and sustainability of the increase. AA and CYR-61 are significantly elevated in the urine at day 1 after renal damage but fail to remain elevated at later time points in spite of persistent renal injury (26, 37). Finally, most of the assays used for measuring urinary biomarkers are either enzymatic or colorimetric assays, thereby preventing high-throughput detection of samples, which is required when handling a large number of samples over extensive time courses.

NGAL is upregulated and can be detected in the kidney (22) and urine of mice three h after cisplatin (20 mg/kg) and has been proposed as an early biomarker for diagnosing AKI (24, 25). These rodent studies have been extended to humans in a recent study indicating that NGAL levels at 2 h is a very powerful predictor of AKI in children after cardio pulmonary bypass (23). Similarly, CYR-61, a secreted protein, is present early in the urine after I/R but currently can only be detected by immunoblotting the urine and kidney extracts at 3–6 h after 30 min bilateral I/R injury (26). Urinary CYR-61 levels are reduced over time despite the continuous progression of injury. Clusterin, a protein associated with programmed cell death and tissue reorganization, as measured by RIA, has been correlated with the elevation of creatinine and NAG in the gentamicin-induced renal injury model in rats (2). Clusterin mRNA and protein levels, however, did not increase until day 5 in the cisplatin-induced renal injury model (35). F-actin is released in the urine in rats at 1 h after 25 min renal ischemia because of actin depolymerizing factor-mediated disruption of microvillar microfilament and apical membrane (34). Increased urinary actin along with IL-6 and IL-8 have also been suggested as useful markers for the prediction of sustained acute renal failure after ischemia in humans (19).

An ideal biomarker to detect AKI in animal studies should be organ and site specific, sensitive to detect minor perturbations in renal function, correlate with the degree of tubular injury, persist throughout the time course of renal injury to indicate progression and regression of injury, be noninvasive, and be quantifiable by a high-throughput method to facilitate large sample size measurements. In addition, it would also add to the merit of the biomarker if it were conserved across species from fish to rodents to humans, allowing for the extrapolation of the results and use of the same marker in preclinical and clinical studies. Kim-1 is expressed predominantly on the apical membrane of the epithelial cells of proximal tubules after injury. An upregulation of Kim-1 in the urine indicates kidney proximal tubular injury (Fig. 5) except when proximal cells have also become dedifferentiated for another reason, such as in renal cell carcinoma (11). Urinary Kim-1 levels increase at least fivefold on day 1 after 5 and 7.5 mg/kg cisplatin, whereas BUN and plasma creatinine increases were seen only from day 3 onward (Fig. 3, A and B). Similar results were obtained in the I/R injury model where 10 min bilateral I/R injury caused a significant increase in urinary Kim-1 without any changes in plasma creatinine, BUN, creatinine

clearance, or proteinuria. Thus Kim-1 is upregulated and shed in the urine with mild insults, which result in minimal injury, thus attesting to the sensitivity and early diagnostic ability of Kim-1 to serve as a biomarker for AKI. An injury-dependent increase in Kim-1 mRNA is observed in the I/R model with progressively increasing *Kim-1* gene expression levels after 10, 20, 30, or 45 min bilateral I/R injury (Fig. 8, A–C). A similar trend in the injury-dependent increase in Kim-1 protein expression is evident from the immunohistochemical staining of Kim-1 on days 0–5 after 5 mg/kg cisplatin (Fig. 5). Thus *Kim-1* gene expression and surface protein expression correlate very well with the degree of renal tubular injury (Fig. 7C).

A significant advantage of measuring Kim-1 as a biomarker for AKI is that it is conserved across species and is upregulated after renal injury in zebrafish (unpublished observations), mice (29), rats (17), nonhuman primates (9), and humans (12) encompassing a complete array of preclinical to clinical risk assessment models. Thus quantitation of urinary Kim-1 is likely to be very useful for the evaluation of kidney injury in animal pathophysiological studies and predictive toxicology and may improve our ability to identify effective therapeutic agents for kidney injury and eliminate nephrotoxic compounds early in the drug development process.

ACKNOWLEDGMENTS

Part of this work was presented at the 44th Annual Society of Toxicology meeting March (5–10, 2005) in New Orleans, LA, and Experimental Biology Meeting (April 2–5, 2005) in San Diego CA.

GRANTS

This work was supported by a postdoctoral fellowship grant from the National Kidney Foundation to V. S. Vaidya, National Institute of Diabetes and Digestive and Kidney Diseases Grants DK-39773 and DK-72381 to J. V. Bonventre, by research Grants G34511M and CO1-40182A-1 from the Mexican Council of Science and Technology, and Academic Support Program (DGAPA) IN208602-3 of the National University of Mexico to N. A. Bobadilla.

REFERENCES

1. Amin RP, Vickers AE, Sistare F, Thompson KL, Roman RJ, Lawton M, Kramer J, Hamadeh HK, Collins J, Grissom S, Bennett L, Tucker CJ, Wild S, Kind C, Oreffo V, Davis JW 2nd, Curtiss S, Naciff JM, Cunningham M, Tennant R, Stevens J, Car B, Bertram TA, and Afshari CA. Identification of putative gene based markers of renal toxicity. *Environ Health Perspect* 112: 465–479, 2004.
2. Aulitzky WK, Schlegel PN, Wu DF, Cheng CY, Chen CL, Li PS, Goldstein M, Reidenberg M, and Bardin CW. Measurement of urinary clusterin as an index of nephrotoxicity. *Proc Soc Exp Biol Med* 199: 93–96, 1992.
3. Bailly V, Zhang Z, Meier W, Cate R, Sanicola M, and Bonventre JV. Shedding of kidney injury molecule-1, a putative adhesion protein involved in renal regeneration. *J Biol Chem* 277: 39739–39748, 2002.
4. Bobadilla NA, Herrera JP, Merino A, and Gamba G. Semi-quantitative PCR: a tool to study low abundance messages in the kidney. *Arch Med Res* 28: 55–60, 1997.
5. Bonventre JV and Weinberg JM. Recent advances in the pathophysiology of ischemic acute renal failure. *J Am Soc Nephrol* 14: 2199–2210, 2003.
6. Branten AJ, Mulder TP, Peters WH, Assmann KJ, and Wetzel JS. Urinary excretion of glutathione S transferases α and π in patients with proteinuria: reflection of the site of tubular injury. *Nephron* 85: 120–126, 2000.
7. Carraway MS, Welty-Wolf KE, Miller DL, Ortell TL, Idell S, Ghio AJ, Petersen LC, and Piantadosi CA. Blockade of tissue factor: treatment for organ injury in established sepsis. *Am J Respir Crit Care Med* 167: 1200–1209, 2003.
8. Davis JW II, Goodsaid FM, Bral CM, Obert LA, Mandakas G, Garner CE II, Collins ND, Smith RJ, and Rosenblum IY. Quantitative gene expression analysis in a nonhuman primate model of antibiotic-induced nephrotoxicity. *Toxicol Appl Pharmacol* 200: 16–26, 2004.
9. Feria I, Richardo I, Juarez P, Ramirez V, Gonzalez MA, Uribe N, Garcia-Torres R, Lopez-Casillas F, Gamba G, and Bobadilla NA. Therapeutic benefit of spironolactone in experimental chronic cyclosporine A nephrotoxicity. *Kidney Int* 63: 43–52, 2003.
10. Han WK, Alinani A, Wu CL, Michaelson D, Loda M, McGovern FJ, Thadhani R, and Bonventre JV. Human kidney injury molecule-1 is a tissue and urinary tumor marker of renal cell carcinoma. *J Am Soc Nephrol* 16: 1126–1134, 2005.
11. Han WK, Bailly V, Abichandani R, Thadhani R, and Bonventre JV. Kidney Injury Molecule-1 (KIM-1): a novel biomarker for human renal proximal tubule injury. *Kidney Int* 62: 237–244, 2002.
12. Han WK and Bonventre JV. Biologic markers for the early detection of acute kidney injury. *Curr Opin Crit Care* 10: 476–482, 2004.
13. Henry RJ, Segalove M, and Sobel C. Turbidimetric determination of proteins with sulfosalicylic and trichloroacetic acids. *Proc Soc Exp Biol Med* 92: 748–751, 1956.
14. Hewitt SM, Dear J, and Star RA. Discovery of protein biomarkers for renal diseases. *J Am Soc Nephrol* 15: 1677–1689, 2004.
15. Ichimura T, Bonventre JV, Bailly V, Wei H, Hession CA, Cate RL, and Sanicola M. Kidney injury molecule-1 (KIM-1), a putative epithelial cell adhesion molecule containing a novel immunoglobulin domain, is up-regulated in renal cells after injury. *J Biol Chem* 273: 4135–4142, 1998.
16. Ichimura T, Hung CC, Yang SA, Stevens JL, and Bonventre JV. Kidney injury molecule-1: a tissue and urinary biomarker for nephrotoxicant-induced renal injury. *Am J Physiol Renal Physiol* 286: F552–F563, 2004.
17. Kelly KJ, Williams WW Jr, Colvin RB, and Bonventre JV. Antibody to intercellular adhesion molecule 1 protects the kidney against ischemic injury. *Proc Natl Acad Sci USA* 91: 812–816, 1994.
18. Kwon O, Molitoris BA, Pescovitz M, and Kelly KJ. Urinary actin, interleukin-6, and interleukin-8 may predict sustained ARF after ischemic injury in renal allografts. *Am J Kidney Dis* 41: 1074–1087, 2003.
19. Liu W, Schob O, Pugmire JE, Jackson D, Zucker KA, Fry DE, and Glew RH. Glycohydrolases as markers of hepatic ischemia-reperfusion injury and recovery. *Hepatology* 24: 157–162, 1996.
20. Livak KJ and Schmittgen TD. Analysis of relative gene expression data using real-time quantitative PCR and the $2[\Delta\Delta C_T]$ method. *Methods* 25: 402–408, 2001.
21. Matthaeus TSLE, Ichimura T, Weber M, Andreucci M, Park KM, and Bonventre JV. Co-regulation of neutrophil gelatinase-associated lipocalin and matrix metalloproteinase-9 in the postischemic rat kidney (Abstract). *J Am Soc Nephrol* 12: 787A, 2001.
22. Mishra J, Dent C, Tarabishi R, Mitsnefes MM, Ma Q, Kelly C, Ruff SM, Zahedi K, Shao M, Bean J, Mori K, Barasch J, and Devarajan P. Neutrophil gelatinase-associated lipocalin (NGAL) as a biomarker for acute renal injury after cardiac surgery. *Lancet* 365: 1231–1238, 2005.
23. Mishra J, Ma Q, Prada A, Mitsnefes M, Zahedi K, Yang J, Barasch J, and Devarajan P. Identification of neutrophil gelatinase-associated lipocalin as a novel early urinary biomarker for ischemic renal injury. *J Am Soc Nephrol* 14: 2534–2543, 2003.
24. Mishra J, Mori K, Ma Q, Kelly C, Barasch J, and Devarajan P. Neutrophil gelatinase-associated lipocalin: a novel early urinary biomarker for cisplatin nephrotoxicity. *Am J Nephrol* 24: 307–315, 2004.
25. Muramatsu Y, Tsujie M, Kohda Y, Pham B, Perantoni AO, Zhao H, Jo SK, Yuen PS, Craig L, Hu X, and Star RA. Early detection of cysteine rich protein 61 (CYR61, CCN1) in urine following renal ischemic reperfusion injury. *Kidney Int* 62: 1601–1610, 2002.
26. Oda H, Shiina Y, Seiki K, Sato N, Eguchi N, and Urade Y. Development and evaluation of a practical ELISA for human urinary lipocalin-type prostaglandin D synthase. *Clin Chem* 48: 1445–1453, 2002.
27. Parikh CR, Jani A, Melnikov VY, Faubel S, and Edelstein CL. Urinary interleukin-18 is a marker of human acute tubular necrosis. *Am J Kidney Dis* 43: 405–414, 2004.
28. Park KM, Byun JY, Kramers C, Kim JI, Huang PL, and Bonventre JV. Inducible nitric-oxide synthase is an important contributor to prolonged protective effects of ischemic preconditioning in the mouse kidney. *J Biol Chem* 278: 27256–27266, 2003.
29. Park KM, Chen A, and Bonventre JV. Prevention of kidney ischemia/reperfusion-induced functional injury and JNK, p38, and MAPK kinase

- activation by remote ischemic pretreatment. *J Biol Chem* 276: 11870–11876, 2001.
31. Rocco MV, Neilson EG, Hoyer JR, and Ziyadeh FN. Attenuated expression of epithelial cell adhesion molecules in murine polycystic kidney disease. *Am J Physiol Renal Fluid Electrolyte Physiol* 262: F679–F686, 1992.
 32. Safirstein RL. Lessons learned from ischemic and cisplatin-induced nephrotoxicity in animals. *Ren Fail* 21: 359–364, 1999.
 33. Sambrook JFE and Maniatis T. *Molecular Cloning: A Laboratory Manual*. New York: Cold Spring Harbor Laboratory, 1989.
 34. Schwartz N, Hosford M, Sandoval RM, Wagner MC, Atkinson SJ, Bamburg J, and Molitoris BA. Ischemia activates actin depolymerizing factor: role in proximal tubule microvillar actin alterations. *Am J Physiol Renal Physiol* 276: F544–F551, 1999.
 35. Silkensen JR, Agarwal A, Nath KA, Manivel JC, and Rosenberg ME. Temporal induction of clusterin in cisplatin nephrotoxicity. *J Am Soc Nephrol* 8: 302–305, 1997.
 36. Star RA. Treatment of acute renal failure. *Kidney Int* 54: 1817–1831, 1998.
 37. Stonard MD, Gore CW, Oliver GJ, and Smith IK. Urinary enzymes and protein patterns as indicators of injury to different regions of the kidney. *Fundam Appl Toxicol* 9: 339–351, 1987.
 38. Thadhani R, Pascual M, and Bonventre JV. Acute renal failure. *N Engl J Med* 334: 1448–1460, 1996.
 39. Tolkkoff-Rubin NE, Rubin RH, and Bonventre JV. Noninvasive renal diagnostic studies. *Clin Lab Med* 8: 507–526, 1988.
 - 39a. United States Food and Drug Administration. *Challenge and Opportunity on the Critical Path to New Medical Products*. www.fda.gov/oc/initiatives/criticalpath/whitepaper.html, 2004.
 40. Usuda K, Kono K, Dote T, Nishiura K, Miyata K, Nishiura H, Shimahara M, and Sugimoto K. Urinary biomarkers monitoring for experimental fluoride nephrotoxicity. *Arch Toxicol* 72: 104–109, 1998.
 41. Vaidya VS, Shankar K, Lock EA, Bucci TJ, and Mehendale HM. Renal injury and repair following S-1, 2 dichlorovinyl-L-cysteine administration to mice. *Toxicol Appl Pharmacol* 188: 110–121, 2003.
 42. Westhuyzen J, Endre ZH, Reece G, Reith DM, Saltissi D, and Morgan TJ. Measurement of tubular enzymuria facilitates early detection of acute renal impairment in the intensive care unit. *Nephrol Dial Transplant* 18: 543–551, 2003.
 43. Wiley RA, Choo HY, and Traiger GJ. The effect of nephrotoxic furans on urinary N-acetylglucosaminidase levels in mice. *Toxicol Lett* 14: 93–96, 1982.
 44. Woods JS. Urinary markers. In: *Methods in Renal Toxicology*, edited by Lash LH. Boca Raton, FL: CRC, 1996, p. 19–33.



Juan M. Mejía-Vilet, Victoria Ramírez, Cristino Cruz, Norma Uribe, Gerardo Gamba and Norma A. Bobadilla

Am J Physiol Renal Physiol 293:78-86, 2007. First published Mar 20, 2007;
doi:10.1152/ajprenal.00077.2007

You might find this additional information useful...

This article cites 50 articles, 27 of which you can access free at:

<http://ajprenal.physiology.org/cgi/content/full/293/1/F78#BIBL>

Updated information and services including high-resolution figures, can be found at:

<http://ajprenal.physiology.org/cgi/content/full/293/1/F78>

Additional material and information about *AJP - Renal Physiology* can be found at:

<http://www.the-aps.org/publications/ajprenal>

This information is current as of October 22, 2007 .

Renal ischemia-reperfusion injury is prevented by the mineralocorticoid receptor blocker spironolactone

Juan M. Mejía-Vilet,^{1,2} Victoria Ramírez,^{1,2} Cristina Cruz,^{1,2}
Norma Uribe,³ Gerardo Gamba,^{1,2} and Norma A. Bobadilla^{1,2}

¹Molecular Physiology Unit, Instituto de Investigaciones Biomédicas, Universidad Nacional Autónoma de México, and Departments of ²Nephrology and ³Pathology, Instituto Nacional de Ciencias Médicas y Nutrición Salvador Zubirán, Mexico City, Mexico

Submitted 14 February 2007; accepted in final form 16 March 2007

Mejía-Vilet JM, Ramírez V, Cruz C, Uribe N, Gamba G, Bobadilla NA. Renal ischemia-reperfusion injury is prevented by the mineralocorticoid receptor blocker spironolactone. *Am J Physiol Renal Physiol* 293: F78–F86, 2007. First published March 20, 2007; doi:10.1152/ajprenal.00077.2007.—Renal ischemia and reperfusion (I/R) injury is the major cause of acute renal failure and may also be involved in the development and progression of some forms of chronic kidney disease. We previously showed that a mineralocorticoid receptor (MR) blockade prevents renal vasoconstriction induced by cyclosporine that leads to acute and chronic renal failure (Feria I, Pichardo I, Juarez P, Ramirez V, Gonzalez MA, Uribe N, Garcia-Torres R, Lopez-Casillas F, Gamba G, Bobadilla NA. *Kidney Int* 63: 43–52, 2003; Perez-Rojas JM, Derive S, Blanco JA, Cruz C, Martinez de la Maza L, Gamba G, Bobadilla NA. *Am J Physiol Renal Physiol* 289: F1020–F1030, 2005). Thus we investigated whether spironolactone administration prevents the functional and structural damage induced by renal ischemia-reperfusion (I/R). Five groups were studied: sham-operated animals, rats that underwent 20 min of ischemia and 24 h of reperfusion, and three groups that received spironolactone 1, 2, or 3 days before I/R, respectively. Renal I/R produced significant renal dysfunction and tubular damage. Spironolactone administration completely prevented a decrease in renal blood flow, the development of acute renal failure, and tubular apoptosis. The protection conferred by spironolactone was characterized by decreasing oxidative stress, as evidenced by a reduction in kidney lipoperoxidation, increasing expression of antioxidant enzymes, and restoration of urinary NO₂/NO₃ excretion. Endothelial nitric oxide synthase expression was upregulated by a mineralocorticoid receptor blockade in I/R groups; in addition, an increase in activating phosphorylation of this enzyme at residue S1177 and a decrease in inactivating phosphorylation at T497 were observed. In conclusion, our study shows that spironolactone administration prevents the renal injury induced by I/R, suggesting that aldosterone plays a central role in this model of renal injury.

endothelial nitric oxide synthase; apoptosis; lipoperoxidation

RENAL ISCHEMIA-REPERFUSION (I/R) injury is the major cause of acute renal failure in both native and transplanted kidneys (22). Ischemic acute renal failure is a syndrome that develops following a transient drop in total or regional blood flow to the kidney. Although reperfusion is essential for the survival of ischemic tissue, there is evidence that reperfusion itself causes additional cellular injury (48). The mechanisms of renal I/R injury involve both vascular and tubular factors, but despite advances in preventive strategies, this

disease continues to be associated with significant morbidity and mortality (21) and there is no successful specific therapy except for supportive care (10).

Recent studies in humans and experimental models have shown that aldosterone plays a pivotal role in the pathophysiology of cardiovascular and renal injury. In this regard, clinical trials have evidenced that mineralocorticoid receptor (MR) blockade improves the survival of patients with chronic heart disease (29, 30, 33, 34) and chronic renal failure (4, 5). The protective effect of MR blockade is associated with decreased fibrosis and vascular inflammation, suggesting that aldosterone is a profibrotic hormone (16, 19). In addition, the effectiveness of MR antagonism in ameliorating glomerular and/or tubulo-interstitial injury has also been documented in several models of nephropathy, including spontaneously hypertensive stroke-prone rats (36, 37), angiotensin II- and nitric oxide synthase inhibitor-treated rats (38), aldosterone-treated rats (15), diabetic nephropathy type 1 and 2 (13), and in a model of unilateral ureteral obstruction (44). We previously observed that aldosterone also plays an important role in nephrotoxicity induced by the immunosuppressant cyclosporine A (CsA), an agent that is extensively used for prevention of allograft rejection (8, 31, 32). In these studies, we observed that in chronic nephropathy an MR blockade reduced structural injury (32) and helped to avoid the progression of renal damage in a model of preexisting chronic CsA nephrotoxicity (31) by mechanisms that involved the reduction of TGF-β expression, lipoperoxidation, and cell death by apoptosis. Interestingly, in the course of these studies, we noticed that an MR blockade prevents the well-known effect of CsA-inducing renal vasoconstriction (2, 7, 8). CsA administration in rats for 7 days was associated with a reduction in renal blood flow by 50%. This reduction was completely prevented by spironolactone (32), suggesting that aldosterone modulates renal vascular tone in this model. In support of these findings, Gros et al. (12) have recently shown that acute aldosterone exposure induced a dose-dependent vasoconstriction through myosin light chain phosphorylation in clonal adult human vascular smooth muscle cells. This effect was prevented by spironolactone, suggesting that aldosterone-mediated vasoconstriction may represent an important pathophysiological mechanism of vascular disease. Thus we reasoned that if aldosterone plays a role in renal vasoconstriction, then spironolactone could be protective against acute I/R injury.

Address for reprint requests and other correspondence: N. A. Bobadilla, Unidad de Fisiología Molecular, Vasco de Quiroga No. 15, Tlalpan, 14000 Mexico City, Mexico (e-mail: nab@biomedicas.unam.mx).

The costs of publication of this article were defrayed in part by the payment of page charges. The article must therefore be hereby marked “advertisement” in accordance with 18 U.S.C. Section 1734 solely to indicate this fact.

MATERIALS AND METHODS

Thirty male Wistar rats (200–300 g) were included and divided into five groups: sham-operated (sham), rats subjected to ischemia-reperfusion (I/R), and three groups of rats that were treated during 1, 2 or 3 days with spironolactone (20 mg/kg by gastric gavage) before I/R was performed (Sp1, Sp2, and Sp3, respectively). This is the most commonly used dose of spironolactone in rats (8, 9, 13, 25, 35, 37, 47).

Kidney I/R injury animal model. Rats were anesthetized by intraperitoneal injection with pentobarbital sodium (30 mg/kg). Animals were placed on a heating pad to maintain a constant temperature and monitored with a rectal thermometer. A midline abdominal incision was made, and both kidneys were exposed. Renal ischemia was induced by nontraumatic vascular clamps over the pedicles for 20 min. After clamps were released, the incision was closed in two layers with 2-0 sutures. Sham-operated animals underwent anesthesia, laparotomy, and renal pedicle dissection only. All animal procedures were followed in accordance with our institutional guidelines for animal care.

Functional parameters. Two hours after renal ischemia, rats were placed in metabolic cages at 22°C with a 12:12-h light-dark cycle and allowed free access to water. Individual 24-h urine samples were collected. Urinary protein excretion was measured by a TCA turbidimetric method (14) and *N*-acetyl- β glucosaminidase (NAG) was measured spectrophotometrically (49). Serum and urine creatinine concentrations were measured with an autoanalyzer (Technicon RA-1000, Bayer, Tarrytown, NY), and renal creatinine clearance was calculated by the standard formula $C = (U \times V)/P$, where U is the concentration in urine, V is the urine flow rate, and P is the serum concentration. Serum aldosterone was quantitatively determined by radioimmunoassay following the procedures described by the manufacturer (DiaSorin, Saluggia, Italy).

Twenty-four hours after renal ischemia-reperfusion, rats were anesthetized with an intraperitoneal injection of sodium pentobarbital (30 mg/kg) and placed on a homeothermic table. The trachea and femoral arteries were catheterized with polyethylene tubing (PE-240 and PE-50). The rats were maintained under euvolemic conditions by infusing 10 ml/kg body wt of isotonic rat plasma during surgery. The mean arterial pressure was monitored with a pressure transducer (model p23 db, Gould) and recorded on a polygraph (Grass Instruments, Quincy, MA). Via a midline abdominal incision, the left renal artery was exposed. An ultrasound transit-time flow probe (IRB, Transonic, Ithaca, NY) was placed around the left renal artery and filled with ultrasonic coupling gel (HR Lubricating Jelly, Carter-Wallace, New York, NY) for recording the renal blood flow.

Histopathological studies. At the end of the experiment, the right kidney was removed and quickly frozen for molecular studies and the left kidney was perfused through the femoral catheter with a phosphate buffer, thereby preserving the mean arterial pressure of each animal. Following blanching of the kidney, the perfusate was replaced by a freshly prepared 10% formalin buffer and perfusion was continued until fixation was completed. After appropriate dehydration, kidney slices were embedded in paraffin, sectioned at 4- μ m and stained via the periodic acid-Schiff technique. Ten subcortical and juxtamedullary fields were recorded from each kidney slide by using a digital camera incorporated in a Nikon microscope. The affected tubular area was analyzed blindly by an expert nephropathologist. Tubular damage was characterized by a loss of brush border, lumen dilatation or collapse, and detachment from basement membrane. Digital microphotographs were recorded for each rat to assess by morphometric analysis the total tubular area (excluding luminal, interstitial, and glomerular areas) and damaged tubular area, delimited by using eclipse net software (magnification $\times 400$). The damaged tubular area was expressed as a proportion of the affected tubular area and total tubular area.

Terminal transferase-dUTP-nick-end labeling assay. Apoptosis in kidney sections was determined by terminal transferase-dUTP-nick-end labeling (TUNEL) assay using an ApopTag in situ apoptosis detection kit (S7101, Chemicon International, Temecula, CA). Slides were prepared by following the procedures previously described (50). A minimum of 10 subcortical and 10 juxtamedullary fields (magnification $\times 400$) per kidney were evaluated in all kidney tissues, and the images were recorded and analyzed blindly. Only tubular cells that contained TUNEL-positive nuclei with the characteristic morphology of apoptosis, including nuclear fragmentation and nuclear condensation, were quantified. TUNEL-positive cells were counted, and the results were expressed as the number of TUNEL-positive nuclei per square millimeter.

Renal lipoperoxidation. Malondialdehyde (MDA), a measure of lipid peroxidation, was assayed in the form of thiobarbituric acid-reactive substances (TBARS) as previously reported (43). Briefly, after homogenization of the tissue, the reaction was performed in an 0.8% aqueous solution of thiobarbituric acid in 15% TCA and heated at 95°C for 45 min, and the mixtures were centrifuged at 3,000 g for 15 min. Supernatant absorbance was read at 532 nm. TBARS were quantified using an extinction coefficient of 1.56×10^5 M/cm and expressed as nanomoles of TBARS per milligram of protein. The tissue protein was estimated using the Bradford method.

RNA isolation and real-time PCR. Total RNA was isolated from each kidney following the guanidine isothiocyanate-cesium chloride method (40) and checked for integrity by 1% agarose gel electrophoresis. Reverse transcription was carried out using 2.5 μ g of total RNA from each rat at 37°C for 60 min using 200 U of the Moloney murine leukemia virus reverse transcriptase (Invitrogen). The mRNA levels of SOD, GPx, catalase, and procaspase-3 were quantified by real-time PCR with the ABI Prism 7300 Sequence Detection System (TaqMan, Applied Biosystems, Foster City, CA). FAM or VIC dye-labeled probes were selected from the Applied Biosystems Assays-on-Demand ABI product line and were specifically used to detect and quantify cDNA sequences without detecting genomic DNA. Primers and probes for SOD, GPx, catalase, and procaspase-3 were ordered as kits: Rn00589772_m1, Rn00577994_g1, Rn00560930_m1, and Rn00563902_m1 (Assays-on-Demand, ABI). As endogenous control, we used eukaryotic 18S rRNA (predesigned assay reagent, ABI, external run) to correct for potential variations in RNA loading or the efficiency of the amplification reaction. The relative quantification of SOD, GPx, catalase, and procaspase-3 gene expression was performed using the comparative CT method (24).

Western blot analysis. Renal proteins were isolated by homogenization and used for immunoblot analysis with rabbit endothelial nitric oxide synthase (eNOS) antibody, phospho-eNOS T495 antibody, or phospho-eNOS S1177 antibody, all used at 1:500 (Cell Signaling Technology). Afterward, membranes were incubated with a secondary antibody, horseradish peroxidase-conjugated rat anti-rabbit IgG (1:2,500, Alpha Diagnostics, San Antonio, TX). To control protein loading and transfer, all membranes were simultaneously probed with an actin antibody (1:2,500) and secondary antibody donkey anti-goat IgG- horseradish peroxidase (Santa Cruz Biotechnology, Santa Cruz, CA). Proteins were detected with an enhanced chemiluminescence kit (Amersham) and autoradiography, following the manufacturer's recommendations. All Western blot analyses were performed within the linear range of protein loads and antibody use. The bands were scanned for densitometric analysis.

Statistical analysis. Results are presented as means \pm SE. Significance of the differences among groups was tested by ANOVA using Bonferroni's correction for multiple comparisons. All comparisons passed the normality test. Statistical significance was defined when the *P* value was <0.05 .

RESULTS

We first investigated whether a prophylactic MR blockade prevented renal dysfunction and structural injury induced by renal I/R in the rat. As shown in Fig. 1, after 24 h of renal reperfusion, rats which underwent renal ischemia developed renal dysfunction that was evidenced by an increase of serum creatinine from 0.56 ± 0.06 to 1.64 ± 0.06 mg/dl and the concomitant reduction of creatinine clearance from 1.4 ± 0.2 to 0.4 ± 0.1 ml/min (Fig. 1, A and B). Renal impairment was, in part, related to renal plasma flow reduction by 33%, without changes in mean arterial pressure (Fig. 1, C and D). In contrast, in the three groups that were pretreated with the MR blocker spironolactone for 1, 2, or 3 days before renal I/R (Sp1, Sp2, and Sp3 groups), the fall in renal plasma flow was completely prevented (Fig. 1C), which was associated with normalization of serum creatinine (Sp1: 0.88 ± 0.2 mg/dl, Sp2: 0.66 ± 0.1 mg/dl, and Sp3: 0.60 ± 0.04 mg/dl) (Fig. 1A) and the concomitant reestablishment of renal function, as shown by the values of creatinine clearance (Fig. 1B).

Light microscopic studies revealed that renal I/R produced severe tubular damage characterized by a loss of brush border, lumen dilatation or collapse, and cellular detachment from tubular basement membranes observed in both renal cortex (Fig. 2, A and E; low and high power, respectively) and outer medulla (not shown). All these lesions were practically absent in rats exposed to spironolactone previous to renal I/R (Fig. 2,

B–H) and were quantitatively confirmed by morphometric analysis of the percentage of injured tubular areas. As a result, the percentage of affected tubular areas in the I/R group was 66.2 ± 0.7 compared with 6.1 ± 1.4 , 9.1 ± 2.5 , and $6.6 \pm 2.0\%$ in the Sp1, Sp2, and Sp3 groups, respectively (Fig. 2I). An assessment of classic markers of tubular injury supported these observations. Proteinuria and NAG excretion increased five- and threefold, respectively, in the I/R group. Accordingly, in rats pretreated with spironolactone, the levels of these tubular injury markers were similar to those found in sham-operated rats and significantly different from the untreated I/R group (Fig. 2, J and K). Figure 3A shows that animals subjected to renal I/R presented a significant elevation of serum aldosterone levels by more than fivefold compared with sham-operated rats. Aldosterone levels were not different among I/R groups. As shown in Fig. 3B, an MR blockade in this model was not associated with an increase in serum potassium levels.

We observed a significant fall in the amount of urinary NO_2/NO_3 excretion by one-half in I/R untreated rats, suggesting that nitric oxide (NO) deficiency contributes not only to reduce renal plasma flow but also to extend renal injury. Also noteworthy was the fact that spironolactone completely prevented the fall in urinary NO_2/NO_3 excretion, as shown Fig. 4A. Thus we analyzed the expression levels and phosphorylation state of eNOS. The eNOS expression levels and phosphorylation in S1177 and T497 residues were not affected by I/R, as

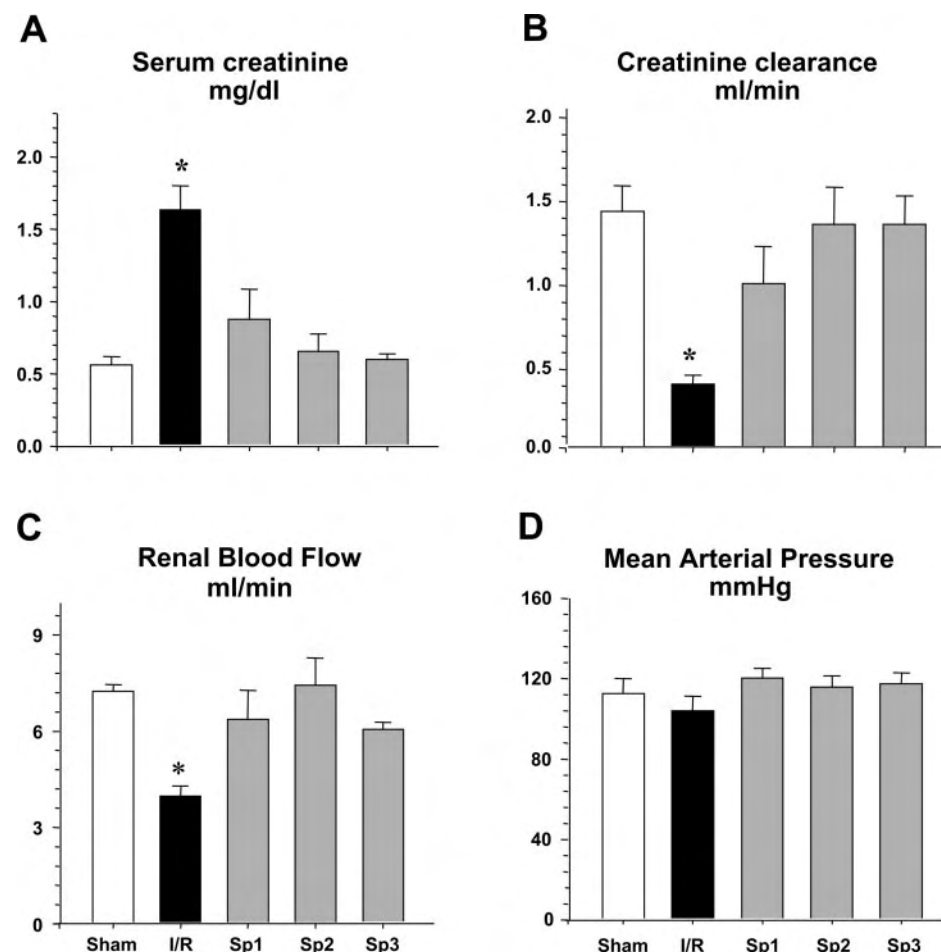


Fig. 1. Renal functional parameters in sham, untreated ischemia-reperfusion (I/R), and spironolactone-treated groups for 1 (Sp1), 2 (Sp2), and 3 (Sp3) days before renal I/R induction, as stated. I/R-induced renal failure was evidenced by a significant increase in serum creatinine (A), together with a reduction of renal creatinine clearance (B) and renal blood flow (RBF; C) without changes in mean arterial pressure (MAP; D) in the I/R untreated group. Renal dysfunction was completely prevented in I/R spironolactone-pretreated rats. * $P < 0.05$ vs. all studied groups.

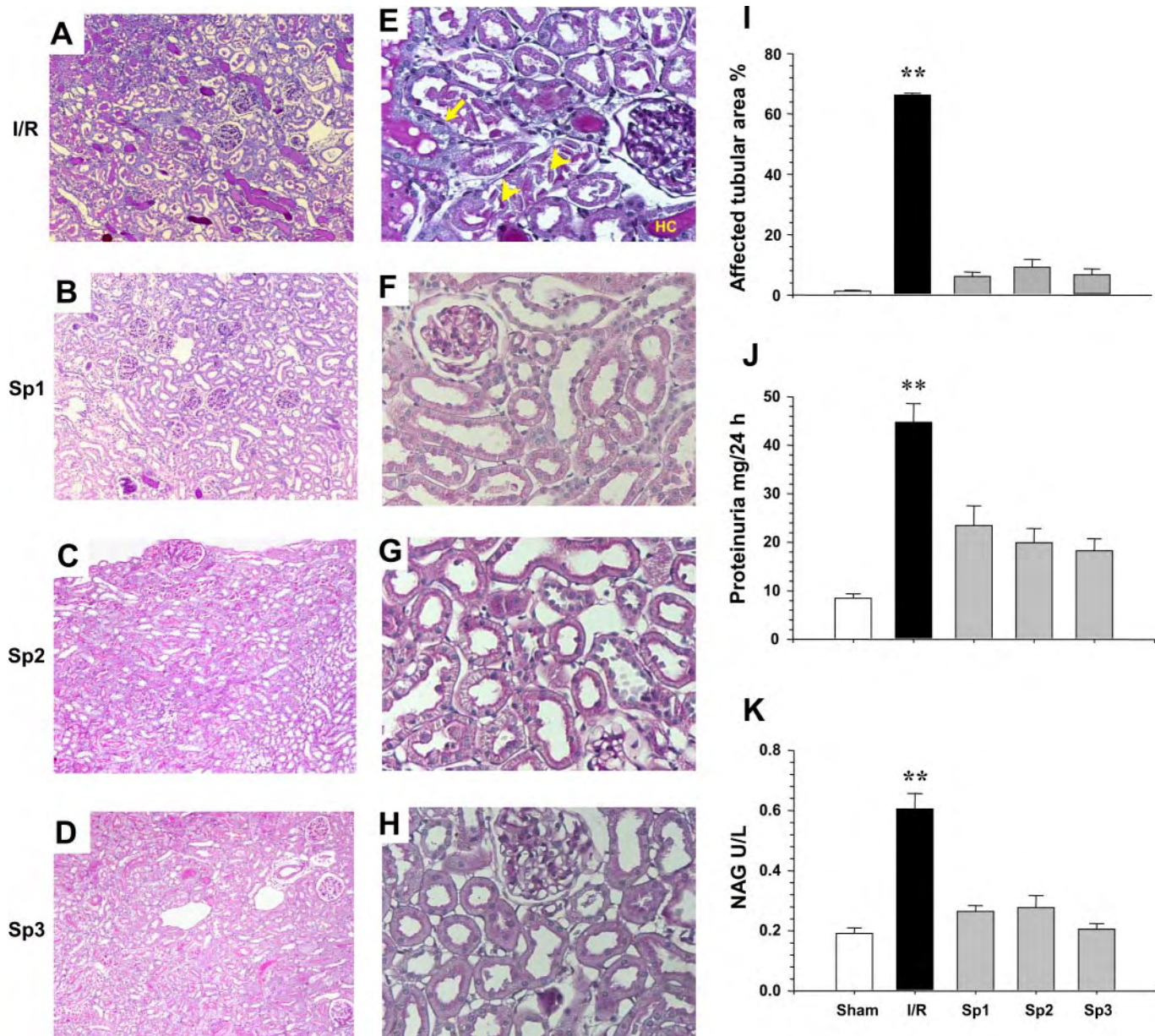


Fig. 2. *A–H*: subcortical histological sections of kidneys stained with periodic acid-Schiff (PAS) from groups studied as stated. Lower-power ($\times 100$; *A–D*) and high-power ($\times 400$; *E–H*) microphotographs are shown. *A* and *E* are representative microphotographs of a kidney section from an I/R untreated rat. Arrowheads in *E* indicate detachment from basement membrane of tubular epithelial cells; yellow arrow indicates tubular dilation, loss of brush border, and flattened epithelial cells, and HC indicates the presence of hyaline cast. These lesions were practically absent in I/R rats treated with spironolactone from 1–3 days (*B–H*). *I*: morphometric quantification of affected tubular area. *J*: urinary protein excretion levels. *K*: urinary N-acetyl- β -glucosaminidase (NAG) excretion. Error bars represent SE. ** $P < 0.05$ vs. all studied groups.

shown in Fig. 4, *B–D*. Kidney eNOS protein levels were significantly increased in rats that received the prophylactic treatment with spironolactone (Fig. 4*B*). In addition, spironolactone treatment was associated with an increase in activating eNOS S1177 phosphorylation (Fig. 4*C*) and a decrease in inactivating eNOS T497 phosphorylation (Fig. 4*D*).

We thus reasoned that spironolactone might also be associated with the prevention of a reperfusion-induced increase in oxidative stress and apoptosis. Therefore, kidney lipoperoxidation and the mRNA levels of antioxidant enzymes were evaluated. Tubular ischemic injury induced by I/R was associated with a significant increase in kidney lipoperoxidation by

threefold, which was prevented by the prophylactic treatment with an MR blocker, since the first day of pretreatment (Fig. 5*A*). The reduction of lipoperoxidation observed in the spironolactone-treated groups was accompanied by a significant increase in SOD and glutathione peroxidase as antioxidant enzymes, while the catalase mRNA levels did not change (Fig. 5, *B–D*).

In situ labeling of cell nuclei by the TUNEL method showed that I/R produced a significant increase in apoptosis cell death measured by positive nuclei stain per square milliliter that was more evident in juxtamedullary areas than in subcortical sections, as shown in Fig. 6, *A* and *B*. These observations were

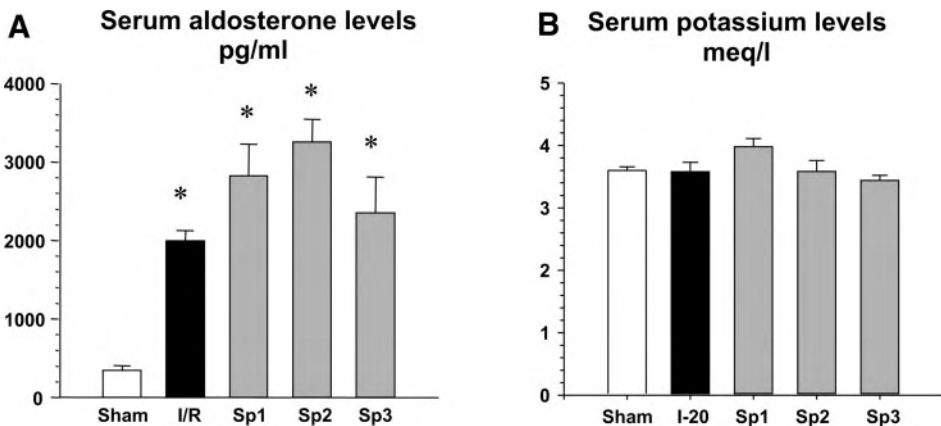


Fig. 3. Effect of I/R and mineralocorticoid (MR) blockade treatment on serum aldosterone and potassium levels. A: all rats that were subjected to I/R presented a marked elevation of serum aldosterone levels compared with the sham-operated group. B: neither renal I/R nor spironolactone treatment modified serum potassium levels. Error bars represent SE. * $P < 0.05$ vs. sham-operated rats.

confirmed by the quantification of positive nuclei per square milliliter, graphically expressed in Fig. 6*I*, showing >100 and 300 positive nuclei/ mm^2 in subcortical and juxtamedullary kidney sections, respectively, of rats that were subjected to renal I/R. Spironolactone pretreatment for 1 day before renal I/R reduced the number of positive nuclei in both areas (Fig. 6, *B* and *C* and *I* and

J). Nevertheless, apoptosis was completely prevented when an MR blockade started 2 or 3 days before I/R (Fig. 6, *C–J*). In accordance with these observations, renal I/R injury produced a significant increase in pro-caspase-3 mRNA levels and this effect was reversed by the pretreatment with a MR blockade administered starting on the first day before I/R (Fig. 6*K*).

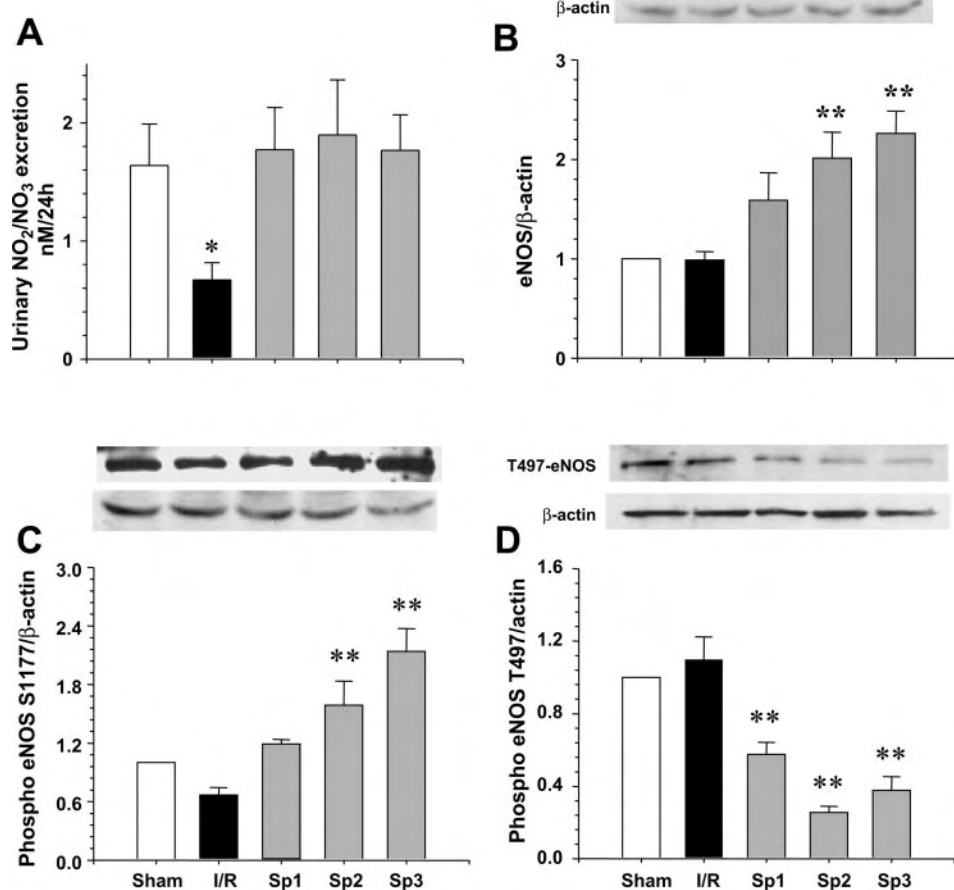


Fig. 4. Renoprotective mechanisms of MR blockade in renal injury induced by I/R. A: renal injury induced by I/R was associated with a significant reduction of urinary nitric oxide (NO) metabolites (NO_2/NO_3), and this effect was prevented by an MR blockade. B–D: effect of spironolactone administration on endothelial nitric oxide synthase (eNOS) expression and eNOS phosphorylation was evaluated by Western blot analysis using specific eNOS and phospho-eNOS antibodies. Renal eNOS expression and phosphorylation were not altered by I/R injury. In contrast, significant changes were observed in treated I/R groups. eNOS protein expression was increased by 1.5- to 2-fold in spironolactone-treated rats. In addition, the amount of phospho-eNOS S1177 was increased, while phospho-eNOS T497 was reduced. Error bars represent SE. * $P < 0.05$ vs. all compared groups. ** $P < 0.05$ vs. sham and I/R groups.

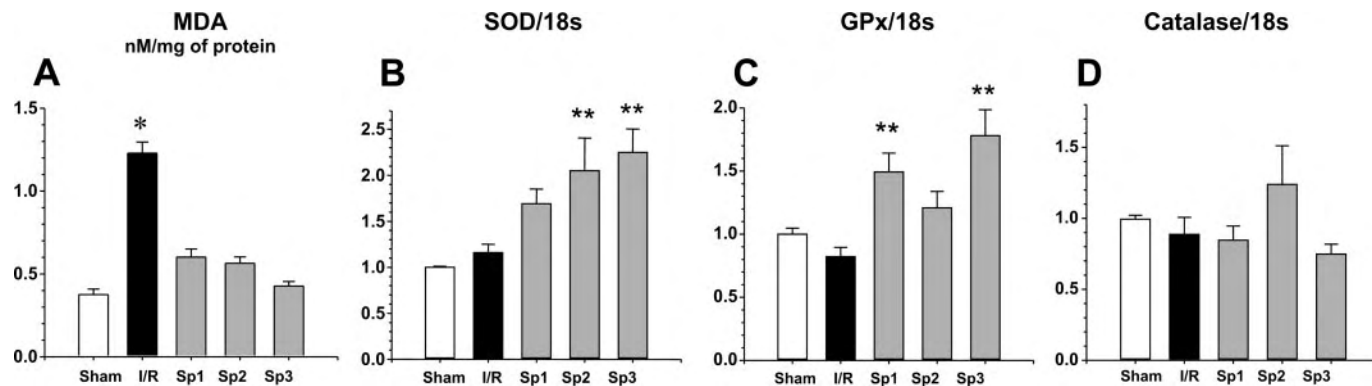


Fig. 5. Effect of renal I/R and MR blockade on renal lipoperoxidation and antioxidant enzymes mRNA levels. *A*: spironolactone administration prevented the kidney lipoperoxidation induced by I/R (malondialdehyde; MDA). This renoprotective effect was associated with increased mRNA levels of SOD and glutathione peroxidase (GPx; *B* and *C*), with no changes in catalase (*D*).

DISCUSSION

In the present study, we show the novel finding that spironolactone administration protects the kidney against I/R injury. Specifically, our data show that pretreatment for 1, 2, or 3 days before rats were subjected to renal I/R prevented 1) renal dysfunction, 2) histological signs of tubular injury evidenced also by a reduction of urinary protein and NAG excretion, and 3) reperfusion injury supported by reduction of kidney lipoperoxidation and cell death by apoptosis.

The mechanisms of renal acute injury induced by I/R seem to be multifactorial and interdependent and involve hypoperfusion, hypoxia, inflammatory responses, and free radical-induced damage. The first step in initiating the pathophysiology of ischemic acute renal failure is renal blood flow reduction (27). In fact, we observed that renal blood flow and creatinine clearance remained significantly lower 24 h after renal I/R compared with sham-operated rats (Fig. 1). These alterations were accompanied by a significant increase in serum aldosterone levels (Fig. 3). There is increasing evidence to support potential roles of aldosterone in the pathogenesis of renal injury (3, 30). Here, we show that administration of spironolactone before induction of renal I/R prevented renal blood flow and renal function reduction, suggesting that aldosterone promotes renal vasoconstriction and plays a potential role in the pathophysiology of acute renal failure. In support of these observations, previous studies from our laboratory showed that spironolactone prevented renal vasoconstriction induced by cyclosporine (8, 32). In addition, Arima et al. (1) demonstrated that aldosterone causes vasoconstriction in afferent and efferent rabbit arterioles, and, more recently, Gros et al. (12) reported that aldosterone mediated a dose-dependent contraction in clonal adult human vascular smooth muscle cells, which was inhibited by spironolactone and eplerenone, suggesting that the vasoconstrictor effect was due to the MR blockade. In this study, in addition of its profibrotic effects, we observed that aldosterone participates in promoting renal vasoconstriction during renal I/R, an effect that was prevented by spironolactone, implying that aldosterone induces renal vasoconstriction by a mechanism that requires the coupling of aldosterone to its receptor. In support of this possibility, a recent study shows that aldosterone induced vasoconstriction by decreasing the endothelial expression of glucose-6-phos-

phate dehydrogenase, which, in turn, decreased the NO availability, and these effects were reversed by spironolactone administration, implying that the MR is involved (23). It has been reported that aldosterone exerts its actions by genomic and nongenomic mechanisms. The first is dependent on the classic MR, which promotes or prevents the transcription of certain genes, whereas the second seems to be mediated by an “unknown receptor,” which mediates fast actions independently of gene transcription (for a review, see Ref. 29). In this regard, it is known that the MR is a protein heterocomplex that includes a steroid-binding protein receptor and heat shock proteins (HSPs) of 56, 70, and 90 kDa. The presence of HSPs actually increases the receptor affinity for binding aldosterone, and when hormone binds to its receptor, HSPs are released. Interestingly, Tumlin et al. (45) reported that HSPs released are capable of activating calcineurin phosphatase. Thus it is possible that by its binding to the MR, aldosterone induces responses by at least two different mechanisms: by the classic pathway at the transcriptional level and by a nongenomic mechanism associated with the effects that occur through HSP release. Thus both genomic and nongenomic mechanisms could be dependent on the aldosterone binding to the classic MR.

As mentioned above, the decrease in renal blood flow is of critical importance in initiating and extending the pathophysiology of acute renal failure. Vasomotor tone is strongly affected by NO derived from eNOS. While NO derived from inducible NOS may contribute to the ischemic injury of renal tubules, there is evidence that the vascular effect of NO derived from eNOS in glomerular afferent arterioles is protective against I/R damage (41). Indeed, decreased eNOS function is one of the features of endothelial dysfunction associated with acute renal failure (11). In this regard, increased eNOS activity induced by ischemic preconditioning protected the kidneys from I/R (51). Also, the inhibition of Rho kinase in rats which underwent renal I/R preserved renal blood flow by improving eNOS function (46). These studies indicate an important role for eNOS activity as a protector against renal I/R. We observed, in the present study, a significant reduction in the amount of NO_2/NO_3 excreted in the urine after 24 h of renal I/R. Intriguingly, spironolactone prevented the reduction of these NO metabolites in the urine, suggesting that the improvement of NO generation is another mechanism associated with

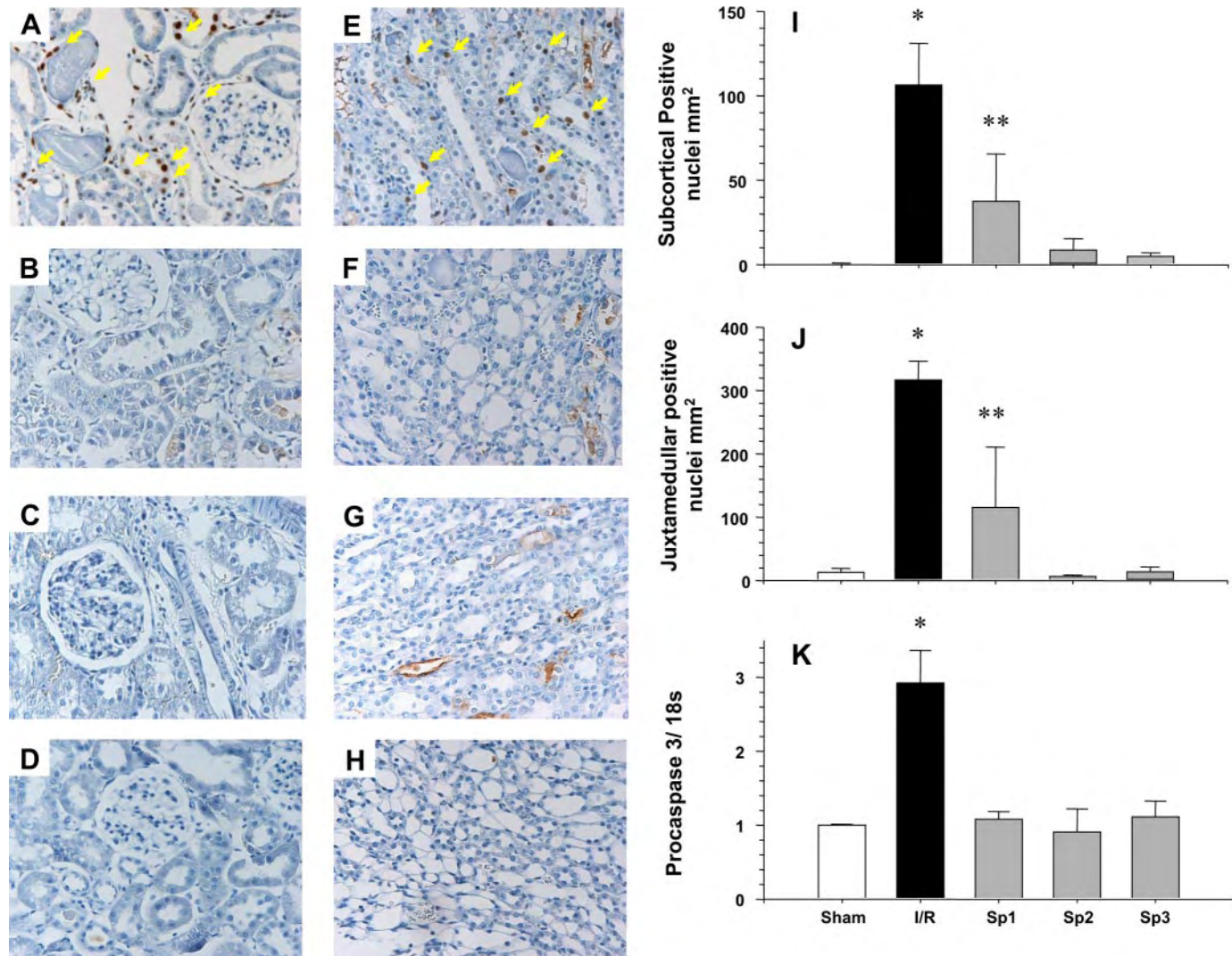


Fig. 6. Apoptotic cellular death. *A–H*: representative subcortical and juxtamedullary kidney sections showing positive nuclei for apoptosis determined by terminal deoxynucleotide transferase-mediated dUTP nick end labeling (TUNEL) assay (coffee brown) in the studied groups, as indicated. *I* and *J*: quantification of TUNEL-positive nuclei (by mm^2) in subcortical and juxtamedullary areas. Note the marked increase in the number of TUNEL-positive cells (arrows) in I/R untreated group (*A* and *E*). A significant reduction was seen in treated I/R groups, which was practically absent when spironolactone was given 2 or 3 days before I/R. I/R injury was associated with an increase in pro-caspase 3 mRNA kidney levels that was reduced by spironolactone pretreatment (*K*). Error bars represent SE. * $P < 0.05$ vs. sham-operated rats. ** $P < 0.05$ vs. all groups.

protection induced by an MR blockade. It is possible that this effect of spironolactone is largely responsible for renal blood flow preservation in I/R spironolactone-treated rats. However, to analyze other possible mechanisms by which spironolactone improved NO production, the amount of eNOS and phosphorylation of active and inactive eNOS was determined. Phosphorylation of serine residue S1177 of eNOS is associated with activation of this enzyme, whereas phosphorylation of threonine residue T497 decreased its activity (42). When the spironolactone-pretreated I/R group was compared with the I/R untreated group, upregulation of eNOS protein levels, increased phosphorylation of residue S1177 of eNOS, and reduced phosphorylation of residue T497 of eNOS were observed. In support of these findings, it has been reported that aldosterone reduces NO generation in human umbilical vein endothelial cells by a mechanism that includes the reduction of eNOS S1177 phosphorylation and increased free radical pro-

duction (28). Thus increased amounts of activated eNOS in the kidney could be responsible for the observed increase in urinary NO_2/NO_3 excretion and reestablishment of renal blood flow in I/R spironolactone-treated animals.

It is well known that hypoxia, as a result of ischemia and subsequent reperfusion, is characterized by increased reactive oxygen species (ROS) and decreased efficacy of the antioxidant system, which lead to tubular cell injury and death (17). In the present study we observed that renal I/R produced significant tubular damage at a histological level, as was evidenced also by the elevation of the amount of urinary protein and NAG excretion as tubular injury markers. Tubular damage observed was associated with an increase in renal TBARS contents as a marker of ROS generation (Fig. 5). Furthermore, a MR prophylactic blockade normalized renal TBARS levels and prevented the development of tubular injury. In support to these observations, it has been demonstrated that aldosterone in-

duced ROS generation by NADPH oxidase activation in cultured adult rat ventricular myocytes and mesangial cells (26, 39). Our results suggest that aldosterone may also contribute to induce ROS generation during a process of I/R. Thus, in addition to preventing renal hypoperfusion, MR antagonism reduced ROS generation and increased the mRNA levels of antioxidant enzymes (SOD and GPx), resulting in the preservation of tubular renal structure, as was shown by the light microscopic findings and the normalization of tubular injury markers.

Ischemic renal injury has been traditionally associated with tubular cell necrosis. However, apoptosis has emerged as a significant mode of cell death during renal I/R (20). Recent reports have demonstrated that interference with the apoptotic program translates into a protective effect during renal ischemia (6, 18), recognizing that the pathways associated with apoptosis may be very critical in the cell injury observed during I/R. In this study, untreated rats that underwent renal I/R presented a significant elevation of cell death by apoptosis in subcortical and juxtamedullary sections. The renoprotective effect of spironolactone was also associated with an important reduction of apoptosis in these sections. Because hypoxia and increased free radical generation resulting from renal hypoperfusion and reperfusion are known to trigger cell death by apoptosis, it is possible that the reduction of apoptosis observed in spironolactone-treated rats may result from the improvement of renal plasma flow (Fig. 1C) and decreased renal tissue lipoperoxidation (Fig. 5A).

In summary, in this study we show that aldosterone plays a central role in renal injury induced by I/R and emphasizes that spironolactone administration for 24–96 h before induction of renal I/R injury prevents the renal dysfunction and structural damage observed in this model. The mechanism of protection includes preservation of renal plasma flow and reestablishment of urinary NO₂/NO₃ excretion that was accompanied by increased expression of eNOS and phosphorylation at its residue S1177, and reduction of lipoperoxidation and cell apoptotic death. Based on our results, it will be intriguing to investigate the potential role of spironolactone in other models of renal ischemia, such as the cold ischemia associated with renal transplantation and I/R in other organs as that occurs in myocardial infarction treated with angioplasty. Our results may open new therapeutic avenues for the prevention of tissue damage in patients that are expected to be exposed to renal I/R, such as renal transplantation, high risk cardiovascular surgery, or I/R in other organs.

ACKNOWLEDGMENTS

We thank Dr. Carlos Larralde and Dr. Steve Hebert for helpful revisions and corrections of the manuscript.

GRANTS

This work was supported by National University of Mexico Grant IN228206 and Mexican Council of Science and Technology Grant 40182 A-1 (to N. A. Bobadilla) and National Institute of Diabetes and Digestive and Kidney Diseases Grant DK-064635 (to G. Gamba).

REFERENCES

- Arima S, Kohagura K, Xu HL, Sugawara A, Abe T, Satoh F, Takeuchi K, Ito S. Nongenomic vascular action of aldosterone in the glomerular microcirculation. *J Am Soc Nephrol* 14: 2255–2263, 2003.
- Bobadilla NA, Tapia E, Franco M, Lopez P, Mendoza S, Garcia-Torres R, Alvarado JA, Herrera-Acosta J. Role of nitric oxide in renal hemodynamic abnormalities of cyclosporin nephrotoxicity. *Kidney Int* 46: 773–779, 1994.
- Brown NJ. Aldosterone and end-organ damage. *Curr Opin Nephrol Hypertens* 14: 235–241, 2005.
- Chrysostomou A, Pedagogos E, MacGregor L, Becker GJ. Double-blind, placebo-controlled study on the effect of the aldosterone receptor antagonist spironolactone in patients who have persistent proteinuria and are on long-term angiotensin-converting enzyme inhibitor therapy, with or without an angiotensin II receptor blocker. *Clin J Am Soc Nephrol* 1: 256–262, 2006.
- Chrysostomou A, Becker G. Spironolactone in addition to ACE inhibition to reduce proteinuria in patients with chronic renal disease. *N Engl J Med* 345: 925–926, 2001.
- Daemen MA, vant'Veer C, Denecker G, Heemskerk VH, Wolfs TG, Clauss M, Vandenameele P, Buurman WA. Inhibition of apoptosis induced by ischemia-reperfusion prevents inflammation. *J Clin Invest* 104: 541–549, 1999.
- English J, Evan A, Houghton DC, Bennett WM. Cyclosporine-induced acute renal dysfunction in the rat. Evidence of arteriolar vasoconstriction with preservation of tubular function. *Transplantation* 44: 135–141, 1987.
- Feria I, Richardo I, Juarez P, Ramirez V, Gonzalez MA, Uribe N, Garcia-Torres R, Lopez-Casillas F, Gamba G, Bobadilla NA. Therapeutic benefit of spironolactone in experimental chronic cyclosporine A nephrotoxicity. *Kidney Int* 63: 43–52, 2003.
- Fiebeler A, Schmidt F, Muller DN, Park JK, Dechend R, Bieringer M, Shagdarsuren E, Breu V, Haller H, Luft FC. Mineralocorticoid receptor affects AP-1 and nuclear factor-kappaB activation in angiotensin II-induced cardiac injury. *Hypertension* 37: 787–793, 2001.
- Friedewald JJ, Rabb H. Inflammatory cells in ischemic acute renal failure. *Kidney Int* 66: 486–491, 2004.
- Goligorsky MS, Brodsky SV, Noiri E. NO bioavailability, endothelial dysfunction, and acute renal failure: new insights into pathophysiology. *Semin Nephrol* 24: 316–323, 2004.
- Gros R, Ding Q, Armstrong S, O'Neil C, Pickering JG, Feldman RD. Rapid effects of aldosterone on clonal human vascular smooth muscle cells. *Am J Physiol Cell Physiol* 292: C788–C794, 2007.
- Han SY, Kim CH, Kim HS, Jee YH, Song HK, Lee MH, Han KH, Kim HK, Kang YS, Han JY, Kim YS, Cha DR. Spironolactone prevents diabetic nephropathy through an anti-inflammatory mechanism in type 2 diabetic rats. *J Am Soc Nephrol* 17: 1362–1372, 2006.
- Henry RJ, Sobel C, Segalove M. Turbidimetric determination of proteins with sulfosalicylic and trichloroacetic acid. *Proc Soc Exp Biol Med* 92: 748–751, 1956.
- Hollenberg NK. Aldosterone in the development and progression of renal injury. *Kidney Int* 66: 1–9, 2004.
- Hostetter TH, Ibrahim HN. Aldosterone in chronic kidney and cardiac disease. *J Am Soc Nephrol* 14: 2395–2401, 2003.
- Jassem W, Heaton ND. The role of mitochondria in ischemia/reperfusion injury in organ transplantation. *Kidney Int* 66: 514–517, 2004.
- Jo SK, Yun SY, Chang KH, Cha DR, Cho WY, Kim HK, Won NH. alpha-MSH decreases apoptosis in ischaemic acute renal failure in rats: possible mechanism of this beneficial effect. *Nephrol Dial Transplant* 16: 1583–1591, 2001.
- Joffe HV, Adler GK. Effect of aldosterone and mineralocorticoid receptor blockade on vascular inflammation. *Heart Fail Rev* 10: 31–37, 2005.
- Kaushal GP, Basnakian AG, Shah SV. Apoptotic pathways in ischemic acute renal failure. *Kidney Int* 66: 500–506, 2004.
- Kelly KJ. Acute renal failure: much more than a kidney disease. *Semin Nephrol* 26: 105–113, 2006.
- Kelly KJ, Molitoris BA. Acute renal failure in the new millennium: time to consider combination therapy. *Semin Nephrol* 20: 4–19, 2000.
- Leopold JA, Dam A, Scribner AW, Liao R, Handy DE, Stanton RC, Pitt B, Loscalzo JL. Aldosterone impairs vascular reactivity by decreasing glucose-6-phosphate dehydrogenase activity. *Nat Med* 13: 189–197, 2007.
- Livak KJ, Schmittgen TD. Analysis of relative gene expression data using real-time quantitative PCR and the $2^{-\Delta\Delta CT}$ method. *Methods* 25: 402–408, 2001.
- McAuley FT, Whiting PH, Thomson AW, Simpson JG. The influence of enalapril or spironolactone on experimental cyclosporin nephrotoxicity. *Biochem Pharmacol* 36: 699–703, 1987.

26. Miyata K, Rahman M, Shokoji T, Nagai Y, Zhang GX, Sun GP, Kimura S, Yukimura T, Kiyomoto H, Kohno M, Abe Y, Nishiyama A. Aldosterone stimulates reactive oxygen species production through activation of NADPH oxidase in rat mesangial cells. *J Am Soc Nephrol* 16: 2906–2912, 2005.
27. Molitoris BA, Sutton TA. Endothelial injury and dysfunction: role in the extension phase of acute renal failure. *Kidney Int* 66: 496–499, 2004.
28. Nagata D, Takahashi M, Sawai K, Tagami T, Usui T, Shimatsu A, Hirata Y, Naruse M. Molecular mechanism of the inhibitory effect of aldosterone on endothelial NO synthase activity. *Hypertension* 48: 165–171, 2006.
29. Ngarmukos C, Grekin RJ. Nontraditional aspects of aldosterone physiology. *Am J Physiol Endocrinol Metab* 281: E1122–E1127, 2001.
30. Nishiyama A, Abe Y. Molecular mechanisms and therapeutic strategies of chronic renal injury: renoprotective effects of aldosterone blockade. *J Pharmacol Sci* 100: 9–16, 2006.
31. Perez-Rojas J, Blanco JA, Cruz C, Trujillo J, Vaidya VS, Uribe N, Bonventre JV, Gamba G, Bobadilla NA. Mineralocorticoid receptor blockade confers renoprotection in preexisting chronic cyclosporine nephrotoxicity. *Am J Physiol Renal Physiol* 292: F131–F139, 2007.
32. Perez-Rojas JM, Derive S, Blanco JA, Cruz C, Martinez de la Maza L, Gamba G, Bobadilla NA. Renocortical mRNA expression of vasoactive factors during spironolactone protective effect in chronic cyclosporine nephrotoxicity. *Am J Physiol Renal Physiol* 289: F1020–F1030, 2005.
33. Pitt B, Remme W, Zannad F, Neaton J, Martinez F, Roniker B, Bittman R, Hurley S, Kleiman J, Gatlin M. Eplerenone, a selective aldosterone blocker, in patients with left ventricular dysfunction after myocardial infarction. *N Engl J Med* 348: 1309–1321, 2003.
34. Pitt B, Zannad F, Remme WJ, Cody R, Castaigne A, Perez A, Palensky J, Witte J. The effect of spironolactone on morbidity and mortality in patients with severe heart failure. Randomized Aldactone Evaluation Study Investigators. *N Engl J Med* 341: 709–717, 1999.
35. Robert V, Heymes C, Silvestre JS, Sabri A, Swynghedauw B, Delcayre C. Angiotensin AT1 receptor subtype as a cardiac target of aldosterone: role in aldosterone-salt-induced fibrosis. *Hypertension* 33: 981–986, 1999.
36. Rocha R, Chander PN, Khanna K, Zuckerman A, Stier CT Jr. Mineralocorticoid blockade reduces vascular injury in stroke-prone hypertensive rats. *Hypertension* 31: 451–458, 1998.
37. Rocha R, Chander PN, Zuckerman A, Stier CT Jr. Role of aldosterone in renal vascular injury in stroke-prone hypertensive rats. *Hypertension* 33: 232–237, 1999.
38. Rocha R, Stier CT Jr, Kifor I, Ochoa-Maya MR, Rennke HG, Williams GH, Adler GK. Aldosterone: a mediator of myocardial necrosis and renal arteriopathy. *Endocrinology* 141: 3871–3878, 2000.
39. Rude MK, Duhaney TA, Kuster GM, Judge S, Heo J, Colucci WS, Siwik DA, Sam F. Aldosterone stimulates matrix metalloproteinases and reactive oxygen species in adult rat ventricular cardiomyocytes. *Hypertension* 46: 555–561, 2005.
40. Sambrook J, Fritsch EF, Maniatis T. *Molecular Cloning: A Laboratory Manual*. Cold Spring Harbor, NY: Cold Spring Harbor Laboratory Press, 1989.
41. Schrier RW, Wang W, Poole B, Mitra A. Acute renal failure: definitions, diagnosis, pathogenesis, and therapy. *J Clin Invest* 114: 5–14, 2004.
42. Sessa WC. eNOS at a glance. *J Cell Sci* 117: 2427–2429, 2004.
43. Singh D, Chander V, Chopra K. Protective effect of catechin on ischemia-reperfusion-induced renal injury in rats. *Pharmacol Rep* 57: 70–76, 2005.
44. Trachtman H, Weiser AC, Valderrama E, Morgado M, Palmer LS. Prevention of renal fibrosis by spironolactone in mice with complete unilateral ureteral obstruction. *J Urol* 172: 1590–1594, 2004.
45. Tumlin JA, Lea JP, Swanson CE, Smith CL, Edge SS, Someren JS. Aldosterone and dexamethasone stimulate calcineurin activity through a transcription-independent mechanism involving steroid receptor-associated heat shock proteins. *J Clin Invest* 99: 1217–1223, 1997.
46. Versteilen AM, Korstjens IJ, Musters RJ, Groeneveld AB, Sipkema P. Rho kinase regulates renal blood flow by modulating eNOS activity in ischemia-reperfusion of the rat kidney. *Am J Physiol Renal Physiol* 291: F606–F611, 2006.
47. Virdis A, Neves MF, Amiri F, Viel E, Touyz RM, Schiffrin EL. Spironolactone improves angiotensin-induced vascular changes and oxidative stress. *Hypertension* 40: 504–510, 2002.
48. Weight SC, Bell PR, Nicholson ML. Renal ischaemia-reperfusion injury. *Br J Surg* 83: 162–170, 1996.
49. Wellwood JM, Price RG, Ellis BG, Thompson AE. A note on the practical aspects of the assay of N-acetyl-beta-glucosaminidase in human urine. *Clin Chim Acta* 69: 85–91, 1976.
50. Wijsman JH, Jonker RR, Keijzer R, van de Velde CJ, Cornelisse CJ, van Dierendonck JH. A new method to detect apoptosis in paraffin sections: in situ end-labeling of fragmented DNA. *J Histochem Cytochem* 41: 7–12, 1993.
51. Yamasawa H, Shimizu S, Inoue T, Takaoka M, Matsumura Y. Endothelial nitric oxide contributes to the renal protective effects of ischemic preconditioning. *J Pharmacol Exp Ther* 312: 153–159, 2005.



Evaluation of oxidative stress in D-serine induced nephrotoxicity

Marisol Orozco-Ibarra ^a, Omar Noel Medina-Campos ^a, Dolores Javier Sánchez-González ^b, Claudia María Martínez-Martínez ^b, Esaú Floriano-Sánchez ^c, Abel Santamaría ^d, Victoria Ramírez ^e, Norma A. Bobadilla ^e, José Pedraza-Chaverri ^{a,*}

^a Facultad de Química, Departamento de Biología, Universidad Nacional Autónoma de México (UNAM), Ciudad Universitaria, 04510, D.F., Mexico

^b Departamento de Biología Celular, Escuela Médico Militar, Universidad del Ejército y Fuerza Aérea, Cerrada de Palomas y Batalla de Celaya, Col Lomas de San Isidro, Delegación Miguel Hidalgo, 11200, D.F., Mexico

^c Departamento de Bioquímica y Biología Molecular, Escuela Médico Militar, Universidad del Ejército y Fuerza Aérea, Cerrada de Palomas y Batalla de Celaya, Col. Lomas de San Isidro, Delegación Miguel Hidalgo, 11200, D.F., Mexico

^d Laboratorio de Aminoácidos Excitadores, Instituto Nacional de Neurología y Neurocirugía Manuel Velasco Suárez, Delegación Tlalpan, 14269, D.F., Mexico

^e Unidad de Fisiología Molecular, Instituto de Investigaciones Biomédicas, Universidad Nacional Autónoma de México, Departamento de Nefrología, Instituto Nacional de Ciencias Médicas y Nutrición Salvador Zubirán, Vasco de Quiroga #15, Delegación Tlalpan, 14000, D.F., Mexico

Received 18 July 2006; received in revised form 6 October 2006; accepted 11 October 2006

Available online 20 October 2006

Abstract

It has been suggested that oxidative stress is involved in D-serine-induced nephrotoxicity. The purpose of this study was to assess if oxidative stress is involved in this experimental model using several approaches including (a) the determination of several markers of oxidative stress and the activity of some antioxidant enzymes in kidney and (b) the use of compounds with antioxidant or prooxidant effects. Rats were sacrificed at several periods of time (from 3 to 24 h) after a single i.p. injection of D-serine (400 mg/kg). Control rats were injected with L-serine (400 mg/kg) and sacrificed 24 h after. The following markers were used to assess the temporal aspects of renal damage: (a) urea nitrogen (BUN) and creatinine in blood serum, (b) kidney injury molecule (KIM-1) mRNA levels, and (c) tubular necrotic damage. In addition, creatinine clearance, proteinuria, and urinary excretion of *N*-acetyl- β -D-glucosaminidase (NAG) were measured 24 h after D-serine injection. Protein carbonyl content, malondialdehyde (MDA), 4-hydroxy-2-nonenal (4-HNE), fluorescent products of lipid peroxidation, reactive oxygen species (ROS), glutathione (GSH) content, and heme oxygenase-1 (HO-1) expression were measured as markers of oxidative stress in the kidney. Additional experiments were performed using the following compounds with antioxidant or pro-oxidant effects before D-serine injection: (a) α -phenyl-*tert*-butyl-nitrone (PBN), a spin trapping agent; (b) 5,10,15,20-tetrakis (4-sulfonatophenyl) porphyrinato iron(III) (FeTPPS), a soluble complex able to metabolize peroxy nitrite; (c) aminotriazole (ATZ), a catalase (CAT) inhibitor; (d) stannous chloride (SnCl_2), an HO-1 inductor; (e) tin mesoporphyrin (SnMP), an HO inhibitor. In the time-course study, serum creatinine and BUN increased significantly on 15–24 and 20–24 h, respectively, and KIM-1 mRNA levels increased significantly on 6–24 h. Histological analyses revealed tubular necrosis at 12 h. The activity of antioxidant enzymes catalase, superoxide dismutase, glutathione peroxidase, and glutathione reductase remained unchanged at all times studied. Protein carbonyl content, MDA, 4-HNE, and ROS remained unchanged at all time-points studied. GSH content decreased transiently on 9 and 12 h. Interestingly, fluorescent products of lipid peroxidation decreased significantly

* Corresponding author at: Facultad de Química, Departamento de Biología, Edificio F, Segundo Piso, Laboratorio 209, Universidad Nacional Autónoma de México (UNAM), Ciudad Universitaria, 04510 México, D.F., Mexico. Tel.: +52 55 5622 3878; fax: +52 55 5622 3878.

E-mail address: pedraza@servidor.unam.mx (J. Pedraza-Chaverri).

on 3–24 h. HO-1 expression was undetectable by Western blot and the immunohistochemistry studies revealed that the intensity of HO-1 staining was weak. The administration of PBN, FeTPPS, ATZ, SnCl₂, and SnMP did not prevent or enhance renal damage induced by D-serine. Our data taken as a whole suggest that oxidative stress is not involved in the early phase of the nephrotoxicity induced by D-serine.

© 2006 Elsevier Ireland Ltd. All rights reserved.

Keywords: D-Serine; Nephrotoxicity; Oxidative stress

1. Introduction

D-Serine is an endogenous ligand for the glycine-binding site on the *N*-methyl-D-aspartate receptor (Mothet et al., 2000). Recent studies have shown that D-serine supplementation reduces the negative symptoms of schizophrenia (Tuominen et al., 2006; Heresco-Levy et al., 2005; Tsai et al., 1998); however, high doses of D-serine have shown to be nephrotoxic (Carone et al., 1985; Carone and Ganote, 1975). D-Serine is reabsorbed in the proximal straight tubules of rat kidney causing selective necrosis (Silbernagl et al., 1999) which is accompanied by aminoaciduria, proteinuria and glucosuria (Carone et al., 1985). In contrast similar doses of L-serine did not produce any nephrotoxic effect (Carone and Ganote, 1975). The mechanism of D-serine-induced toxicity is not yet completely understood. It has been suggested that tyrosine catabolism (Williams and Lock, 2004) and D-amino acid oxidase (D-AAO, EC 1.4.3.3) activity (Williams and Lock, 2005; Maekawa et al., 2005) may be involved in D-serine toxicity. In this regard, Williams and Lock (2005) found that the administration of sodium benzoate, an inhibitor of D-AAO, prevents D-serine induced nephrotoxicity. D-AAO catalyzes the oxidative deamination of D-amino acids, including D-serine, to produce the corresponding α-keto acids plus ammonia and hydrogen peroxide (H₂O₂) (Nagata, 1992), the last is a reactive oxygen specie (ROS). In the kidney, D-AAO is localized within the peroxisomes of tubular epithelial cells (Pilone, 2000). The H₂O₂ production by D-AAO and the protective effect of reduced glutathione (GSH) administration on D-serine induced tubular dysfunction and renal GSH depletion (Silbernagl et al., 1997) may suggest the participation of oxidative stress in D-serine induced nephrotoxicity. However, the possible participation of oxidative stress in this experimental model has not been fully explored. Therefore, the aim of the present study was to assess if oxidative stress is involved in the renal damage induced by D-serine in rats using several approaches including: (a) the determination of a number of markers of oxidative damage [e.g. heme oxygenase-1 (HO-1) expres-

sion, ROS determination and GSH content], (b) the determination of the activity and/or content of several antioxidant enzymes [e.g. catalase (CAT), superoxide dismutase (SOD) and glutathione peroxidase (GPx)], and (c) the use of compounds with antioxidant [e.g. α-phenyl-*tert*-butyl-nitrone (PBN), 5,10,15,20-tetrakis (4-sulfonatophenyl) porphyrinato iron (III) (FeTPPS)] or pro-oxidant [e.g. 3-amino-1,2,4-triazole (ATZ) effects.

2. Materials and methods

D-Serine, L-serine, PBN, ATZ, *p*-nitrophenyl-N-acetyl-β-D-glucosaminide, 2,4-dinitrophenylhydrazine (DNPH), streptomycin sulphate, guanidine, 1-methyl-2-phenylindole, trimethoxypropane, 5,5'-dithiobis-(2-nitrobenzoic acid) (DTNB), GSH, oxidized glutathione (GSSG), glutathione reductase (GSH-Rx), NADPH, 2-vinylpyridine, acrylamide, bis-acrylamide, nitro blue tetrazolium (NBT), 2',7'-dichlorofluorescein (DCF), and deoxyribonucleoside triphosphate (dNTP), were purchased from Sigma Chemical Co. (St. Louis, MO, USA). Trichloroacetic acid (TCA), SnCl₂, HCl, H₂O₂, sulfosalicylic acid, acetonitrile and methanol were purchased from Mallinckrodt Baker Inc. (Phillipsburg, NJ, USA). Tin mesoporphyrin (SnMP) was purchased from Frontier Scientific Inc. (Logan, UT, USA). Anti-HO-1, anti-Mn-SOD, and anti-Cu/Zn-SOD antibodies and recombinant rat HO-1 protein (used as a western blot control) were purchased from StressGen Biotechnologies Co. (Victoria, BC, Canada). Anti-CAT antibodies and FeTPPS were purchased from Calbiochem (San Diego, CA, USA). Anti-α-actin antibodies were purchased from Chemicon International, Inc. (Temecula, CA, USA). Anti-4-hydroxy-2-nonenal (4-HNE) antibodies were from Oxis International, Inc. (Portland, OR, USA). Dichlorodihydrofluorescein diacetate (DCFH-DA) was from Molecular Probes (Eugene, OR, USA). Commercial kits were used to measure creatinine (Bayer, cat # B014569-01) and BUN (Spinreact, cat # 1001325). Declere was from Cell Marque (Hot Springs, AR, USA). ABC-kit Vectastain was from Vector Laboratories (Orton Southgate, Peterborough, UK). Diaminobenzidine substrate was from DAKO Corporation (Carpinteria, CA, USA). Moloney murine leukemia virus reverse transcriptase and random hexamers were from Invitrogen (Carlsbad, CA, USA). The KIM-1 primer and probe was ordered as kit: RN00597703_m1 (Assays-on-Demand, ABI).

3. Experimental design

3.1. Animals

Male Sprague–Dawley (Harlan Teklad, Mexico City, Mexico) rats weighting initially 180–200 g were used along the study. Rats were maintained in stainless steel metabolic cages to collect 24-h urine. Animals were sacrificed by decapitation, blood was collected to obtain serum and both kidneys were dissected and immediately frozen in liquid nitrogen. Experimental protocols followed the guidelines of Norma Oficial Mexicana (NOM-ECOL-087-1995); all procedures were made to minimize animal suffering.

3.2. Time-course study

Animals were sacrificed 3, 6, 9, 12, 15, 20, and 24 h after D-serine administration (400 mg/kg, i.p.). Control group was formed by rats treated with L-serine 400 mg/kg i.p. and sacrificed 24 h later. Kidneys were removed to evaluate the histological damage and to perform immunohistochemical analyses, as well as to assess the activity and content of some antioxidant enzymes, and the content of HO-1, protein carbonyl, GSH, and malondialdehyde (MDA). Blood serum was obtained to determine the concentration of creatinine and blood urea nitrogen (BUN). In addition, 24 h after D- or L-serine injection, total protein and N-acetyl- β -D-glucosaminidase (NAG) activity were measured in the urine samples collected. We studied the animals 24 h after L-serine or D-serine injection taking into account that in a previous study we found a peak of renal damage evaluated by proteinuria and urinary excretion of NAG at this time point (unpublished observations).

3.3. Effect of PBN, FeTPPS, ATZ, SnCl₂, and SnMP on D-serine nephrotoxicity

In additional groups of animals ($n=6$ rats/group), we tried to modulate the renal damage induced by D-serine using compounds able to protect against oxidative/nitrosative damage (PBN and FeTPPS) or to enhance it (ATZ). PBN and FeTPPS were given i.p. 30 min before D-serine administration at a dose of 100 mg/kg (Pedraza-Chaverri et al., 1992) and 15 mg/kg (Chirino et al., 2004), respectively. ATZ was given i.p. (1 g/kg) (Pedraza-Chaverri et al., 1999) 24 h before D-serine administration.

Furthermore we tested if the modulation of HO-1 expression/activity was able to alter D-serine induced nephrotoxicity. HO-1 was induced by a single i.p. injection of SnCl₂ (100 mg/kg) (Barrera et al., 2003) and HO was inhibited by a single i.p. injection of SnMP (15 mg/kg) (Wang et al., 2001) 12 h and 3 h, respectively, before D-serine injection. Rats were sacrificed 24 h after D-serine administration. SnMP inhibits both the inducible HO-1 and constitutive HO-2 isoforms and SnCl₂ induces specifically the HO-1 isoform (Akagi et al., 2005; da Silva et al., 2001).

3.4. Biochemical markers of renal injury

Creatinine in serum and urine was measured in a creatinine analyzer (Bayer RA1000) (Miles Inc., Diagnostic Division, Tarrytown, NY, USA) using a commercial kit. These data were used to calculate creatinine clearance with the standard formula. Urea was also measured using a commercial kit; BUN was obtained correcting the urea value by a 2.14 factor (Woo et al., 1979). NAG activity was measured using p-nitrophenyl-N-acetyl- β -D-glucosaminide as substrate and proteinuria was measured by a turbidimetric method using TCA (Barrera et al., 2003).

3.5. Histological and immunohistochemical analyses

For light microscopy, kidney tissue was fixed by immersion in buffered formalin (pH 7.4) and embedded in paraffin. For histological analysis, sections (3 μ m) were stained with hematoxylin and eosin. For immunohistochemistry, kidney sections (3 μ m) were deparaffined and then boiled in Declere to unmask antigen sites; the endogenous activity of peroxidase was quenched with 0.03% H₂O₂ in absolute methanol. Kidney sections were incubated overnight at 4 °C with 1:200 dilution of mouse anti 4-HNE monoclonal antibodies or 1:500 dilution of rabbit anti HO-1 polyclonal antibodies in phosphate buffered saline (PBS). Bound antibodies were detected with avidin-biotinylated peroxidase complex ABC-kit Vectastain and diaminobenzidine substrate. After appropriate washing in PBS, slides were counterstained with hematoxylin. All specimens were examined by light microscopy Axiovert 200M (Carl Zeiss, Germany). The percentage of positive cells was determined with a computerized image analyzer KS-300 3.0 (Carl Zeiss, Germany). This software detects positive cells in brown and automatically determines the percentage per field. All sections were incubated under the same conditions with the same concentration of antibodies and in the same running, so the immunostaining was comparable among the different experimental groups. For the negative control, preimmune goat serum was used instead of the primary antibodies (Sánchez-González et al., 2004).

3.6. Renal mRNA levels of KIM-1

3.6.1. RNA isolation

Total RNA was isolated in a pool including four rats of each group following the guanidine isothiocyanate-cesium chloride method (Sambrook et al., 1989). Integrity of isolated total RNA was examined by 1% agarose gel electrophoresis and RNA concentration was determined by UV-light absorbance at 260 nm (Beckman DU640, Brea, CA, USA). Reverse transcription (RT) was carried out using 2.5 μ g of total RNA from renal cortex of each rat. RT was performed at 37 °C for 60 min in a total volume of 20 μ l using 200 U of the Moloney murine leukemia virus reverse transcriptase, 100 pmol of random hexamers, 0.5 mM of each dNTP, and 1 \times RT buffer [75 mM KCl, 50 mM Tris–HCl, 3 mM MgCl₂, 10 mM dithiothreitol (DTT), pH 8.3].

3.6.2. Real-time PCR

The renal mRNA levels of KIM-1 were quantified by real-time PCR on the ABI Prism 7300 Sequence Detection System (TaqMan, Applied Biosystems ABI, Foster City, CA, USA) as previously reported (Vaidya et al., 2006; Perez-Rojas et al., in press). FAM or VIC dye-labeled probes were selected from the Applied Biosystems Assays-on-Demand ABI product line and were specifically used to detect and quantify cDNA sequences without detecting genomic DNA. For KIM-1 and 18S rRNA expression FAM and VIC probes were used, respectively. The FAM and VIC were used as fluorescent reporter dyes to detect amplification products. Validation of amplification efficiency was made for every primer/probe set and was calculated for each run. As endogenous control, we used eukaryotic 18S rRNA (pre-designed assay reagent Applied by ABI, external run) to correct for potential variation in RNA loading or efficiency of the amplification reaction. Standard curves for each primer/probe were computed from a series of serial template dilutions from 0.187 through 187 ng. PCR was carried out in 96-well plates on cDNA equivalent to 3.5 ng of total RNA. Thermal cycling conditions were 10 min at 95 °C followed with 40 cycles at 95 °C for 1 min, and 60 °C for 1 min. Data were collected using the ABI PRISM 7300 SDS analytical thermal cycler (Applied Biosystems). Each individual sample was tested in triplicate. The relative quantification KIM-1 gene expression was performed using the comparative Ct method (Livak and Schmittgen, 2001). The threshold cycle (CT) is defined as the fractional cycle number at which the reporter fluorescence reaches a certain level (i.e., usually 10 times the standard deviation of the baseline). In all experiments, 18S eukaryotic rRNA was used as control. Negative controls were included in the reaction plate.

3.7. Assay of reactive oxygen species (ROS)

ROS formation was estimated according to previous reports (Ali et al., 1992; Pérez-Severiano et al., 2004), making discrete modifications to adapt the method for kidney homogenates. Kidney tissue samples (55 mg) were obtained and homogenized in 2.2 ml of saline solution (0.9% NaCl). Aliquots of 1.5 ml were incubated with 0.5 ml of 5 μM DCFH-DA at 37 °C for 60 min. Fluorescence signals were recorded at the end of the incubation at an excitation wavelength of 488 nm and an emission wavelength of 525 nm in a Perkin-Elmer LS55 luminescence spectrometer. A standard curve was constructed using increasing concentrations of DCF incubated in parallel. Results were expressed as nmol of DCF formed/mg of protein/min. For this and other experimental procedures, protein concentrations were measured according to the method described by Lowry et al. (1951).

3.8. Protein carbonyl content

Protein carbonyl groups, a relatively stable marker of protein oxidation by ROS, were detected by their reactivity with DNPH to form protein hydrazones in renal cortex (Barrera et al., 2003). Homogenates were prepared in phosphate buffer

(pH 7.4) and incubated with streptomycin sulphate during 12 h. Then, homogenates were incubated with DNPH and vortexed continuously at room temperature for 1 h. Samples were precipitated with TCA and centrifuged at 2236 × g at 4 °C for 10 min. The pellet was washed with ethanol/ethyl acetate (1:1) to remove free DNPH reagent, samples were centrifuged at 2236 × g at 4 °C for 10 min. Washing procedure was repeated two times. The resulting protein pellet was resuspended in guanidine 6 M. Samples were incubated at 37 °C for 15–30 min to aid dissolution of the protein. The concentration of DNPH was determined at its maximum wavelength (360 nm) and the molar absorption coefficient of 22,000 M⁻¹ cm⁻¹ was used to quantify the levels of protein carbonyls. Blanks were prepared by replacing DNPH by HCl. The samples were then read against the blanks. Samples were spectrophotometrically analyzed against a blank of guanidine solution (6 M guanidine with 2 mM potassium phosphate).

3.9. Renal MDA content

A solution of 1-methyl-2-phenylindole in a mixture of acetonitrile/methanol (3:1) was added to the renal homogenates. The reaction was started by adding 37% HCl. The absorbance (A) at 586 nm was measured upon incubation of the reaction mixture at 45 °C for 40 min. For each series of assays, a blank (in which the sample was replaced by water) was included, and its postreaction absorbance was further subtracted from the A value. For each assay homogenate, a sample blank in which the reagent was replaced by acetonitrile/methanol (3:1, v/v) was included. It was used a standard curve of trimethoxypropane (Gerard-Monnier et al., 1998) and the results were expressed as nmol of MDA per mg of protein.

3.10. Assay of lipid fluorescent products

Lipid peroxidation was assessed in kidney tissue by discrete modifications to the assay of lipid fluorescent products previously reported by Pérez-Severiano et al. (2004) and Santamaría et al. (2003). Briefly, kidney tissue samples (50 mg) were homogenized in 3 ml of isotonic saline solution. Aliquots of 1 ml were added to 4 ml of a chloroform-methanol mixture (2:1, v/v). After vortexing for 10 s, the mixture was ice-cooled for 45 min to allow phase-separation. The fluorescence of the chloroform layer was measured in a Perkin-Elmer LS55 luminescence spectrometer at 370 nm of excitation and 430 nm of emission wavelengths. The sensitivity of the equipment was adjusted with a standard curve of quinine (original stock containing 0.1 μg/ml of quinine in 50 mM H₂SO₄). Results were expressed as relative fluorescence units (RFU) per mg of protein.

3.11. Renal glutathione content

GSH was determined by following the rate of reduction of DTNB by GSH at 412 nm. The quantification of GSSG was performed using the Griffith's method (Hermes-Lima and Storey, 1996; Griffith, 1980). Briefly, frozen tissue samples

were homogenized in ice-cold 5% (w/v) sulfosalicylic acid (previously bubbled with nitrogen gas for 10 min), then further bubbled with nitrogen gas for 10 s and centrifuged at 15,000 × g for 5 min. Supernatants were removed and immediately used to measure total glutathione, expressed as GSH-equivalents (GSH-eq = GSH + 2GSSG), thus preventing any acid hydrolysis. The assay for GSH-eq was performed in potassium phosphate buffer, pH 7.2, containing sample, NADPH and DTNB. The absorbance at 412 nm was recorded up to stabilization, after which GSH-Rx was added. The rate of reduction of DTNB was compared to a GSH standard curve. To determine GSSG, extracts prepared in 5% (w/v) sulfosalicylic acid were mixed with 2-vinylpyridine (prepared in ethanol) and the pH adjusted to 7.0 with NaOH. The GSH derivation was completed after 1 h incubation at room temperature, after which GSSG alone was quantified in the same way that GSH-eq determination. A standard curve of GSSG was done in the presence of ethanol to correct its effect on the assay. GSH content was calculated as the difference between total glutathione and GSSG content.

3.12. Western blot analyses

Total kidney and kidney microsomal proteins were separated by SDS-PAGE and transferred to nitrocellulose membranes (Amersham; Piscataway, USA). Membranes were incubated with 5% milk in 10 mM Tris-HCl (pH 7.4), 150 mM NaCl, 0.05% Tween-20 (TBS) buffer at 4 °C overnight. After washing with TBS, membranes were incubated with anti-HO-1 (1:2000), anti-CAT (1:400), anti Mn-SOD (1:4000), anti Cu/Zn-SOD (1:5000), or anti β-actin (1:1000) antibodies for 1 h at room temperature under constant shaking. Membranes were then washed and probed with horseradish peroxidase-conjugated donkey anti-rabbit IgG (Amersham) at a dilution of 1:2000. Chemiluminescence detection was performed with the Amersham ECL detection kit according to the manufacturer's instructions (Barrera et al., 2003).

3.13. Activity of antioxidant enzymes

Renal CAT activity was assayed by a method based on the decomposition of H₂O₂ by CAT contained in the samples (Aebi, 1984). This reaction follows a first-order kinetic given by the equation $k = 2.3/t \log A_0/A$, where k is the first-order reaction rate constant, t is the time over which was measured the decrease of H₂O₂ (15 s), and A_0/A is the optical density at times 0 and 15 s, respectively. The results were expressed in k /mg protein. SOD activity in kidney homogenates was assayed by a previously reported method (Oberley and Spitz, 1984), based in the NBT reduction to formazan. The amount of protein that inhibits NBT reduction to 50% of maximum was defined as one unit of SOD activity. Results were expressed as U/mg protein. Renal GPx activity was assayed by a method previously described (Lawrence and Burk, 1976). When GPx reduces H₂O₂, the enzyme consumes GSH and produces GSSG which is reduced to GSH by GSH-Rx using

NADPH. In this method the NADPH consumption is measured at 340 nm. Results were expressed as U/mg protein. Renal GSH-Rx activity was assayed by a method previously reported (Carlberg and Mannervik, 1975). The NADPH consumption in the reaction was measured at 340 nm. Results were expressed as U/mg protein. One unit of GPx or GSH-Rx is defined as the amount of enzyme that oxidizes 1 μmol of NADPH per minute.

3.14. Statistics

Data were expressed as mean ± S.E.M. Data were analyzed with the software Prism 3.02 (GraphPad, San Diego, CA, USA) by one-way analysis of variance followed by Dunnett post test or Bonferroni multiple comparisons method, as appropriate. Comparisons between two groups were performed by non-paired *t*-test. $p < 0.05$ was considered significant.

4. Results

4.1. Renal damage induced by D-serine

D-Serine administration induced a significant time-dependent increase of serum creatinine and BUN on 15–24 and 20–24 h, respectively. Creatinine and BUN values increased five- and three-fold, respectively, compared to L-serine treated rats (Fig. 1). The increase observed in serum creatinine revealed renal dysfunction induced by D-serine, thus creatinine clearance was significantly reduced from 1.26 ± 0.1 ml/ml in L-serine treated rats to 0.12 ± 0.03 ml/min in D-serine-treated rats ($p < 0.001$). Tubular damage was evinced by the increase

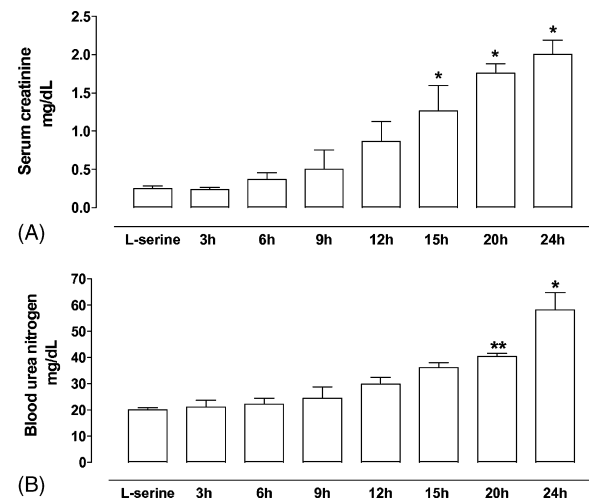


Fig. 1. Time-course study of (A) serum creatinine and (B) blood urea nitrogen after a single i.p. injection of D-serine (400 mg/kg). Control rats were injected with L-serine (400 mg/kg) and sacrificed 24 h later. Data are mean ± S.E.M. $n = 4$ rats (3–20 h) and 10 rats (24 h). * $p < 0.001$ and ** $p < 0.05$ vs. L-serine.

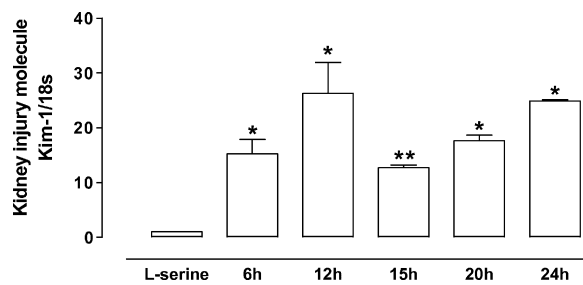


Fig. 2. Time-course study of kidney injury molecule (KIM-1) mRNA levels after a single i.p. injection of D-serine (400 mg/kg). Control rats were injected with L-serine (400 mg/kg) and sacrificed 24 h later. Data are mean \pm S.E.M. $n=4$ rats for each time. * $p<0.001$ and ** $p<0.05$ vs. L-serine. SEM in the L-serine group was very small.

of KIM-1 mRNA levels which were detected earlier than creatinine and BUN. Thus, KIM-1 increased more than 10-fold on 6–24 h after D-serine administration (Fig. 2). These findings were highlighted with the significant increase of urinary NAG and total protein excretion (16 and 4-times, respectively) detected 24 h after D-serine administration (Fig. 3) and tubular necrosis observed by histological analysis (data not shown).

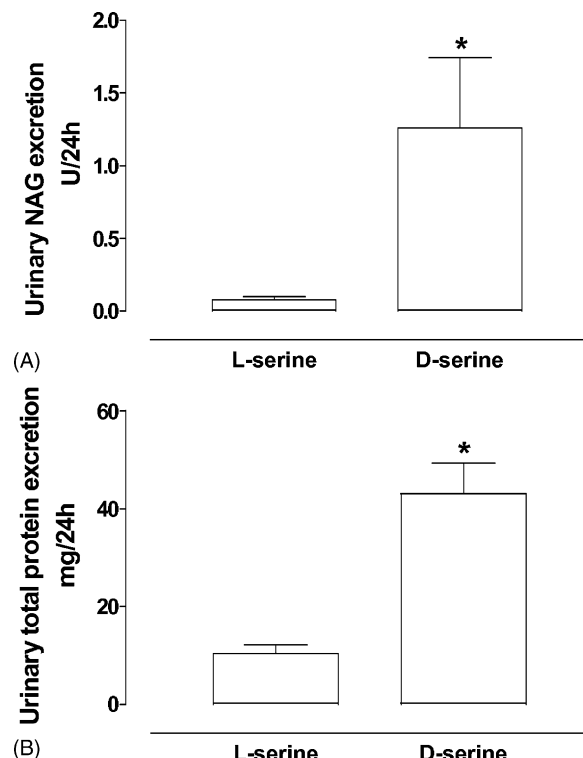


Fig. 3. Urinary excretion of (A) N -acetyl- β -D-glucosaminidase (NAG) and (B) total protein 24 h after a single i.p. injection of D-serine (400 mg/kg) or L-serine (400 mg/kg). Data are mean \pm S.E.M. $n=15$ rats for each group. * $p<0.001$ vs. L-serine.

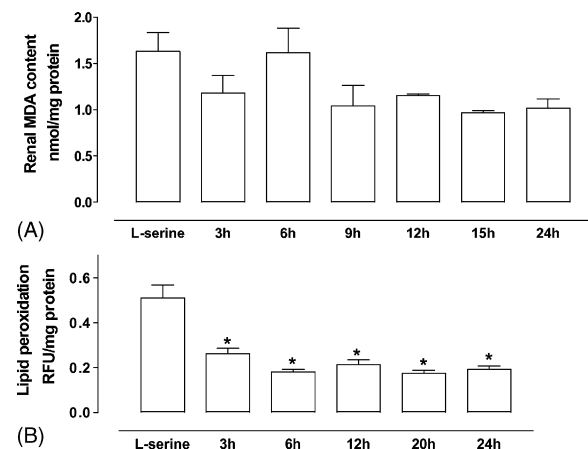


Fig. 4. Time-course study of changes in renal (A) MDA content and (B) lipid fluorescent products after a single i.p. injection of D-serine (400 mg/kg). Control rats were injected with L-serine (400 mg/kg) and sacrificed 24 h later. Data are mean \pm S.E.M. $n=4$ (3–15 h) and 10 (24 h). Changes in renal MDA content were not significative. * $p<0.001$ vs. L-serine. RFU: relative units of fluorescence.

4.2. Oxidative damage markers

In spite of renal dysfunction and structural damage induced by D-serine administration, renal ROS content was similar at all periods of time studied and renal protein carbonyl content remained unchanged in D-serine treated rats (data not shown). In order to evaluate oxidative stress we looked for renal lipid peroxidation by measuring MDA, 4-HNE, and fluorescent products of lipid peroxidation. Also GSH content and HO-1 expression were measured. But, we did not find any significant

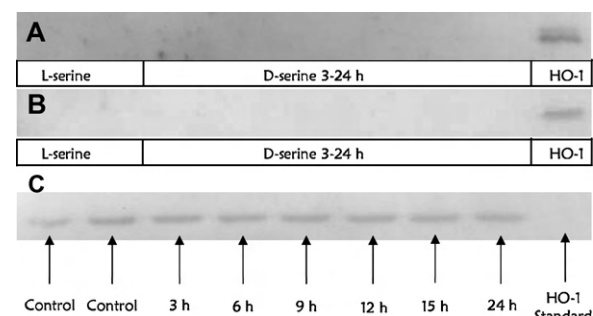


Fig. 5. Effect of D-serine or L-serine on renal HO-1 content measured by western blot. Analysis was performed 3, 6, 9, 12, 15, and 24 h after a single injection of D-serine (400 mg/kg) and 24 h after a single injection of L-serine (400 mg/kg). Panel A shows the result when it was used total renal homogenate, and panel B shows the result when it was used renal microsomes. L-serine and D-serine were unable to induce changes in HO-1 expression. Recombinant rat HO-1 protein (5 ng, right lane) was used as a western blot control and β -actin was used as a loading control (panel C). A representative image of western blot is shown in each panel.

Table 1

Glutathione content in kidneys from L-serine (control) and D-serine treated rats (3–24 h)

	GSH-eq*	GSSG*	GSH*	GSH/GSSG	(GSHeq/GSH) × 100
Control	5.4 ± 0.2	0.29 ± 0.07	4.8 ± 0.2	17.7 ± 3.5	89.1 ± 2.1
3 h	4.6 ± 0.3	0.29 ± 0.02	4.0 ± 0.3	14.3 ± 1.2	87.4 ± 1.0
6 h	5.8 ± 0.4	0.32 ± 0.02	5.2 ± 0.9	16.3 ± 2.2	88.6 ± 1.5
9 h	3.2 ± 0.6**	0.30 ± 0.01	2.6 ± 0.6**	8.7 ± 1.5	80.4 ± 3.3
12 h	3.3 ± 0.6**	0.33 ± 0.03	2.6 ± 0.6**	9.7 ± 3.7	79.1 ± 5.5
15 h	3.8 ± 0.9	0.25 ± 0.04	3.3 ± 0.9	13.3 ± 2.2	86.1 ± 2.5
24 h	4.1 ± 0.4	0.25 ± 0.02	3.6 ± 0.4	14.8 ± 2.4	87.1 ± 1.5

L-Serine and D-serine were given as a single i.p. injection at a dose of 400 mg/kg. L-Serine injected rats were sacrificed 24 after. Total glutathione is expressed as GSH-equivalents (GSH-eq=GSH+2GSSG). Data are mean ± S.E.M. n=4 (3–15 h), and 10 (24 h). * mmol/g tissue; ** p<0.05 vs. control.

change in renal MDA (Fig. 4A) and 4-HNE was undetected by immunostaining (data not shown). Moreover, renal lipid fluorescent products levels decreased significantly from 3 to 24 h (Fig. 4B) and GSH content and GSH-eq diminished transiently on 9 and 12 h (Table 1). In addition, HO-1 expression was undetectable in kidney (Fig. 5). The immunohistochemical studies revealed that the intensity of HO-1 staining was weak (Fig. 6).

4.3. Antioxidant enzymes

Renal activity of total SOD, GPx, and GSH-Rx was similar at all periods of time studied after D-serine administration (data not shown). D-Serine administration decreased CAT activity about 33% at 24 h. Also, we determined the renal protein content of CAT, Mn-SOD, and Cu/Zn-SOD by western blot, but in accord with the

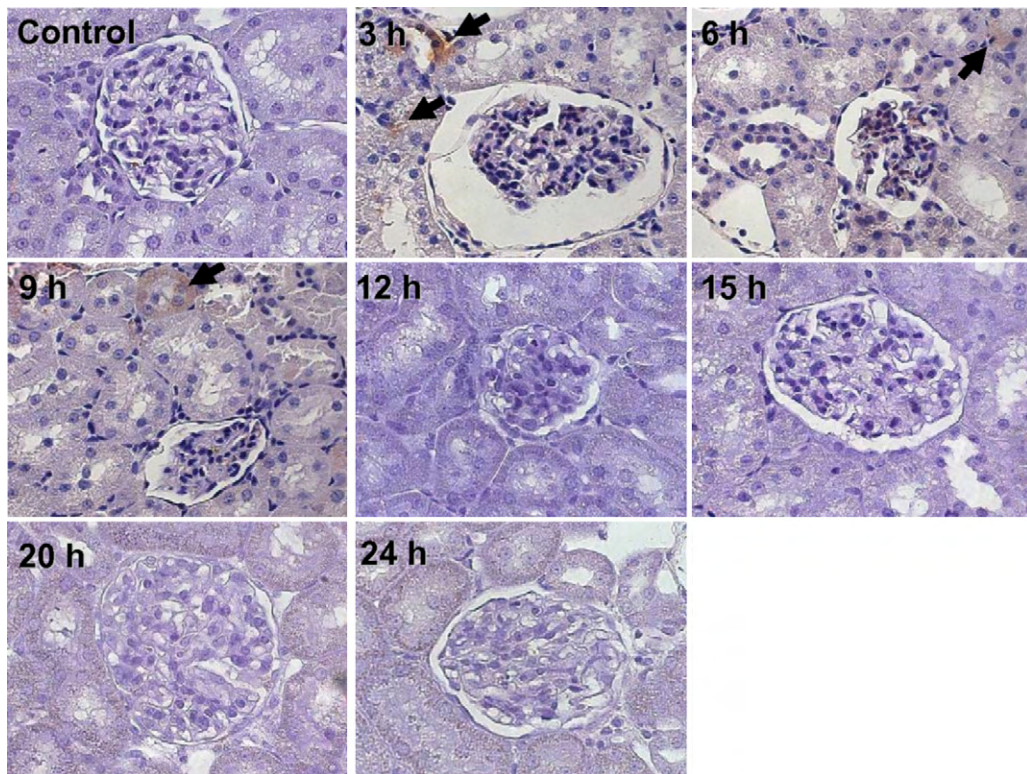


Fig. 6. Effect of a single i.p. injection of D-serine (400 mg/kg) on renal HO-1 expression measured by immunohistochemical analysis at the following time-points 3, 6, 9, 12, 15, 20, and 24 h. Control rats were injected with L-serine (400 mg/kg) and sacrificed 24 h later. A weak HO-1 immunostaining in brown (arrows) was observed on 3, 6 and 9 h, particularly in some distal tubular segments. Later, the immunostaining decreases until being done almost imperceptible but generalized to 12, 15, 20 and 24 h. Pictures are representative ($n \geq 6$ slides), panels represent 400× magnification.

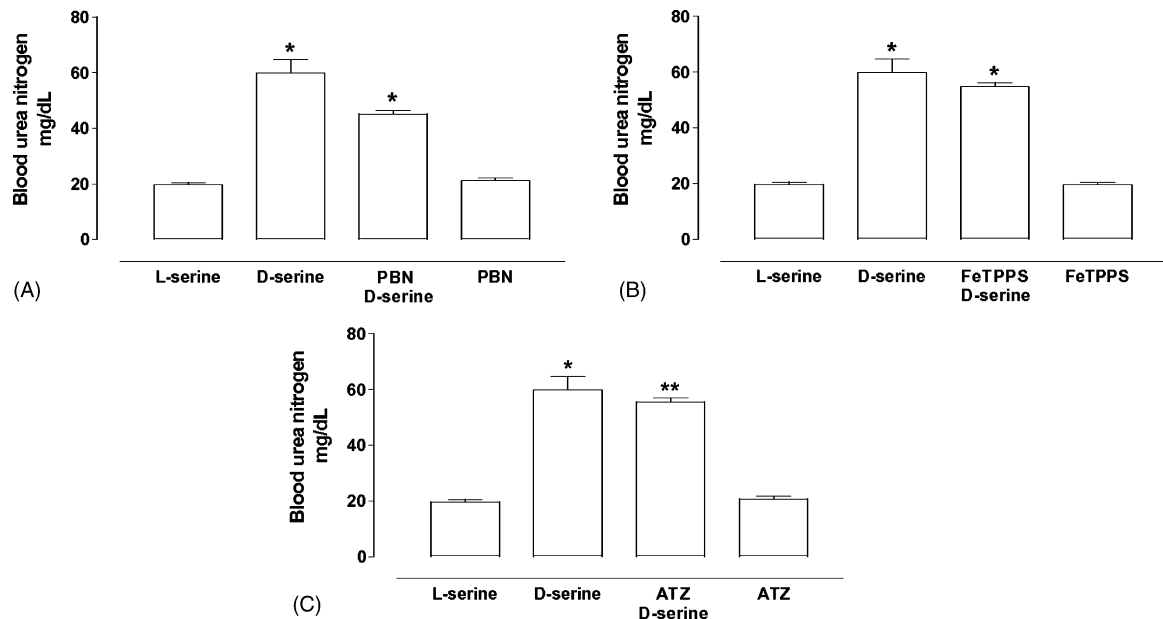


Fig. 7. Effect of (A) PBN (100 mg/kg), (B) FeTPPS (15 mg/kg) or (C) ATZ (1 g/kg) on blood urea nitrogen 24 h after a single i.p. injection of d-serine (400 mg/kg). PBN and FeTPPS were given 30 min before d-serine. ATZ was given 24 h before d-serine. Control rats were injected with the same doses of L-serine, PBN, FeTPPS or ATZ. Data are mean \pm SEM. $n=6$ for each group. * $p<0.001$ and ** $p<0.01$ vs. L-serine.

activity results of these enzymes, d-serine administration did not modify the amount of these proteins (data not shown).

4.4. Effect of PBN, FeTPPS, ATZ, SnCl₂ and SnMP on d-serine nephrotoxicity

Administration of PBN, FeTPPS or ATZ was unable to modify the d-serine induced nephrotoxicity evaluated by the following markers: BUN (Fig. 7), serum creatinine, proteinuria and urinary excretion of NAG (Table 2). In order to determine if the modulation of HO-1 was able to alter d-serine induced nephrotoxicity,

we treated a group of rats with SnCl₂, a potent HO-1 inducer (Kappas and Maines, 1976), and a group of rats with SnCl₂ plus an HO inhibitor (SnMP). The administration of SnCl₂ or SnCl₂ + SnMP did not attenuate the renal damage induced by d-serine (Fig. 8). Urinary NAG excretion (U/24 h) in the groups studied was: L-serine: 0.13 ± 0.03 , d-serine: $2.84 \pm 1.11^*$, d-serine + SnCl₂: $3.86 \pm 0.37^*$, d-serine + SnCl₂ + SnMP: $4.00 \pm 1.14^*$ (* $p<0.05$ versus L-serine). The renal damage was not exacerbated as judged by serum creatinine, creatinine clearance, and urinary excretion of total protein and NAG. Interestingly, BUN was exacerbated in SnCl₂ and SnCl₂ + SnMP groups.

Table 2
Effect of PBN, FeTPPS or ATZ on renal injury markers in rats with d-serine induced nephrotoxicity

	Total protein excretion (mg/24 h)	NAG excretion (U/24 h)	Serum creatinine (mg/dl)
L-Serine ($n=16$)	10.4 ± 1.9	0.08 ± 0.02	0.54 ± 0.06
d-Serine ($n=15$)	$43.1 \pm 6.2^*$	$1.26 \pm 0.48^*$	$2.86 \pm 0.37^*$
d-Serine			
PBN ($n=4$)	$42.9 \pm 7.6^*$	$0.60 \pm 0.10^*$	$2.80 \pm 0.38^*$
FeTPPS ($n=6$)	$60.7 \pm 7.0^*$	$1.06 \pm 0.32^*$	$3.10 \pm 0.04^*$
ATZ ($n=4$)	$51.0 \pm 6.7^*$	$1.15 \pm 0.40^*$	$3.07 \pm 0.10^*$
PBN ($n=5$)	11.1 ± 1.4	0.01 ± 0.00	0.38 ± 0.07
FeTPPS ($n=5$)	6.3 ± 2.1	0.02 ± 0.02	0.27 ± 0.03
ATZ ($n=5$)	6.5 ± 0.9	0.06 ± 0.04	0.28 ± 0.02

Data are mean \pm S.E.M. * $p<0.001$ vs. L-serine. PBN: a-phenyl-*tert*-butyl-nitrone; FeTPPS: 5,10,15,20-tetrakis (4-sulfonatophenyl) porphyrinato iron(III); ATZ: aminotriazole; NAG: *N*-acetyl-p-d-glucosaminidase.

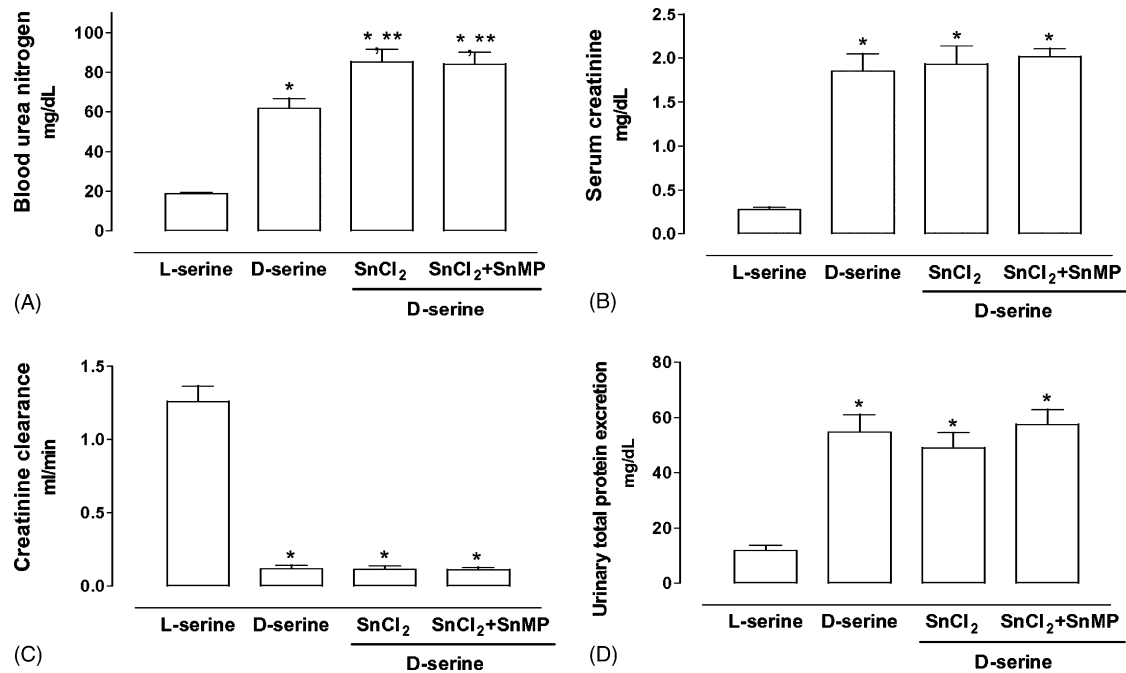


Fig. 8. Effect of SnCl₂ and tin mesoporphyrin (SnMP) on blood urea nitrogen (A), serum creatinine (B), creatinine clearance (C), and proteinuria (D) 24 h after a single i.p. injection of d-serine (400 mg/kg). SnCl₂ (100 mg/kg) and SnMP (15 mg/kg) were given 12 h and 3 h, respectively, before d-serine. L-Serine and d-serine were given at a dose of 400 mg/kg and the rats were sacrificed 24 h later. Data are mean \pm S.E.M. $n=6$ for each group. * $p<0.001$ vs. L-serine and ** $p<0.05$ vs. d-serine.

4.5. HO-1 expression in rats treated with PBN, FeTPPS, ATZ, SnCl₂, and SnMP

HO-1 was not detected in kidneys of rats treated with PBN, FeTPPS, and ATZ with or without d-serine (data not shown). In contrast, the HO-1 induction in the groups of rats treated with SnCl₂ was confirmed by western blot (Fig. 9) and by immunostaining (Fig. 10).

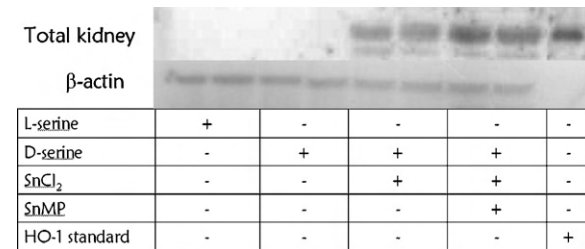


Fig. 9. Effect of SnCl₂ and tin mesoporphyrin (SnMP) on renal HO-1 content measured by western blot in d-serine injected rats. Rats were sacrificed 24 h after a single injection of 400 mg/kg of d-serine or L-serine. SnCl₂ (100 mg/kg) and SnMP (15 mg/kg) were given 12 h and 3 h, respectively, before L-serine. $n=6$ for each group.

4.6. Experiments with a higher dose of d-serine

In an additional group of animals, rats were injected i.p. with 800 mg/kg of d-serine and control rats were injected i.p. with L-serine (800 mg/kg). Both groups of rats were sacrificed 24 h later. Renal damage was made evident by the increase in BUN and serum creatinine and by the decrease in creatinine clearance as well as by the increase in urinary excretion of protein and NAG (Table 3). In spite of this renal damage, MDA and protein carbonyl content levels in kidney remained unchanged compared to L-serine treated rats (Table 3) and renal HO-1 expression was undetectable by western blot suggesting lack of oxidative stress. In good agreement with the previous data, the administration of SnCl₂ was unable to prevent the increase in BUN and serum creatinine or the decrease in creatinine clearance induced by d-serine. In addition, the renal activity of SOD, GPx and GSH-Rx remained unchanged in these animals (data not shown).

5. Discussion

It has been suggested that d-AAO and oxidative stress may be involved in d-serine induced nephrotoxicity (Williams and Lock, 2005; Maekawa et al., 2005;

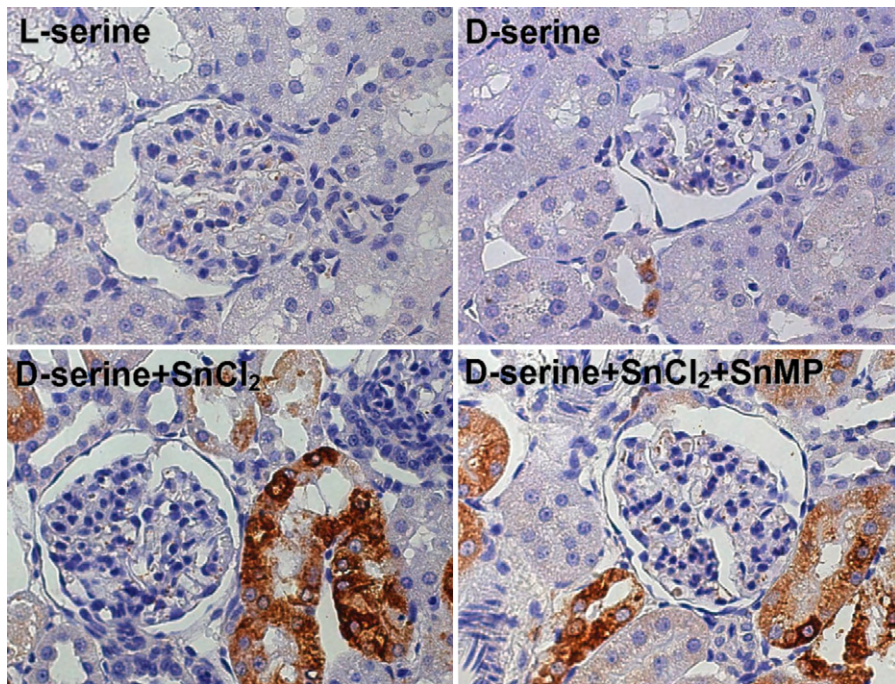


Fig. 10. Effect of SnCl_2 and tin mesoporphyrin (SnMP) on renal HO-1 expression evaluated by immunohistochemical analysis. HO-1 was expressed copiously in the groups injected with SnCl_2 in proximal tubules whereas the immunostaining was weak in the D-serine group. The doses of reagents and time of study are given in the legend to Fig. 8. Pictures are representative ($n \geq 6$ slides), panel represents $400\times$ magnification.

Silbernagl et al., 1997). H_2O_2 is produced during D-serine metabolism by the enzyme D-AAO and this ROS may be a source of the highly reactive hydroxyl radicals. This fact and the protective role of GSH observed in this experimental model (Silbernagl et al., 1997) support the role of oxidative stress in D-serine-induced nephrotoxicity as has been shown in several models of

nephrotoxicity including those produced by $\text{K}_2\text{Cr}_2\text{O}_7$ (Barrera et al., 2003), maleate (Pedraza-Chaverri et al., 2006), and ischemia and reperfusion, cisplatin, gentamicin, lipopolysaccharide, myoglobin, and cyclosporine A (reviewed by Ueda et al., 2001).

Based on the above data, we measured an array of oxidative stress markers in D-serine injected rats including HO-1 expression, because this enzyme has been used as an oxidative stress marker in other models of renal damage including those induced by maleate (Pedraza-Chaverri et al., 2006), cyclosporine A (Galletti et al., 2005), and cisplatin, glycerol, ischemia and reperfusion, HgCl_2 , and in acute inflammatory nephropathies (reviewed by Kanakiriya and Nath, 2001).

The nephrotoxicity induced by D-serine injection was made evident by established markers of renal injury including BUN, serum creatinine, KIM-1 mRNA levels, and urinary excretion of total protein and NAG. Serum creatinine and BUN increased significantly 15 and 20 h after D-serine injection. In addition, renal KIM-1 mRNA levels increased 6 h after D-serine injection confirming that KIM-1 is an early biomarker of nephrotoxicity as has been postulated previously (Vaidya et al., 2006). The increase in the urinary excretion of total protein and NAG at 24 h and the tubular necrosis observed by histological studies confirmed additionally the nephrotoxicity

Table 3
Effect of a higher dose of D-serine (800 mg/kg) on renal injury markers in rats with D-serine induced nephrotoxicity

	L-Serine (800 mg/ml)	D-Serine (800 mg/ml)
Blood urea nitrogen (mg/dl)	20.41 ± 1.71	$68.56 \pm 7.3^*$
Serum creatinine (mg/dl)	0.33 ± 0.05	$2.47 \pm 0.31^*$
Urinary total protein excretion (mg/24 h)	9.63 ± 4.43	$49.7 \pm 15.35^*$
Urinary NAG excretion (U/24 h)	0.082 ± 0.04	$1.59 \pm 0.8^*$
Creatinine clearance (ml/min)	0.74 ± 0.19	$0.08 \pm 0.01^*$
Renal MDA content (nmol/mg protein)	1.17 ± 0.26	1.01 ± 0.32
Renal protein carbonyl content (nmol DNPH/mg protein)	3.15 ± 0.6	3.32 ± 0.51

Data are mean \pm S.E.M. * $p < 0.001$ vs. L-serine. $n = 6$ for each group.
* $p < 0.001$ vs. L-serine.

induced by D-serine in our experimental conditions. In spite of this renal damage we were unable to observe an increase in the oxidative stress markers in the kidney of rats treated with D-serine. ROS formation and MDA, and protein carbonyl levels were not altered significantly and 4-HNE was undetected by immunostaining in this experimental model. The lack of 4-HNE immunostaining at the kidney cortex, the renal site of D-serine induced toxicity, is consistent with the MDA data obtained in the whole kidney. Furthermore, fluorescent products of lipid peroxidation decreased after D-serine injection; at present, it is unclear why this marker decreased in D-serine injected rats. We are tempting to speculate that D-serine may be interfering with this determination. It was found a decrease in the content of GSH and GSH-eq, but this was a transient effect observed only on 9 and 12 h. Taken into account the lack of evidence of oxidative stress with the majority of the markers measured we can not reach the conclusion that oxidative stress is involved in D-serine induced nephrotoxicity. Additional studies are required to study GSH metabolism in this experimental model.

Interestingly, it has been observed that the renal lesions induced by D-serine are unusual. Ganote et al. (1974) observed that mitochondria from kidneys of D-serine treated animals retain their pycnotic configuration long after the cell is necrotic, rather than swelling and accumulating calcium, or developing amorphous densities in the matrix as occurs in most other forms of cellular injury. They also found that the condensed mitochondria do not show dilation of the intracristal spaces. The above observations suggest that the effect of D-serine on mitochondria is different from other renal toxins which may be involved, at least in part, in the lack of oxidative damage observed in our experimental model. In addition, it is possible that the α-ketoacid produced by the action of the enzyme D-AAO on D-serine (hydroxypyruvate) (Williams et al., 2005) may have H₂O₂ scavenging activity which prevents that oxidative stress be evident. Hydroxypyruvate is structurally related to pyruvate which is a known H₂O₂ scavenger (Salahudeen et al., 1991). However, more studies are required to address more precisely this point.

Western blot analysis performed with samples obtained from the whole kidney revealed that HO-1 expression was not induced; the immunohistochemical studies were consistent since revealed only a very weak and/or localized HO-1 immunostaining. This protein has been considered as a marker of oxidative stress in several experimental models (Zarkovic, 2003; Calabrese et al., 2005; Miwa et al., 2004; Schipper et al., 1998; Browne et al., 1999). In a previous study (Barrera et

al., 2003) we found only a discrete increase in HO-1 expression in association with oxidative stress in rats with K₂Cr₂O₇-induced nephrotoxicity. The lack of functional role of HO-1 protein in D-serine treated rats was obtained by the pharmacological manipulation of HO-1 expression and HO activity. Western blot and immunohistochemical analyses revealed that HO-1 was copiously expressed by the pretreatment with SnCl₂. Neither HO-1 induction nor HO inhibition was able to modify D-serine induced nephrotoxicity. The manipulation of HO-1 expression/activity has a profound effect on the development of damage induced by oxidative stress (Barrera et al., 2003; Kanakiriya and Nath, 2001; Nath, 2006; Pedraza-Chaverri et al., 2006). These data strongly argue against a role of oxidative damage in D-serine induced nephrotoxicity.

It was observed that pretreatment with SnCl₂ increased significantly BUN values in D-serine + SnCl₂ and D-serine + SnCl₂ + SnMP groups compared to L-serine treated groups suggesting an exacerbation of renal dysfunction. However, we were unable to see this exacerbation with the other markers of renal injury (serum creatinine, creatinine clearance, and urinary excretion of total protein and NAG). Taking all the renal function data as a whole, we could conclude that SnCl₂ does not exacerbate the renal dysfunction observed in D-serine-treated animals. The effect observed on BUN could probably be related to a direct effect of SnCl₂ on nitrogen metabolism but not to changes in HO-1 expression (the exacerbation was also observed in the D-serine + SnCl₂ + SnMP group).

It is known that SnCl₂ injection decreases CYP450 content which is secondary to the increase in HO activity (da Silva et al., 2001). Taking into account that SnCl₂ injection was without effect on D-serine induced nephrotoxicity; our data may suggest that CYP450 is not involved in D-serine induced nephrotoxicity.

We also used an array of compounds with antioxidant or prooxidant properties. It has been shown that PBN (Pedraza-Chaverri et al., 1992) and FeTPPs (Chirino et al., 2004) are able to reduce the damage associated with oxidative/nitrosative stress in renal ischemia and reperfusion and cisplatin nephrotoxicity, respectively. In contrast, it has been shown that the administration of ATZ enhances the renal oxidative damage induced by puromycin aminonucleoside (Pedraza-Chaverri et al., 1999). These compounds were unable to protect or enhance the renal damage in our experimental model, which strongly suggests that oxidative stress is not involved in the development of this damage. We also found that the activity of several antioxidant enzymes including CAT, SOD, GPx, and GSH-Rx and the renal

content of CAT, Mn-SOD, and Cu/Zn-SOD remained unchanged in D-serine treated rats. This suggests that there is no deficiency in the renal antioxidant enzymes, which is consistent with the majority of oxidative stress markers obtained in the present work.

In conclusion, the results in this work taken as a whole suggest that oxidative stress is not involved in D-serine-induced nephrotoxicity, at least in our experimental conditions. To further explore the mechanisms by which D-serine induces nephrotoxicity, the potential role of cytokines and chemokines, altered eicosanoid metabolism, and the disbalance between vasoconstrictor (e.g. endothelin-1, thromboxane A₂, platelet activating factor) and vasodilator (e.g. prostacyclin) factors deserve to be considered.

Acknowledgements

This work was supported by DGAPA (Grant Nos. IN227103 and IX203504). Axiovert 200M confocal microscope was donated by Fundacion Gonzalo Rio Arronte IAP México.

References

- Aebi, H., 1984. Catalase in vitro. *Meth. Enzymol.* 105, 121–126.
- Akagi, R., Takahashi, T., Sassa, S., 2005. Cytoprotective effects of heme oxygenase in acute renal failure. *Contrib. Nephrol.* 148, 70–85.
- Ali, S.F., LeBel, C.P., Bondy, S.C., 1992. Reactive oxygen species formation as a biomarker of methylmercury and trimethyltin neurotoxicity. *Neurotoxicology* 13, 637–648.
- Barrera, D., Maldonado, P.D., Medina-Campos, O.N., Hernandez-Pando, R., Ibarra-Rubio, M.E., Pedraza-Chaverri, J., 2003. HO-1 induction attenuates renal damage and oxidative stress induced by K₂Cr₂O₇. *Free Radic. Biol. Med.* 34, 1390–1398.
- Browne, S., Ferrante, R., Beal, M., 1999. Oxidative stress in Huntington's disease. *Brain Pathol.* 9, 147–163.
- Calabrese, V., Lodi, R., Tonon, C., D'Agata, V., Sapienza, M., Scapagnini, G., Mangiameli, A., Pennisi, G., Stella, A.M., Butterfield, D.A., 2005. Oxidative stress, mitochondrial dysfunction and cellular stress response in Friedreich's ataxia. *J. Neurol. Sci.* 233, 145–162.
- Carlberg, I., Mannervik, B., 1975. Purification and characterization of the flavoenzyme glutathione reductase from rat liver. *J. Biol. Chem.* 250, 5475–5480.
- Carone, F.A., Ganote, C.E., 1975. D-Serine nephrotoxicity. *Arch. Pathol.* 99, 658–662.
- Carone, F.A., Nakamura, S., Oldman, B., 1985. Urinary loss of glucose, phosphate and protein by diffusion into proximal straight tubules injured by D-serine and maleic acid. *Lab. Invest.* 52, 605–610.
- Chirino, Y.I., Hernandez-Pando, R., Pedraza-Chaverri, J., 2004. Peroxynitrite decomposition catalyst ameliorates renal damage and protein nitration in cisplatin-induced nephrotoxicity in rats. *BMC Pharmacol.* 4, 20.
- da Silva, J.L., Zand, B.A., Yang, L.M., Sabaawy, H.E., Lianos, E., Abraham, N.G., 2001. Heme oxygenase isoform-specific expression and distribution in the rat kidney. *Kidney Int.* 59, 1448–1457.
- Ganote, C.E., Peterson, D.R., Carone, F.A., 1974. The nature of D-serine-induced nephrotoxicity. *Am. J. Pathol.* 77, 269–282.
- Gerard-Monnier, D., Erdelmeier, I., Regnard, K., Moze-Henry, N., Yadan, J.C., Acudiere, J., 1998. Reactions of 1-methyl-2-phenylindole with malondialdehyde and 4-hydroxyalkenals. Analytical applications to a colorimetric assay of lipid peroxidation. *Chem. Res. Toxicol.* 11, 1176–1183.
- Galletti, P., Di Gennaro, C.I., Migliardi, V., Indaco, S., Della Ragione, F., Manna, C., Chioldini, P., Capasso, G., Zappia, V., 2005. Diverse effects of natural antioxidants on cyclosporin cytotoxicity in rat renal tubular cells. *Nephrol. Dial. Transplant.* 20, 1551–1558.
- Griffith, O.W., 1980. Determination of glutathione and glutathione disulfide using glutathione reductase and 2-vinylpyridine. *Anal. Biochem.* 106, 207–212.
- Heresco-Levy, U., Javitt, D.C., Ebstein, R., Vass, A., Lichtenberg, P., Bar, G., Catinari, S., Ermilov, M., 2005. D-Serine efficacy as add-on pharmacotherapy to risperidone and olanzapine for treatment-refractory schizophrenia. *Biol. Psychiatry* 57, 577–585.
- Hermes-Lima, M., Storey, K.B., 1996. Relationship between anoxia exposure and antioxidant status in the frog *Rana pipiens*. *Am. J. Physiol.* 271, R918–R925.
- Kanakiriya, S., Nath, K.A., 2001. Heme oxygenase and acute renal injury. In: Molitoris, B.A., Finn, W.F. (Eds.), *Acute Renal Failure*. W.B. Saunders Co., Philadelphia, pp. 78–88.
- Kappas, A., Maines, M.D., 1976. Tin: a potent inducer of heme oxygenase in kidney. *Science* 192, 60–62.
- Lawrence, R.A., Burk, R.F., 1976. Glutathione peroxidase activity in selenium-deficient rat liver. *Biochem. Biophys. Res. Commun.* 71, 952–958.
- Livak, K.J., Schmittgen, T.D., 2001. Analysis of relative gene expression data using real-time quantitative PCR and the 2-(Delta Delta C(T)) method. *Methods* 25, 402–408.
- Lowry, O.H., Rosebrough, N.J., Farr, A.L., Randall, R.J., 1951. Protein measurement with the Folin-phenol reagent. *J. Biol. Chem.* 193, 265–275.
- Maekawa, M., Okamura, T., Kasai, N., Hori, Y., Summer, K.H., Konno, R., 2005. D-Amino-acid oxidase is involved in D-serine-induced nephrotoxicity. *Chem. Res. Toxicol.* 18, 1678–1682.
- Miya, H., Kubo, T., Morita, S., Nakanishi, I., Kondo, T., 2004. Oxidative stress and microglial activation in substantia nigra following striatal MPP+. *Neuroreport* 15, 1039–1044.
- Mothet, J.P., Parent, A.T., Wolosker, H., Brady Jr., R.O., Linden, D.J., Ferris, C.D., Rogawski, M.A., Snyder, S.H., 2000. D-Serine is an endogenous ligand for the glycine site of the N-methyl-D-aspartate receptor. *Proc. Natl. Acad. Sci. U.S.A.* 97, 4926–4931.
- Nagata, Y., 1992. Involvement of D-amino acid oxidase in elimination of D-Serine in mouse brain. *Experientia* 48, 753–755.
- Nath, K.A., 2006. Heme oxygenase-1: a provenance for cytoprotective pathways in the kidney and other tissues. *Kidney Int.* 70, 432–443.
- Oberley, L.W., Spitz, D.R., 1984. Assay of superoxide dismutase activity in tumor tissue. *Meth. Enzymol.* 105, 457–464.
- Pedraza-Chaverri, J., Granados-Silvestre, M.D., Medina-Campos, O.N., Hernandez-Pando, R., 1999. Effect of the in vivo catalase inhibition on aminonucleoside nephrosis. *Free Radic. Biol. Med.* 27, 245–253.
- Pedraza-Chaverri, J., Murali, N.S., Croatt, A.J., Alam, J., Grande, J.P., Nath, K.A., 2006. Proteinuria as a determinant of renal expression of heme oxygenase-1: studies in models of glomerular and tubular proteinuria in the rat. *Am. J. Physiol. Renal Physiol.* 290, F196–F204.

- Pedraza-Chaverri, J., Tapia, E., Bobadilla, N., 1992. Ischemia-reperfusion induced acute renal failure in the rat is ameliorated by the spin-trapping agent alpha-phenyl-*N-tert*-butyl nitron (PBN). *Renal Fail.* 14, 467–471.
- Perez-Rojas, J., Blanco, J.A., Cruz, C., Trujillo, J., Vaidya, V.S., Uribe, N., Bonventre, J.V., Gamba, G., Bobadilla, N.A., in press. Mineralocorticoid receptor blockade confers renoprotection in preexisting chronic cyclosporine nephrotoxicity. *Am. J. Physiol. Renal Physiol.*
- Pérez-Severiano, F., Rodríguez-Pérez, M., Pedraza-Chaverri, J., Maldonado, P.D., Medina-Campos, O.N., Ortiz-Plata, A., Sánchez-García, A., Villeda-Hernández, J., Galván-Arzate, S., Aguilera, P., Santamaría, A., 2004. S-Allylcysteine, a garlic-derived antioxidant, ameliorates quinolinic acid-induced neurotoxicity and oxidative damage in rats. *Neurochem. Int.* 45, 1175–1183.
- Pilone, M.S., 2000. D-Amino acid oxidase: new findings. *Cell Mol. Life Sci.* 57, 1732–1747.
- Sánchez-González, D.J., Moro, M.A., Castillo-Henkel, C., Herrera-González, N., Hernández-Pando, R., Larios-Medina, F.J., Cobilt, R., Blanco, J.A., Pedraza-Chaverri, J., Villanueva, C., 2004. Ozone exposure induces iNOS expression and tyrosine nitration in rat aorta. *Environ. Toxicol. Pharmacol.* 17, 1–7.
- Salahudeen, A.K., Clark, E.C., Nath, K.A., 1991. Hydrogen peroxide-induced renal injury. A protective role for pyruvate in vitro and in vivo. *J. Clin. Invest.* 88, 1886–1893.
- Sambrook, J., Fritsch, E.F., Maniatis, T., 1989. Molecular Cloning a Laboratory Manual. Cold Spring Harbor Laboratory Press, New York.
- Santamaría, A., Salvatierra-Sánchez, R., Vázquez-Román, B., Santiago-López, D., Villeda-Hernández, J., Galván-Arzate, S., Jiménez-Capdeville, M.E., Ali, S.F., 2003. Protective effects of the antioxidant selenium on quinolinic acid-induced neurotoxicity in rats: in vitro and in vivo studies. *J. Neurochem.* 86, 479–488.
- Schipper, H.M., Liberman, A., Stopa, E.G., 1998. Neural heme oxygenase-1 expression in idiopathic Parkinson's disease. *Exp. Neurol.* 150, 60–68.
- Silbernagl, S., O'Donovan, D.J., Völker, K., 1997. D-Serine nephrotoxicity is mediated by oxidative damage. *Pflügers Arch.* 433, R37 (Abstract).
- Silbernagl, S., Volker, K., Dantzler, W.H., 1999. D-Serine is reabsorbed in rat renal pars recta. *Am. J. Physiol.* 276, F857–F863.
- Tsai, G., Yang, P., Chung, L., Lange, N., Coyle, J., 1998. D-Serine added to antipsychotics for the treatment of schizophrenia. *Biol. Psychiatry* 44, 1081–1089.
- Tuominen, H., Tiihonen, J., Wahlbeck, K., 2006. Glutamatergic drugs for schizophrenia. *Cochrane Database Syst. Rev.* 2, CD003730.
- Ueda, N., Mayeux, P.R., Baliga, R., Shah, S.V., 2001. Oxidant mechanisms in acute renal failure. In: Molitoris, B.A., Finn, W.F. (Eds.), *Acute Renal Failure*. W.B. Saunders Co., Philadelphia, pp. 60–77.
- Vaidya, V.S., Ramirez, V., Ichimura, T., Bobadilla, N.A., Bonventre, J.V., 2006. Urinary kidney injury molecule-1: a sensitive quantitative biomarker for early detection of kidney tubular injury. *Am. J. Physiol. Renal Physiol.* 290, F517–F529.
- Wang, W.P., Guo, X., Koo, M.W., Wong, B.C., Lam, S.K., Ye, Y.N., Cho, C.H., 2001. Protective role of heme oxygenase-1 on trinitrobenzene sulfonic acid-induced colitis in rats. *Am. J. Physiol. Gastrointest. Liver Physiol.* 281, G586–G594.
- Williams, R.E., Lock, E.A., 2004. D-Serine-induced nephrotoxicity: possible interaction with tyrosine metabolism. *Toxicology* 201, 231–238.
- Williams, R.E., Lock, E.A., 2005. Sodium benzoate attenuates D-serine induced nephrotoxicity in the rat. *Toxicology* 207, 35–48.
- Williams, R.E., Major, H., Lock, E.A., Lenz, E.M., Wilson, I.D., 2005. D-Serine-induced nephrotoxicity: a HPLC-TOF/MS-based metabolomics approach. *Toxicology* 207, 179–190.
- Woo, J., Treuting, J.J., Cannon, D.C., 1979. Metabolic intermediates and inorganic ions. In: Henry, J.B. (Ed.), *Clinical Diagnosis and Management by Laboratory Methods*. Saunders Company.
- Zarkovic, K., 2003. 4-hydroxynonenal and neurodegenerative diseases. *Mol. Aspects Med.* 24, 293–303.



RenaStick: A Rapid Urine Test for Early Detection of Kidney Injury.

Journal:	<i>Journal of the American Society of Nephrology</i>
Manuscript ID:	JASN-2008-12-1300
Manuscript Type:	Original Article - Basic Research
Date Submitted by the Author:	24-Dec-2008
Complete List of Authors:	Vaidya, Vishal; Harvard Medical School, Renal Division Ford, Glen; BioAssay Works, L.L.C Waikar, Sushrut; Brigham and Women's Hospital, Renal Division Wang, Yizhuo; Brigham and Women's Hospital, Renal Division Clement, Matthew; Brigham and Women's Hospital, Renal Division Ramirez, Victoria; Instituto de Investigaciones Biomédicas and Instituto Nacional de Ciencias Médicas y Nutrición Salvador Zubirández México, Molecular Physiology Unit Glaab, Warren; Merck Research Laboratories, Safety Assessment Troth, Sean; Merck Research Laboratories, Safety Assessment Sistare, Frank; Merck Research Laboratories, Safety Assessment Prozialeck, Walter; Midwestern University, Department of Pharmacology Edwards, Joshua; Midwestern University, Department of Pharmacology Bobadilla, Norma A; Instituto de Investigaciones Biomédicas and Instituto Nacional de Ciencias Médicas y Nutrición Salvador Zubirán, Molecular Physiology Unit Mefferd, Stephen; BioAssay Works, L.L.C Bonventre, Joseph; Brigham and Womens Hospital, Renal Division; Brigham and Women's Hospital, Renal Division
Keywords:	acute renal failure, drug nephrotoxicity, kidney



1
2 **RenaStick: A Rapid Urine Test for Early Detection of Kidney Injury.**
3

4 Vishal S. Vaidya^{1¶}, Glen Ford², Sushrut S. Waikar¹, Yizhuo Wang¹, Matthew Clement¹, Victoria
5
6 Ramirez³, Warren E. Glaab⁴, Sean P. Troth⁴, Frank D. Sistare⁴, Walter C. Prozialeck⁵, Joshua
7
8 R. Edwards⁵, Norma A. Bobadilla³, Stephen Mefferd², and Joseph V. Bonventre¹.
9
10

11
12
13
14 ¹Renal Division, Department of Medicine, Brigham and Women's Hospital, Harvard Medical
15 School, Boston, MA 02115; ²BioAssay Works, L.L.C., Ijamsville, MD 21754; ³Molecular
16 Physiology Unit, Instituto de Investigaciones Biomédicas, Universidad Nacional Autónoma de
17 México and Instituto Nacional de Ciencias Médicas y Nutrición Salvador Zubirán, Mexico City,
18 Mexico; ⁴Merck Research Laboratories, Safety Assessment, West Point, PA, 19486;
19
20
21
22
23
24
25
26 ⁵Department of Pharmacology, Midwestern University, Downers Grove, IL, 60515.
27
28
29
30
31
32
33
34
35
36
37
38
39

40 **Running Title:** RenaStick to Detect Kidney Injury
41
42

43 **Abstract: 193 words**
44
45

46 **Text: 1492 words**
47
48
49
50
51
52
53
54
55
56
57
58
59
60

40 **¶Correspondence may be addressed to:**
41
42

43 *Vishal S. Vaidya, PhD*, Brigham and Women's Hospital, Harvard Medical School, Harvard
44 Institutes of Medicine, Renal Division, Rm 550, 4 Blackfan circle, Boston, MA 02115. Tel: 617-
45 525-5974. Fax: 617-525-5965. E-Mail: vvaidya@partners.org
46
47
48
49
50
51
52
53
54
55
56
57
58
59
60

ABSTRACT

Kidney injury molecule-1 (Kim-1) is the first marker of kidney injury deemed qualified by the FDA and EMEA to monitor drug-induced kidney injury in preclinical studies and on a case-by-case basis in clinical trials. We report development and evaluation of a rapid direct lateral flow immunochromatographic assay that detects urinary Kim-1 within 15 minutes. The intensity of the Kim-1 band in rat RenaStick correlated very well with the levels of Kim-1 as measured by microbead-based assay ($r^2 = 0.91$; $p<0.0001$), histopathological damage and renal Kim-1 immunostaining in dose and time dependent manner following kidney injury induced by Cadmium, Gentamicin or 20 min bilateral renal ischemia/reperfusion. In humans, median urinary KIM-1 band intensity was significantly higher in patients with acute kidney injury (AKI) than in healthy volunteers ($p<0.05$). RenaStick also enabled temporal evaluation of kidney injury and recovery in patients who developed postoperative AKI following a cytoreductive surgery with intraoperative local cisplatin administration for malignant mesothelioma. In summary, RenaStick allows sensitive detection of Kim-1 thereby serving as a convenient, quick and clear 'yes or no' diagnostic assay for kidney damage to facilitate rapid and early detection of kidney injury in preclinical and clinical studies.

1 It is estimated that by 2015, more than 700,000 individuals in the United States will have end
2 stage renal disease (ESRD) and more than 107,000 ESRD related deaths will occur annually(4).
3
4 Acute Kidney injury (AKI) is an important risk factor for progression to ESRD(11) and therefore
5 early detection of AKI prior to significant loss of kidney function would permit more timely
6 diagnosis of AKI, prediction of injury severity, and safety assessment during drug development.
7
8 Current metrics such as serum creatinine (SCr) and blood urea nitrogen (BUN) lack the
9 sensitivity and/or specificity to adequately detect kidney damage(3, 11, 12). Recently, the
10 Critical Path Institute's Preventive Safety Testing Consortium (PSTC) identified kidney injury
11 molecule-1 (Kim-1 or KIM-1 in humans) as an early diagnostic biomarker for monitoring acute
12 kidney tubular toxicity in preclinical studies and the FDA and EMEA encouraged its use for
13 safety monitoring on a case-by-case basis in clinical trials
14 (<http://www.fda.gov/bbs/topics/NEWS/2008/NEW01850.html>). In a multi-site preclinical rat
15 toxicology study involving 17 studies, we showed that urinary Kim-1 not only outperformed the
16 conventional markers such as BUN, serum creatinine (SCr) and urinary NAG for assessing
17 renal injury, but did so achieving an ROC-AUC of 0.91 to 0.99, the highest performing biomarker
18 of all those we have examined to date(13). Urinary Kim-1 has been shown to be a sensitive and
19 early diagnostic indicator of renal injury in a variety of acute and chronic kidney injury models (8,
20 14, 18, 6, 9, 16). Human studies have confirmed the promise of KIM-1 for the diagnosis and
21 prediction of outcome of AKI(5, 7, 15, 17).
22

23 Urinary Kim-1 measurements have been performed using microsphere-based Luminex
24 xMAP technology(13, 15) that requires 3-4 hours of assay time and is dependent on a large
25 analyzer(2). The objective of this study was to develop and evaluate a greater ease-of-use
26 direct lateral flow immunochromatographic assay (LFIA) that has visual read out and is
27
28
29
30
31
32
33
34
35
36
37
38
39
40
41
42
43
44
45
46
47
48
49
50
51
52
53
54
55
56
57
58
59
60

1 sensitive, specific and high throughput thereby allowing rapid (within minutes) point of care
2 detection of urinary Kim-1 in rats and humans.
3
4
5
6
7
8

9 *Development and evaluation of rat and human RenaStick.*

10
11 Colloidal gold nanoparticles were coated with previously tested mouse monoclonal anti-Kim-
12 1 antibody against rat Kim-1 ectodomain or rabbit polyclonal antibody against human KIM-1 (13-
13 15). When the sample containing Kim-1 is added to the sample well, the colloidal sphere
14 complex bound to Kim-1 rapidly migrates by capillary action through a nitrocellulose membrane
15 to a test-line that is coated with another epitopically distinct antibody against Kim-1. The
16 presence of detectable levels of the Kim-1 in the test sample results in the formation of a dark
17 red test-line within minutes as the gold spheres containing Kim-1 are deposited on the test line
18 (Supplementary Fig. 1a). The assay range was found to be linear from 1 ng/ml to 20 ng/ml (n=4)
19 (Supplementary Figures 1b-c and 2a-b). The lower limit of detection was 0.5 ng/ml for rat
20 RenaStick and 0.8 ng/ml for human RenaStick (n=4). The analytical recovery for rat and human
21 Kim-1 was within the acceptable range from 78 % to 108 % for 5 ng/ml (Supplementary Figures
22 1 d and 2c) and 75 % to 106 % for 1 ng/ml (data not shown).

23
24
25
26
27
28
29
30
31
32
33
34
35
36
37
38
39
40
41
42 *Evaluation of rat RenaStick in preclinical models of kidney injury.*

43
44 We evaluated whether Cadmium (Cd) induced nephrotoxicity can be sensitively detected by
45 RenaStick. Cadmium is a widely disseminated industrial and environmental pollutant with the
46 kidney as the primary target of toxicity following chronic low levels of exposure(9). In control rats
47 urine Kim-1 levels were undetectable (Fig. 1a), consistent with the results of the microbead
48 based assay (Supplementary Table 1), and consistent with the absence of histological damage
49 (Fig. 1f) and lack of kidney Kim-1 protein expression (Fig. 1j). Kim-1 was detected after 0.6
50
51
52
53
54
55
56
57
58
59
60

1 mg/kg (Fig. 1b) of Cd administration for 5 days/week for 4 weeks with a further increase seen
2 following 1.2 mg/kg (Fig. 1 c & e) and following 2.4 mg Cd/kg (Fig. 1 d & e). The intensity of the
3 Kim-1 band correlated very well with the levels of Kim-1 as measured by microbead-based
4 assay (Supplementary Table 1a), histopathological damage (Fig. 1 g-i) and renal Kim-1
5 immunostaining (Fig. 1 k-m). Even the individual variability among the four rats in the same
6 group was clearly distinguished by the RenaStick band intensities and correlated with the
7 microbead assay, demonstrating the sensitivity of the RenaStick.
8
9

10 Gentamicin is an important antibiotic with nephrotoxic side effects in humans(1). Gentamicin
11 administration for 9 days resulted in a distinct dose dependent increase in the rat urinary Kim-1
12 band intensity paralleling the Kim-1 values measured using the microbead-based method (Fig. 2
13 a-c, Supplementary Table 1b). The conventional markers of kidney injury, BUN and SCr, were
14 elevated significantly only following the 120 mg/kg/day dose (Fig. 2 e & f) when significant
15 tubular degeneration and necrosis was observed histologically (Fig. 2i). Mild histological
16 damage, as defined by single cell necrosis, dilation of tubules and basophilia was evident in the
17 40 mg/kg/day group (Fig. 2h). This milder injury was sensitively detected by the RenaStick
18 assay for urinary Kim-1 (Fig. 2 b & d, Supplementary Table 1b).
19
20

21 Ischemia/reperfusion (I/R) results in acute kidney injury showed that 9 hours after 20 min of
22 bilateral I/R (Fig. 3 c & i, Supplementary Table 1c) there was ~ 4-fold increase in Kim-1 by the
23 RenaStick assay as compared to sham. Kim-1 levels peaked at 24 h (Fig. 3 e & i) and returned
24 to levels persistently above baseline at 96 and 120 h after reperfusion (Fig. 3 g & h,
25 supplementary Table 1c). This time course correlated with histological changes of the kidney
26 marked by single cell necrosis and sloughing of cells in tubules at 9 h (Fig. 3k) followed by
27 proximal tubular necrosis with associated inflammation and cast formation at 18 and 24 h (Fig.
28 3l) and subsequently regeneration and restoration of damaged epithelium at 120 h (Fig. 3m).
29
30
31
32
33
34
35
36
37
38
39
40
41
42
43
44
45
46
47
48
49
50
51
52
53
54
55
56
57
58
59
60

1 The amount of Kim-1 urinary excretion detected by RenaStick correlated well with Kim-1 protein
2 expression in the kidney (Fig. 3 o-q).
3
4
5
6
7
8

9 *Evaluation of human RenaStick in patients with or without various forms of acute kidney injury*
10 (*AKI*).
11
12

13 We tested the ability of RenaStick to identify human KIM-1 in samples from patients with
14 and without AKI. Supplementary Table 2 shows the results of KIM-1 quantification using a
15 microbead based assay, and Figures 4a-c show the corresponding results using RenaStick.
16 Median urinary KIM-1 band intensity was significantly higher in AKI patients than in healthy
17 volunteers ($p<0.05$). The quantification between RenaStick and the microbead-based assay was
18 comparable, with a Pearson correlation coefficient of 0.88 ($p < 0.0001$) (data not shown).
19 Supplementary Table 3 and Figure 4 d-f show how Renastick performs on serially collected
20 urine from two patients who developed postoperative AKI following a cytoreductive surgery with
21 intraoperative local cisplatin administration for malignant mesothelioma. In each patient,
22 preoperative and 6h samples were negative according to RenaStick, and also measured below
23 800 pg/ml on the microbead based assay. At 24h, peak KIM-1 levels were identified by both
24 techniques, with decreasing values at subsequent time points.
25
26
27
28
29
30
31
32
33
34
35
36
37
38
39
40
41
42
43

44 The opportunity to use the same marker for both the preclinical and clinical setting facilitates
45 clinical monitoring of toxicity that has been demonstrated at higher doses in preclinical
46 development or in a single test species and human relevance is suspect. Rat RenaStick
47 sensitively detects 2-3 fold increases in urinary Kim-1, which have been shown to exceed the
48 threshold defining early and mild reversible kidney tubular injury by histopathology(13). Human
49 RenaStick sensitively detects KIM-1 levels exceeding 800 pg/ml, which we showed to be an
50
51
52
53
54
55
56
57
58
59
60

optimal cutoff (75% sensitivity, 89% specificity) in a cross sectional study of patients with and without AKI(15). Levels measured by a microbead based assay were found to be comparable to levels using rat RenaStick ($r^2=0.91$) and human renaStick ($r^2=0.88$) ($p < 0.0001$), suggesting that RenaStick can replace the more cumbersome and time intensive ELISA based systems for quantification of KIM-1. Our results from two patients undergoing surgery demonstrate the clinical applicability of RenaStick: levels of KIM-1 were undetectable before and 6h surgery, and became detectable (> 800 pg/ml) at 24h when they peaked and declined thereafter. Since urinary KIM-1 levels are undetectable in rats or humans without any proximal tubular damage the RenaStick serves as a convenient, quick and clear 'yes or no' diagnostic assay for kidney damage.

One limitation of RenaStick is the quantification of absolute values of KIM-1. Because of the kidney's ability to dilute and concentrate the urine, levels of biomarkers are often expressed as a ratio to the urinary concentration of creatinine, which accounts for variations in urinary flow rate. Creatinine dipsticks are available, and could be used alongside KIM-1 to aid interpretation.

In summary, we report the development of first point of care diagnostic dipstick assay for the first kidney toxicity biomarker qualified by the FDA and EMEA. A point of care device for detection of Kim-1 in urine should facilitate predictive safety assessment in preclinical studies and evolution of clinical trial safety monitoring with respect to kidney injury(10) and aid in development of effective preventative strategies.

CONCISE METHODS**Animals.**

All animals were maintained in respective central animal facility over wood chips free of any known chemical contaminants under conditions of $21 \pm 1^{\circ}\text{C}$ and 50-80% relative humidity at all times in an alternating 12 h light-dark cycle. Rats were fed with commercial rodent chow (Teklad rodent diet # 7012), given water *ad lib*, and were acclimated for 1-week prior to use. All animal maintenance and treatment protocols were in compliance with the Guide for Care and Use of Laboratory animals as adopted and promulgated by the National Institutes of Health and were approved by respective Institutional Animal Care and Use Committees (IACUC).

Experimental design for rat RenaStick evaluation.

Cadmium-induced kidney toxicity model: Male Sprague Dawley rats ($n=4/\text{group}$) weighing 275-300 g were maintained in individual plastic cages received varying doses of CdCl_2 (Cd dose of 0.6, 1.2, or 2.4 mg/kg/5 days per week for 4 weeks) subcutaneously as previously reported(9). Control group animals ($n=4$) received daily injections of the saline vehicle alone.

Gentamicin-induced kidney toxicity study: Male Sprague Dawley rats (265-316 g) received a daily intraperitoneal (ip) injection of either vehicle (0.9% sodium chloride) or 40 or 120 mg/kg/day gentamicin sulfate ($n=5$ rats/dose group) for 9 days and were necropsied on day 10.

Renal Ischemia-reperfusion studies: Fifty-six male Wistar (W) rats weighing approximately 270-300 g were anesthetized with an intraperitoneal injection of pentobarbital sodium (30 mg/kg) and placed on a homeothermic table to maintain core body temperature at 37°C , by means of a rectal probe attached to a temperature regulator which was in turn attached to a homeothermic blanket. A midline laparotomy was made, renal pedicles were isolated, and bilateral renal ischemia was induced by clamping the renal pedicles for 0 or 20 min as described previously(14). Occlusion was verified visually by change in the color of the kidneys to a paler

1 shade and reperfusion by a blush. Reperfusion commenced when the clips were removed. The
2 rats were divided in groups of eight rats each after 9, 18, 24, 72, 96 and 120 h of reperfusion. A
3 group of 4 rats underwent sham surgery and served as controls. Rats (n=4) per group were
4 immediately placed in metabolic cages at 22 °C. Individual urine samples were collected at 9, 18,
5 10 24, 72, 96 and 120 h after reperfusion for analysis of Kim-1. Another set of rats (n=4) was
6 11 12 13 14 15 16 sacrificed by overdose of pentobarbital (200 mg/kg, ip) at 9, 18, 24, 72, 96 and 120 h after
reperfusion.

17 To confirm the results obtained from RenaStick urinary Kim-1 was measured using
18 previously described microbead based assay(13).
19
20
21
22
23
24
25 **Urine Collection.**
26

27 Urine was collected prior to necropsy (18 hr +/- 2 hr collection period) and the rats were
28 placed in standard metabolic cages and fasted prior to collection. Urine samples were collected
29 from individual animals into containers surrounded by dry ice and were stored at -80 °C until
30 thawing for urinalysis. After the initial thawing at 22 °C, samples were placed on wet ice and
31 volume measurement was performed (precipitates were allowed to settle by gravity and were
32 discarded). Typically, 2.5 ml urine samples were used for routine clinical chemistry urinalysis
33 (Roche Modular Analyzer): manual specific gravity, pH, protein, glucose, creatinine, occult
34 blood, creatinine, and ketones were measured. For the remaining urine volumes, small aliquots
35 were made and stored at -80 °C until biomarker analysis to avoid repeated freeze-thaw cycles.
36
37
38
39
40
41
42
43
44
45
46
47
48
49
50

51 **Blood Collection & Clinical Chemistry.** 52

53 Rats were fasted overnight prior to necropsy and bled from the vena cava with 2 ml collected
54 into a serum separator tube and centrifuged 1,500 X g for 10 min at 4 °C. An additional 2 ml of
55
56
57
58
59
60

1 collected blood was placed into an EDTA collection tube and centrifuged 900 X g for 15 min at
2 4°C to isolate plasma. Isolated plasma and serum samples were stored at -80°C until use.
3 Blood urea nitrogen (BUN) (mg/dL) and creatinine were measured using a standard clinical
4 chemistry analyzer (Roche-Modular).
5
6
7
8
9

10
11
12
13 **Histopathology.**
14

15 At necropsy, tissues were collected from Cadmium or Gentamicin treated rats for histology
16 soon after the last blood collection and exsanguination. Both kidneys (5 mm section including
17 the papilla, cortex, and medulla) were isolated from each animal and placed in 10% neutral
18 buffered formalin (NBF). In renal I/R study one kidney was perfused via the left ventricle with
19 phosphate-buffered saline and then with 4 % paraformaldehyde lysine periodate (PLP) for
20 10 min for histology. Tissues were fixed for a minimum of 24 hr, processed and embedded in
21 paraffin. Embedded tissues were cut into 4-6 micron sections and stained with hematoxylin and
22 eosin (H&E). Tissues from control and treated animals were examined microscopically using a
23 light microscope.
24
25
26
27
28
29
30
31
32
33
34
35

36
37
38
39 **Immunohistochemical or Immunofluorescence visualization of Kim-1.**
40

41 For immunohistochemistry paraformaldehyde lysine periodate-fixed tissue sections (in
42 ischemia/reperfusion injury study), (5µm) were deparaffinized in xylene, rehydrated with a series
43 of alcohol washes and then incubated for 20 min at 95°C in a citrate buffer solution (Zymed
44 Laboratories, #00-5000, South San Francisco, CA). The samples were then processed for
45 visualization of Kim-1 using a monoclonal anti-rat Kim-1 antibody (MARKE-2) and the same
46 labeling protocol for paraffin embedded tissue samples as described previously(14). For
47 immunofluorescence staining of Kim-1 in Cadmium study sections were thawed, washed with
48
49
50
51
52
53
54
55
56
57
58
59

PBS, fixed in -20°C methanol, and blocked in 1.5% normal goat serum in PBS (blocking solution) for 30 min. Sections were then incubated for 1 h with monoclonal anti-rat Kim-1 antibody (MARKE-2) (5 µg/ml) diluted in the blocking solution. The sections were washed with PBS and incubated with anti-mouse FITC conjugated (1:75 dilution, Pierce) in PBS for 30 min. At the final step, sections were washed with PBS and mounted with Vector Shield mounting reagent (Vector) containing 12.5 µg/ml DAPI to identify nuclei. As a negative control, the same concentration of mouse IgG (5 µg/ml) was used for the primary antibody.

Selection of participants and urine sample collection.

Urine samples from patients with and without elevated urinary KIM-1 levels (1000 pg/ml) were obtained from our cross sectional study on urinary biomarkers of AKI(15). Urine samples had been kept frozen at -80C and then thawed for quantitation by RenaStick and repeat measurement of KIM-1 as previously described(15). Patients without elevated urinary KIM-1 levels were healthy volunteers (N = 9) and critically ill patients with no clinical evidence of AKI (N = 3). Patients with elevated urinary KIM-1 levels had acute tubular necrosis (N = 7) and recent cardiac catheterization (N = 3); two patients had no other identifiable clinical evidence of acute kidney injury.

Serial pre- and post-operative urine samples were obtained from two patients with postoperative AKI from cytoreductive surgery with intraoperative local cisplatin administration for malignant mesothelioma. Urine samples were obtained pre-operatively, 6h postoperatively, and then every day for up to five days. The Institutional Review Board approved the protocols for recruitment and sample collection.

Urine was collected from spontaneous voids or from indwelling Foley catheters. Urine dipstick analysis was performed (Multistix 8 SG, Bayer Corporation), followed by centrifugation

1 and microscopic examination of the urine sediment (Olympus microscope). The urine
2 supernatant was aliquoted into 1.8 ml eppendorf tubes and frozen within 2 hours of collection at
3 -80 °C. At the time of assay samples were thawed, vortexed, and centrifuged at 14,000 rpm at 4
4 °C and supernatant was pipetted for KIM-1 measurement.
5
6
7
8
9

10
11
12
13 **Development and Evaluation of direct lateral flow immunochromatographic assay for**
14 **measurement of Kim-1.**
15
16

17
18 *Coupling of gold nanoparticles to Kim-1 capture antibodies:* Forty nm gold nanoparticles
19 obtained from BioAssay Works were coated with mouse monoclonal anti Kim-1 antibody
20 (MARKE-1)(14) or rabbit polyclonal antibody against human KIM-1(15) by adjusting the pH of
21 the gold particles with a bicarbonate buffer to slightly above the isoelectric point of the Kim-1
22 antibody. Approximately two hundred (200) molecules of antibody were coated onto each gold
23 sphere, blocked with BSA and sprayed on polyester ribbon. The ribbon was air-dried at 37°C for
24 two hours and stored in a desiccated chamber. BioAssay Works' nitrocellulose membrane was
25 striped with a 2 mg/ml solution of another epitopically distinct anti Kim-1 antibody at a rate of 1
26 µl per square cm. A control line of goat anti-mouse for rat RenaStick and anti-rabbit for human
27 RenaStick was also striped down at the same rate. The striped down membrane and air-dried
28 ribbon were assembled in overlapping fashion on a plastic laminate (see Supplementary Figure
29 1a). Strips were cut 4 mm-wide and placed in plastic immunochromatographic housing.
30
31
32
33
34
35
36
37
38
39
40
41
42
43
44
45
46
47
48
49
50
51
52
53
54
55
56
57
58
59
60

Evaluation of the assay: Positive and negative Kim-1 urine samples were diluted two-fold in
a TRIS-buffered saline solution and 150 µL of the mixture was added to the sample well of the
immunochromatographic housing. Results were read within fifteen minutes. Kim-1 antigen
detection levels in urine starting at 500 pg/ml were realized with a dose-response covering a
three-log range. The inter assay variability was determined by adding diseased urine samples

1 containing low (1.3 ng/ml), medium (8.6 ng/ml) and high (19 ng/ml) levels of Kim-1 to nine
2 RenaSticks (n=3 each) was less than 10 % (data not shown).
3
4
5
6
7
8

9 *Quantitation of Kim-1 band intensities.*

10 The strips were read using a CAMAG Thin Layer Chromatography (TLC) 3 Scanner,
11 CAMAG Scientific Inc., Wilmington, NC. The CAMAG scanner is designed for densitometric
12 measurement of thin-layer chromatograms and other objects up to 200x200mm in size. The
13 scanner was set to read at a wavelength of 546 in the light absorption-mode at a scanning
14 speed of 5 mm per second. The scanning produces peaks and the peak height correlates with
15 the signal. The band intensity units were represented on Y-axis in the respective injury models
16 with respect to either dose or time on X-axis using Prism 4 software, GraphPad Software, Inc.
17 La Jolla, CA. Statistical comparison between control and treated was obtained by two tailed
18 student t-test and a p value less than 0.05 was assessed as statistically significant.
19 Comparisons between quantitated Kim-1 band intensity and log-transofrmed Kim-1
20 measurements by the microbead assay were assessed by the Pearson correlation coefficient.
21
22
23
24
25
26
27
28
29
30
31
32
33
34
35
36
37
38
39
40
41
42
43
44
45
46
47
48
49
50
51
52
53
54
55
56
57
58
59
60

ACKNOWLEDGEMENT

This work was supported by K99/R00 ES016723 grant by NIEHS to VSV; Center for Integration of Medicine and Innovative Technology (CIMIT) grant (W81XWH-07-2-0011) to JVB and VSV, NIH grants DK39773, DK72831 and DK74099 to JVB, ES06478 to WCP, and by research grants 48483 from the Mexican Council of Science and Technology (CONACYT) and DGAPA IN228206-3 of National University of Mexico to NAB.

COMPETING FINANCIAL INTERESTS

Dr. Bonventre is an inventor on KIM-1 patents.

1
2
REFERENCES

- 3
4
5
6
7
8
9
10
11
12
13
14
15
16
17
18
19
20
21
22
23
24
25
26
27
28
29
30
31
32
33
34
35
36
37
38
39
40
41
42
43
44
45
46
47
48
49
50
51
52
53
54
55
56
57
58
59
60
1. Appel, GB & Neu, HC: Gentamicin in 1978. *Ann Intern Med*, 89: 528-38, 1978.
 2. Carson, RT & Vignali, DA: Simultaneous quantitation of 15 cytokines using a multiplexed flow cytometric assay. *J Immunol Methods*, 227: 41-52, 1999.
 3. Dieterle, F, Marrer, E, Suzuki, E, Grenet, O, Cordier, A & Vonderscher, J: Monitoring kidney safety in drug development: Emerging technologies and their implications. *Curr Opin Drug Discov Devel*, 11: 60-71, 2008.
 4. Gilbertson, DT, Liu, J, Xue, JL, Louis, TA, Solid, CA, Ebben, JP & Collins, AJ: Projecting the number of patients with end-stage renal disease in the United States to the year 2015. *J Am Soc Nephrol*, 16: 3736-41, 2005.
 5. Han, WK, Bailly, V, Abichandani, R, Thadhani, R & Bonventre, JV: Kidney Injury Molecule-1 (KIM-1): a novel biomarker for human renal proximal tubule injury. *Kidney Int*, 62: 237-44, 2002.
 6. Ichimura, T, Hung, CC, Yang, SA, Stevens, JL & Bonventre, JV: Kidney injury molecule-1: a tissue and urinary biomarker for nephrotoxicant-induced renal injury. *Am J Physiol Renal Physiol*, 286: F552-63, 2004.
 7. Liangos, O, Perianayagam, MC, Vaidya, VS, Han, WK, Wald, R, Tighiouart, H, MacKinnon, RW, Li, L, Balakrishnan, VS, Pereira, BJ, Bonventre, JV & Jaber, BL: Urinary N-acetyl-beta-(D)-glucosaminidase activity and kidney injury molecule-1 level are associated with adverse outcomes in acute renal failure. *J Am Soc Nephrol*, 18: 904-12, 2007.
 8. Perez-Rojas, J, Blanco, JA, Cruz, C, Trujillo, J, Vaidya, VS, Uribe, N, Bonventre, JV, Gamba, G & Bobadilla, NA: Mineralocorticoid receptor blockade confers renoprotection in preexisting chronic cyclosporine nephrotoxicity. *Am J Physiol Renal Physiol*, 292: F131-9, 2007.
 9. Prozialeck, WC, Vaidya, VS, Liu, J, Waalkes, MP, Edwards, JR, Lamar, PC, Bernard, AM, Dumont, X & Bonventre, JV: Kidney injury molecule-1 is an early biomarker of cadmium nephrotoxicity. *Kidney Int*, 72: 985-93, 2007.
 10. Sistare, FD & DeGeorge, JJ: Preclinical predictors of clinical safety: opportunities for improvement. *Clin Pharmacol Ther*, 82: 210-4, 2007.
 11. Uchino, S, Kellum, JA, Bellomo, R, Doig, GS, Morimatsu, H, Morgera, S, Schetz, M, Tan, I, Bouman, C, Macedo, E, Gibney, N, Tolwani, A & Ronco, C: Acute renal failure in critically ill patients: a multinational, multicenter study. *JAMA*, 294: 813-8, 2005.
 12. Vaidya, VS, Ferguson, MA & Bonventre, JV: Biomarkers of Acute Kidney Injury. *Annu Rev Pharmacol Toxicol*, 48: 463-493, 2008.
 13. Vaidya, VS, Ozer, JS, Dieterle, F, Collings, FB, Ramirez, V, Troth, S, Muniappa, N, Thudium, D, Gerhold, D, Holder, D, Bobadilla, NA, Marrer, E, Perentes, E, Cordier, A, Vonderscher, J, Maurer, G, Goering, PL, Sistare, F & Bonventre, JV: Kidney injury molecule-1 outperforms traditional biomarkers of kidney injury in a multisite preclinical biomarker qualification studies. Submitted, 2008.
 14. Vaidya, VS, Ramirez, V, Ichimura, T, Bobadilla, NA & Bonventre, JV: Urinary kidney injury molecule-1: a sensitive quantitative biomarker for early detection of kidney tubular injury. *Am J Physiol Renal Physiol*, 290: F517-29, 2006.
 15. Vaidya, VS, Waikar, SS, Ferguson, MA, Collings, FB, Sunderland, K, Gioules, C, Bradwin, G, Matsouaka, R, Betensky, RA, Curhan, GC & Bonventre, JV: Urinary biomarkers for sensitive and specific detection of acute kidney injury in humans. *Clinical and Translational Science*, 1: 200-208, 2008.
 16. van Timmeren, MM, Bakker, SJ, Vaidya, VS, Bailly, V, Schuurs, TA, Damman, J, Stegeman, CA, Bonventre, JV & van Goor, H: Tubular kidney injury molecule-1 in protein-overload nephropathy. *Am J Physiol Renal Physiol*, 291: F456-64, 2006.

- 1
2
3
4
5
6
7
8
9
10
11
12
13
14
15
16
17
18
19
20
21
22
23
24
25
26
27
28
29
30
31
32
33
34
35
36
37
38
39
40
41
42
43
44
45
46
47
48
49
50
51
52
53
54
55
56
57
58
59
60
17. van Timmeren, MM, Vaidya, VS, van Ree, RM, Oterdoom, LH, de Vries, AP, Gans, RO, van Goor, H, Stegeman, CA, Bonventre, JV & Bakker, SJ: High Urinary Excretion of Kidney Injury Molecule-1 Is an Independent Predictor of Graft Loss in Renal Transplant Recipients. *Transplantation*, 84: 1625-1630, 2007.
18. Zhou, Y, Vaidya, VS, Brown, RP, Zhang, J, Rosenzweig, BA, Thompson, KL, Miller, TJ, Bonventre, JV & Goering, PL: Comparison of kidney injury molecule-1 and other nephrotoxicity biomarkers in urine and kidney following acute exposure to gentamicin, mercury, and chromium. *Toxicol Sci*, 101: 159-70, 2008.

For Peer Review

1 **Figure 1. Urinary Kim-1 measurements using rat RenaStick (a-e), histological damage (f-i)**
2
3
4
5
6 **and Kim-1 immunostaining (j-m) following cadmium induced kidney injury.** Male Sprague
7 Dawley rats (n=4/group) were injected subcutaneously with varying doses of CdCl₂ (Cd dose of
8 0.6, 1.2, or 2.4 mg/kg) or saline 5 days per week for 4 weeks. (a-d) After 4 weeks rats were
9 placed in metabolic cages and urine was collected. Seventy microlitres of urine sample from
10 each rat was mixed with 70 µl of TRIS-buffered saline solution, added to the RenaStick sample
11 well and incubated for 15 minutes. (e) Each RenaStick was scanned using CAMAG TLC
12 scanner and the densitometric units obtained were plotted. * Statistically higher than
13 control/sham (p<0.05). (f-i) At necropsy samples of both kidneys were isolated from each animal
14 and placed in 10% neutral buffered formalin (NBF) for H & E staining and histology assessment.
15
16 (j-m) In addition, non-fixed cryosections of the kidney tissue were processed for the
17 immunoflourescent visualization of Kim-1. Representative photomicrographs of H & E stained
18 kidney sections and immunostaining for Kim-1 respectively from following groups: (f, j) control,
19
20 (g, k) 0.6 mg Cd/kg, (h, l) 1.2 mg Cd/kg, (i, m) 2.4 mg Cd/kg. All fields were chosen from outer
21 renal cortex. Arrows in panels from b-d indicate retraction and sloughing of cells, tubular
22 congestion and necrosis. The fluorescent images in panel's j-m indicate Kim-1 staining in the
23 apical membrane of the proximal tubules in similar fields of the outer renal cortex.
24
25
26
27
28
29
30
31
32
33
34
35
36
37
38
39
40
41
42
43
44
45
46
47
48
49
50
51
52
53
54
55
56
57
58
59
60

Figure 2. Urinary Kim-1 measurements using rat RenaStick (a-d), clinical chemistry (e, f)
 and histological damage (g-i) following gentamicin induced kidney toxicity. Male Sprague
Dawley rats received Gentamicin sulfate at 0, 40, or 120 mg/kg/day (n=5 rats/dose group) for 9
days and urine samples were collected on day 10 by keeping rats in metabolic cages. (a-c)
Urinary Kim-1 was measured from each rat by mixing 70 µl of urine sample with 70 µl of
TRIS-buffered saline solution and adding it to the RenaStick sample well. Results were read in

1 15 minutes. (d) Each RenaStick was scanned using CAMAG TLC scanner and the
2 densitometric units obtained were plotted. * Represents statistically higher than control ($p<0.05$).
3
4 On day 10 for animals were necropsied for evaluation of (e) blood urea nitrogen (BUN), (f)
5 serum creatinine and (g-i) histomorphologic evaluation of kidneys (H&E staining). All fields were
6 chosen from outer stripe of outer medulla (OSOM). Arrows in panel's g and i indicate sloughing
7 of cells, tubular dilation and necrosis. Bar represents 50 μm .
8
9
10
11
12
13
14

15
16
17
18 **Figure 3. Urinary Kim-1 measurements using rat RenaStick (a-i), kidney histopathology (j-
19 m) and immunohistochemistry for Kim-1 (n-q) over time following 20 min bilateral renal
20 ischemia/reperfusion injury.**
21
22

23 Male Wistar rats were subjected to 0 (sham) or 20 min of bilateral ischemia by clamping the
24 renal pedicles for 20 min and then removing the clamps and confirming reperfusion. (a-h) Rats
25 were placed in metabolic cages and urine was collected at 6, 9, 18, 24, 72, 96 and 120 h
26 following reperfusion. Urinary Kim-1 was measured from each rat by mixing 70 μl of urine
27 sample with 70 μl of TRIS-buffered saline solution and adding it to the RenaStick sample well.
28 Results were read in 15 minutes. (i) Each RenaStick was scanned using CAMAG TLC scanner
29 and the densitometric units obtained were plotted. * Represents statistically higher than sham
30 ($p<0.05$). (j-q) Rats were euthanized at various times and kidney tissue was collected:
31 Representative photomicrographs of H & E stained kidney sections and immunohistochemistry
32 for Kim-1 respectively from following time points: (j, n) 0 h (sham control); (k, o) 9 h; (i, p) 24 h;
33 (m, q) 120 h. All fields were chosen from the outer stripe of outer medulla (OSOM). Arrows in
34 panels from k-m indicate sloughing of cells, tubular dilation and necrosis. Panel's o-q show Kim-
35 1 staining in the apical membrane of the proximal tubules in the OSOM region. Bar represents
36 50 μm .
37
38
39
40
41
42
43
44
45
46
47
48
49
50
51
52
53
54
55
56
57
58
59
60

1 **Figure 4. Urinary Kim-1 measurements using human RenaStick in (a-c) cross sectional**
2 **study involving twenty-four patients with or without acute kidney injury and (d-f)**
3 **prospective study in two patients with cisplatin induced kidney toxicity over time.**

14 **SUPPLEMENTARY FIGURES**

17 **Figure 1. Characteristics of rat RenaStick.** (a) Principle of lateral flow
18 immunochromatographic assay. (b) Visual concentration dependent decrease in Kim-1 band
19 intensity was observed in rat RenaStick. (c) The density of the Kim-1 band was quantitated
20 using a CAMAG thin layer chromatography (TLC) scanner and a standard curve was obtained
21 by plotting the concentration of recombinant rat Kim-1 protein on the X-axis and corresponding
22 densitometric units on the Y-axis. The X-axis is broken in to three segments for better data
23 representation. (d) The analytical recovery was determined by adding a known concentration of
24 recombinant rat Kim-1 ectodomain (5 ng/ml) into buffer or urine samples from control or treated
25 rats (n=3 each). Arrow indicates band corresponding to Kim-1.

42 **Figure 2. Characteristics of human RenaStick.** (a) Visual concentration dependent decrease
43 in KIM-1 band intensity was observed in human RenaStick. (c) The density of the KIM-1 band
44 was quantitated using a CAMAG thin layer chromatography (TLC) scanner and a standard
45 curve was obtained by plotting the concentration of recombinant human KIM-1 protein on the X-
46 axis and corresponding densitometric units on the Y-axis. The X-axis is broken in to two
47 segments for better data representation. (d) The analytical recovery was determined by adding
48 a known concentration of recombinant human KIM-1 ectodomain (5 ng/ml) into buffer or urine

1 samples from patients with or without kidney injury (n=3 each). Arrow indicates band
2 corresponding to KIM-1.
3
4
5
6
7
8
9
10
11
12
13
14
15
16
17
18
19
20
21
22
23
24
25
26
27
28
29
30
31
32
33
34
35
36
37
38
39
40
41
42
43
44
45
46
47
48
49
50
51
52
53
54
55
56
57
58
59
60

For Peer Review

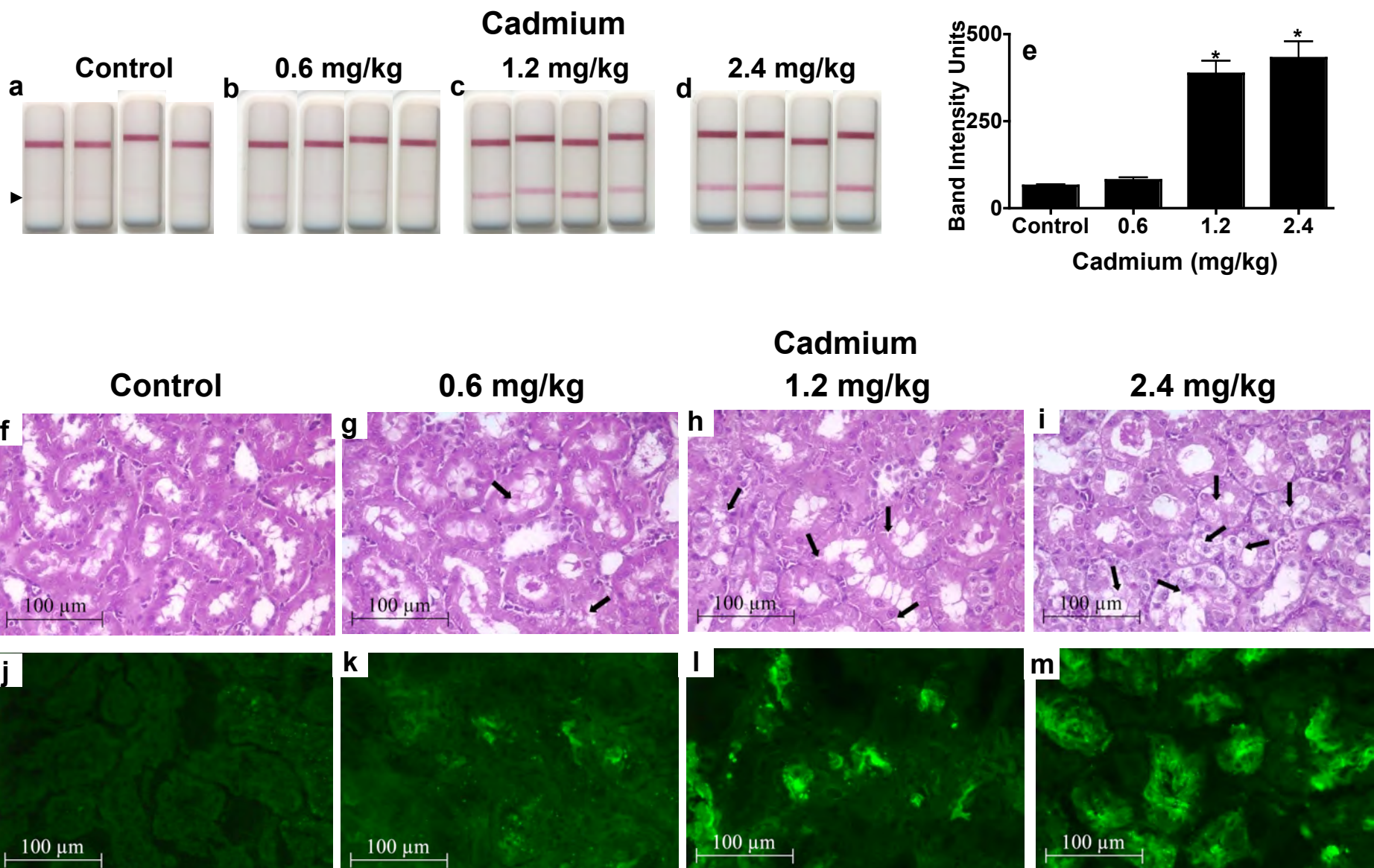
Figure. 1

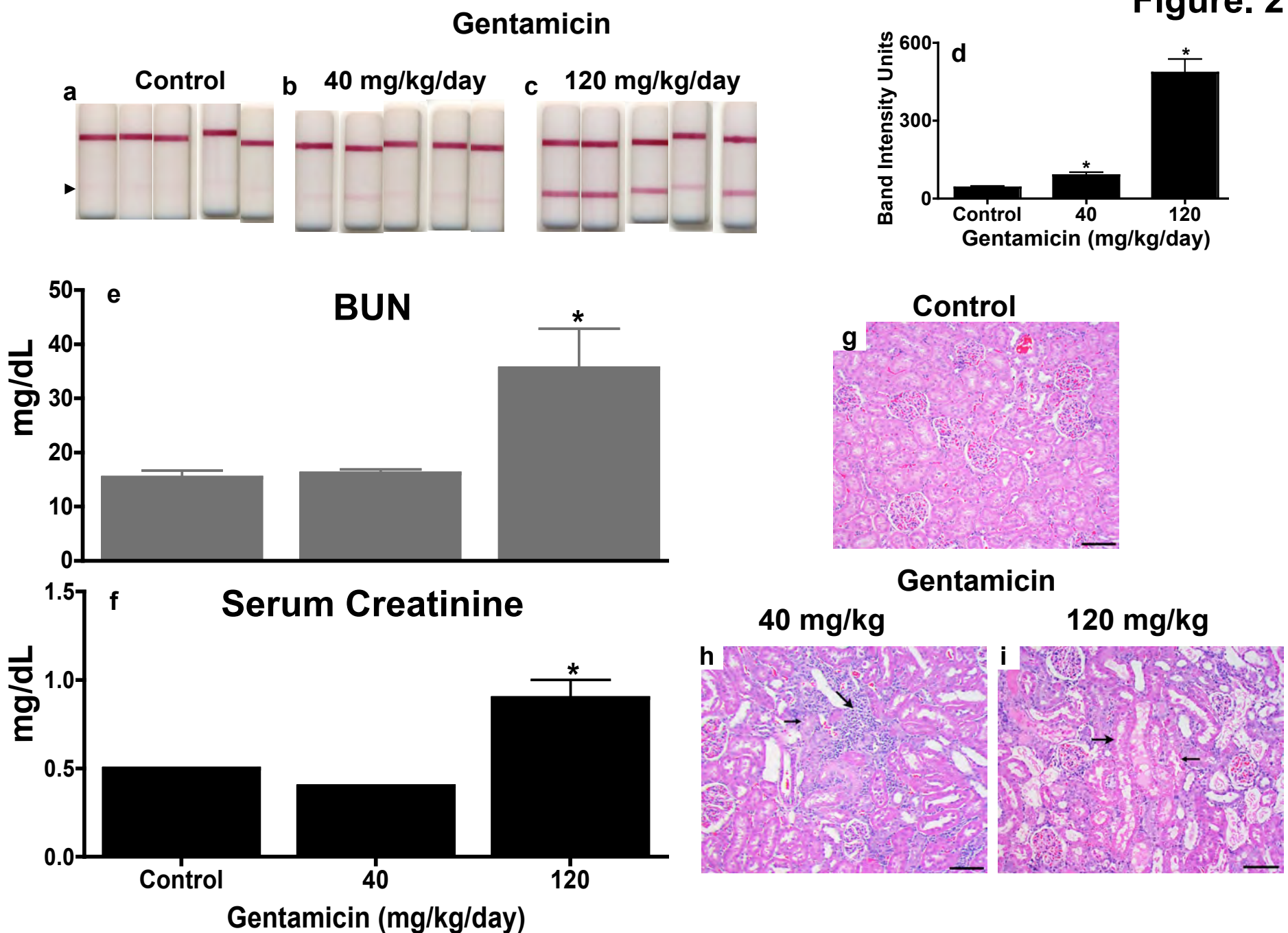
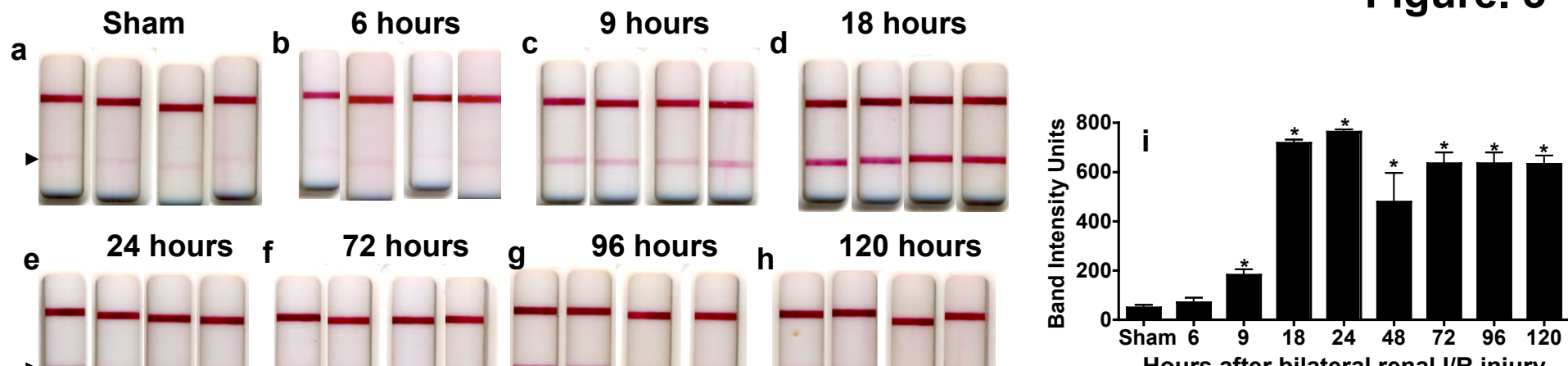
Figure. 2

Figure. 3

20
21
22
23
24
25
26
27
28
29
30
31
32
33
34
35
36
37
38
39
40
41
42
43
44
45
46
47
48
49

Hours after bilateral renal I/R injury

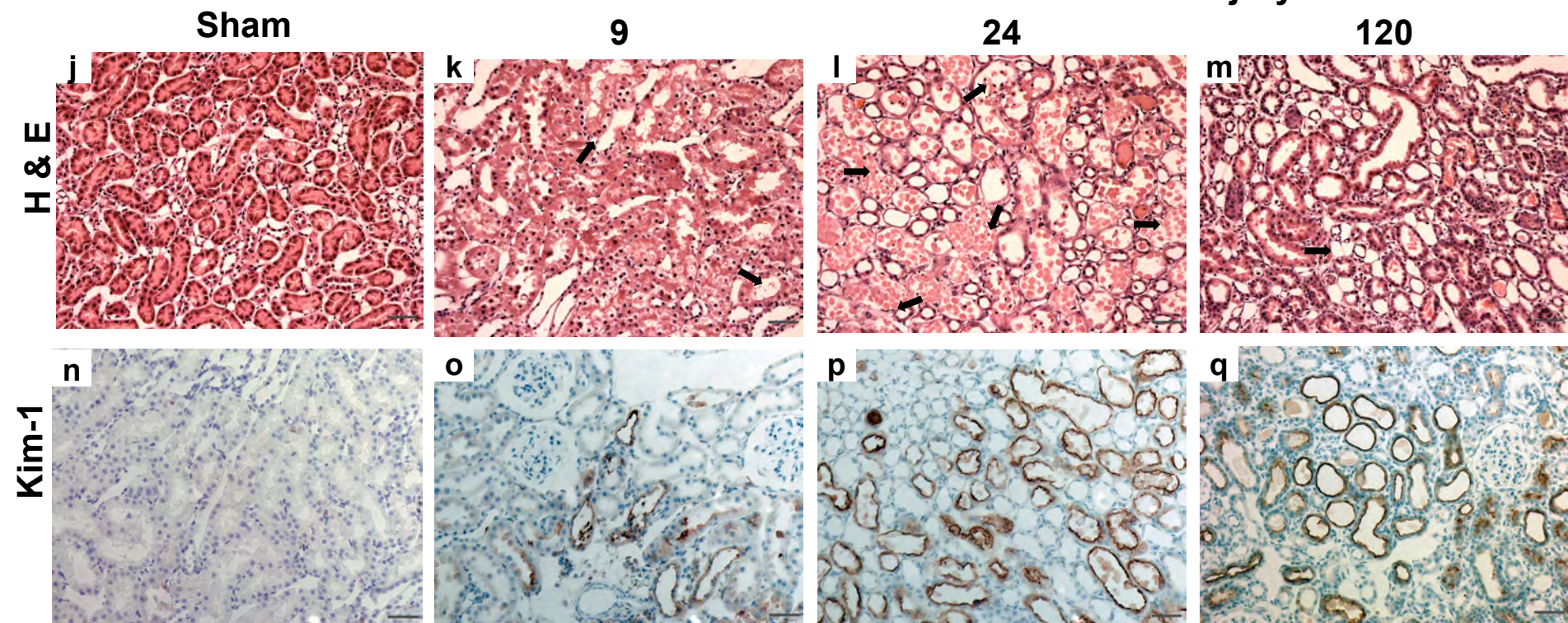
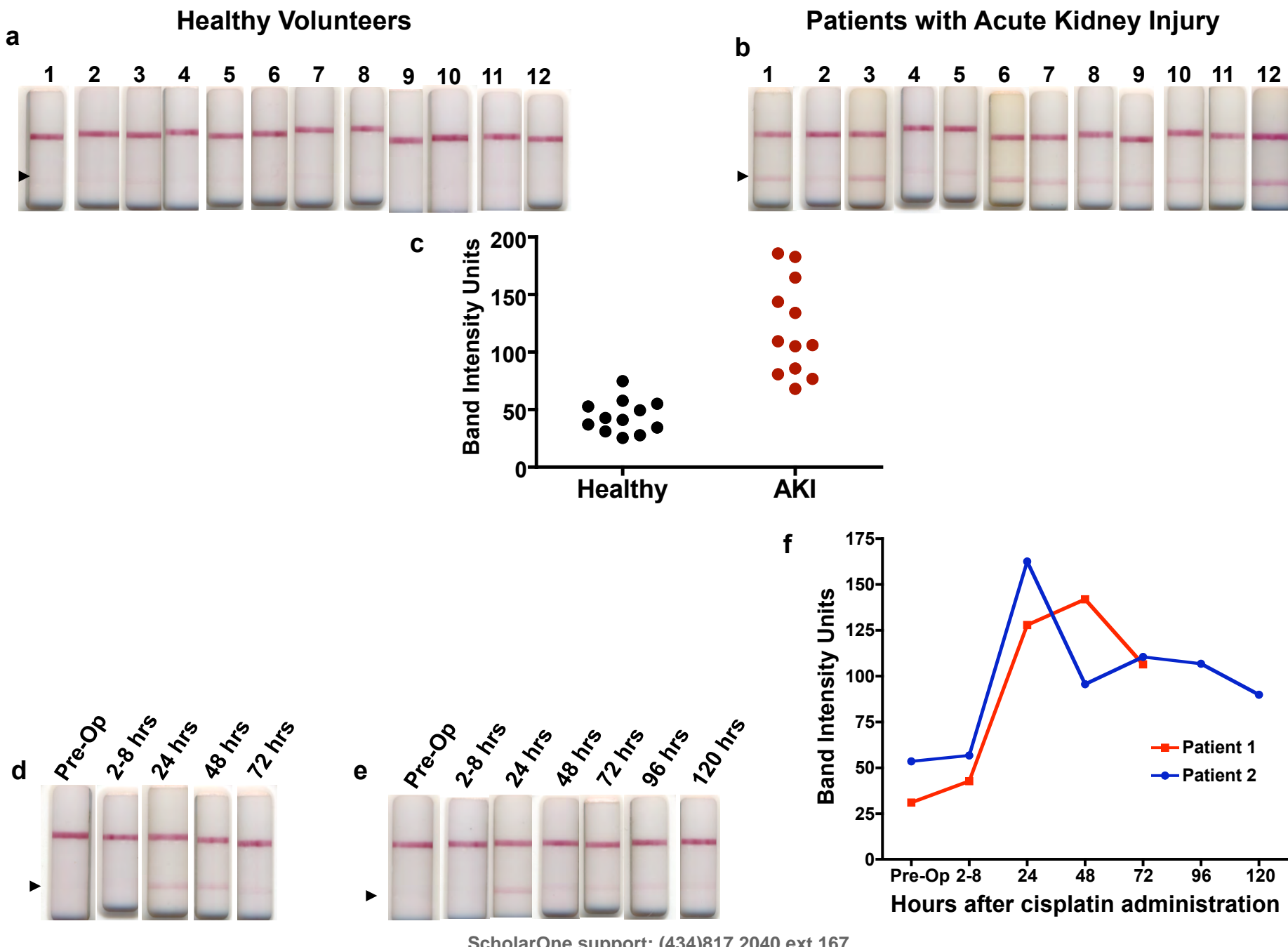
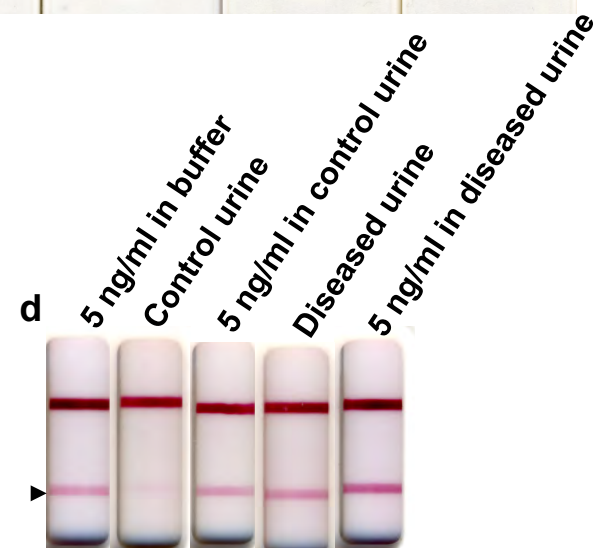
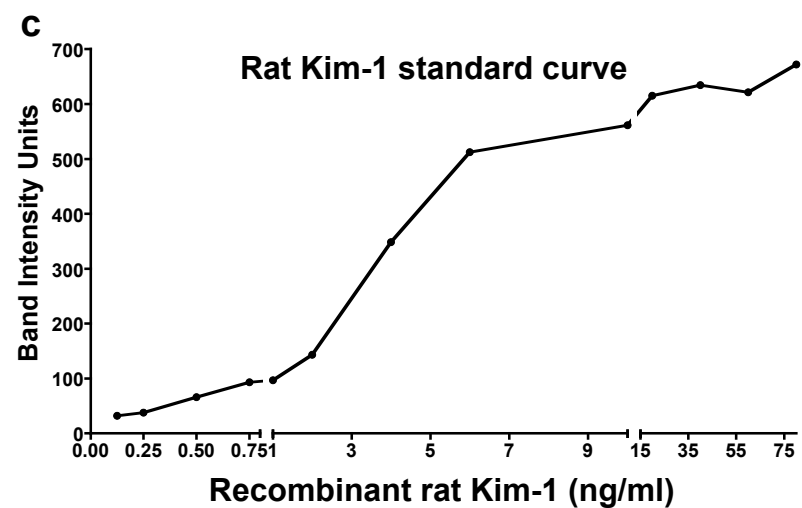
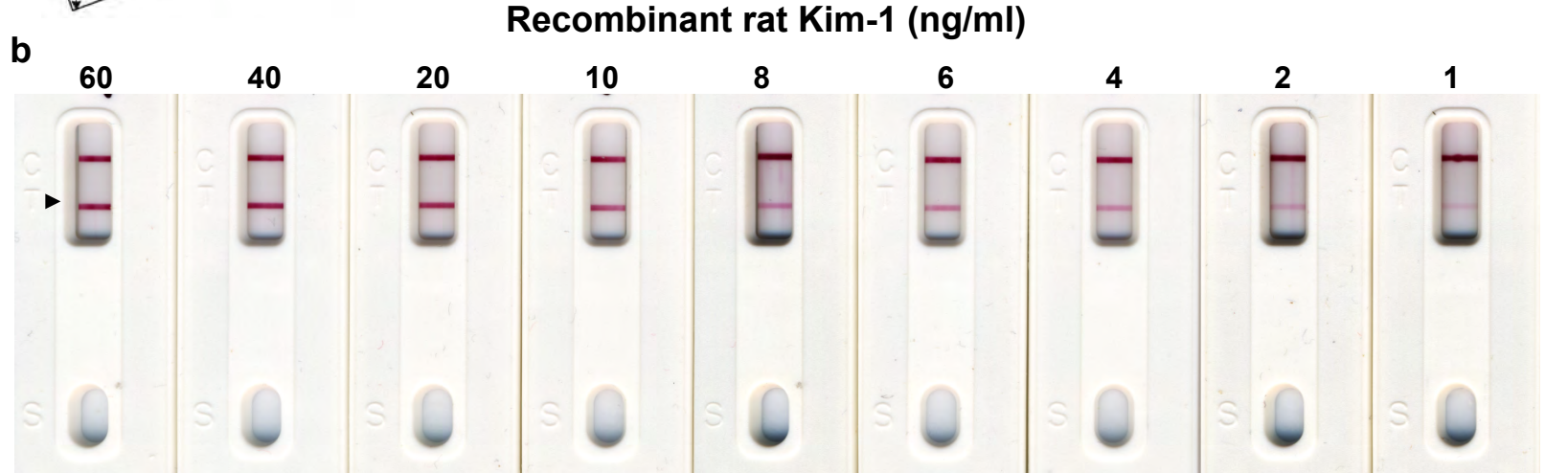
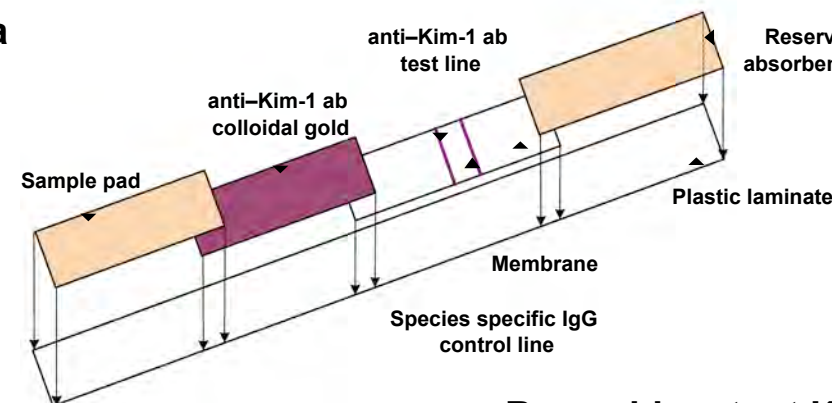
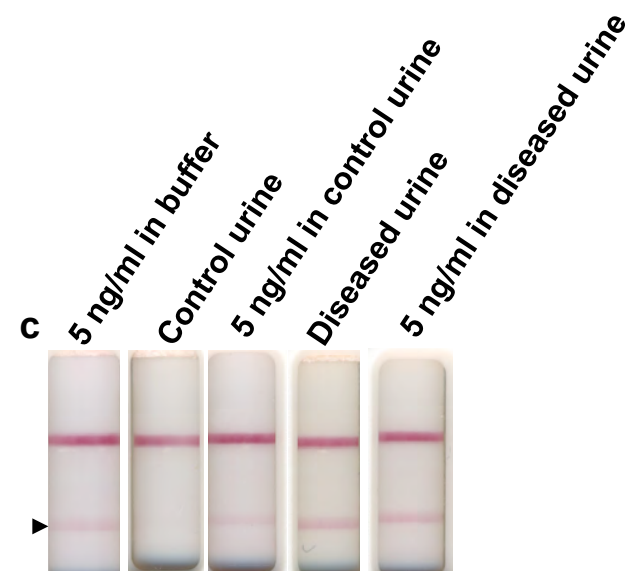
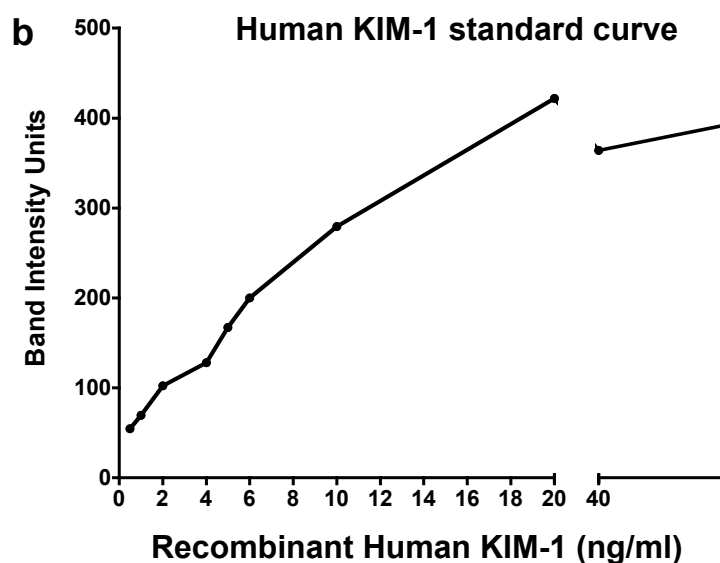
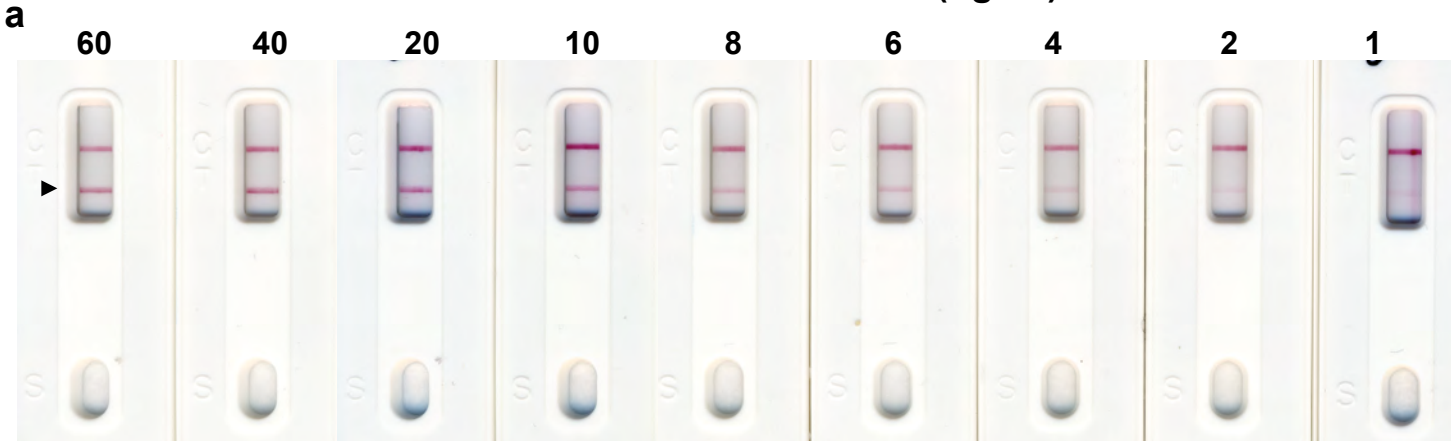


Figure. 4

Supplementary Figure. 1



Supplementary Figure. 2**Recombinant Human KIM-1 (ng/ml)**

1 **SUPPLEMENTARY TABLE 1: Urinary Kim-1 values measured by microbead based xMAP technology in three mechanistically
2 different kidney injury models caused by a) Cadmium, b) Gentamicin or c) 20 min bilateral ischemia/reperfusion injury.**

5 a) Cadmium toxicity 6 model	Control	0.6 mg/kg	1.2 mg/kg	2.4 mg/kg				
7	183.5	358.7	1351.8	2471.4				
8	Urinary Kim-1 (pg/ml) 9 measured after 4 weeks	317.8	199	1849.6				
10		192.5	185.2	3402.7				
11		225.3	207.3	1816.6				
12				5127				
13								
14 b) Gentamicin toxicity 15 model	Control	40 mg/kg/day	120 mg/kg/day					
16	239.1	611.7	22226.5					
17	Urinary Kim-1 (pg/ml) 18 measured after 10 days	235.5	931.6	19087.9				
19		232	569	10846.3				
20		234	569.5	2596.6				
21		200.7	851	11930.5				
22								
23 c) Ischemia/Reperfusion 24 injury model	Sham	6	9	18	24	72	96	120
25	Urinary Kim-1 (pg/ml) 26 measured at different time 27 points following 28 reperfusion	118.9	150.9	769	4212.9	22160.6	5574.9	5057.6
29		225.3	114.1	709.3	5218.3	46097.8	5610.3	3623.9
30		140.4	69.8	512.6	8627.2	10311.4	2391.2	5087
31		192.5	202.9	1137	9085.7	14209.9	5674.5	4701.2
32								1793.3
33								2261.5
34								1320.4
35								

1 **SUPPLEMENTARY TABLE 2: Urinary KIM-1 values measured by microbead based xMAP technology in patients with or without**
2 **acute kidney injury.**

5	Healthy Volunteers	Acute kidney injury
7	Patient 1	265.74
8	Patient 2	227.09
9	Patient 3	91.39
10	Patient 4	172.99
11	Patient 5	467.87
12	Patient 6	102.98
13	Patient 7	179.35
14	Patient 8	176.46
15	Patient 9	391.64
16	Patient 10	249.49
17	Patient 11	241.02
18	Patient 12	97.56
19	Patient 1	3755.07
20	Patient 2	1152.76
21	Patient 3	11038.52
22	Patient 4	1079.53
23	Patient 5	2313.62
24	Patient 6	5113.29
25	Patient 7	3222.66
26	Patient 8	1319.39
27	Patient 9	1062.23
28	Patient 10	1309.99
29	Patient 11	1492.79
30	Patient 12	13500.26

1 **SUPPLEMENTARY TABLE 3: Urinary KIM-1 values measured by microbead based xMAP technology in patients with acute kidney
2 injury following cisplatin administration.**

5 Time of urine collection following 6 cisplatin administration	7 Patient 1	8 Patient 2
7 Pre-Op	11.58	143.00
9 2-8 hours	50.28	100.45
10 24 hours	4785.38	7834.17
11 48 hours	5365.37	1714.50
12 72 hours	1168.11	2381.15
13 96 hours	--	2177.99
14 120 hours	--	564.58